# *In vivo* toxicological evaluation of peptide conjugated gold nanoparticles for potential application in colorectal cancer diagnosis

**O.B. Adewale**



**2018**

# *In vivo* toxicological evaluation of peptide conjugated gold nanoparticles for potential application in colorectal cancer diagnosis

**Olusola Bolaji Adewale**

**215317041**

**Submitted in fulfilment of the requirements for the degree of**

***Philosophiae* Doctor**

**in**

**Biochemistry**



**Faculty of Science**

**Department of Biochemistry and Microbiology**

**Nelson Mandela University**

**April 2018**

**Promoter: Prof S Roux**

**Co-Promoter: Dr H Davids**

**DECLARATION**

I, Olusola Bolaji Adewale, student number 215317041, hereby declare that the thesis: *In vivo* toxicological evaluation of peptide conjugated gold nanoparticles for potential application in colorectal cancer diagnosis, for the degree of *Philosophiae* Doctor is my own work and that it has not previously been submitted for assessment or completion of any postgraduate qualification to another University or for another qualification.

……

Olusola B. Adewale

**TABLE OF CONTENTS**

**ABSTRACT**

Colorectal cancer (CRC) is among the leading cause of cancer-related deaths in South Africa and worldwide. Efforts are being made at finding improved diagnostic tools, as early detection (before metastasis) is a major factor in CRC treatment. Colonoscopy is the most reliable detection method, but is a specialised and expensive procedure, which is invasive, not readily available and not patient-friendly. There is a risk of developing interval cancers, as colonoscopies are performed every 10 years after the age of 40. The development of non-invasive, cost efficient and readily available diagnostic tools to CRC, which can be performed at more regular intervals, using tumour-targeting molecular imaging agents, is of urgent attention.

Gold nanoparticles (AuNPs) possess several physicochemical properties, including ease of synthesis, biocompatibility, and the ability to be conjugated by ligands or biomolecules such as polyethylene glycol (PEG) and peptides for improved stability, tissue targeting and selectivity. These factors potentiate the role in biomedical applications, including cancer theranostics. Conjugation of AuNPs with a targeting molecule (e.g. antibody or peptide) is directed against cancer cell receptors. The peptides, p.C, p.L, and p.14, bind to CRC cells *in vitro*. Conjugation of AuNPs with these peptides should be investigated for CRC diagnosis *in vivo*, as it is hypothesised to allow examinations at shorter intervals through imaging techniques. This could reduce the risk of interval cancers, but before developing this novel tool, *in vivo* toxicity evaluations are essential. This study was therefore aimed at investigating the short- and long-term toxicological effects of a single intravenous injection of peptides (p.C, p.L, and p.14) conjugated to AuNPs in a healthy rat model.

Citrate-capped AuNPs were synthesised by the citrate-reduction method, and conjugated with each peptide (biotinylated) using a combination of PEG (99% PEG-OH and 1% PEG-biotin) as a stabilising agent and linker, via biotin-streptavidin interaction. Healthy male Wistar rats were intravenously injected with 14 nm citrate-AuNPs, PEG-, p.C-PEG, p.L-PEG, and p.14-PEG-AuNPs (100 µg/kg body weight), and the control rats were injected with phosphate buffered saline. The animals were monitored for behavioural, physiological, biochemical, haematological and

histological changes, as well as inflammatory responses. Phase 1 rats were sacrificed 2 weeks post-injection to determine the immediate or acute toxicity of the AuNPs, while phase 2 animals were sacrificed 12 weeks post-injection, to investigate the delayed or persistence toxicity of the AuNPs.

Results revealed no significant toxicities ($p>0.05$) with the citrate, PEG-, p.C-PEG and p.14-PEG-AuNPs over 12 weeks post-exposure, as evidenced by biochemical assays such as serum marker enzymes, liver and kidney function markers, and cholestatic indicators; haematological parameters; oxidative stress markers; and histopathological examinations. P.L-PEG-AuNPs, however, caused significant toxicity ($p<0.05$) to rats, as evidenced by increased relative liver weight, increased malondialdehyde levels, and total white blood cell counts 2 weeks post-exposure when compared to the control group. This was, however, reversed during the 12 weeks post-exposure. Further, there were no evidence of inflammatory responses, using pro-inflammatory markers including phospho IkB-α (p-IkB-α), interleukin 18 (IL-18) and interferon-γ (IFN-γ), as indicated by immunohistochemical staining of the liver, spleen, kidney and colon of rats 2 weeks post-injection of AuNPs.

Citrate, PEG-, p.C-PEG, and p.14-PEG-AuNPs did not induce immediate, acute or persistent toxicity, while p.L-PEG-AuNPs induced a transient acute toxicity.

It can be concluded that 14 nm spherical citrate-AuNPs at 100 µg/kg body weight is a good candidate for biomedical applications, and as a suitable carrier for diagnostic and/or therapeutic molecules. Combination of 99% PEG-OH and 1% PEG-biotin is an appropriate option for stabilising AuNPs in biological environment, and conjugating secondary diagnostic or therapeutic biomolecules or agents to citrate-capped AuNPs. Peptide-conjugated AuNPs are suitable for the development into a diagnostic tool for CRC *in vivo*.

**ACKNOWLEDGEMENTS**

My sincere appreciation to the Almighty God, the Alpha and Omega, the Holy Trinity One God for being the All in All of my studies and this research. His grace was sufficient for me during these trying few years. Thank you, my faithful Father. Glory be to Your Holy name. Amen.

My profound gratitude to my supervisor, Prof S Roux, and co-supervisor, Dr H Davids, for your mentorship. Your approach towards science has provided me the confidence to forge ahead in my carrier.

- To Prof S Roux, a mother and woman per excellent, I really appreciate you for your listening ear always towards the success of this work, even when not convenient. I have learnt a lot through you in science and lifestyle in general. I will forever be grateful.
- Dr H Davids, your rigorous, insightful and tireless contribution to this work is highly appreciated. Thank you very much.

I appreciate Dr N Wickens for his tireless efforts in the histological analyses. I learnt a lot from your wealth of scientific experience. Also, to Dr Tarryn Fick (Veterinary surgeon) for your dedicated support to this project, most especially in injecting the rats and for your special skill in training. Thank you. I also thank Prof Meyer for providing the peptides for this work, thank you very much.

I thank the National Research Foundation, South Africa and RCD, Nelson Mandela University for funding this project, and especially during the hard periods, I appreciate your support.

My appreciation to all postgraduate students, and members of staff of the Department of Biochemistry and Microbiology, Nelson Mandela University for your assistance during this study. Thank you to Lawyer and Jabu.

To my laboratory colleagues: Lynn, Disang, Ngozi (sister and friend), Hlumisa, Jean, Onye, Zona, Njabulo, Thabo, and Nomfundo. You are all wonderful, I will never forget your support in making this work a success.

A special thank you to Aare Afe Babalola (Founder, Afe Babalola University, Ado-Ekiti, ABUAD); the management of ABUAD; staff of the Department of Chemical Sciences; ABUAD Cooperative Multipurpose Limited for coming to my aid during the trying periods; and all the staff of Biochemistry program, ABUAD, permit me not to mention names, you are all wonderful.

To my humble Rev. Frs - Peter Adeusi, Anthony Bankole, Kelvin Fakehinde and Anthony Arowolo, thank you for your prayers and encouragement.

To these special people: Prof. Abiodun Ojo and Prof A. Onasanya, I will never forget your support in making me, you both are exceptionally wonderful, God bless you; Dr B.E. Oyinloye, Prof. Agunbiade, Prof. O.I. Oloyede, Prof N.E.J. Orhue, Abdulkadr Lukman, Dr S. Elaigwu, Olori Abiodun Ayeoba and family, Mrs Esther Adeogun, Mrs Olufunke Ogunyemi, Mr Jide, Abbey, Austin, Amaka and Jethro. Thank you all for your prayers and encouragement always.

I will never forget James Omoleye and family, Adewale Fadaka (my bobo), Dr Oluwole Alese, Mr Lanre Bankole and family, Mrs Toyin Awogbami, and a wonderful friend Oyebanji Ibitoye, your support and encouragement inspire me. My unreserved appreciation to Scholastica Anadozie, words are not enough to express my gratitude for your support towards my study since many years ago, and for the confidence and trust you have in me. Thanks a lot.

To my most amiable and lovely wife, Mojisola Janet Adewale, I appreciate your love, perseverance and endurance. I know it was not easy during this study, I thank God for the courage given you. Also, my lovely sons, Oluwajoba, IfeOluwa and IbukunOluwa Adewale, I really appreciate your endurance and prayers.

My parents: Mr Odekunle Adewale and Mrs Asabi Adewale, I so much appreciate your prayers, support and encouragement always. I also appreciate Mrs C.O. Adewale, Mr Sunday and Mrs

‘Funke Animasahun and family, Mr Olusola and Mrs ‘Seun Oladunjoye and family, as well as Ojo, Bisi and Dayo Adewale for your support.

I remember Late Adebowale Samuel Adewale. May his soul rest in peace. Amen.

## CONFERENCE PRESENTATIONS

1. Lynn Cairncross, **Olusola Adewale**, Hajierah Davids, Mervin Meyer, Saartjie Roux. Peptide – gold nanoparticles for colorectal cancer diagnosis: Assessment of the in vivo uptake and toxicity in rats. Annual MSc and PhD presentations, Department of Biochemistry and Microbiology, Conference centre, North Campus, Nelson Mandela University, South Africa, 3rd June 2016, **Oral presentation.**

2. **Olusola Adewale,** Hajierah Davids, Saartjie Roux. Acute toxicity assessment of peptide-gold nanoparticles for diagnosis of colorectal cancer. Annual MSc and PhD presentations, Department of Biochemistry and Microbiology, Conference centre, North Campus, Nelson Mandela University, South Africa, 9th June 2017, **Oral presentation.**

3. **Olusola Adewale,** Lynn Cairncross, Hlumisa Xakaza, Nicolas Wickens, Hajierah Davids & Saartjie Roux. Evaluation of acute toxicity of peptide conjugated gold nanoparticles: Potential agent in the diagnosis of colorectal cancer. 14th International Conference on Nanosciences and Nanotechnologies, Porto Palace Conference Centre and Hotel, Thessaloniki, Greece, 4-7 July 2017, **Poster presentation.**

## MANUSCRIPTS

1. O.B. Adewale, H. Davids, L. Cairncross & Saartjie Roux (2017). Toxicological behaviour of gold nanoparticles on various models: Influence of physicochemical properties and other factors. (***Manuscript ready for submission***).

2. O.B. Adewale, L. Cairncross, H. Xakaza, N. Wickens, H. Davids, S. Roux (2017). Acute toxicity assessment of peptide-gold nanoparticles for diagnosis of colorectal cancer. (***Manuscript ready for submission***).

## LIST OF ABBREVIATIONS

| | |
|---|---|
| 4-HNE | 4-hydroxy-2-nonenal |
| 5’-NT | 5’-nucleotidase |
| 8-OHdG | 8- hydroxydeoxyguanosine |
| A/G | Albumin/Globulin ratio |
| AchE | Acetylcholine esterase |
| AFM | Atomic force microscopy |
| ALB | Albumin |
| ALP | Alkaline phosphatase |
| ALT | Alanine aminotransferase |
| ANOVA | One-way analysis of variance |
| AO | Acridine orange |
| AST | Aspartate aminotransferase |
| Au | Gold |
| $Au^0$ | Gold atom |
| $Au^{3+}$ | Gold (III) ions |
| Au-CHIT-H | Surface densities of 0.1 wt% Chitosan in solution |
| Au-CHIT-L | Surface densities of 0.001 wt% Chitosan in solution |
| AuNCs | Gold nanoclusters |
| AuNPs | Gold nanoparticles |

| | |
|---|---|
| BALB/c | Bagg albino |
| BAS | Basophils |
| BCA | Bicinchoninic acid |
| BIL | Bilirubin |
| BSA | Bovine serum albumin |
| BTV | Bluetongue virus |
| BUN | Blood urea nitrogen |
| C57BL/6 | C57 black 6 |
| Ca | Calcium |
| CALNN | Pentapeptide: cysteine–alanine–leucine–asparagine–asparagine |
| CAT | Catalase |
| CFE | Colony forming efficiency |
| CHO22 | Chinese hamster ovary |
| Chol-VLDL | Cholesterol-Very low-density lipoprotein |
| CK | Creatine kinase |
| $Cl^-$ | Chloride ion |
| CPK-MB | Creatinine phosphokinase-MB |
| CR | Creatine |
| CRC | Colorectal cancer |
| CREA | Creatinine |

| | |
|---|---|
| CT | Computed tomography |
| CTAB | Cetyltrimethylammonium bromide |
| CTB | CellTiter-Blue® |
| CTC | Computed tomographic colonography |
| CV | Central vein |
| DCBE | Double-contrast barium enema |
| DLC | Differential leukocyte count |
| DLS | Dynamic light scattering |
| DMEM | Dulbecco's Modified Eagle's Medium |
| DNP | Dinitrophenyl |
| DNPH | 2,4-dinitrophenylhydrazine |
| DPBS | Dulbecco's phosphate-buffered saline |
| ECG | Electrocardiogram |
| EDC | 1-Ethyl-3-(3-dimethylaminopropyl)-carbodiimide |
| EE | Endosomes |
| EGFP | Enhanced green fluorescent protein |
| EGFR | Epidermal growth factor receptor |
| ELISA | Enzyme-linked immunosorbent assay |
| EMH | Extramedullary hematopoiesis |
| EOS | Eosinophils |

| | |
|---|---|
| ESR | Erythrocyte sedimentation rate |
| FBS | Fetal bovine serum |
| FDA | Food and Drug Administration |
| FIT | Fecal immunochemical test |
| FTIR | Fourier transform infrared |
| GABA | Gamma amino-butyric acid |
| GFAAS | Graphite furnace atomic absorption spectroscopy |
| GFB | Glomerular filtration barrier |
| gFOBT | Guaiac-based fecal occult blood test |
| GFR | Glomerular filtrate rate |
| GGT | Gamma-glutamyltranspeptidase |
| GLDH | Glutamate dehydrogenase |
| GLOB | Globulin |
| GLU | Glucose |
| GPx | Glutathione peroxidase |
| GR | Glutathione reductase |
| GSH | Glutathione |
| $HAuCl_4.3H_20$ | Gold(III) chloride trihydrate |
| HB | Haemoglobin |
| H&E | Haematoxylin and eosin |

| | |
|---|---|
| $H_2$DCFDA | Carboxy-2',7'-dichlorofluorescein diacetate |
| $HAuCl_4$ | Tetrachloroaurate |
| HCl | Hydrochloric acid |
| HCT | Hematocrit |
| HDF-f | Human dermal fibroblast-fetal |
| hESCs | Human Embryonic Stem Cells |
| $HNO_3$ | Nitric acid |
| HRTEM | High resolution transmission electron microscopy |
| HS | Heparin sulphate |
| HUVECs | Human umbilical vein endothelial cells |
| ICAM | Intercellular adhesion molecule |
| ICP-AES | Inductively-coupled plasma atomic emission spectroscopy |
| ICP-MS | Inductively-coupled plasma mass spectrometry |
| ICP-OES | Inductively-coupled plasma optical emission spectrometry |
| ICR | Institute for Cancer Research |
| IFN-γ | Interferon-γ |
| IgE | Immunoglobulin E |
| IgG | Immunoglobulin G |
| IHC | Immunohistochemistry |
| *IκB* | Inhibitor of κappaB |

| | |
|---|---|
| IKK | IκB kinase |
| IL | Islets of Langerhans |
| IL-1 | Interleukin 1 |
| IL-2 | Interleukin 2 |
| IL-6 | Interleukin 6 |
| IL-8 | Interleukin 8 |
| 1L-18 | Interleukin 18 |
| IP | Inorganic phosphorus |
| $K^+$ | Potassium ion |
| $K_2HPO_4$ | Dipotassium hydrogen phosphate |
| KCl | Potassium chloride |
| $KH_2PO_4$ | Potassium dihydrogen phosphate |
| $L^\bullet$ | Lipid radical |
| LDH | Lactate dehydrogenase |
| LOH | Loss of heterozygosity |
| $LOO^\bullet$ | Lipid peroxyl radical |
| LOOH | Lipid hydroperoxide |
| LYM | Lymphocytes |
| Lys | Lysosomes |
| MAP | Multiple antigenic peptide |

| | |
|---|---|
| MAPK | Mitogen-activated protein kinase |
| MCH | Mean corpuscular haemoglobin |
| MCHC | Mean corpuscular haemoglobin concentration |
| MCV | Mean corpuscular volume |
| MDA | Malondialdehyde |
| MDH | Malate dehydrogenase |
| MEEE | 2-(2-(2-mercaptoethoxy)ethoxy)ethanol |
| MES | 2-mercaptoethanesulfonic acid |
| Mg | Magnesium |
| MON | Monocytes |
| MP | Macropinosomes |
| MPA | 3-mercaptopropionic acid |
| MPS | 3-mercaptopropanesulfonate |
| MPV | Mean platelet volume |
| MSA | Mercaptosuccinic acid |
| MTT | 3-(4,5-dimethylthiazolyl-2)-2,5-diphenyltetrazolium bromide |
| MUA | 11-mercaptoundecanoic acid |
| MVB | Multivesicular bodies |
| N/R | Not reported |
| $Na^+$ | Sodium ion |

| | |
|---|---|
| NAA | Neutron activation analysis |
| $Na_2HPO4$ | Disodium hydrogen phosphate |
| $Na_3C_6H_5O_7$ | Trisodium citrate |
| $NaBH_4$ | Sodium borohydrate |
| NaCl | Sodium chloride |
| $NAD^+$ | Nicotinamide adenine dinucleotide (oxidised) |
| NADH | Nicotinamide adenine dinucleotide |
| $NaH_2PO_4$ | Sodium dihydrogen phosphate |
| NaOH | Sodium hydroxide |
| NEU | Neutrophils |
| *NF-kB* | Nuclear factor-kappaB |
| NHCME | Human colon mucous epithelium cells |
| NHS | N-hydroxy sulfo-succinimide |
| NO | Nitric oxide |
| NPs | Nanoparticles |
| OECD | Organization for economic co-operation and development |
| P | Phosphorus |
| PAA | Polyacrylic acid |
| PAH | Polyelectrolyte poly(allylamine) hydrochloride |
| PALS | Periarteriolar lymphoid sheath |

| | |
|---|---|
| PAP | Pro-apoptotic peptide |
| PCR | Polymerase chain reaction |
| PCT | Plateletcrit |
| PCV | Packed cell volume |
| PDI | Polydispersity index |
| PDW | Platelet distribution width |
| PEG | Polyethylene glycol |
| PEI2 | Polyethylenimine |
| PI3-K | Phosphoinositide 3-kinase |
| PLAL | Pulsed laser ablation in liquids |
| PLP | Pyridoxal phosphate |
| PLT | Platelet |
| PT | Prothrombin time |
| qRT-PCR | Quantitative real-time polymerase chain reaction |
| RAPD-PCR | Random amplified polymorphic DNA- polymerase chain reaction |
| RBC | Red blood cells |
| RDW | Red cell distribution width |
| RET | Reticulocyte |
| ROS | Reactive oxygen species |
| RP | Red pulp |

| | |
|---|---|
| RT-PCR | Real time-polymerase chain reaction |
| SC | Surface coating |
| SD | Standard deviation |
| SDH | Sorbital dehydrogenase |
| SEM | Scanning electron microscopy |
| siRNA | Small interfering RNA |
| SOD | Superoxide dismutase |
| TAC | Total antioxidant capacity |
| TAT | Trans-activator of transcription |
| TBA | Thiobarbituric acid |
| TBARS | Thiobarbituric acid reactive substances |
| TBIL | Total bilirubin |
| TCA | Trichloroacetic acid |
| TCHOL | Total cholesterol |
| TEM | Transmission electron microscope |
| TG | Triglycerides |
| TMAT | N,N,N-trimethylammoniumethanethiol |
| *TNF-α* | Tumour necrotic factor-alpha |
| TOAB | Tetraoctylammonium bromide |
| TP | Total protein |

| | |
|---|---|
| TPPMS | Triphenylphosphine monosulfonate |
| TUNEL | Terminal deoxynucleotidyl transferase-mediated dUTP nick-end labelling |
| UA | Uric acid |
| UDP | Uridine diphosphate |
| UN | Urea nitrogen |
| UV-Vis | Ultraviolet-Visible |
| VEGF | Vascular endothelial growth factor |
| WBC | White blood cells |
| WP | White pulp |
| WST-1 | Water-soluble tetrazolium-1 |

**LIST OF FIGURES**

## LIST OF TABLES

# CHAPTER ONE

## INTRODUCTION

Colorectal cancer (CRC) is the third most common cancer and the fourth leading cause of cancer-related deaths worldwide. The incidence and mortality cases are estimated to increase by 60% by 2030 (Arnold *et al.*, 2017). The most effective treatment option for CRC to date remains surgery, which is costly and has associated side effects, such as damage to surrounding organs, a high rate of post-operative recurrence, and the development of adhesions and thromboses. Chemotherapy that often follows surgery lacks tissue selectivity. Worldwide, the major challenge to CRC treatment is early detection. Current treatment options are often started too late, typically after metastasis has occurred. The most reliable detection method is a colonoscopy, but it is a specialized and expensive procedure, it is invasive, not readily available and not patient-friendly. Colonoscopy should normally be performed once every 10 years, after the age of 40, during which time cancers (interval cancers) may develop (Richter *et al.*, 2015). These could arise from failing to detect all polyps (another challenge to colonoscopy) during a colonoscopy (Rabinsky *et al.*, 2016). There is therefore a need for the development of effective non-invasive, cost efficient and readily available diagnostic tools to CRC, which can be performed at regular intervals, using tumour-targeting molecular imaging agents.

Recently, the use of nanoparticles (NPs) has expanded into biomedical research, in the form of vectors of antisense cancer drugs, agents for molecular imaging, and as targeting and therapeutic agents in cancer theranostics. Gold NPs (AuNPs) are well-suited for biomedical applications as they are characterised by ease of synthesis, biocompatibility, ease of shape control, and the ability to easily incorporate secondary molecules (Thakor *et al.*, 2011; Elia *et al.*, 2014). Such molecules, including ligands, antibodies, nucleic acids and peptides, afford selectivity (Bohl Kullberg *et al.*, 2002; Goodman *et al.*, 2004; Alkilany *et al.*, 2014).

Following the interest of AuNPs in biomedical applications, research into the possible toxic or adverse effects of these particles are of utmost importance. Various conflicting toxicological

evaluation studies on AuNPs have been reported using *in vitro*, *in vivo*, and *in ovo* models. Some researchers have reported its safety in fish (Kunjiappan *et al.*, 2015), mice (Lasagna-Reeves *et al.*, 2010), rats (Venkatpurwar *et al.*, 2012; Jo *et al.*, 2015), rabbits (Glazer *et al.*, 2011) and various cell lines (Venkatpurwar *et al.*, 2012; Uchiyama *et al.*, 2014), although the toxic effect of AuNPs have also been reported in each of these models (Ghahnavieh *et al.*, 2014; Boyles *et al.*, 2015; Ferreira *et al.*, 2015; Shetty *et al.*, 2015; Senut *et al.*, 2016). These conflicting results could be linked to differences in the protocols and models used. Differences in size, shape, morphology, surface charge, surface chemistry, and concentration of AuNPs injected, as well as the model (cell- or animal-based) and the route of administration used, could account for these discrepancies (Fratoddi *et al.*, 2015; Jo *et al.*, 2015; Schmid *et al.*, 2017).

In this study, AuNPs were conjugated with biotinylated peptides (p.C, p.L and p.14). These peptides were shown to selectively bind to CRC cells *in vitro* (Wang *et al.*, 2012; Mazyambe, 2013). It is thus hypothesised that these peptides can be useful in CRC diagnosis *in vivo*. It is therefore important to investigate the toxic effects of these conjugated NPs (p.C-, p.L- and p.14-polyethylene glycol (PEG)-AuNPs) *in vivo*.

To our knowledge, no reports on either the short- or long-term effects of a single intravenous injection of these conjugated AuNPs in the diagnosis of CRC have been published. A single intravenous injection in healthy rats was considered to mimic the potential diagnostic applications. This procedure could allow examinations through imaging techniques that can be performed more regularly with shorter intervals between examinations, thereby reducing the risk of interval cancers. If proved to be safe, the conjugated AuNPs could be developed for early CRC-patient-friendly imaging, thereby improving the current methods of CRC detection and prevention. This study was therefore aimed at investigating the short- and long-term effects of peptide-conjugated AuNPs using the rat model.

A literature review follows in chapter two which discusses the problem (colorectal cancer), potential solution (AuNPs), and nanotoxicty (study focus).

# CHAPTER TWO

# LITERATURE REVIEW

## 2.1 COLORECTAL CANCER

Colorectal cancer originates in the cells lining the lumen of the colon and rectum. The colon, together with the rectum, forms the large intestine, which is the last segment of the digestive tract (Figure 2.1).

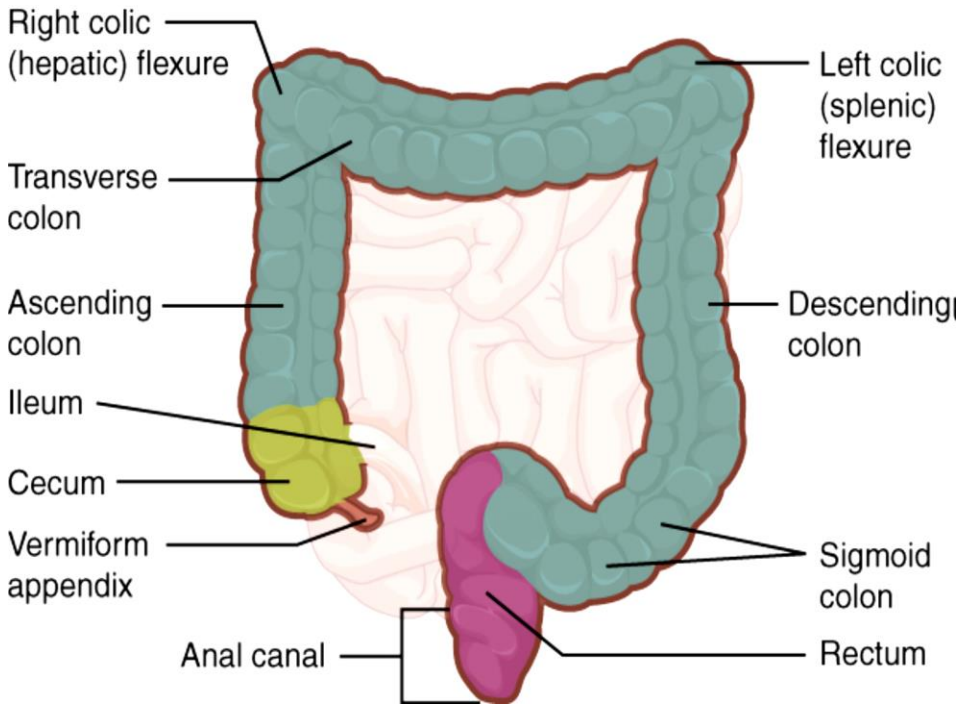


**Figure 2.1:** Anatomy of the colon and rectum. Adapted from Openstax (2013).

Colorectal cancer often begins as a polyp (an abnormal growth of tissue in an organ), that forms on the luminal wall of the colon or rectum. Removal of these polyps, upon early detection, can prevent the progression of CRC, thereby reducing incidence and mortality rates (Zauber *et al.*,

2012). Colorectal cancer is one of the most common malignant tumours of the gastrointestinal tract. It is difficult to cure, and has a high post-operative recurrence rate (De Jong *et al.*, 2009; Kobayashi and Sugihara, 2012).

Colorectal cancer can be described by stage, depending on the size of the tumour, how far it has grown into the colon or rectal wall, and whether the cancer has metastasised to lymph nodes or secondary sites (American Cancer Society, 2017). There are five numerical stages of CRC (Figure 2.1), which include:

Stage 0 – This is when cancer cells are located in the luminal wall of the colon or rectum. This is typically confined to the surface of a polyp, also referred to as *carcinoma in situ*.

Stage 1 – It is when cancer cells have spread from the inner lining into the middle layers of the muscular wall of the colon or rectum.

Stage 2 – In this stage, cancer cells have spread to the outside surface of the colon or rectum, which may also involve surrounding tissues, but not *lymph nodes*.

Stage 3 – It is when cancer cells have spread to the nearby *lymph nodes*.

Stage 4 – This is when cancer cells have metastasised to secondary sites, such as the liver or lungs (Herbst, 2017).

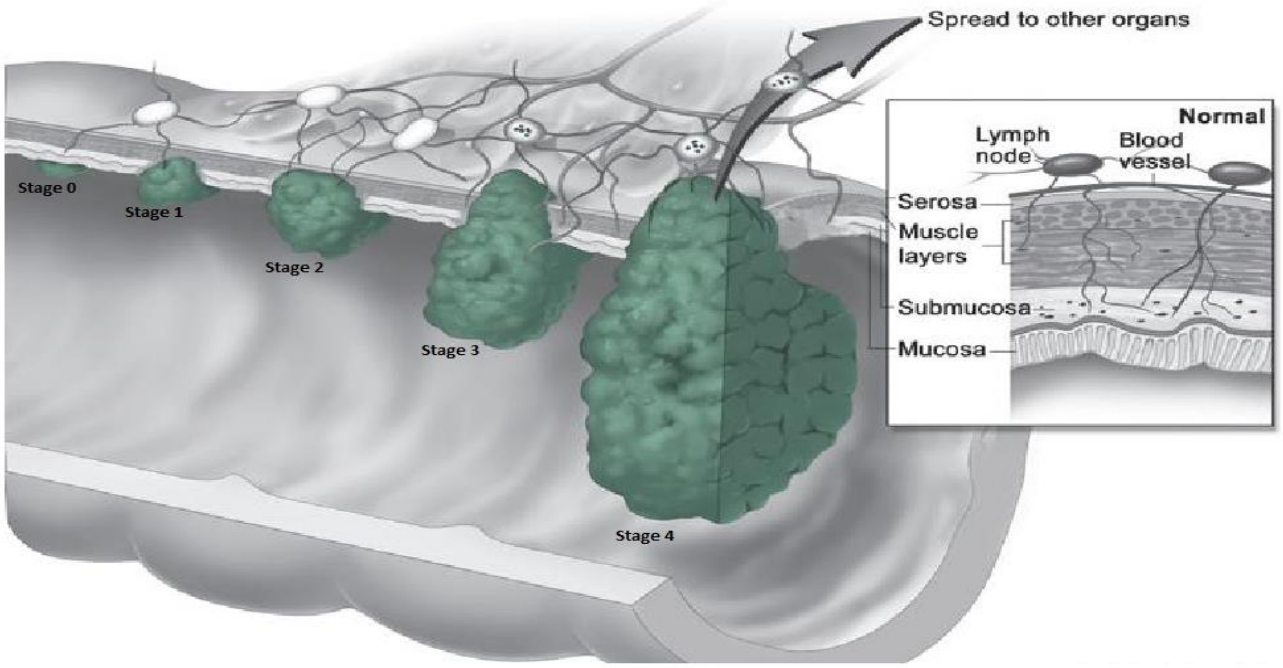


**Figure 2.2:** Stages of colorectal cancer. Adapted and edited from American Cancer Society (2014).

### 2.1.1 Incidence and mortality rates of colorectal cancer

Globally, CRC is the third most common type of cancer in both men and women (American Cancer Society, 2016). The incidence rates of CRC were reported to be higher in more developed regions, such as Australia, New Zealand, Europe, Northern America and South Korea, when compared to less developed regions including Africa and South-Central Asia (American Cancer Society, 2015; Torre *et al.*, 2015). In 2012, approximately 693,900 deaths resulted from CRC, accounting for 8% of all cancer deaths worldwide (American Cancer Society, 2015). In 50 years and older, mortality rates of CRC patients have declined since 1980. This was linked to changes in risk factors, such as decreased smoking and increased use of non-steroidal anti-inflammatory drugs, various screening tests that aid detection, and the subsequent removal of early-stage cancer and pre-cancerous polyps (Edwards *et al.*, 2010; American Cancer Society, 2016). Although the incidence rate declined by 4.5% per year among adults above 50 years of age, there was an increased

incidence (1.8% per year) among adults younger than 50 years of age (American Cancer Society, 2016).

The incidence rates of CRC between Blacks and Whites in the United States were predominantly higher in Whites than in Black populations for both sexes prior to 1980. As from 1989, however, incidence rates were higher in Blacks than in Whites for both men and women. These changes may result from differences in socio-economic status, racial differences in risk factors of CRC, as well as greater access by the Whites to recommended screening tests that detect and remove pre-cancerous polyps (Lansdorp-Vogelaar *et al.*, 2012). The overall incidence and mortality rates of CRC are about 30% to 40% higher in men than in women (American Cancer Society, 2014), which may be linked to the protective role of endogenous oestrogens against CRC formation (Murphy *et al.*, 2015).

In African countries, the incidence rate of CRC in 2008 was 6 per 100,000 people, with a mortality rate of 5 per 100,000 people (Morhason-Bello *et al.*, 2013). In the Global Cancer Statistics of 2012, Southern Africa has the highest incidence and mortality rates of CRC when compared to other regions of Africa (Torre *et al.*, 2015). The incidence rates of CRC increased in West Africa (Nigeria and Ghana) from 1954 to 2007. This was linked to lifestyle and diet changes, lack of or inadequate medical facilities, as well as high cost of procedures and treatment (Irabor, 2017). In 2012, which is the most recently reported formal statistics of CRC for South Africa, the incidence rate was highest among Whites, followed by Blacks, Coloured groupings, and then Asians, in both men and women (Graham *et al.*, 2012).

### 2.1.2 Symptoms of colorectal cancer

Symptoms of CRC include loss of appetite and weight, rectal bleeding and blood in stool, change in stool shape, a feeling that the bowel is not completely empty, and cramping pains in the lower abdomen. Blood loss from the tumour can lead to anaemia in some cases, resulting in symptoms such as excessive fatigue. As early stages of CRC are asymptomatic, screening for CRC is needed (American Cancer Society, 2014; Herbst, 2017).

### 2.1.3 Risk factors for colorectal cancer

Several factors increase the risk of developing CRC. These can be categorised into behavioural factors, heredity- and medical-associated factors. Behavioural factors include tobacco smoking, high or moderate alcohol consumption (> 12.5 grams/day), diet (high consumption of red and processed meat, low calcium intake) (Raskov *et al.*, 2014), physical inactivity, as well as being overweight, and obesity. Hereditary factors include a family history of adenomas, Lynch syndrome or familial adenomatous polyposis (Herbst, 2017). Medical factors associated with increased risk include individuals with chronic inflammatory bowel disease, such as ulcerative colitis or Crohns disease, a history of adenomatous polyps, and type-2 diabetes (American Cancer Society, 2016; American Cancer Society, 2017). If high risk individuals are identified and screened early, it could reduce the incidence and mortality rates of CRC (American Cancer Society, 2017).

### 2.1.4 Screening and diagnosis of colorectal cancer

Colorectal cancer is currently screened and diagnosed by: (1) structural (visual) examinations, including flexible sigmoidoscopy, computed tomographic colonography (CTC), double-contrast barium enema (DCBE) and colonoscopy, and (2) stool tests, such as the guaiac-based faecal occult blood test (gFOBT), the faecal immunochemical test (FIT) and the FIT-DNA test (American Cancer Society, 2014; American Cancer Society, 2017).

1. Structural examinations

    a. Flexible sigmoidoscopy: This involves the insertion of a sigmoidoscope through the rectum into the colon, providing a visual examination of the lower part of the colon and the rectum. The procedure does not require sedation or a specialist, and is quick, with few complications and minimal bowel preparation. There are, however, some limitations associated with this procedure. These include limited availability, inability to remove large polyps, failure to view the entire colon and risk of infection or bowel tear (American Cancer Society, 2014; American Cancer Society, 2017). If there are

polyps or a tumour present, the patient is referred for a colonoscopy to examine the entire colon (American Cancer Society, 2014)

b. Computed tomographic colonography: This is also known as virtual colonoscopy. It is a non-invasive imaging procedure that gives detailed, cross-sectional, two- or three-dimensional images of the entire colon and rectum with the use of an X-ray machine. Limitations to this procedure include exposure to low-dose radiation, and an inability to remove polyps or perform biopsies. Patients with polyps larger than 5 mm in size or other abnormal results are further examined by colonoscopy (American Cancer Society, 2014; American Cancer Society, 2017). Another challenge is its non-specificity to tumours; there is thus a need for suitable contrast and CRC-specific targeting agents to enhance imaging (Mody *et al.*, 2010)

c. Double-contrast barium enema: In this procedure, barium sulphate is introduced into the colon (via the rectum) to partially fill and open the colon. Air is then introduced to expand the colon and increase the quality of X-rays. The entire colon can be visualised with few complications, and no sedation is necessary. The procedure is less sensitive than colonoscopy, as DCBE cannot visualize small polyps or cancers. Other disadvantages include a level of false positive results, inability to remove polyps, exposure to low-dose radiation, a limited number of radiologists adequately trained to perform the procedure, and the requirement for a colonoscopy if abnormalities are detected (American Cancer Society, 2017).

d. Colonoscopy: A colonoscopy allows for a direct visual examination of the colon and rectum. It is the most sensitive method for the detection of CRC (Rockey *et al.*, 2005), and it is done every 10 years (Herbst, 2017). A colonoscope is used to visualize the entire colon. If a polyp is present, it may be removed during the procedure. Colonoscopy, however, has a highest risk of complications when compared to other screening procedures. These include high cost of the procedure, the need for complete bowel cleansing, use of sedation, as well as a high risk of bowel tears and bleeding,

especially in the removal of polyps (American Cancer Society, 2014; American Cancer Society, 2017).

2. Stool-based test

The stool-based test, is non-invasive, and requires no bowel cleansing or sedation. These tests are generally less sensitive than the structural procedures, with possibilities of false-positive results (Liss *et al.*, 2013; American Cancer Society, 2017).

a. Guaiac-based faecal occult blood test: This is a non-invasive test that requires the use of guaiac to detect blood in the stool. Several stool samples from multiple bowel movements are required (Schreuders *et al.*, 2016). In gFOBT, blood can be detected from any source (including meat in the diet). Patients are therefore restricted from red meat and nonsteroidal anti-inflammatory drugs for 3 days prior to the test to avoid false-positive results, and from vitamin C, to avoid false-negative results. Other limitations to this test include failure to detect most polyps and the requirement of multiple stools. If abnormalities are detected, colonoscopy is necessary (American Cancer Society, 2014; American Cancer Society, 2017).

b. Faecal immunochemical test: The FIT is a non-invasive test that uses antibodies against haemoglobin to screen for blood in the stool. It is convenient, and requires no dietary restrictions. It is specific for blood from the colorectum (American Cancer Society, 2017). The FIT is more effective and less expensive when compared to the gFOBT test (Goede *et al.*, 2017), and the faecal haemoglobin concentrations can be measured both qualitatively and quantitatively with FIT (Schreuders *et al.*, 2016). Disadvantages, however, include non-capturing of most polyps and possibilities of false-positive results. Blood does not appear in the stool during the early phases, therefore early detection is not possible. Colonoscopy is necessary if abnormalities are detected (American Cancer Society, 2014; American Cancer Society, 2017).

c. Faecal immunochemical test-DNA test: This is a non-invasive test, which requires a single stool sample. It is called “Cologuard” and referred to as a multi-targeted test - it can detect both blood as well as mutated DNA from large adenomas and CRC in the stool (American Cancer Society, 2017). This test was approved in 2014 for CRC screening by the Food and Drug Administration (FDA) in the United States. This screening test is more expensive when compared to gFOBT and FIT alone, but has low specificity (Schreuders *et al.*, 2016). There are possibilities of failure to detect most polyps in the small adenomas, which also limits early detection. In case of abnormalities, patients are referred for colonoscopy examination (American Cancer Society, 2017).

Incidence of CRC is increasing in younger patients. In 2012, the diagnosed cases of CRC in South Africa among 0-39 years of age was highest in Blacks, followed by Whites, Coloureds, and lowest among Asians (Herbst, 2017). Research on frequent screening procedures, which are more sensitive and specific, less expensive, non-invasive, and does not induce discomfort for patients than the current procedures, are therefore encouraged. This should be focused in areas of developing regions, where there is an increasingly growing westernised lifestyle and aging population (Torre *et al.*, 2015). These include African, Asian, and South American countries where CRC screening initiatives are rare (American Cancer Society, 2014; American Cancer Society, 2015).

### 2.1.5 Treatment options for colorectal cancer

The first–line treatment of CRC is surgery. For cancers that have not metastasised, surgical removal of the tumour may be the most effective treatment (American Cancer Society, 2014).

The main types of treatment that can be used for CRC and their possible side effects include:

a. Surgery - Stage 0 CRC may be treated by removing the cancer cells by colonoscopy. Extensive surgery is needed to remove large cancerous part of the colon and rectum. If cancerous cells are detected after the removal of polyps, this is followed by chemotherapy, or preceded by chemotherapy and radiation therapy in case of a rectal

tumour that has spread to surrounding tissues and lymph nodes. Limitations of surgery include pain associated with the procedure, post-operative bleeding, damage to nearby organs, and loss of sexual function in the case of men (American Cancer Society, 2014; American Cancer Society, 2017).

b. Radiation therapy – This involves the use of high-energy rays to destroy CRC cells. It is performed as pre-operatively or post-operatively, usually combined with adjuvant chemotherapy. It is used to slow the growth or shrink the tumour, and is more useful in rectal cancer than colon cancer (Häfner and Debus, 2016; Herbst, 2017). Adverse effects associated with radiation therapy include: skin irritation at the site of radiation, which ranges from redness to blistering and peeling; rectal irritation, causing painful bowel movements, diarrhoea or blood in the stool; bowel incontinence; pain associated with urination or blood in the urine; and sexual problems (impotence in men and infertility in women) (American Cancer Society, 2014; American Cancer Society, 2017).

c. Chemotherapy – Surgery and radiotherapy are commonly used in the treatment of locally confined cancers, while chemotherapy targets both locally confined cancer cells and metastatic cancer cells. Adjuvant chemotherapy in CRC prevents local recurrence or distant metastases (Andre and Schmiegel, 2005; Herbst, 2017). Chemotherapeutic agents, such as Oxaliplatin, 5'-Fluorouracil, Irinotecan and Capecitabine are used in CRC treatment. Use is limited due to several dose-limiting side effects, and the ability of tumours to rapidly develop resistance (American Cancer Society, 2017).

d. Targeted therapy involves the use of agents that antagonise growth factor receptors, epidermal growth factor receptor (EGFR) and vascular endothelial growth factor (VEGF), which are overexpressed in a variety of tumours - activation of these receptors initiates signalling pathways that promote cell proliferation, cell division, tumour migration, angiogenesis, and inhibits apoptosis (Andre and Schmiegel, 2005; Hagan *et al.*, 2013). Limitations to this treatment option for CRC include: acne-like rash dry skin, swelling or pain in the fingernails or toenails, caused by the EGFR inhibitors (e.g. cetuximab), and

nose bleeds, thromboses in the arteries or veins, hypertension, proteinuria, anorexia or kidney damage, caused by the VEGF inhibitors (e.g. bevacizumab) (Hagan *et al.*, 2013; American Cancer Society, 2014).

In most cases, the major challenge to the success of these treatments is the inability to detect the tumour before it metastasises. Nanotechnology is a technique which has promising potential to address early diagnosis of CRC, as well as treatment.

## 2.2 NANOTECHNOLOGY

Nanotechnology is a branch of science that deals with the controlled manipulation, in terms of design, synthesis and applications, of materials and devices at one billionth of a meter ($10^{-9}$ meter). Nanostructured materials are categorised based on various divisions, including 1) zero-dimensional nanomaterials, which include quantum dots, nanospheres, NPs array, hollow cubes, and core–shell NPs; 2) one-dimensional nanomaterials, such as nanorods, nanowires, nanotubes, nanoribbons, and nanobelts; 3) two-dimensional nanomaterials, including nanoplates, nanosheets, nanodisks, and nanowalls; and 4) three-dimensional nanomaterials, which include dendritic structures, nanocones, nanoflowers, and nanocoils (Tiwari *et al.*, 2012).

### 2.2.1 Nanoparticles

Nanoparticles are smaller than 100 nm in diameter, and have enhanced physicochemical properties when compared to their bulk materials. These properties include larger surface areas, lower melting points, as well as unique optical and magnetic properties. Due to these and other properties, NPs have been used widely in many fields, such as biomedicine, chemistry, electronics and photochemistry (Horikoshi and Serpone, 2013).

There are different types of metallic NPs, including AuNPs, silver NPs, iron NPs, platinum NPs and zinc NPs. Gold NPs are preferred in biomedical applications due to their unique properties, such

as ease of synthesis, stability, high biocompatibility, excellent biodistribution, low toxicity, and the ability to be conjugated with other biomolecules (Lan *et al.*, 2013; Tiwari *et al.*, 2014).

### 2.2.2 Gold nanoparticles

Gold NPs are the most suitable for biomedical use because of the ability to be applied in various sizes (1 nm – > 100 nm) and diverse shapes, such as nanospheres, nanocages, nanoshells and nanorods (Khan *et al.*, 2014; Kong *et al.*, 2017). Other shapes include prisms, triangles, tetrahedral, sub-octahedral, octahedral, decahedral, icosahedral multiple twined and irregular shaped (Khan *et al.*, 2014). Gold NPs are important in cancer diagnosis and therapy because of their unique and optical properties (tunable) due to the shape, size and large surface area, as well as the ability to diffuse into the target cells (Lan *et al.*, 2013; Khan *et al.*, 2014; Oni *et al.*, 2014; Kong *et al.*, 2017).

#### *2.2.2.1 Synthesis of gold nanoparticles*

The synthesis of AuNPs can be grouped under two main principles: “top-down” method and “bottom-up” method.

The top-down methods require the removal of matter from the bulk gold (Au) material to produce desired sizes and shapes of AuNPs. The major disadvantage is the high cost of production of AuNPs. Examples of this method include photolithography and electron beam lithography (Sreeprasad and Pradeep, 2013).

On the other hand, the bottom-up method involves the synthesis of desired AuNPs by reduction. Examples of this method include the chemical, electrochemical, photochemical, thermal reduction and sonochemical methods (Sreeprasad and Pradeep, 2013).

The synthesis of AuNPs can be broadly divided into three major methods based on the materials required for the production, which are physical, chemical and biological methods.

### A. Physical methods

Pulsed laser ablation in liquids (PLAL) is the most commonly used physical method for the synthesis of AuNPs. It is an easy "top-down" technique, which can be used to prepare AuNPs by the irradiation of a focused pulsed laser beam onto the surface of bulk Au material in aqueous biocompatible media. There is an interaction between the electromagnetic field of the laser radiation and the surface of the Au atoms producing ionised species on the surface of the Au. These electrons form Au clusters by their attraction to the electronic cloud through electromagnetic forces (Torres-Mendieta *et al.*, 2016). The formed clusters then coalesce and form a colloidal solution of AuNPs. The stability of the colloidal AuNPs formed is dependent on the electrical repulsion effect due to the negative charges on the AuNPs (Correard *et al.*, 2014). The laser ablation method can therefore produce stable colloidal NPs without the presence of a ligand or reagent. The method is advantageous in the synthesis of low toxic AuNPs due to the stability, biocompatibility, and the absence of contaminants. Disadvantages include broader particle size distribution, low efficiency in the formation of NPs, and the possibility of agglomeration (Phuoc, 2014; Al-Azawi and Bidin, 2015).

### B. Chemical methods

There are several types of chemical methods commonly used in the synthesis of AuNPs. These include the Turkevich-Fens, Brust–Schiffrin, and Seeded-growth methods.

#### i. The Turkevich-Fens method

The Turkevich-Fens method, also known as the citrate-reduction method, is the most commonly and easily used method for the synthesis of colloidal AuNPs with different diameters (Turkevich *et al.*, 1951; Frens, 1973). This method involves the boiling of hydrogen tetrachloroaurate ($HAuCl_4$) solution with sodium citrate solution. Sodium citrate reduces Au (III) ($Au^{3+}$) ions in $HAuCl_4$ to Au atoms ($Au^0$). The sizes of the AuNPs formed are dependent on the ratio of the sodium citrate to Au atoms, with a larger ratio leading to smaller diameters, i.e. increase in the

amount of sodium citrate added reduces the size of the resulting AuNPs. This was reported in the Turkevich modified method by Frens (1973). Sodium citrate also acts as the stabilising/capping agent, which stabilises AuNPs by binding to its surface, thereby resulting in negatively-charged AuNPs. These repel each other and prevent aggregation (electrostatic repulsion). This method is cheap, non-hazardous, and can synthesise easy-to-control-sized AuNPs (Dobrowolska *et al.*, 2015).

### ii. The Brust–Schiffrin method

The Brust–Schiffrin method was formulated by Brust *et al.* (1994) to produce small-sized AuNPs (core diameter of usually 1-6 nm). The method involves the phase transfer (aqueous phase to organic phase) of Au salt from aqueous solution by tetraoctylammonium bromide (TOAB) (a phase-transfer catalyst) to an organic solvent (e.g. toluene). In the presence of a thiol (dodecanethiol), there is a reduction of the Au at the interphase of sodium borohydrate ($NaBH_4$), which results in the production of thiolate-protected AuNPs. The thiol stabilises the AuNPs, thereby preventing aggregation, while $NaBH_4$ acts as the reducing agent. The size of the AuNPs produced depends on the ratio of Au to the thiol, i.e. an increased thiol concentration results in smaller-sized AuNPs (Shah *et al.*, 2014a). The advantage of the Brust–Schiffrin method is that the synthesised AuNPs can be dried, the powder stored for a long period of time and can later be redispersed again (Sreeprasad and Pradeep, 2013). Toxicity of the Au cluster formed from the dodecanethiol has, however, been reported (Dreaden *et al.*, 2012a).

### iii. The seeded-growth method

The seeded growth method, also known as the seed-mediated growth method, is used in the synthesis of AuNPs with varied sizes and shapes (Carbo-Argibay and Rodriguez-Gonzalez, 2016), whereas the Turkevich and Brust–Schiffrin methods are mostly used in the synthesis of spherical AuNPs. This method involves two steps: 1) the synthesis of seed (small and mono-dispersed spherical) NPs (sizes between 2 and 7 nm) by the reduction of Au salts with a strong reducing agent ($NaBH_4$, for example); 2) the growth of small particles generated in the first step into larger

particles. Here, the small seed particles generated are added to additional Au salt solution in the presence of a weak reducing agent, such as ascorbic acid. The ascorbic acid prevents further growth of AuNPs, thereby directing the structure of the particles. The shape and size of AuNPs produced is dependent on the concentration of seeds, concentration of Au salts, reducing agents, as well as the structure-directing agent (Shah *et al.*, 2014a), i.e. a low concentration of seeds produces many particles of bigger sizes. Different reducing agents, such as hydroxylamine, citrate, $NaBH_4$ in citrate, and ascorbic acid have been used to generate different AuNP shapes, most especially nanorods, and larger sizes compared to the seed particles (Carbo-Argibay and Rodriguez-Gonzalez, 2016).

Other methods used in the synthesis of AuNPs include the electrochemical and photochemical reduction, as well as sonochemical and solvothermal methods (Sreeprasad and Pradeep, 2013; Shah *et al.*, 2014a).

### C. Biological methods

The biological methods, generally called green chemistry, involve the use of biological systems, such as plant and plant materials (Vijayakumar and Ganesan, 2012; Kunjiappan *et al.*, 2015; Tripathi *et al.*, 2016; Alizadeh *et al.*, 2017), bacteria (Kalishwaralal *et al.*, 2010; Sadhasivam *et al.*, 2012), algae (Ramakrishna *et al.*, 2016) and fungi (Mukherjee *et al.*, 2001) in the synthesis of AuNPs. The extracts from these materials contain phytochemicals or compounds that act as reducing, capping and stabilising agents, thereby allowing more biocompatibility to biosynthesised NPs (Shah *et al.*, 2014a; Ramakrishna *et al.*, 2016). It also involves the use of biological components or biomolecules, such as enzymes, amino acids and proteins, lipids, carbohydrates and nucleic acids. These compounds contain amine, hydroxyl and/or carbonyl functional groups capable of reducing $Au^{3+}$ ions to $Au^0$. The AuNPs are capped by these groups to form stabilised AuNPs of different sizes and shapes (Ramakrishna *et al.*, 2016). Benefits associated with these approaches include simplicity, cost-effectivity and efficiency, eco-friendliness and reduced toxicity (Sadhasivam *et al.*, 2012; Ramakrishna *et al.*, 2016; Tripathi *et*

*al.*, 2016). The disadvantages of this approach include the inability to control the size and morphology of AuNPs due to the diverse nature of phytochemicals present in the biological materials, as well as high poly-dispersity and long-term stability of the synthesised NPs (Dauthal and Mukhopadhyay, 2016).

#### *2.2.2.2 Characterisation of gold nanoparticles*

Gold NPs are characterised by their physicochemical properties, including size, surface charge, surface chemistry, stability and morphology, using Ultraviolet-Visible (UV-Vis) spectroscopy, scanning electron microscopy (SEM), atomic force microscopy (AFM), transmission electron microscopy (TEM), high resolution transmission electron microscopy (HRTEM), Fourier transform infrared (FTIR) spectroscopy, as well as Zeta potential and dynamic light scattering (DLS) measurements (Patra and Baek, 2014; Tiwari *et al.*, 2014).

##### 2.2.2.2.1 Ultraviolet-Visible Spectroscopy

Ultraviolet-Visible spectroscopy involves the absorption of light by molecules in the UV-Vis region. It is useful in the estimation of size, concentration, stability and aggregation level of AuNPs, because of the optical properties (plasmon resonance). Colloidal AuNPs are red in colour, with absorbance peaks between 500 and 550 nm, depending on the size of the NP (Patra and Baek, 2014). The absorption in the visible region of the electromagnetic spectrum affects the colour of the NPs, and undergo electronic transitions, because the surface electron cloud of NPs tends to vibrate and absorb the electromagnetic radiation of a particular energy state (Shamaila *et al.*, 2016). The colour change is a characteristic of the size and conformation of AuNPs with the plasmon resonance. During aggregation, there is a colour change (for example, from red to blue for colloidal AuNPs), indicating the shift of the absorption band to longer wavelengths, which is caused by dipole-dipole electric interactions between the particles (Sujitha and Kannan, 2013). For conjugated AuNPs, the plasmon resonance spectrum shifts into the red region by a few nanometres (increase in wavelength), which is due to an increase in the local refractive index at

the surface of AuNPs (Zhou *et al.*, 2015; D'agata *et al.*, 2017). This is the basis of the increase in the wavelength of conjugated-AuNPs when compared to the unconjugated AuNPs.

#### 2.2.2.2.2 Transmission Electron Microscopy and High-Resolution Transmission Electron Microscopy

The TEM provides an image of the internal structure of a sample, sufficiently thin (about 1000 Å) to allow for the transmission of electrons. It measures the size and aggregation state of AuNPs, providing information on the composition, crystallography and morphology of the NPs. This is obtained by the transmission and interaction of high energy electrons scattered through the thin NP sample as it passes through the beam (Lu and Barron, 2010). In HRTEM, the transmitted beam interferes with diffracted (scattered) beams, of which the relative phases of the beams determine the contrast across the sample - thus, phase-contrast imaging (Smith, 2015). This produces the atomic structure images (lattice fringes) of the particles.

#### 2.2.2.2.3 Measurement of Zeta potential and dynamic light scattering

The Zeta potential and DLS measurements of NPs are usually performed using the Zetasizer Nanoseries. These two parameters are important in confirming the sizes and surface charge of NPs (Bhattacharjee, 2016). Zeta potential provides information about the stability, surface charges, surface chemistry, and dispersity nature of NPs in suspension (Patra and Baek, 2014; Duque *et al.*, 2016; Jyoti *et al.*, 2016). It was reported that NPs with high positive or negative zeta potentials (above +30 mV or -30 mV) are considered stable and of good quality, devoid of aggregation (Bhatia, 2016; Ramakrishna *et al.*, 2016; Tripathi *et al.*, 2016). A high negative zeta potential of AuNPs gives an indication of the stability, as well as reduced or no aggregation of the NPs, due to electrostatic repulsion (Duque *et al.*, 2016; Ramakrishna *et al.*, 2016). The DLS provides information about the size distribution and particle size (hydrodynamic radius) (Bhattacharjee, 2016).

#### 2.2.2.2.4 Fourier Transform Infrared Spectroscopy

Fourier transform infrared spectroscopy is widely used for the detection of functional groups and characterising covalent bonding information of a compound or mixtures of compounds. This can be achieved by measuring the vibrational frequencies of the chemical bonds or functional groups present (Belliraj *et al.*, 2015). The large surface area-to-volume ratio of AuNPs can be modified by various agents or targeting molecules, resulting in functionalised-NPs suitable for biomedical applications (Khan *et al.*, 2014). These functional groups can be detected by FTIR spectroscopy (Ghodake and Lee, 2011; Belliraj *et al.*, 2015; Botha *et al.*, 2015). The FTIR spectra of the functionalised-NPs contain additional peaks or specific wavelengths when compared to other molecules present in the NP (Belliraj *et al.*, 2015).

Other means of characterising NPs include 1) agarose gel electrophoresis that separates NPs based on charge, size, shape and surface chemistry as they migrate in an electric field (Sosibo *et al.*, 2015; Zheng *et al.*, 2015); 2) atomic force microscopy, which provides information about the size, morphology and size distribution of NPs (Bhatia, 2016); and 3) scanning electron microscopy, through direct visualization by scanning with a focused beam of electrons that interact with the NP atoms, measures the size, shape and surface morphology of NPs (Ahmed and Aljaeid, 2016).

### 2.2.2.3 Properties of gold nanoparticles

Gold, in its pure form, is regarded as the most valuable unreactive metal (chemically inert). It is non-toxic, and resistant to corrosion and rust, and is able to retain its brilliant glow for many years without deteriorating (Sau and Goia, 2012). In comparison to bulk Au, AuNPs have more enhanced physical and chemical properties, with larger surface area and quantum size effects (Khan *et al.*, 2014).

The AuNP is classified into physical, chemical and optical properties, based on its application in biomedicine.

#### 2.2.2.3.1 Physical properties

Gold NPs are wine-red in solution (in contrast to bulk Au that is yellowish in colour) and exhibit various sizes and shapes (Khan *et al.*, 2014).

#### 2.2.2.3.2 Chemical properties

The chemical properties of AuNPs are dependent on the size and shape of the particles (Amendola *et al.*, 2014). Such properties include the melting point (temperature), catalytic activity, fluorescence, electrical conductivity, magnetic permeability and chemical reactivity (Sreeprasad and Pradeep, 2013).

The melting point of AuNPs increases with size, and is usually lower than the melting point of the bulk material, although the melting point of AuNPs above 20 nm tend to reach that of bulk Au (Bensebaa, 2012). When AuNPs are supported by substrate, the melting point reduces due to the free surface/volume ratio of the NPs. The contact angle between the particle and the substrate is also a determining factor (Luo *et al.*, 2012). The catalytic activity of functionalised or unfunctionalised-AuNPs is size dependent, as small-sized (0.5-5 nm) particles are the most active. The catalytic reactions involved include: 1) hydrogenation reactions, such as hydrogenation of nitro compounds and hydrogenation of α, β-unsaturated compounds; 2) oxidation reactions, such as the gas phase aerobic oxidation of carbon monoxide; and 3) nucleophilic additions (Sreeprasad and Pradeep, 2013; Amendola *et al.*, 2014). The fluorescence intensities and quenching effects of AuNPs are size-, shape-, concentration- and surface chemistry-dependent (Zhi-Juan *et al.*, 2007; Abdelhalim *et al.*, 2012; Xue *et al.*, 2013). Gold NPs also exhibit quantum size effects, i.e. the ability of the NPs to change the optical and electronic properties of AuNPs as the size decreases to a few nanometres (usually less than 3 nm) (Daniel and Astruc, 2004).

#### 2.2.2.3.3 Optical properties

Upon excitation of AuNPs with an electromagnetic field of the incident light, there is a production of an intense absorption peak (from 500 to 550 nm) as the core size of AuNPs increase from 1 to 100 nm in aqueous solution. This is attributed to the collective oscillation of electrons on the particle surface, known as surface plasmon resonance (band) (Yeh *et al.*, 2012). This plasmon resonance effect (nanoscale electronic effect) enables AuNPs to absorb and scatter electromagnetic radiation of wavelengths larger than identically-sized non-plasmonic NPs. The plasmon resonance effect is highly dependent on the environment, particle size, shape, surface chemistry, core charge and aggregation state (Yeh *et al.*, 2012). When these characteristics are altered, the frequency can be shifted over a wide range of wavelengths. For example, variations in size and shape of NPs can adjust the surface plasmon resonance, leading to particles with engineered optical properties suitable for different biomedical applications. The plasmon resonance of spherical AuNPs occurs in the visible region, which confers the characteristic red colour in solution. This colour, however, changes to blue/violet when the plasmon frequency is altered by a reduction in the average distance between the AuNPs (Sperling *et al.*, 2008).

### *2.2.2.4 Properties of gold nanoparticles for biomedical applications*

The unique properties (size, shape and morphology, surface charge, biocompatibility, and the ability to be functionalised by secondary molecules) exhibited by AuNPs allow the suitability in the field of biomedicine. Gold NPs bind to a wide range of molecules with functional groups, with a high affinity for the Au surface via surface modifiers (for example, sulphur-containing compounds, PEG, amines and organic phosphates). These modifiers enable colloidal stability, and compatibility of AuNPs to biomolecules such as amino acids, DNA and peptides, thereby providing promising characteristics for desired applications (Sau and Goia, 2012).

#### *2.2.2.5 Applications of gold nanoparticles in biomedicine*

Promising applications of AuNPs in nanomedicine include plasmon-based labelling and imaging, optical and electrochemical sensing, and diagnostics, which can facilitate early detection and treatment of cancers, such as prostate cancer (Peng *et al.*, 2010; Oh *et al.*, 2015), bladder cancer (Eissa *et al.*, 2014), lung, breast and colorectal cancers (Peng *et al.*, 2009; Peng *et al.*, 2010), as well as in the treatment of hepatitis (Shawky *et al.*, 2010) and tuberculosis (Hussain *et al.*, 2013; Tsung-Ting *et al.*, 2013; Ng *et al.*, 2015).

Another area of interest is the use of AuNPs as antibacterial therapy, photothermal therapy and radiofrequency-mediated thermal therapy (Boisselier and Astruc, 2009; Abadeer and Murphy, 2016), as well as delivery vehicles for genetic materials (Pissuwan *et al.*, 2011), imaging agents (Lu *et al.*, 2010; Oh *et al.*, 2015), and drugs (Brown *et al.*, 2010; You *et al.*, 2010) for cancers and Alzheimer's disease (Gao *et al.*, 2015), diabetes (Karthick *et al.*, 2014), heart disease (Spivak *et al.*, 2013), hepatitis (Lee *et al.*, 2012), tuberculosis (Malathi *et al.*, 2013), rheumatoid arthritis (Lee *et al.*, 2014), and obesity (Chen *et al.*, 2013a).

#### *2.2.2.6 Functionalisation of gold nanoparticles*

One of the major advantages of AuNPs is the ability to be functionalised by secondary molecules, due to the small size and large surface area (Khan *et al.*, 2014). This functionalisation enables good stability, biocompatibility, specificity and selectivity. The stability of AuNPs is very important because of the high ionic and protein concentrations in the physiological environment. Gold NPs are functionalised by agents such as polymers (e.g. PEGs), antibodies, cell surface receptors, nucleic acids, peptides, proteins, and drugs, depending on the proposed applications. Functional group linkers, such as amines, carboxylates, cyanides, isothiocyanate thiolates, and phosphines are used for the conjugation of these biomolecules and ligands onto the surface of AuNPs. For example, PEG, a commonly used stabiliser, is attached to the surface of the AuNPs by a thiol linker, allowing for further conjugation to other biomolecules through electrostatic interactions (Dreaden *et al.*, 2012b). Generally, these biomolecules or ligands can replace the original

stabiliser or be attached to the original stabiliser on the surface of AuNPs by bioconjugate chemistry. A good example is the displacement of the bond formed between citrate (reducing and stabilising agent) and the Au surface during the synthesis of spherical AuNPs (Turkevich method), by stronger bonds, such as thiols (PEGs) (Dreaden *et al.*, 2012b).

#### *2.2.2.7 Uptake, biodistribution and bioaccumulation of gold nanoparticles*

Transport of molecules into and out of the cell is regulated by the cell membrane, which serves as a barrier that protects the intracellular milieu from extracellular materials. Charged and large polar molecules are transported across the membrane into the cell via active transport systems, and generally, the uptake of several macromolecules occur via endocytosis (Kettiger *et al.*, 2013).

Nanoparticles are generally taken up in a similar manner to biomolecules, depending on the size, shape, surface charge, surface functionality, dose, species, and chemical composition (Iversen *et al.*, 2011; Kulkarni and Feng, 2013; Zhang *et al.*, 2016; Jia *et al.*, 2017). These particles are recognised by the Kupffer cells, and internalised by endocytotic pathways, such as macropinocytosis, and receptor-mediated (clathrin-mediated) and caveolin-mediated endocytosis (Zhang *et al.*, 2016). The receptor-mediated endocytotic pathway (Figure 2.3) explains how NPs and other substances are incorporated into the cell (endocytosis), and are enveloped within the phagosomes, macropinosomes (MP) or endosomes (EE). These then form multivesicular bodies (MVB), and further fuse with lysosomes (Lys). Several enzymes within the lysosomes degrade the NPs and other biological substances (Iversen *et al.*, 2011).

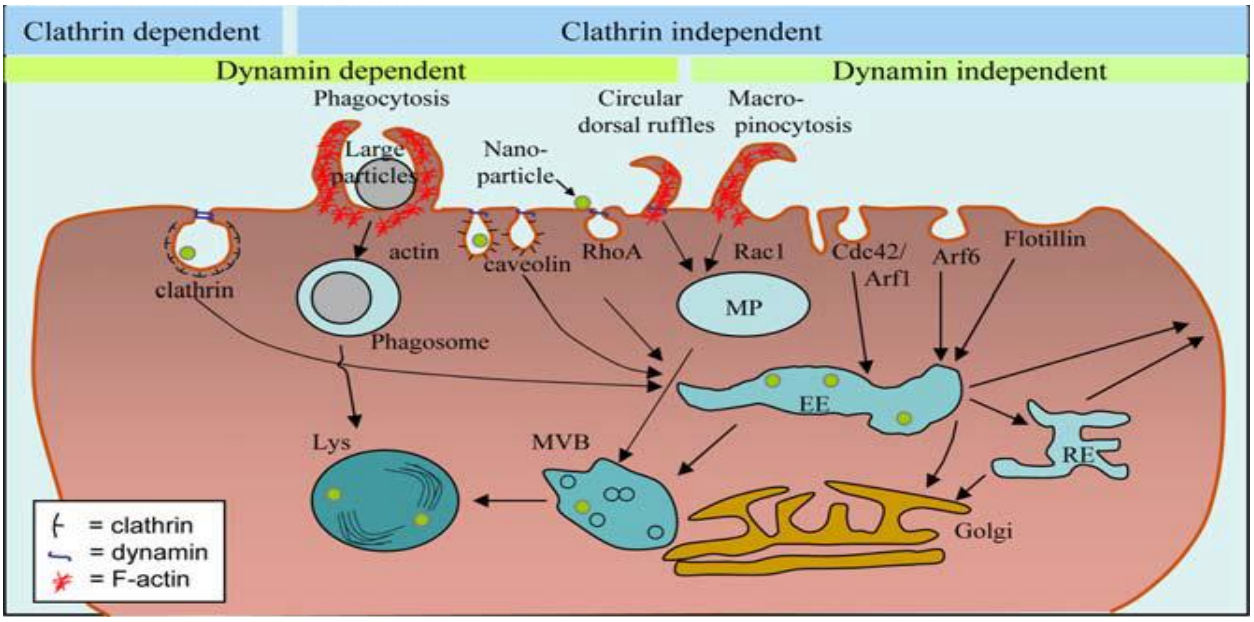


**Figure 2.3**: Mechanisms of endocytosis and intracellular transport. Adapted from Iversen *et al.* (2011). EE (Endosomes); Lys (Lysosomes); MP (Macropinosomes); MVB (Multivesicular bodies).

On exposure of AuNPs to biological systems, there is an interaction with biological components. The AuNPs are distributed to various organs and tissues before elimination. Tissue distribution of AuNPs is dependent on the size, shape, surface charge, surface modification, and route of administration (De Jong *et al.*, 2008; Elci *et al.*, 2016; Alalaiwe *et al.*, 2017; Jia *et al.*, 2017).

Different sized NPs (10, 50, 100 and 250 nm) accumulate in the liver after 24 h, which could be linked to the high perfusion of blood through it. The 10-nm sized AuNPs were distributed to the blood, spleen, liver, kidney, lung, testes, heart, thymus and brain in rats, while the larger particles (50, 100 and 250 nm) were limited to the blood, liver and spleen (De Jong *et al.*, 2008). Intravenous administration of 13 nm-sized PEG-AuNPs to mice were distributed primarily to the liver and spleen after 5 mins to 7 days post-injection (Cho *et al.*, 2009a). This indicates that the liver and spleen are the primary organs of distribution, and that the smaller-sized AuNPs are distributed to many organs, thereby explaining the role of size in the distribution of AuNPs.

Organo-specific distribution of AuNPs functionalised with various agents, such as 15 nm AuNPs functionalised with 11-mercaptoundecanoicacid (MUA), was accumulated in mice brain within 24 h, while the AuNCs (3 nm glutathione (GSH)-AuNCs and bovine serum albumin (BSA)-AuNCs) accumulated in the kidney, and in the liver and spleen, respectively (Escudero-Francos *et al.*, 2017). Here, the differences in the distribution/accumulation could be linked to the shape, size and surface functionality of the AuNPs.

Negatively-charged and neutral AuNPs were mostly distributed and accumulated in the liver, whereas positively-charged AuNPs were accumulated in several other organs, mostly in the kidney (Wang *et al.*, 2016b; Jia *et al.*, 2017). The accumulation of positively-charged AuNPs in the kidney was reportedly linked to the interaction with the negatively-charged glomerulus membrane. Both the negatively- and positively-charged functionalised-AuNPs accumulated in the red pulp of the spleen, which contrasted with the neutral particles that accumulated in the white pulp and margin of the spleen. Negatively-charged NPs were broadly distributed in the liver, while the positively-charged and neutral NPs were mostly found in the hepatocytes and Kupffer cells, respectively (Elci *et al.*, 2016).

On the dependency of route of administration in the distribution and accumulation of AuNPs, the amount of Au 24 h after intravenous administration of 5 nm PEG-AuNPs (1, 2 and 5 kDa) was higher in the liver than in the spleen or kidney, based on the relative organ weight. In contrast, the concentration of Au 48 h after oral administration of PEG-AuNPs was higher in kidney than in the liver or spleen (Alalaiwe *et al.*, 2017), which was in agreement with the study of Smith *et al.* (2013). In another study, the concentration of 10 nm AuNP in the blood, liver and spleen were higher 24 h after intravenous injection than intervaginal space injection in the tarsal tunnel (Shi *et al.*, 2016). Maximum accumulation was observed in the spleen and kidneys 7 days after an intravenous administration of AuNPs consisting of a mixture of bipyramid (100 nm in length) and spherical (40 nm) NPs (Zagainova *et al.*, 2010). Further, 15 nm AuNPs were found to cross the blood-brain barrier, and deposited in the brain (Sonavane *et al.*, 2008).

It could thus be deduced that the liver and spleen presented with the highest levels of accumulation post-intravenous injection (24 h up to 2 months) (Balasubramanian *et al.*, 2010; Rambanapasi *et al.*, 2016; Jia *et al.*, 2017), suggesting that the clearance mechanism of AuNPs could be linked to the hepatobiliary system (Rambanapasi *et al.*, 2016). This can also be attributed to the fact that NPs are taken up by reticulo-endothelial organs (liver and spleen) (Hornos Carneiro and Barbosa, 2016), with the spleen having a higher filtering efficacy, and both organs having a high number of phagocytic cells and capillary beds (Chanda *et al.*, 2010; Elci *et al.*, 2016).

The uptake, biodistribution and bioaccumulation provides more information on the applications of AuNPs in diagnosis and therapy rather than toxicity, as AuNPs are distributed and accumulate in various tissues and body fluids for short or extended periods without inducing toxicity (Fraga *et al.*, 2014; Tiwari *et al.*, 2014; Rambanapasi *et al.*, 2016; Shi *et al.*, 2016; Zong *et al.*, 2017). Factors such as size, surface chemistry and charge, dose and route of administration mainly influence the toxicity of NPs (Fraga *et al.*, 2014; Jia *et al.*, 2017).

Gold can quantitatively be determined in biological system using various techniques including inductively-coupled plasma mass spectrometry (ICP-MS), inductively-coupled plasma optical emission spectrometry (ICP-OES) or inductively-coupled plasma atomic emission spectroscopy (ICP-AES), graphite furnace atomic absorption spectroscopy (GFAAS), and neutron activation analysis (NAA) (Pan-Bartneck, 2010).

### 2.2.3 Peptides

Peptides are molecules derived from dehydration-condensation reactions, involving two or more amino acids linked by peptide bonds. Peptides exist in natural as well as synthesised forms. Peptides are signalling molecules that specifically bind to receptors, such as G protein-coupled receptors, on the cell surface (due to high selectivity) and trigger intracellular effects (Fosgerau and Hoffmann, 2015). Peptides have been involved in the diagnosis and treatment of several diseases, such as cancers (Rabinsky *et al.*, 2016), asthma (Chen *et al.*, 2016), diabetes (Xia *et al.*, 2017), and heart failure (De Sa and Chen, 2008; Roberts *et al.*, 2015a).

#### *2.2.3.1 Use of peptides in cancer*

Peptides play important roles in the diagnosis, prognostic predictors and treatment of various cancers (Xiao *et al.*, 2015), including breast cancer (Haggag *et al.*, 2017), CRC (Comstock *et al.*, 2014; Rabinsky *et al.*, 2016), lung cancer (Wang *et al.*, 2014a; Zhang *et al.*, 2014), pancreatic cancer (Roy *et al.*, 2014) and prostate cancer (Han *et al.*, 2015). The advantages of using peptides in cancers include ease of synthesis and modification, small size and low molecular weight, good compatibility, specificity, tumour-targeting ability, high receptor affinity, and low toxic effects on normal tissues (Thundimadathil, 2012; Shapira *et al.*, 2014; Fosgerau and Hoffmann, 2015; Michalska *et al.*, 2016; Marqus *et al.*, 2017).

Peptides are used directly as drugs or as drug carriers, radionuclides carriers, in hormonal therapy, and as vaccines; and as diagnostic tools and biomarkers in cancer progression to target and bind receptors (Thundimadathil, 2012). Peptides can thus act directly as anticancer drugs or as tumour-targeting agents, or can be used in combination with nanomaterials, thereby enhancing effective delivery and affording clinical efficacy (Xiao *et al.*, 2015).

#### *2.2.3.2 Peptides and the diagnosis of colorectal cancer*

Peptides are used in the diagnosis of CRC - several studies on the detection of protein markers in the blood or the stool of CRC patients have been reported (Kim *et al.*, 2008; Shah *et al.*, 2014b; Shapira *et al.*, 2014; Solé *et al.*, 2014). The diagnostic potential of peptides is based on the overexpression of peptide receptors (G-protein coupled receptors) in CRC and several other cancers. Peptides used in cancer diagnosis induce humoral responses, which lead to the secretion of auto-antibodies used for the diagnosis (Shapira *et al.*, 2014).

Combinational peptide library technology has made it possible to identify peptides that possess binding specificity for tumour receptors (Shadidi and Sioud, 2003b), which can be used in CRC diagnosis. Various peptides specific for colorectal cancer have been identified. These include HNP1–3 (Albrethsen *et al.*, 2006), P1, P10, P13, P14, and P20 (Wang *et al.*, 2012), CPAA-783-

EPPT1 (Bloch *et al.*, 2012) p.L and p.C (Mazyambe, 2013), and serum C-peptide (Comstock *et al.*, 2014). Only three will be discussed here, as these were the focused peptides in this study.

#### 2.2.3.2.1 P.C

P.C has an amino acid sequence CVFSSSYSSSG. It was derived from the phage display peptide library, and binds specifically to prostate-specific antigens (Wu *et al.*, 2000). It has high binding specificity towards human colorectal adenocarcinoma cells (HT-29 cells), with no binding to non-cancerous fibroblast cells (Kmst-6 cells) (Mazyambe, 2013).

#### 2.2.3.2.2 P.L

P.L, with an amino acid sequence LTYSPWY, was derived from the phage display peptide libraries, and strongly binds to the glioma cell line, BT4C (Shadidi and Sioud, 2003a), and breast cancer cells (Shadidi and Sioud, 2003b). It was reported that p.L specifically binds to HT-29 cells when compared to human epithelial colorectal adenocarcinoma cells (Caco-2 cells), human cervical cancer cells (HeLa cells), human liver cancer cells (HepG2 cells) and Kmst-6 cells (Mazyambe, 2013).

#### 2.2.3.2.3 P.14

P.14, alongside four other peptides (P1, P10, P13, and P20), derived from a phage display peptide library, binds favourably and specifically to a human CRC cells (LoVo cells), with no binding to normal human colon mucous epithelium cells (NHCME). It has an amino acid sequence PDHERPM, with highest specificity for LoVo cells, and was regarded as a potential vector for targeting CRC (Wang *et al.*, 2012).

As p.14, p.L and p.C bind selectively to CRC cell lines, these peptides have been identified as suitable peptides for use in the development of a diagnostic tool or as a targeted drug delivery system in CRC.

### 2.2.4 Peptide–gold nanoparticle conjugates

Gold NPs have been functionalised or conjugated with several peptides, and have been designed for various biomedical applications (Roma-Rodrigues *et al.*, 2016; Borglin *et al.*, 2017). These include: conjugation of AuNPs with peptide VG-21 through 1-ethyl-3-(3-dimethylaminopropyl) carbodiimide (EDC) chemistry, as the delivery agent for biomolecules, drugs, fluorophores, and Small interfering RNA (siRNA) (Tiwari *et al.*, 2014); AuNPs were functionalised with Trans-activator of transcription (TAT) peptide via streptavidin-biotin chemistry, for drug delivery or biolabeling (Sosibo *et al.*, 2015); multiple antigenic peptide (MAP)-functionalised AuNPs for detecting bluetongue virus (BTV)-specific antibodies in serum (Saxena *et al.*, 2012); a pro-apoptotic peptide (PAP) was conjugated to AuNPs through thiol–Au interaction, for cancer therapy (Chen *et al.*, 2013c); a gastrin-releasing peptide (specific for prostate, breast and lung cancer) – Bombesin, was conjugated to AuNPs using the disulphide and carboxylic acid groups of thioctic acid as linker, for targeting tumour cells (Chanda *et al.*, 2010); AuNPs were conjugated with a peptide (ACP) having an amino acid sequence WKRAKLAK, using alpha-lipoic acid as a linker, for cancer therapy (Akrami *et al.*, 2016); CRGDK and p12 were conjugated to AuNPs by amide bonds, for cancer targeting and therapy, respectively (Kumar *et al.*, 2012).

#### *2.2.4.1 Approaches for conjugating peptides to AuNPs*

The presence of peptides on the surface of AuNPs enhance the stability, specificity and biocompatibility of the particles. The functionalisation of citrate-reduced AuNPs by peptides can be categorised into chemical reduction, ligand exchange, and chemical conjugation methods (Zong *et al.*, 2017).

##### 2.2.4.1.1 Chemical reduction method

This method involves the reduction of chloroaurate (III) ions by tyrosine or serine in the peptide sequence. Tyrosine competes with the $Cl^-$ of $AuCl_4^-$, which leads to the reduction of $Au^{3+}$ to $Au^0$ by the C-terminal tyrosine, and the N-terminal free amino group of the peptide attach to the gold

surface, producing colloidal peptide-AuNP (Toroz and Corni, 2011; Ramesh *et al.*, 2015). One limitation to this approach is that only small-sized conjugated-AuNPs can be synthesised, and by increasing the concentration of the peptide, the possibility of aggregation increases (Zong *et al.*, 2017).

#### 2.2.4.1.2 Ligand exchange method

The ligand exchange method is used in the synthesis of AuNPs capped with cysteine-containing peptides and involves the displacement of one ligand for the other. In this method, the citrate reduction method is used first to synthesise citrate-capped AuNPs, followed by the introduction of another ligand-containing peptide (e.g. cysteine-capped peptide). This results in ligand exchange, producing peptide-AuNPs (Zong *et al.*, 2017). Limitations associated with this method include the inability to determine the amount of ligand exchanged, possibilities of incomplete ligand exchange, and irreversible aggregation of the NPs (Nicol *et al.*, 2015).

#### 2.2.4.1.3 Chemical conjugation

Chemical conjugation of a peptide involves the use of water-soluble stabilising agents. These serve as capping agents and linkers between synthesised colloidal AuNPs and peptides due to the active binding sites (Zong *et al.*, 2017). In this approach, peptides are not conjugated directly onto the surface of AuNPs but thiolated, leading to the formation of strong Au-sulphur bonds. Polyethylene glycol serves as a stabilising agent for the nanoconjugate, and prevents non-specific interactions of AuNPs with other biomolecules (Sosibo *et al.*, 2015; Jazayeri *et al.*, 2016).

Methods used in the covalent conjugation of peptides to AuNPs include the maleimide-thiol chemistry, EDC–N-hydroxy sulfo-succinimide (NHS) bioconjugation, and Cu(I) catalysed click chemistry (Capehart *et al.*, 2014).

Maleimide-thiol chemistry: It involves the conjugation of primary amines to thiol (sulfhydryl) groups, such as PEG. The maleimide group reacts specifically with sulfhydryl groups, resulting in

the formation of an irreversible and stable thioether (3-thiosuccinimidyl ether) linkage at pHs ranging from 6.5 and 7.5 (Conde *et al.*, 2014). Maleimide chemistry has been used in the conjugation of peptide to AuNPs through maleimide-thiol (PEG) coupling (Oh *et al.*, 2010). Major limitations to this approach include the hydrolysis of imido groups of the maleimide conjugate in aqueous buffer to form a non-reactive maleamic acid derivative at pH above 8.0 (Kalia and Raines, 2010; Conde *et al.*, 2014), and the inability of maleimides to react with certain amino acids, such as histidine, methionine and tyrosine (Koniev and Wagner, 2015).

The EDC–NHS bioconjugation method: This is a type of carbodiimide chemistry approach, which involves covalent immobilization of peptides to PEGylated-AuNPs. In this approach, EDC reacts with a carboxyl group attached to or on a molecule, forming an intermediate (amine-reactive O-acylisourea), which is attacked by a primary amine (a nucleophile), forming an amide bond. The reaction involves the use of sulfo-NHS in conjunction with EDC to avoid the inactivation of the intermediate, as it is easily displaced in water. The sulfo-NHS forms a stable amine-reactive sulfo-NHS ester with the carboxylic group, and the formation of an amide bond occurs by the hydrolysis of sulfo-NHS in the presence of amine (Bartczak and Kanaras, 2011; Conde *et al.*, 2014). Sulfo-NHS increases the stability and solubility of the active intermediate, which reacts with the nucleophile. Different peptides have been functionalised with oligo-ethylene glycol-capped AuNPs using this approach (Bartczak and Kanaras, 2011; Roma-Rodrigues *et al.*, 2016). The advantage of this approach is the formation of negatively-charged particles, which prevent aggregation during the reaction. Experimental conditions, such as the concentrations of EDC and sulfo-NHS added, the ratio of EDC/NHS, the amount of peptide added, the reaction time, and pH are factors that influences the degree of peptide coupling using this approach (Conde *et al.*, 2014).

Click chemistry: This involves facile covalent coupling of peptides to functionalised AuNPs, making use of the catalytic product (copper(I)-catalysed 1,2,3-triazole) of a reaction between azides and terminal acetylenes. This method is highly selective and specific, dependable, and compatible with aqueous and organic reaction systems (Brennan *et al.*, 2006). Copper(I)-

mediated click chemistry is, however, limited by the extended time (3 days) of the reaction (Capehart *et al.*, 2014).

Other non-covalent techniques used in the synthesis of peptide-conjugated AuNPs (peptide-AuNPs) include the electrostatic, hydrophobic, and affinity based non-covalent interactions.

Electrostatic interaction: This is a non-covalent interaction between the positively-charged group of peptides and negatively-charged AuNPs (Capehart *et al.*, 2014). It is known for its stability in aqueous solutions. Several limitations, such as the assembly of particles leading to large hydrodynamic radii of AuNPs, the sensitivity of the method to external environmental conditions such as pH and ionic strength, and the lack of control over the extent of functionalisation due to restrictions in the charge of the molecules to be used (Tauran *et al.*, 2013; Wang *et al.*, 2014b), are associated with this method.

Hydrophobic interactions result in the formation of non-covalent bonds between the AuNP surface and the hydrophobic side of a peptide. In this method, there are electrostatic interactions between negatively-charged AuNPs and positively-charged groups and the N-terminal region of the peptide (Jazayeri *et al.*, 2016).

Affinity-based non-covalent interactions: This method involves the conjugation of AuNPs with groups providing affinity sites for the binding of peptides. Such groups include avidin and streptavidin, which links AuNPs to biotinylated peptides. The streptavidin-biotin interaction is one of the strongest non-covalent affinities known (Sorenson *et al.*, 2015). Streptavidin is isolated from *Streptomyces avidinii*, with a molecular weight of about 60 kDa. It is a tetrameric protein, and each monomer is capable of binding one biotin or biotinylated compound. Streptavidin maintains its native structure under a wide range of pHs, buffer conditions, heat and proteolysis. The binding of biotin to streptavidin promotes the stability of the complex. Biotin has the greatest binding affinity to streptavidin and their molecular recognition reaction can take place in a wide range of pH and temperatures. Streptavidin has a low isoelectric point of about 5, enabling the

reduction of non-specific binding at a common pH working range. This method was used in the synthesis of TAT peptide-conjugated AuNPs (Sosibo *et al.*, 2015).

#### *2.2.4.2. Peptide-conjugated AuNPs in CRC diagnosis*

In the diagnosis of CRC, peptides specific for CRC binds to receptors on the tumour cells (Shapira *et al.*, 2014). The AuNPs can be viewed by imaging techniques. X-ray based computed tomography (CT) is an efficient, available, convenient and affordable imaging and diagnostic tool used in hospitals. Gold, in the form of AuNPs, is an excellent candidate as an X-ray CT contrast agent, as opposed to the currently used CT contrasting agent (iodine) which lacks the ability to be conjugated to biological molecules or tumour markers, and associated renal toxicity (Ahn *et al.*, 2013). The presence of targeted peptides on the surface of AuNPs allows tumour specificity and selectivity, as AuNPs may not be targeted without conjugation to specific biomarkers. It was reported that selective X-ray attenuation obtained from peptide-AuNPs on targeted cancer cells is stronger than that obtained from normal or untargeted cells (Popovtzer *et al.*, 2008). This potentiates the use of peptide-AuNPs for molecular imaging of CRC, thereby enhancing the diagnosis.

Since the peptide-AuNPs is more visible on cancer cells (highly concentrated in tumour site) than normal and untargeted cells, the question remains: 1. What is the fate of the peptide-AuNPs injected in normal patients (without tumour) during CRC screening? 2. What happens to the peptide-AuNPs after tumour imaging in CRC patients?

As a first step to answer the questions above, it is necessary to investigate the possible toxic effects of these peptide-AuNPs after a single injection to healthy rats.

## 2.3 NANOTOXICOLOGY

### 2.3.1 Toxicology

Toxicology is the branch of medical and biological sciences that studies the interaction of substances with the living systems; thus, affecting the normal biological and physiological processes in the body. This can be used to predict safe exposure level of substances. A fundamental principle of toxicology is that no substance is safe if given in a large amount, but it can be considered safe if given in small amount (low dose), and results into a non-detectable impact on normal biological processes. These substances can also, at one point, be harmful if the exposure duration is increased (Society of Toxicology, 1999).

Toxicity is any adverse or toxic effect that a substance produces on exposure to biological systems. Toxicity studies are performed based on the exposure of chemicals or substances to experimental animals, and can be divided into categories, including single or multiple dose (acute) and repeated dose (sub-acute, sub-chronic or chronic) exposure (Casarett and Klaassen, 2008).

Acute toxicity is an adverse effect that is manifested within a relatively short time (ranging from almost immediately to several days) after a single or multiple exposure of a substance within 24 h. These adverse effects may produce biochemical lesions, impairments in the functional integrity of organs, or mortality (Chinedu *et al.*, 2013). Acute toxicity studies investigate the effect of a substance within 14 days of administration. If acute toxicity studies in animals are designed towards providing primary safety data to support single-dose safety study in humans, parameters such as clinical pathology and histopathology should be investigated for maximum effect and reversibility (FDA, 1996).

Sub-acute and sub-chronic toxicity studies involve investigating the effect of repeated exposure of substances (3 to 4 doses) in animals for 14 to 28, and 90 days, respectively. Chronic toxicity studies investigate the effect of substances after repeated exposure for more than 3 months

(Casarett *et al.*, 1996; Roberts *et al.*, 2015b). These studies are done to evaluate clinical observations, analysis of blood, and tissue histopathology.

Nanotoxicology is the study of the adverse effects of NPs on biological systems or the environment. Several diseases have been implicated on exposure of the body to NPs, including cancers, neurodegenerative diseases, asthma, bronchitis, heart disease, and damage to other internal organs (Figure 2.4) (Buzea *et al.*, 2007).

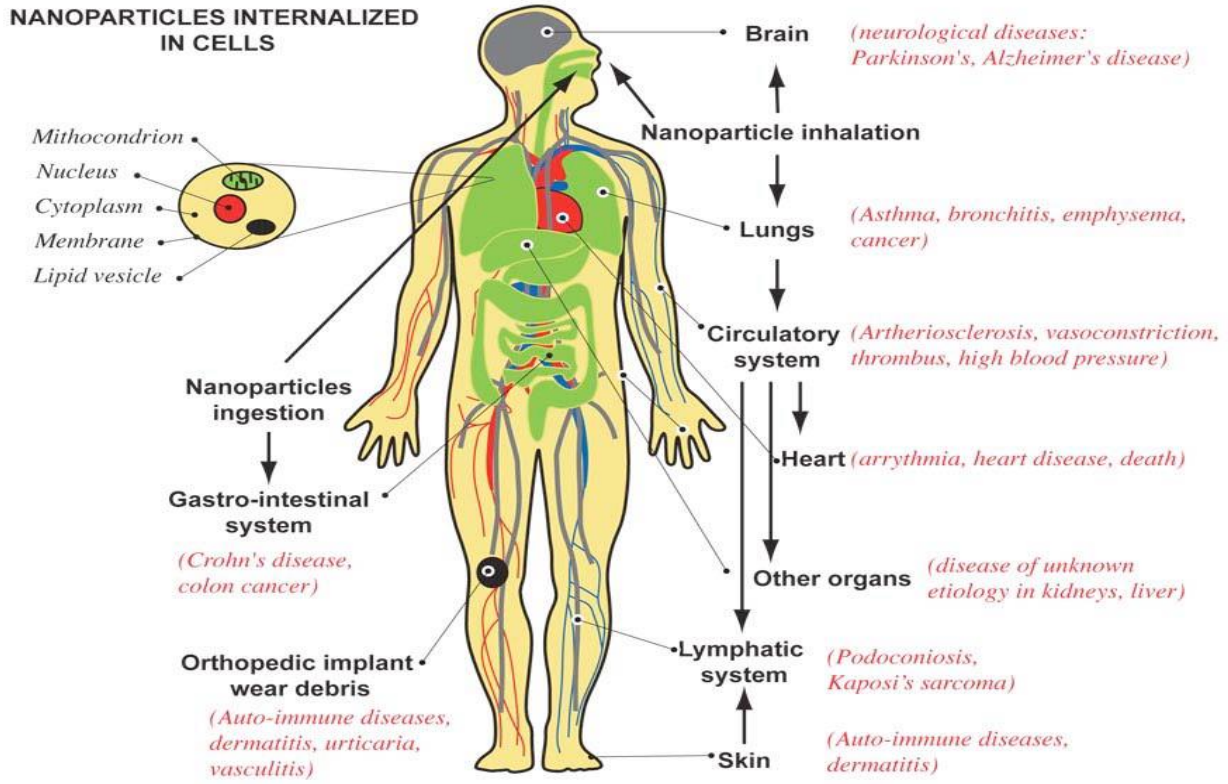


**Figure 2.4:** Exposure of nanoparticles to various organs of human body and associated diseases. Adapted from Buzea *et al.* (2007).

It was observed that most guidelines used in toxicity testing, which involve the exposure of chemicals via oral route (OECD, 2008), may not be applicable to NPs, due to their exceptional properties and applications. The following needs proper attention towards designing a route of administration of NPs *in vivo*: 1) parenteral route of administration, such as intravenous, could be the best option for NPs in targeted disease diagnosis and therapy, as intravenous

administration ensures complete dose delivery into systemic circulation (Casarett and Klaassen, 2008); 2) oral administration of AuNPs was more toxic than intravenous administration (Zhang *et al.*, 2010), which might be linked to an effect on the mucosal cells of the gastrointestinal tract (Section 2.3.2.1.9); 3) long-term toxicity or reversibility studies of NPs after a single or repeated injection should be considered (Yah, 2013). This is because the application of NPs in diagnosis requires a single exposure at a given time, and the long-term accumulation of these particles might induce adverse effects on biological system (Shin *et al.*, 2015).

Parameters, such as the morphological, physiological and biochemical, as well as histopathological changes should be investigated alongside mortality in acute toxicity studies. This is necessary due to lack of standardised guidelines for investigating the toxic effects of NPs *in vivo*, as AuNPs possess several physicochemical properties related to its toxicity (Yah, 2013). It is therefore noteworthy to investigate the effect (most especially *in vivo*) of NPs based on intended applications with respect to exposure in humans.

### 2.3.2 Toxicity of gold nanoparticles

Several toxicological studies on AuNPs using various *in vitro*, *in vivo* and *in ovo* models have been reported (Fraga *et al.*, 2014; Jo *et al.*, 2015; Berce *et al.*, 2016; Senut *et al.*, 2016; Tripathi *et al.*, 2016). There are however, few toxicological reports of AuNPs in the animal model, which is the preferred system for the toxicological evaluation of a novel agent due to the complexity in terms of absorption, distribution, metabolism, and excretion (Alkilany and Murphy, 2010; Jia *et al.*, 2017). The toxicologic behaviour of AuNPs are guided by their small size, shape and surface charges (Yah, 2013). Although AuNPs are useful in medical applications due to their inert nature, high biocompatibility and conjugation to other biomolecules (Oni *et al.*, 2014; Shapira *et al.*, 2014), there are a number of conflicting results concerning their toxicity (Buzea *et al.*, 2007; Sperling *et al.*, 2008). Researchers have reported the safety of AuNPs (Schulz *et al.*, 2012; Chen *et al.*, 2013a; Fraga *et al.*, 2013; Uchiyama *et al.*, 2014; Kunjiappan *et al.*, 2015) as well as the toxicity (Cho *et al.*, 2009a; Pan *et al.*, 2009; Hwang *et al.*, 2012; Khan *et al.*, 2012; Kim *et al.*, 2013).

The section of this chapter integrates available literature (toxicological studies from 2009 to 2017) to better understand factors that may contribute to the toxicity or safety of AuNPs.

#### *2.3.2.1 Factors influencing the toxicity of gold nanoparticles*

Several factors (Figure 2.5) are important in predicting the toxicity of AuNPs *in vitro, in ovo* and most especially, *in vivo*. Numerous studies have indicated that toxicity is highly dependent on the physicochemical properties of NPs, even though many of these unique properties make them appealing to nanomedicine and biological applications (Zhang, 2015).

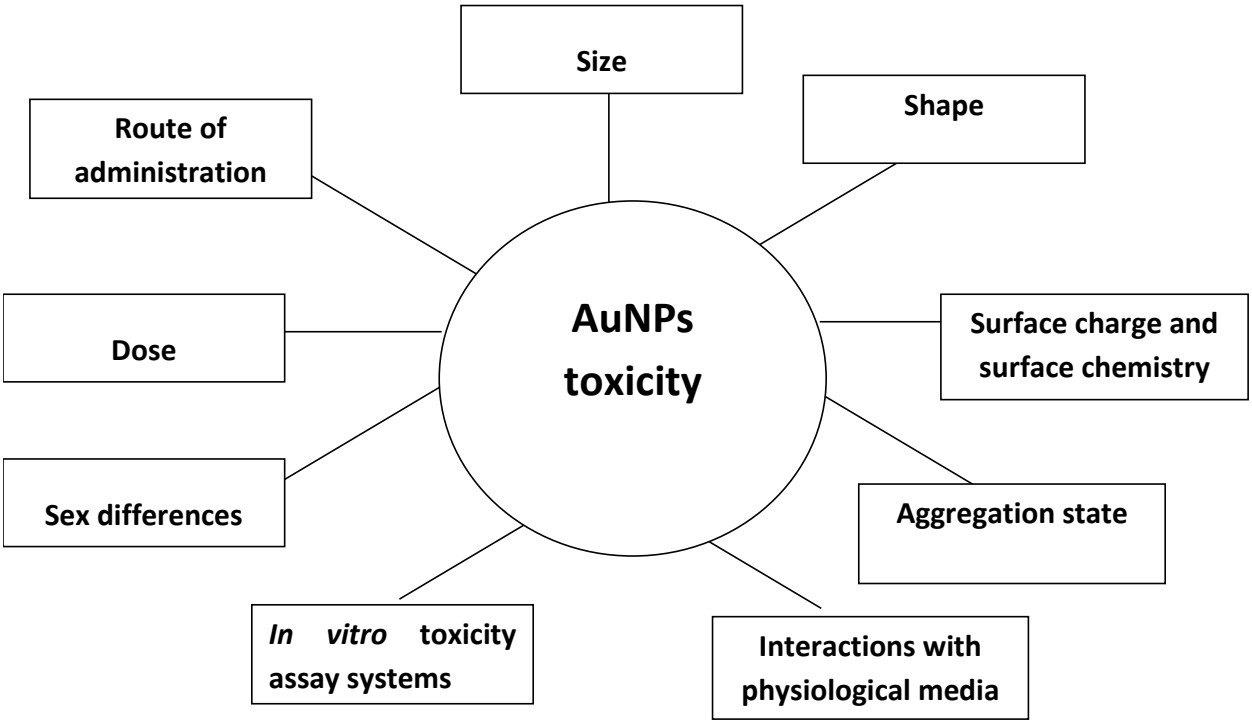


**Figure 2.5:** Factors influencing the toxicity of gold nanoparticles

2.3.2.1.1 Size

The size of NPs influences the biological activity of the cell (Fadeel and Garcia-Bennett, 2010). Small-sized AuNPs (< 5 nm) are more toxic than larger ones *in vitro* (Table 2.1) (Pan *et al.*, 2009; Boyoglu *et al.*, 2013; Coradeghini *et al.*, 2013), and in zebrafish (Kim *et al.*, 2013; Truong *et al.*,

2013). The toxicity of small-sized AuNPs may result from the presence of a high surface area relative to the total mass, thereby increasing the interaction with biomolecules (Shang *et al.*, 2014). This assumption may not be generalised, as only a few contradictory studies using small-sized AuNPs have been reported *in vivo*. Non-toxic effects have been reported, as shown in Table 2.3 (Chen *et al.*, 2009; Cho *et al.*, 2009b) and Table 2.5 (Glazer *et al.*, 2011).

In a study by Zhang *et al.* (2009), it was reported that AuNPs smaller than 20 nm in diameter are useful for *in vivo* applications, as these are more readily excreted via the urinary and hepatobiliary systems of the body. There is however no guidance as to the size of the AuNPs be after conjugation with different conjugants. Reported research on size may be complicated by the stability of the conjugating agent or the possible toxicity of capping agent. More studies are therefore suggested, most especially with AuNPs at low concentrations (Zhang *et al.*, 2010).

2.3.2.1.2 Shape

The shape of AuNPs is thought to be an important factor in establishing the cellular or biological responses to AuNPs (Schaeublin *et al.*, 2012; Tian *et al.*, 2015). Gold NPs exhibit shapes, such as nanospheres, nanotriangles, nanoprisms and nanorods. Other shapes include tetrahedral, sub-octahedral, octahedral, decahedral, icosahedral, multiple twined and irregular shapes (Khan *et al.*, 2014).

The toxicity studies of spherical AuNPs and nanorods have mostly been studied and compared. This may be connected to: (1) the popularity of spherical AuNPs with regards to their small size (< 100 nm), ease of synthesis and conjugation with other molecules, as well as the absorption wavelength in the visible spectral region (500-600 nm), and (2) the superiority of Au nanorods in terms of the absorption cross-section (longitudinal and transverse), as compared to other Au nanostructures (Makkouk and Madsen, 2013).

Cellular uptake of rod-shaped AuNPs is lower than spherical AuNPs (Chithrani *et al.*, 2006). Uptake of AuNPs is important in designing AuNPs for biomedical use. Gold nanorods were more

toxic to cells in culture when compared to spherical AuNPs (Murphy *et al.*, 2008), as shown in Table 2.1 (Alkilany *et al.*, 2009). This toxicity was caused by cetyltrimethylammonium bromide (CTAB), which is essential for the synthesis of Au nanorods using the seed-growth Au nanorod synthesis method (Alkilany *et al.*, 2009; Zhang, 2013). Citrate-stabilised spherical AuNPs showed no significant cytotoxicity on cells (MDCK and HEp-2) when compared to CTAB-capped Au nanorods (Zhang, 2013). The toxicity of Au nanorods can therefore be reduced if coated with other polymer molecules, such as PEG, phosphatidylcholine and poly(acrylic acid) (Niidome *et al.*, 2006; Takahashi *et al.*, 2006; Murphy *et al.*, 2008).

Substantial adverse effects were induced by PEG-Au nanorods in cells, whereas exposure of cells to 3-mercaptopropanesulfonate (MPS)-Au nanospheres did not show toxicity (Schaeublin *et al.*, 2012). It was further clarified that the surface coatings (PEG and MPS) were biocompatible. Gold nanorods conjugated with PEG or citric acid ligands are less toxic when compared to spherical AuNPs in human keratinocyte cells (HaCaT) and human breast cancer cells (MCF-7) (Clichici and Filip, 2015), which contradicts the report by Schaeublin *et al.* (2012). In a study by Wang *et al.* (2016c), it was shown that CTAB-coated spherical, rod and polyhedral AuNPs resulted in developmental toxicity in zebrafish embryo, in a shape-dependent manner, with spherical AuNPs exhibiting greater toxicity when compared with nanopolyhedrons and nanorods. More toxicological studies on AuNPs are thus encouraged, taking into consideration the size and other properties.

#### 2.3.2.1.3 Surface chemistry and surface charge

Gold NPs are coated, stabilised, functionalised or conjugated with different organic moieties to improve their stability, thereby forming a protective layer on the surface of the particles, whilst preventing aggregation in biological fluids (Bogdanov *et al.*, 2015). These have shown low cytotoxicity, with excellent biodistribution abilities (Tiwari *et al.*, 2011). A number of these agents, including nucleic acids, drugs, antibodies, PEG (Nelson *et al.*, 2013), siRNA (Hou *et al.*, 2013; Nelson *et al.*, 2013), peptides (De La Fuente and Berry, 2005; Jin *et al.*, 2013) and

methoxypoly-ethylene glycol-graft-poly(L-lysine) copolymer (Bogdanov *et al.*, 2015) have been used to facilitate the application of AuNPs in nanomedicine. These functionalised AuNPs are used for gene transfection and silencing, targeted drug or gene delivery (Jin *et al.*, 2013), intracellular detection, bioimaging (Chanda *et al.*, 2010), cancer studies (Oyelere *et al.*, 2007; Bartczak *et al.*, 2013) and as biosensors (Wang *et al.*, 2010).

Polyethylene glycol, as a conjugating agent, has gained popularity due to its amphiphilic and solubility characteristics, thereby protecting the AuNPs and ensuring a high degree of biocompatibility and affinity of the nanocarrier for cell membranes (Pissuwan *et al.*, 2011; Sosibo *et al.*, 2015).

The toxic effect of a gene-delivery vector (based on the ability of AuNPs to transfect CRC (HCT-116) cells with enhanced green fluorescent protein (EGFP) expression vector) was investigated by Almeida (2014). In this study, no toxicity was recorded with 14 nm AuNP-based formulations (PEG-AuNP-functionalised with quaternary ammonium and pEGFP vector (AuNP-PEG-R4N$^{+}$-pEGFP)) when compared with a commercial transfection reagent, Lipofectamine 2000 (a cationic liposome), 48 h post-exposure to cells.

Stabilisation of AuNPs with two PEG molecules (1% PEG-biotin and 99% PEG-OH) promotes stability and prevents the aggregation of AuNPs. The PEG-OH was used because of its versatility with regards to solubility and biological compatibility, while PEG-biotin allows the immobilization of streptavidin – a linker between PEGylated biotin on the surface of AuNPs and biotinylated TAT peptide. This approach decreased the risk of introducing toxic reagents during the coupling reaction, and provides a suitable design of multilayered nanoconjugates for various applications in nanomedicine. Although PEG serves as a promising coating agent for AuNPs, toxicological studies are suggested to ascertain the success of PEGylated AuNPs-based formulations for nanomedicine applications (Sosibo *et al.*, 2015).

Gold NPs coated with high-molecular-weight (5 kDa) PEG were more stable and devoid of aggregation than the AuNPs coated with low-molecular-weight (2 kDa) PEG (Zhang *et al.*, 2009; Zhai *et al.*, 2015), suggesting less toxicity.

Addition of too much PEG (though no information on the type of PEG referred to) onto the surface of AuNPs minimises binding interactions between surfaces and protein disease targets, which is a key factor to be considered in the potential application of AuNPs as therapeutic agents.

Several challenges regarding the use of these capping, stabilising or conjugating agents for AuNPs have been reported, including i) possible toxic effects of chemicals and capping agents, which include citrate (Table 2.1) (Vijayakumar and Ganesan, 2012), CTAB, as shown in Table 2.1 (Alkilany *et al.*, 2009), sodium borohydride, polyelectrolyte poly(allylamine (PAH) (Bozich *et al.*, 2014) and hydrazinium hydroxide, used in the synthesis of AuNPs, limiting usage in nanomedicine, and ii) high cost of preparation (Ghosh *et al.*, 2012; Ramakrishna *et al.*, 2016).

To this end, researchers have worked on the synthesis of NPs by biological methods (green chemistry) and physical methods (laser ablation in liquids).

The biological methods involve the use of biological systems such as plant and plant materials (Vijayakumar and Ganesan, 2012; Kunjiappan *et al.*, 2015; Tripathi *et al.*, 2016), bacteria (Kalishwaralal *et al.*, 2010; Sadhasivam *et al.*, 2012), algae (Ramakrishna *et al.*, 2016) and fungi (Mukherjee *et al.*, 2001) in the synthesis of AuNPs. Benefits associated with these approaches include simplicity, cost-effectivity and efficiency, eco-friendliness and low toxicity (Sadhasivam *et al.*, 2012; Ramakrishna *et al.*, 2016; Tripathi *et al.*, 2016).

Limited toxicity studies have been reported on these biosynthesised AuNPs. Non-toxic effects of spherical herbal-AuNPs up to 100 µg/ml (average size 70 nm), using the leaf extract of *Achyranthes aspera* on cultured spleenocyte cells, have been reported (Tripathi *et al.*, 2016). This approach was successful in cell culture, and the stability (up to 2 months) of the synthesised particles was achieved at 25 $^{0}$C and pH 10, with the pH adjusted to the normal physiological range

for medicinal use. In using this approach, physiological parameters including a pH range from 7.35 to 7.45, a temperature of 37 $^{0}$C, and stability at different salt (NaCl) concentrations, should be emphasised. More detailed toxicity studies, with improved production or synthesis of biosynthesised AuNPs be done, so as to address the limitations to this approach, which include particle aggregation, non-uniform shapes with biological materials and poor mono-dispersity (Clichici and Filip, 2015).

The physical methods (such as laser ablation in liquid) provide a free-ligand synthesised NPs (Rehbock *et al.*, 2014). This method has several advantages, such as simple procedural steps; high purity-synthesised colloidal NPs free of chemical reagents (free-ligand); and excellent colloidal stability of NPs (Elsayed *et al.*, 2013; Tiedemann *et al.*, 2014). The stability of ligand-free AuNPs (without stabilising agents) in a variety of media may result from the partial oxidation of the Au surface during the process of ablation, thereby resulting in positively-charged AuNPs (Tiedemann *et al.*, 2014).

Gold NPs, synthesised by pulsed laser ablation of Au wire in liquid-flow, were coated with BSA to prevent the formation of protein corona upon exposure to biological proteins. No adverse effects were recorded after 2 h incubation of porcine spermatozoa with BSA-coated AuNPs (20 nm, 10 μg/mL). Also, no sign of toxicity was observed when porcine cumulus–oocyte complexes were exposed to 6 nm and 20 nm AuNPs-BSA (10 μg/mL) and 6 nm BSA/citrate-coated AuNPs (10 and 30 μg/mL) (Tiedemann *et al.*, 2014).

In another study, spherical AuNPs were synthesised by femtosecond laser ablation in three different liquid media (pure deionised water, PEG and dextran solutions). The toxic effects of these NPs (0.1 μg/L to 10,000 μg/L) were investigated in the human glioblastoma (U87-MG) and neuroblastoma (SK-N-SH) cell lines after 72 h. No obvious cytotoxicity was induced (Correard *et al.*, 2014).

It should be noted that although the ligand-free AuNPs decreased interference of ligands with toxicological assays and particle properties, the following points need to be considered: 1) the

ligand-free AuNPs need to be stabilised with agents such as BSA before exposure to a biological environment. This is to prevent the adsorption of proteins to the surface of the NPs, which could form a protein corona (Rehbock *et al.*, 2014; Tiedemann *et al.*, 2014). This corona influences the biological nature of the particles; 2) in designing AuNPs as a drug carrier or delivery tool for therapeutic or diagnostic purposes, which requires conjugation with capping, stabilising, coating or conjugating agents, it is important to investigate the biocompatibility and toxic effects of these agents, which are important in the synthesis of the bioconjugating nanomaterials; and 3) the capping agents introduced to the free-ligand AuNPs influence the size of the AuNPs (Correard *et al.*, 2014; Torres-Mendieta *et al.*, 2016).

Nevertheless, there is no method that can be regarded as the best in the synthesis of AuNPs, since each of these methods have several disadvantages.

*Surface charge*

The effect of surface charge was reported by Goodman *et al.* (2004), where 2 nm cationic AuNPs were moderately toxic, whereas, the anionic counterpart at the same concentration was non-toxic in cells. The difference was related to the interactions of the cationic NPs with the negatively-charged cell membrane, thereby leading to membrane disruption.

The effect of charge was also observed in zebrafish embryo. Neutral (2-(2-(2-mercaptoethoxy)ethoxy)ethanol) (MEEE)-AuNP (no charge) did not cause behavioural defects, while negatively-charged (2-mercaptoethanesulfonic acid) (MES)-AuNP and positively-charged (N,N,N-trimethylammoniumethanethiol) (TMAT)-AuNP resulted in larval behavioural abnormalities, which persisted into adulthood (Truong *et al.*, 2012). In another study, the surface functionalisation of 1.3 nm AuNPs with a cationic ligand monolayer (TMAT-AuNPs) played a significant role in the toxicity results observed in zebrafish embryos (Kim *et al.*, 2013).

#### 2.3.2.1.4 Aggregation state

Aggregation of NPs (facilitated by surface charge, size and surface chemistry) influences cellular toxicity (Yang *et al.*, 2014; Moore *et al.*, 2015). It was reported that cationic and oligocationic species resulted in particle aggregation (Yang *et al.*, 2007), while negatively-charged AuNPs repel each other and inhibit aggregation (Basu *et al.*, 2007).

A number of coating agents, including lipids (Yang *et al.*, 2014) and polymers (Fratoddi *et al.*, 2015), and the presence of BSA and proteins in the cellular medium, prevent the aggregation of NPs (Yang *et al.*, 2014; Moore *et al.*, 2015).

#### 2.3.2.1.5 Interactions with physiological media and biological fluids

Nanoparticles interact with the components of a typical cell growth medium such as serum proteins, essential amino acids, vitamins, ionic salts, and other chemicals, including trace metals and antibiotics. These constituents influence the physiochemical properties, such as surface charge, aggregation state and surface chemistry (Alkilany and Murphy, 2010), and the hydrodynamic behaviour of NPs (Moore *et al.*, 2015). The presence of a high concentration of electrolytes in media results in the destabilisation of NPs (Vesaratchanon *et al.*, 2007), which could influence the ability of AuNPs to interact with cells (Alkilany and Murphy, 2010).

On exposure to biological fluids, AuNPs interact with proteins, nucleic acids, lipids and polysaccharides. On interaction, the physicochemical properties of both AuNPs and proteins change, and induce a number of physiological and pathological changes, which include blood coagulation, aggregation of proteins, complement activation, and changes in the configuration of bound proteins (Pfeiffer *et al.*, 2014; Wang *et al.*, 2015).

Proteins such as ubiquitin, tumour necrosis factor, serum albumin, polypeptides, fibrinogen, or cytochrome C, are easily adsorbed onto the surface of AuNPs to form protein corona. This causes: (1) changes in the structures of adsorbed proteins (Deng *et al.*, 2011); (2) loss of original targeting

capabilities of proteins (Salvati *et al.*, 2013); and (3) induction of several cellular responses, such as activation of caspase-related pathways, apoptosis, increased lysosomal permeability or inflammatory responses (Ma *et al.*, 2011; Wang *et al.*, 2015).

2.3.2.1.6 Interference of gold nanoparticles with *in vitro* toxicity assay systems

It is difficult to draw meaningful conclusions with regards to the toxicity of AuNPs based on the use of these methods because of differences in the size of the AuNPs used and the cell types implemented (Vetten *et al.*, 2013), and variations in shape, concentration, surface charge and surface chemistry. The contradictory cytotoxicity results obtained with the different assay methods were reportedly caused by possible interference of the tested AuNPs with these assay systems (Kroll *et al.*, 2009; Vetten *et al.*, 2013). This could be linked to high surface area, which leads to increased adsorption capacity; optical properties that causes interference with fluorescence or visible light absorption detection systems as they absorb light in the visible region (about 520 nm); and magnetic properties, which leads to interference with methods based on redox reactions (Kroll *et al.*, 2009; Dhawan and Sharma, 2010). As a result, the methods adopted for traditional toxicological studies cannot directly be applied to NP toxicological studies.

The provision of a standardised NP reference material for toxicological studies, through which comparison of data can be made across different studies, has been suggested (Dhawan and Sharma, 2010). Colony forming efficiency (CFE) assay is well-defined, and compared to other *in vitro* toxicity screening assays has advantages that include lack of interference (because it is a label-free test) and higher sensitivity. This method was reportedly tested by twelve laboratories in France, Italy, Japan, Poland, the Republic of Korea, South Africa and Switzerland, which are related to the organization for economic co-operation and development (OECD) working party of manufactured nanomaterials (Ponti *et al.*, 2014). This test has been used in different *in vitro* systems to assess cytotoxicity of a wide range of nanomaterials such as AuNPs (Coradeghini *et al.*, 2013), silica NPs (Uboldi *et al.*, 2012) and multi-wall carbon nanotubes (Ponti *et al.*, 2010).

The CFE assay was therefore suggested to serve as a first-choice method in defining dose-effect relationships for other *in vitro* assays in the early toxicity screening of NPs (Ponti *et al.*, 2014).

#### 2.3.2.1.7 Gender differences

In *in vivo* models, the toxicity of AuNPs may be influenced by sex differences. Some factors to be considered when choosing a sex of an *in vivo* model include: (i) larger percent of fat in relation to the total body weight of females compared to males; (ii) the anatomical differences in the reproductive system and associated hormone cycles between males and females; and (iii) faster total clearance of most substances in males compared to females (Schwartz, 2003).

In a study by Chen *et al.* (2013b), no significant toxicological responses were noted in the reproductive system in both male and female mice upon intraperitoneal injection of 200 µL PEG-AuNPs (Table 2.3). Gold NPs caused more serious hepatotoxicity and infection in male mice than female mice, suggesting that sex differences may be one of the important elements of *in vivo* toxicity of AuNPs (Chen *et al.*, 2013b).

#### 2.3.2.1.8 Dose

The total concentration of AuNPs administered to an organism for a specific period of exposure could influence the toxicity of the particles. Various conflicting results have been reported on the dosage of AuNPs. No literature has reported the safe dose of these particles without emphasis on other factors, such as size, shape and route of administration. Since the doses used in animal studies were generally higher than the actual doses humans are exposed to, and since NP pharmacokinetics is dose-dependent, a low-dose model, as shown in Table 2.3 (Zhang *et al.*, 2010), is therefore important (Libutti *et al.*, 2010; Lin *et al.*, 2015).

The dose in a rat model for low and medium doses are ~0.01 and ~1.0 mg/kg (10 and 1000 µg/kg) respectively, and was therefore extrapolated to simulate low-dose kinetics of AuNPs, since pharmacokinetics is dose-dependent, and because the actual doses tested in animals are higher

than the doses humans are exposed to. Based on this, a scientific basis for researchers to select the most appropriate animal model and dosing paradigms for conducting future nanomaterial studies, so as to increase the research relevance to humans is needed (Lin *et al.*, 2016a). In choosing dose for toxicity studies, the purpose of application of AuNPs should be considered.

#### 2.3.2.1.9 Routes of administration

The administration route of AuNPs could influence the toxicity of the particles. Injection via the tail vein (intravenous) is the most promising route for AuNPs because it is a superficial and easily assessable procedure for animals, and showed the lowest toxicity of AuNPs, as reported by Zhang *et al.* (2010) (Table 2.3).

Oral delivery of NPs may have an effect on the mucosal cells of the gastrointestinal tract as a result of morphologic and physiologic absorption barriers (Jung *et al.*, 2000). Mucosal cells play an important role in oral administration of AuNPs. No significant damage was noted to the stomach on oral administration of AuNPs, which indicates good absorption of the particles. Slight damage to the intestine was also reported, which may be an indication for the toxicity of the AuNPs (Zhang *et al.*, 2010). No literature could be found on the effect of the digestive enzymes on the surface coatings of the NPs.

Intraperitoneal injection in rats is less toxic than oral administration at a dose of 1100 µg/kg AuNPs (Zhang *et al.*, 2010).

#### 2.3.2.1.10 Clearance and excretion

Nanoparticles with optimum clearance characteristics tend to reduce the risk of toxicity, as a result of the reduction in the duration of exposure to the body. Nanoparticles (quantum dots) with diameters < 5.5 nm are easily excreted via the kidney (Choi *et al.*, 2007), as the filtration-size threshold of glomerular capillary walls is typically 6-8 nm, where particles with hydrodynamic diameters smaller than 6 nm undergoes rapid urinary excretion (Choi *et al.*, 2007; Yu and Zheng,

2015; Zhang *et al.*, 2016). The kidney cleared 1.9 nm AuNPs and excreted the particles 5 h after intravenous injection in mice (Hainfeld *et al.*, 2006), indicating that these particles are small enough to cross the glomerular filter.

Larger NPs (> 6 nm) in the systemic circulation, which were not excreted in urine, can be eliminated from the blood by the reticuloendothelial system. These are accumulated in the liver and spleen, or entrapped by the mononuclear phagocyte system and cleared via the hepatobiliary system, or retained in the body for months (Longmire *et al.*, 2008; Alkilany and Murphy, 2010; Zhang *et al.*, 2016). An over-time elimination of 40 nm AuNPs was primarily by the Kupffer cells of the liver, with the NPs found inside the lysosome/endosome-like vesicles in a clustered manner (Sadauskas *et al.*, 2009). It was concluded, based on their extrapolated data, that most of the AuNPs remain in the liver of the mouse, even for the normal life span, since the clearance of these particles may be very slow.

Surface chemistry is another factor that influences the excretion of AuNPs. It was found that 20 nm PEG-AuNPs were cleared from the blood without further accumulation in the liver and spleen (Perrault *et al.*, 2009). In a study by Zhang *et al.* (2012), it was reported that 36% Au in GSH- and 1% Au in BSA-protected Au nanoclusters were excreted in the urine after 24 hours. Also, 94% and < 5% Au in GSH- and BSA-Au nanoclusters, respectively, were metabolised by renal clearance after 28 days. This resulted in a significant reduction in the toxicity of GSH-Au nanoclusters, whereas, the BSA-Au nanoclusters accumulated in the liver and spleen, leading to the irreparable toxicity response.

It can therefore be concluded that the size of AuNPs and surface chemistry contributes to its elimination from the body.

#### *2.3.2.2 Models previously used to screen the toxicity of AuNPs*

A number of researchers have reported the safety of naked or conjugated AuNPs (Glazer *et al.*, 2011; Schulz *et al.*, 2012; Venkatpurwar *et al.*, 2012; Chen *et al.*, 2013a; Fraga *et al.*, 2013;

Correard *et al.*, 2014; Uchiyama *et al.*, 2014; Jo *et al.*, 2015; Kunjiappan *et al.*, 2015), as well as the toxicity (Pan *et al.*, 2009; Hwang *et al.*, 2012; Khan *et al.*, 2012; Kim *et al.*, 2013; Ghahnavieh *et al.*, 2014; Boyles *et al.*, 2015; Ferreira *et al.*, 2015; Shetty *et al.*, 2015; Senut *et al.*, 2016), using various *in vitro*, *in vivo* and *in ovo* models (Figure 2.6).

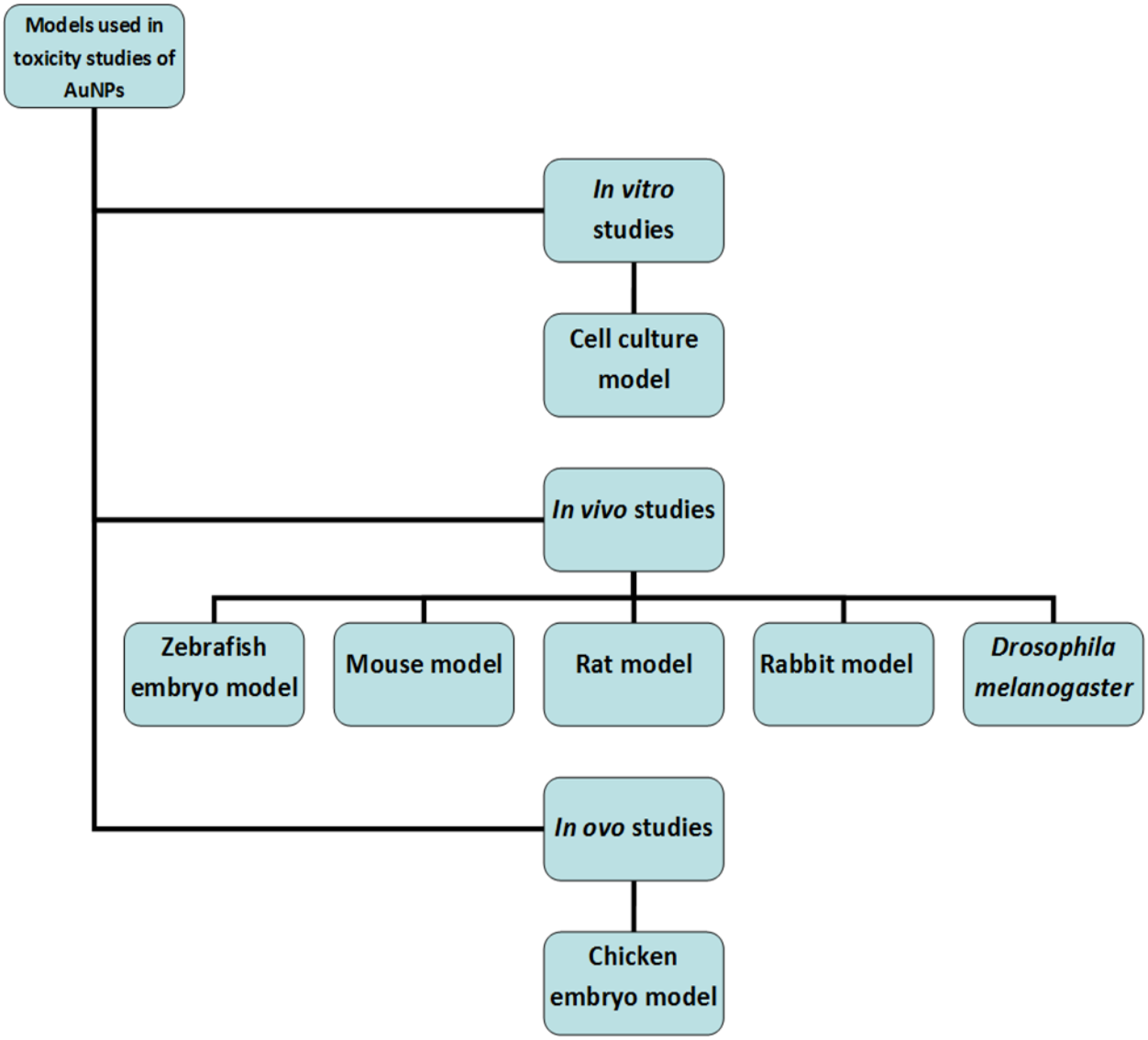


**Figure 2.6:** Models used in screening the toxicity of AuNPs

There are, however, few toxicological reports of AuNPs in the animal model, which is the preferred system for the toxicological evaluation of a novel agent (Zhang *et al.*, 2010).

#### 2.3.2.2.1 *In vitro* assessment of the toxicity of AuNPs

Most toxicological studies are conducted *in vitro* in immortalised cell lines, using standard toxicological assays such as the 3-(4,5-dimethylthiazolyl-2)-2,5-diphenyltetrazolium bromide (MTT) assay and the lactate dehydrogenase (LDH) assay, which measures the mitochondrial enzymatic activity and disruption of the cell membrane, respectively (Senut *et al.*, 2016), CFE assay, which measures the ability of a single cell to form a colony (Ponti *et al.*, 2014), as well as the carboxy-2',7'-dichlorofluorescein diacetate ($H_2$DCFDA) assay and water-soluble tetrazolium-1 (WST-1) assay, which measures reactive oxygen species (ROS) and cell proliferation, respectively (Jo *et al.*, 2015). The high proliferation rate of cell lines, simple procedures (which can be automated), low cost, short experimental period and precise applied concentration of testing materials, make cell-based screening tests popular (Pan-Bartneck, 2010).

##### *2.3.2.2.1.1 Cell-based toxicity screening tests*

Cell culture assays are suitable for the study of basic mechanisms that include endocytosis, death pathways and the interactions between AuNPs and subcellular components. Several cell lines have been used to assess the effects of AuNPs (Venkatpurwar *et al.*, 2012; Belliraj *et al.*, 2015; Jo *et al.*, 2015) (Table 2.1).

**Table 2.1:** Evaluation of AuNPs in different cell lines

| Cell line used | AuNPs characteristics | Concentration | Time of exposure | Assay methods | Toxicity findings | Ref. |
|---|---|---|---|---|---|---|
| HT-29 cells | **SC:** CTAB, PAA, PAH; **Size:** 65 x 15 nm; **Shape:** Rods; **Charge (zeta potential):** +ve (+40 mV for CTAB-AuNPs and +35 mV for PAH-AuNPs in aqueous solution), −ve (−45 mV for PAA-AuNPs in aqueous solution; all changed to −20 mV in serum protein) | $4x10^{-4}$ µM | 96 h | MTT | Cytotoxicity observed by CTAB-capped Au nanorods was caused by free CTAB in solution, and not the shape and metal (Au or Ag) ions. Over-coating the CTAB capped rods with PAA or PAH (regardless of charge) reduced the toxicity. | Alkilany *et al.* (2009) |
| HeLa cells | **SC:** PEG and MPA (AuNP-MPA-PEG); **Size:** 3.7 nm; **Shape:** Spherical; **Charge (zeta potential):** N/R | 0.08–100 µM | 6–72 h | MTT | Presence of the particles in the nucleus without obvious cytotoxicity. | Gu *et al.* (2009) |
| HeLa cells | **SC:** TPPMS, GSH; **Size:** 1.4 and 15 nm for TPPMS-AuNPs and 1.1 nm for GSH-AuNPs; **Shape:** Spherical; **Charge (zeta potential):** −ve (−42 mV for 1.4 TPPMS-AuNPs in distilled water; −48 mV | 5600 µM | 48 h | MTT, flow cytometry, fluorescence microscopy and DNA gene arrays | 1.4 nm TPPMS-AuNPs was more toxic than the 15 nm NPs and the induced necrosis (1.4 nm) was by oxidative stress. The toxicity was reportedly dependant on the ability of | Pan *et al.* (2009) |

| | | | | | | |
|---|---|---|---|---|---|---|
| | for 1.4 TPPMS-AuNPs + GSH in NaOH and +25 mV in HCl solution) | | | | small-sized AuNPs to trigger the intracellular formation of ROS from dioxygen. GSH-AuNPs (1.1 nm) were less toxic than TPPMS-AuNPs, with no induction of oxidative stress. The reduced toxicity was linked to the presence of the thiol group in GSH. | |
| HDF-f cells | **SC:** Citrate; **Size:** 20 nm; **Shape:** Spherical; **Charge (zeta potential):** N/R | 10, 50, 100, 200, 300 µM | 72 h | MTT | No toxicity or cell death was observed up to 300 µM, but cell morphology was altered at increased concentrations. | Qu and Lu (2009) |
| PC-3 cells | **SC:** PEG; **Size:** 30-90 nm; **Shape:** Spherical, rod; **Charge (zeta potential):** −ve and +ve (−34 ± 1.3 mV, −30 ± 2.4 mV and −38 ± 0.3 mV for plain AuNPs at 30, 50 and 90 nm respectively; −22 ± 1.3 mV, | $1.5x10^{-3}$ µM | 88 h | MTT, LDH | No LDH leakage was observed up to 0.034 µM. Spherical and rod PEG-AuNPs (as high as $1.5x10^{-3}$ µM) did not affect proliferation of PC-3 cells over 88 h. | Arnida *et al.* (2010) |

| | | | | | | |
|---|---|---|---|---|---|---|
| | −20 ± 2.0 mV and −18 ± 3.3 mV for spherical PEG-AuNPs at 30, 50 and 90 nm core sizes respectively; +24 ± 1.0 mV +17 ± 2.2 mV for rod PEG-AuNPs 10×35 and 10×45 nm core sizes, respectively) | | | | | |
| A549 cells | **SC:** Citrate; **Size:** 15 nm; **Shape:** N/R; **Charge (zeta potential):** N/R | 200-2000 µM | 4 h and 24 h | Real-time PCR, ELISA | No observed adverse effects – oxidative stress and inflammatory cytokines were not induced. | Brandenberger *et al.* (2010) |
| MRC-5 cells | **SC:** FBS; **Size:** 20 nm; **Shape:** N/R; **Charge (zeta potential):** −ve (−11.3±1.1 mV) | 0.001 µM | 72 h | Oxidative stress PCR array, Lipid hydroperoxide assay, Western blotting | Lipid peroxidation and oxidative damage were noted. Up-regulation of antioxidants, stress response genes, and protein expression were observed. | Li *et al.* (2010) |
| Dendritic cells from | **SC:** Citrate; **Size:** 10 nm; **Shape:** Spherical; **Charge (zeta potential):** −ve (−13 mV) | 500 µM | 4 h, 24 h and 48 h | Flow cytometry | Non-toxic and no activation of dendritic cells. | Villiers *et al.* (2010) |

| | | | | | | |
|---|---|---|---|---|---|---|
| C57BL/6 mice | | | | | | |
| VERO cells | **SC:** Porphyran; **Size:** 14 nm; **Shape:** Spherical; **Charge (zeta potential):** −ve (−31 mV) | 10, 50 or 100 µM | 24 h | MTT | No toxicity. | Venkatpurwar *et al.* (2012) |
| PC-3 and MCF-7 cells | **SC:** Citrate, starch, gum Arabic; **Size:** 20 and 21 nm; **Shape:** N/R; **Charge (zeta potential):** −ve (−30 to −35 mV for citrate-, starch- and gum Arabic-AuNPs) | *20, 50, 80, 110, and 140 µg/mL | 24 h | MTT, LDH and neutral red cell assay | At high concentrations, citrate-stabilised AuNPs showed significant cytotoxicity compared to starch- and gum Arabic-stabilised AuNPs. This was due to the acidic nature of citrate. The phytochemicals within starch and gum Arabic contributed to the non-toxicity of the AuNPs. | Vijayakumar and Ganesan (2012) |
| HEp-2 cells | **SC:** N/R; **Size:** 3, 10, 25, and 50 nm; **Shape:** Spherical; **Charge (zeta potential):** −ve (−38.2 mV for 3 nm, −49 mV for 10 nm, −34 mV for 25 nm, −40 mV for 50 nm) | *0.5 to 50 µg/mL | 1, 2, 4, 12, and 24 h | MTT | 3 and 10 nm AuNPs induced significant toxicity, as small-sized AuNPs effectively entered the cytoplasm and nucleus, thereby damaging the cellular and nuclear membranes - this indicates size-dependent toxicity. | Boyoglu *et al.* (2013) |

| | | | | | | |
|---|---|---|---|---|---|---|
| Balb/3T3 cells | **SC:** Citrate; **Size:** 5, and 15 nm; **Shape:** N/R; **Charge (zeta potential):** −ve (−26 ± 11 mV for 5 nm, −30 ± 12 mV for 15 nm) | 10 to 300 µM | 2, 24 and 72 h | CFE | 5 nm AuNPs induced cytotoxicity at 72 h (at ≥ 50 µM), whereas no toxicity was observed for 15 nm AuNPs at all concentrations tested. This indicates size-dependent toxicity. | Coradeghini *et al.* (2013) |
| HepG2 cells | **SC:** Citrate and MUA; **Size:** 20 nm; **Shape:** Spherical; **Charge (zeta potential):** −ve (− 44.7+7.5 mV for Cit-AuNPs; - 37.3+8.4 mV for MUA-AuNPs) | 0–200 µM | 24 h, 72 h | MTT, LDH and comet assay | No significant cytotoxicity; DNA damage was observed with lower concentrations of Cit- but not with MUA-AuNPs. | Fraga *et al.* (2013) |
| MCF-7, PC-3 and CHO22 cells | **SC:** Citrate; **Size:** 3, 5, 6, 8, 10, 17, 30 and 45 nm; **Shape:** N/R; **Charge (zeta potential):** N/R | *10, 40, 70, 100, and 130 µg/mL | 24 h, 72 h | MTT, LDH and neutral red cell assay | 3 nm, 8 nm, and 30nm AuNPs caused cell death within 24 h at higher concentrations, whereas 5 nm, 6 nm, 10 nm, 17 nm, and 45nm AuNPs were non-toxic up to three- to four-fold higher concentrations at 72 h. | Vijayakumar and Ganesan (2013) |
| THP-1 cells | **SC:** Citrate, Chitosan (CHIT-L and CHIT-H); **Size:** 10 nm, sizes of chitosan- | *0.8–3.2 and 0.6–2.5 µg/ml | 4 and 24 h | LDH and CTB | Chitosan-functionalised AuNPs induced cytotoxicity and pro-inflammatory | Boyles *et al.* (2015) |

| | | | | | | |
|---|---|---|---|---|---|---|
| | AuNPs was 7 nm; **Shape:** N/R; **Charge (zeta potential):** −ve (−45 ± 0.2 mV for citrate-AuNPs) and +ve (+23±1.0 mV and +65 ± 1.0 mV for CHIT-L- and CHIT-H-AuNPs respectively) | | | | responses. This indicates charge-dependent toxicity. | |
| INT-407 cells | **SC:** Citrate; **Size:** 5 to 15 nm; **Shape:** Spherical; **Charge (zeta potential):** −ve (−3.37 ± 0.28 mV). | *4, 8 and 13 µg/mL | 24 h, 7 days | WST-1, LDH, MTT and $H_2$DCFDA | No cytotoxic effects on cells in terms of inhibition of cell proliferation, membrane damage, and oxidative stress after short term (24 h) exposure up to 13 µg/mL. Exposure at 7 days revealed potential toxicity at high concentrations (13 µg/mL). The toxicity is dependent on exposure time and concentration. | Jo *et al.* (2015) |
| HUVECs | **SC:** Citrate; **Size:** 12 nm; **Shape:** N/R; **Charge (zeta potential):** −ve (− 30 mV to − 10 mV in biological medium). | *0.5 µ g/mL to 64 µ g/mL | 24 h, up to 2 months | Calcein Am/Ethidium homodimer staining and MTT assay | There was a significant decrease in cell viability after 24 hr at higher concentrations (> 8 µ g/mL) in 5 % serum-containing | Gunduz *et al.* (2017) |

| | | | | | | |
|---|---|---|---|---|---|---|
| | | | | | medium. In 10 % serum-containing medium, cell viability was higher at higher concentrations than in 5 % serum-containing medium. Over two months, there was no cell death or ROS formation after accumulation of AuNPs, but there was elevated endoplasmic reticulum stress, which tends to reduce as the AuNPs taken up were depleted. | |

A549 (Human alveolar epithelial-like cell); Au-CHIT-H (Surface densities of 0.1 wt% Chitosan in solution); Au-CHIT-L (Surface densities of 0.001 wt% Chitosan in solution); Balb/3T3 (mouse fibroblast cell line); C57BL/6 (C57 black 6); CFE (colony forming efficiency); CHO22 (Chinese hamster ovary); CTAB (Cetyltrimethylammonium bromide); CTB (CellTiter-Blue®); ELISA (Enzyme-linked immunosorbent assay); FBS (Fetal bovine serum); GSH (Glutathione); $H_2$DCFDA (carboxy-2',7'-dichlorofluorescein diacetate); HDF-f (Human dermal fibroblast-Fetal); HeLa (Human cervical cancer cells); HEp-2 (Human epithelial type 2); HepG2 (Human liver cells); HT-29 (Human colon carcinoma cells); HUVECs (Human umbilical vein endothelial cells); IgG (Immunoglobulin G); INT-407 (Human intestinal cells); LDH (Lactate dehydrogenase); MCF-7 (Human breast adenocarcinoma cell line); MPA (3-mercaptopropionic acid); MRC-5 (human lung fibroblasts); MTT (3-(4,5-dimethylthiazolyl-2)-2,5-diphenyltetrazolium bromide); MUA (11-mercaptoundecanoic acid); N/R (not reported); PAA (polyacrylic acid); PAH (polyelectrolyte poly(allylamine) hydrochloride); PC-3 (Human prostate cancer cell lines); PCR (Polymerase chain reaction); PEG (Polyethylene glycol); SC (Surface coating); THP-1 (Human monocytic cell line); TPPMS (Triphenylphosphine monosulfonate); VERO (Normal monkey kidney cell line); WST-1 (water-soluble tetrazolium-1); *values were reported in mass concentrations, not in molar concentration (μM).

The various toxicities observed are dependent on the size, charge, surface coating, assay type and time of exposure (Table 2.1). For instance, large-sized citrate-AuNPs (> 5 nm) were not toxic to cells - the negative charge on the citrate causes the particles to repel the negatively-charged cell membranes (Boyles *et al.*, 2015). Small-sized AuNPs are obtained from a higher concentration of sodium citrate used in the synthesis (Qu and Lu, 2009; Chen and Wen, 2011), leading to increased acidity of the citrate-AuNPs, hence toxicity. It is suggested that the amount of sodium citrate be reduced to the level at which the stability and safety of AuNPs are guaranteed, depending on the desired size of the AuNPs under investigation. The results of cell-based toxicity could also be influenced by the type of assay employed (Vijayakumar and Ganesan, 2013). Surface modifications of AuNPs with agents, such as biomolecules, ligands, and polymers, also contribute largely to the reduction in the toxicity of AuNPs, irrespective of the size. This could result from the exchange of citrate on the surface of AuNPs with these ligands or biomolecules (Pan *et al.*, 2009; Simpson *et al.*, 2011).

Generally, the disadvantages of using cell-based assays include: (1) the genome and the proliferation pattern of commonly used tumour cell lines are not comparable with normal, healthy cells; and (2) the metabolism, routes of exposure and organ-specific toxicity of intact animals cannot be mimicked in cell culture (Pan-Bartneck, 2010). This approach does not represent the complexity and defence system of the whole organism, as it only reveals the toxicity at a cellular level (Joubert *et al.*, 2013) which may not correspond to animal-based results (Jia *et al.*, 2017). In view of this and other reasons, animal-based models should be more emphasised in the final analysis of AuNPs toxicity (Jia *et al.*, 2017), although the cell culture model provides initial basic toxicity information.

*2.3.2.2.1.2 Human Embryonic Stem Cells (hESCs)*

Advantages of using hESCs with reference to other systems (e.g. animal-derived) include: (1) the unlimited self-renewal capabilities and continuous growth of hESCs in culture; (2) the ability of these cells to differentiate into various specialised cell types over an extended period of time;

and (3) the ability to prevent interspecies variability, which makes this a more suitable model in predicting human responses to toxins (Senut *et al.*, 2016).

The effect of different conjugating agents with AuNPs of varying sizes (1.5 nm Thiolate-, 4 nm mercaptosuccinic acid (MSA)- and 14 nm citrate-AuNPs) on hESCs was determined (Senut *et al.*, 2016). Cells exposed to 1.5 nm naked AuNPs (0.1 µg/ml) disintegrated into single cells within 48 h, suggesting cell death; 1.5 thiolate-AuNPs (0.1 µg/ml) was toxic to hESC; 4 nm MSA-AuNPs decreased DNA methylation while DNA hydroxymethylation increased. The 14 nm citrate-AuNPs did not produce any significant toxic effects on the hESCs at concentrations as high as 10 µg/ml. This is size- and surface chemistry-dependent toxicity, as small-sized particles presented adverse effects on hESCs, with no significant toxicity with citrate-capped AuNPs.

This is the first report on the use of hESCs to evaluate the toxicity of AuNPs. It is therefore suggested that more studies, including the use of hESCs at different concentrations and surface groups of the AuNPs, be performed.

2.3.2.2.2 Determination of the in vivo toxicity of AuNPs

The pharmacokinetics and safety of AuNPs should be evaluated in laboratory animals (including zebrafish, mice and rats) prior to application in humans. It is thus crucial to understand interspecies differences in the pharmacokinetics of NPs before generated data in laboratory animals can be used to establish comparisons in humans (Lin *et al.*, 2016a).

*2.3.2.2.2.1 Studies using the zebrafish model*

The zebrafish (*Danio rerio*) is a widely used vertebrate model for toxicity studies. Various characteristics, such as small size, easy maintenance, transparency of embryos and the requirement of low amounts of testing compounds, makes zebrafish suitable for use as an *in vivo* screening model. Several zebrafish embryos can easily be acquired, where critical organs may be

fully developed within 7 days. The larvae are transparent, thereby enabling easy visualization of the internal organs and tissues (Crawford *et al.*, 2008).

Studies have indicated some similarities between zebrafish and humans, including: 1) diploid genome structure (Barbazuk *et al.*, 2000; Lieschke and Currie, 2007); 2) heart rates, action potential shape and duration, as well as electrocardiogram (ECG) morphology (Verkerk and Remme, 2012); and 3) drug metabolism - similar phase I and phase II metabolism, which may be attributed to the highly conserved genetic expression profiles in the liver (Lam *et al.*, 2006; Hung *et al.*, 2012).

The zebrafish model, though more complex than cultured cell models, is invasive and less expensive than large-scale biocompatibility studies in rats or mice (Rizzo *et al.*, 2013). Few studies have, however, been reported using this model (Table 2.2).

**Table 2.2:** Effect of AuNPs on zebrafish

| Model used | AuNPs characteristics | Exposure; Dose/concentration | Time of exposure | Parameters investigated for toxicity | Findings | Ref. |
|---|---|---|---|---|---|---|
| Zebrafish embryos | **SC:** TMAT; **Size:** 1.3 nm; **Shape:** Spherical; **Charge (zeta potential):** +ve (N/R) | Waterborne; 100 µL 80 - $5x10^4$ µg/L | 5 days | Behavioural activity assessment; apoptosis using the AO staining and TUNEL assay; gene expression by qRT-PCR; IHC of transcription factors regulating eye and pigmentation development. | Disruption of the progression of eye development and pigmentation, as well as embryonic mortality. The toxicity was due to covalent addition of the positively-charged TMAT on the AuNPs surface. | Kim *et al.* (2013) |

| | | | | | | |
|---|---|---|---|---|---|---|
| Zebrafish embryos | **SC:** TMAT, MES and MEEE; **Size:** 1.5 nm; **Shape:** N/R; **Charge (zeta potential):** −ve (−13.3 mV for MES-AuNPs), +ve (+8.71 mV for TMAT-AuNPs, and +2.91 mV for MEEE-AuNPs) | Waterborne; 100 µL 0 - 250 µg/L | 48 h | Gene expression by qRT-PCR | Pathways involved in inflammation and immune responses were affected. Embryo mortality was induced by TMAT-AuNPs, with no mortality after exposure to MES- and MEEE-AuNPs. Sub-lethal malformations were observed when exposed to MES-AuNPs, with no adverse responses on exposure to MEEE-AuNPs. The toxicity was attributed to surface chemistry. | Truong *et al.* (2013) |
| Adult zebrafish | **SC:** Citrate; **Size:** 14 nm; **Shape:** Spherical; **Charge (zeta potential):** −ve (−50 mV) | $1.6x10^4$ and $5.5 x10^4$ µg/kg dry weight; 0.25 and 0.8 µg/L released in water column | 20 days | Brain and muscle AChE activity; genotoxicity analysis by RAPD-PCR, and gene expression using RT-PCR | Modifications of genome composition, gene expressions, and DNA alterations were observed, as well as increased activity of acetylcholinesterase. | Dedeh *et al.* (2015) |

| | | | | | | |
|---|---|---|---|---|---|---|
| Adult zebrafish | **SC:** Mannose; **Size:** 16.5 ± 2.0 nm (spherical), 47.6 ± 3.0 × 12.3 ± 1.5 nm (Rod), 42.3 ± 2.5 × 16.1 ± 1.0 (nanostar); **Shape:** spherical, nanorod, and nanostar; **Charge (zeta potential):** −ve (−22 ± 1.2 and −27.5 ± 1.0 mV for spherical and nanostar, respectively, in water; −16.8 ± 0.3 and −6.9 ± 0.5 mV, respectively, in DMEM); +ve for nanorod (30.9 ± 1.3 mV in water, and 5.42 ± 0.6 mV in DMEM) | Intraperitoneal; 2 µl contain 5 µg/g single dose | 120 h | Mortality test | No toxicity was observed up to 120 h | Sangabathuni *et al.* (2017) |

AChE (Acetylcholinesterase); AO (Acridine orange); DMEM (Dulbecco's Modified Eagle's Medium); IHC (Immunohistochemistry); MEEE (2-(2-(2-mercaptoethoxy)ethoxy)ethanol); MES (2-mercaptoethanesulfonic acid); qRT-PCR (Quantitative real-time polymerase chain reaction); N/R (Not reported); RAPD-PCR (random amplified polymorphic DNA- polymerase chain reaction); SC (Surface coating); TMAT (N,N,N-trimethylammoniumethanethiol); TUNEL (Terminal deoxynucleotidyl transferase-mediated dUTP nick-end labelling).

The toxicity of AuNPs could result from covalent modification of AuNPs with ligands, although there was no toxicity with the ligand (TMAT) alone on the embryo (Table 2.2). This describes the role of surface chemistry on the toxicity of AuNPs. Larger-sized citrate-AuNPs (> 5 nm) can be considered non-toxic to cells when compared to the toxicity observed with adult zebrafish. The difference might be longer exposure period (20 days) of the AuNPs to zebrafish.

The zebrafish embryo assay is not a representative replacement for other *in vivo* models, such as mice and rats, but it is suitable as an intermediate screening tool between preliminary toxicity assessments in cells and more detailed and translationally relevant follow-up toxicity assessments in higher organisms (Rizzo *et al.*, 2013).

*2.3.2.2.2.2 Studies using mice as an in vivo model*

Mice, another *in vivo* model used in toxicity screening of AuNPs, have several advantages. These include closer similarities to human in all mammalian organs and physiological features, possibilities of performing pharmacokinetic and toxicokinetic studies, as well as easy access and possibilities of withdrawing more blood for analyses (Vliegenthart *et al.*, 2014). Conflicting results have been reported on the toxicity of AuNPs, which could be due to differences in size, surface chemistry, surface charge, dose and route of administration, using the *in vivo* mouse model (Table 2.3).

**Table 2.3:** Effect of AuNPs in mice

| Model used | AuNPs characteristics | Route of administration; Dose | Time of exposure | Parameters investigated for toxicity | Findings | Ref. |
|---|---|---|---|---|---|---|
| Male BALB/c mice | **SC:** Citrate; **Size:** 3, 5, 8, 17, 12, 37, 50, and 100 nm; **Shape:** Spherical; **Charge (zeta potential):** N/R | Intraperitoneal; 8000 µg/kg/week | 21 days | Animal behaviour, body weight assessment, and mortality; tissue histopathology using H&E staining followed by *ex vivo* imaging of tissues by CARS Microscopy. | 8 to 37 nm induced death, with abnormalities in the liver, lung and spleen. The 3 and 5 nm size AuNPs did not produce toxicity. | Chen *et al.* (2009) |
| Male BALB/c mice | **SC:** PEG; **Size:** 13 nm; **Shape:** Spherical; **Charge (zeta potential):** N/R | Intravenous; Single injection of 170, 850 or 4260 µg/kg | 5 min, 30 min, 4 h, 24 h, or 7 days | Detection of apoptosis by TUNEL assay; mRNA expression of adhesion molecules (*E-selectin* and *ICAM-1*), chemokines (*MCP-1*, *MIP-1α*, *MIP-1β* and *CCL-5*), and cytokines (*IL-1β*, *IL-6*, *IL-10*, and *TNF-α*) by RT-PCR; liver histopathology by H&E staining. | Acute inflammation and apoptosis by AuNPs was observed in the liver in a dose-dependent manner. | Cho *et al.* (2009a) |
| Male BALB/c mice | **SC:** PEG; **Size:** 4 and 100 nm; **Shape:** | Intravenous; A single injection of 4260 µg/kg | 5 min, 30 min, | Liver microarray analysis of apoptosis, cell cycle, inflammatory and | No histopathological changes in the liver, but the PEG-AuNPs | Cho *et al.* (2009b) |

| | | | | | | |
|---|---|---|---|---|---|---|
| | Spherical; **Charge (zeta potential):** N/R | | 4 h, 24 h, or 7 days | immune response, and metabolic process genes by GeneSifter® microarray data analysis system; apoptosis and inflammatory/immune responses by qRT-PCR, and tissue histopathology by H&E staining. | influenced apoptosis, cell cycle, inflammation, and metabolic processes in the liver after 30 min of injection. | |
| Male C57BL/6J mice | **SC:** N/R; **Size:** 20 and 100 nm; **Shape:** N/R; **Charge (zeta potential):** N/R | Intravenous; Single dose of $1x10^6$ µg/kg | 7 days | TUNEL assay was performed to detect apoptosis; tissue histopathology by H&E staining. | 20 nm AuNPs passed through the blood–retinal barrier but did not induce retinal toxicity, 100 nm AuNPs were not detected in the retina. | Kim *et al.* (2009) |
| Male C57BL/6 mice | **SC:** Citrate; **Size:** 12.5 nm; **Shape:** regular; **Charge (zeta potential):** − ve **(**−53 mV) | Intraperitoneal; 40, 200, and 400 µg/kg/day | 8 days | Behavioural examination, body and organ weights; serum biochemical analysis (TBIL and ALP for liver function, and UA, BUN, CREA for kidney function); haematological parameters (RBC, WBC, HB, HCT, MCV, MCH, MCHC, RDW, LYM, NEU, | No evidence of toxicity was observed. | Lasagna-Reeves *et al.* (2010) |

| | | | | | | |
|---|---|---|---|---|---|---|
| | | | | MON, EOS, BAS, and PLT); tissue histopathology using H&E staining. | | |
| Male ICR mice | **SC:** Citrate; **Size:** 13.5 nm; **Shape:** Spherical; **Charge (zeta potential):** N/R | Oral; 200 µl at 137.5, 275, 550, 1100 and 2200 µg/kg/day | 14 days | Body and organ weights; haematological parameters (HCT, HB, PLT, RBC, and WBC). | No apparent toxicity at low concentrations (137.5–275 µg/kg). Decreased body weight, RBC levels, and HCT were observed at high concentrations (550–1100 µg/kg). | Zhang *et al.* (2010) |
| Male ICR mice | **SC:** Citrate; **Size:** 13.5 nm; **Shape:** Spherical; **Charge (zeta potential):** N/R | Oral, Intraperitoneal and Intravenous; 1100 µg/kg/day | 28 days | Body and organ weights; haematological parameters (HCT, HB, PLT, RBC, and WBC). | Highest toxicity was observed in oral and intraperitoneal administration routes, while the intravenous (tail vein) route showed the lowest toxicity. | Zhang *et al.* (2010) |
| Male mice | **SC:** PEG; **Size:** 5, 10, 30 and 60 nm; **Shape:** Spherical; **Charge (zeta potential):** − ve (−2.96, −1.55, −1.97, | Intraperitoneal; A single dose of 4000 µg/kg | 28 days | Body and organ weights; haematological parameters (HCT, HB, PLT, RBC, WBC, MCV, MCH, and MCHC); biochemical parameters (ALT, AST, BUN, GLOB, CREA, TP, ALB, and TBIL). | Damage to the liver with 10 and 60 nm, as revealed by significant increases in the activities of ALT and AST; Damage to the kidney with 60 nm, as revealed by the significant decrease in | Zhang *et al.* (2011) |

| | | | | | | |
|---|---|---|---|---|---|---|
| | and −1.65 mV for 5, 10, 30 and 60 nm respectively) | | | | the level of CREA; Increased WBC and RBC counts in 10 and 60 nm indicates an inflammatory response and effect on the haematopoietic system, respectively. | |
| Male mice | **SC:** PEG; **Size:** 15 nm; **Shape:** Spherical; **Charge (zeta potential):** N/R | Intravenous; Single dose of 5000 µg/kg | 1 or 7 days. | Apoptotic response was determined with TUNEL analysis; total RNA by qRT-PCR analysis; histological analysis with Oil red O and H&E staining; biochemical analysis (ALT, AST, TP, ALB, CAT, SOD, GPx); cytochrome C levels in the livers with immunoblot assay; lipid peroxidation by immunofluorescence staining using antibody against 4-HNE. | Liver damage was observed. | Hwang *et al.* (2012) |
| Swiss male mice | **SC:** Citrate; **Size:** 50 nm; **Shape:** | Acute: Intravenous (Single | Acute (6, 12, 24, 48 and | Physical observation; urinalysis; biochemical parameters (AST, LDH, | Toxicity was observed in both exposures, most especially with higher | Sengupta *et al.* (2013) |

| | | | | | | |
|---|---|---|---|---|---|---|
| | Spherical; **Charge (zeta potential):** N/R | injection of 1000, 2000 and 10000 µg/kg; Chronic: Intraperitoneal (1000 and 2000 µg/kg/day) | 72 h); Chronic (15, 30, 60 and 90 days) | urea, and creatinine); haematological analysis (RBC, HB, WBC and differential WBC); tissue histopathology by H&E staining. | doses (2000 and 10000 µg/kg), while mortality was recorded during the chronic study (2000 µg/kg). The toxicity was dose-, time- and exposure frequency-dependent. | |
| Male mice | **SC:** Citrate; **Size:** 21 nm; **Shape:** Spherical; **Charge (zeta potential):** N/R | Intraperitoneal; Single dose of 7850 µg/kg | 1 h, 24 h and 72 h | Food intake, body and organ weights; biochemical analysis (ALT, blood glucose, and urinalysis); morphology of the kidney by H&E staining; mRNA expression by qRT-PCR. | No detectable toxicity to vital organs; results correlated with significant fat loss and inhibition of inflammatory effects. | Chen *et al.* (2013a) |
| Male and female mice | **SC:** PEG; **Size:** 4.4, 22.5, 29.3, and 36.1 nm; **Shape:** Spherical; **Charge (zeta potential):** −ve (−6.01, −1.92, −1.89, and −0.98 mV for | Intraperitoneal; 4000 µg/kg | Injection every 2 days for 28 days | Body and organ weights; biochemical parameters (ALT, AST, BUN, CREA, TP, ALB, GLOB, TBIL); haematology (WBC, RBC, HCT, MCV, HB, PLT, MCH, and MCHC); tissue histopathology by H&E staining. | More significant liver toxicity in male mice as revealed by significant increases in the levels of ALT and AST; possibilities of infection in male mice, as revealed by significant increases in WBC and RBC counts; no | Chen *et al.* (2013b) |

| | | | | | | |
|---|---|---|---|---|---|---|
| | 4.4, 22.5, 29.3, and 36.1 nm respectively) | | | | significant toxicological response in the reproductive system in both female and male mice. | |
| Male mice | **SC:** Citrate; **Size:** 10 nm; **Shape:** Spherical; **Charge (zeta potential):** N/R | Intraperitoneal; $2.5x10^4$, $5x10^4$ and $1x10^5$ µg/kg/day | 14 days | Body weights; biochemical assay ALT and AST); haematological parameters (WBC, RBC, HB, PLT, HCT, MCV, MCH, MCHC, RDW). | Significant increase in the RBC count and AST levels in the $5x10^4$ µg/kg/day, which is an indication of toxicity. | Ghahnavieh *et al.* (2014) |
| Male Crl:CD1(ICR) mice | **SC:** Tween® 20; **Size:** 20 nm; **Shape:** Spherical; **Charge (zeta potential):** − ve (− 23.2mV) | Intravenous; Acute (Single injection of 100, 250, 500, 750, 1,000, 1,250, 1,500, 1,750, and 2,000 µg/kg); Sub-chronic (1,100 µg/kg/day) | 14 days; 21 days | Body and organ weights; biochemical assays (ALT, AST, and BIL); haematological parameters (RBC, HB, WBC, LYM, MON, NEU, HCT, and PLT); histology of the liver and decalcified bone was performed using H&E staining. | No severe clinical or behavioural alteration at all concentrations in the acute toxicity test. In the sub-chronic test, it was found to be hepatotoxic. | Berce *et al.* (2016) |
| Male BALB/c mice | **SC:** PEG; **Size:** 10, 30 and 50 nm; **Shape:** Spherical shape | Tail vein (Intravenous); 400 µg/kg/day for 14 days | 2 weeks, 4 weeks and 12 weeks, | Heart weight to body weight ratio, and two-dimensional echocardiography was | No effect on cardiac systolic function, and no cardiac fibrosis or infiltration of | Yang *et al.* (2016) |

| | | | | | | |
|---|---|---|---|---|---|---|
| | observed (As seen on the TEM image provided); **Charge (zeta potential):** N/R | | | performed to examine cardiac structure; Sirius red staining to detect cardiac interstitial collagen; IHC to detect inflammatory cells; histopathology of the heart using H&E staining; expression of collagen I gene by RT-PCR | inflammatory cells by the three sizes; 10 nm AuNPs for 2 weeks resulted in reversible cardiac hypertrophy, 30 and 50 nm AuNPs did not affect cardiac size over 12 weeks; administration of 50 nm AuNPs for 12 weeks decreased the synthesis of collagen, while 10 and 30 nm AuNPs did not affect collagen synthesis. | |

4-HNE (4-hydroxy-2-nonenal); ALB (Albumin); ALP (Alkaline phosphatase); ALT (Alanine transaminase); AST (Aspartate transaminase); BALB/c (Bagg albino); BAS (Basophils); BIL (Bilirubin); b.w. (Body weight); BUN (Blood urea nitrogen); C57BL/6, (C57 black 6); C57BL/6J (C57 black 6, from Jackson Lab); CARS (Coherent Anti-Stoke Raman Scattering); CAT (Catalase); *CCL-5* (Chemokine ligand 5); CREA (Creatinine); DPBS (Dulbecco's phosphate buffered saline); EOS (Eosinophils); GLOB (Globulin); GPx (Glutathione peroxidase); HCT (Haematocrit); H&E (Haematoxylin and eosin); HB (Haemoglobin); *ICAM-1* (Intercellular Adhesion Molecule 1); ICR (Institute for Cancer Research); IHC (Immunohistochemistry); *IL-1β* (Interleukin-1β), *IL-6* (Interleukin-6); *IL-10* (Interleukin-10); LDH (Lactate dehydrogenase); LYM (Lymphocytes); MCH (mean corpuscular haemoglobin); MCHC (mean corpuscular haemoglobin concentration); *MCP-1* (Monocyte chemoattractant protein-1/); MCV (mean corpuscular volume); *MIP-1α* (Macrophage Inflammatory Protein 1 alpha); *MIP-1β* (Macrophage Inflammatory Protein-1 beta); MON (Monocytes); mRNA (Messenger ribonucleic acid); NEU (Neutrophils); N/R (Not reported); PEG (Polyethylene glycol); PLT (Platelets); qRT-PCR (Quantitative real time-polymerase chain reaction); RBC (Red blood cells); RDW (red cell distribution width); SC (Surface coating); SOD (Superoxide dismutase); TBIL (Total bilirubin); TEM (Transmission electron microscope); *TNF-α* (Tumour necrotic factor-*α*); TP (Total protein); TUNEL (Terminal deoxynucleotidyl transferase dUTP nick end labelling); UA (Uric acid); UN (Urea nitrogen); WBC (white blood cells).

Large-sized (> 5 nm) citrate-AuNPs were toxic to mice (Table 2.3), most of which were injected intraperitoneally and at high doses. Intravenous injection of large-sized PEG-AuNPs to mice resulted in toxicity, and could be due to high doses of particles injected and/or the molecular weight of PEG and/or the duration of exposure. This was compared with other reports with large-sized citrate-AuNPs, and even at repeated injections, no toxicity via oral, intraperitoneal or intravenous administrations were noted. This contradicts the report of Cho *et al.* (2009b), where toxicity was observed at the genetic level, 30 mins after intravenous injection of PEG-AuNPs (Table 2.3), of which the assay and duration of exposure of NPs must be considered.

*2.3.2.2.2.3 Studies using rats as an in vivo model*

Rats and pigs are more appropriate representative models of humans than mice in animal-to-human extrapolation of AuNPs pharmacokinetics, although the dose, size, age and/or species/strain/breed are factors as well (Lin *et al.*, 2016a). The spleen capillaries in rats and humans are both sinusoidal, where a large volume of blood flows through open-circulation routes with NP filtration at inter-endothelial cell slits, unlike the mouse spleen capillaries that are non-sinusoidal (Cesta, 2006). Further, the liver capillaries of mice, rats, pigs and humans are all sinusoidal with open fenestrae, but the average number of fenestrae per square micrometre in mice is lower than that of rats and humans (Braet and Wisse, 2002). In addition, there are other parameters, such as surface coating, corona formation, as well as physiological parameters, including organ weight fraction of body weight and plasma volume fraction of body weight, which greatly affects the pharmacokinetics of NPs (Lin *et al.*, 2016b). In these, most especially the physiological parameters, rats are closer to humans than mice (Lin *et al.*, 2016a). Several researchers have reported the toxicity of AuNPs using the rat model (Table 2.4).

**Table 2.4:** Effect of AuNPs in rats

| Model used | AuNPs characteristics | Route of administration; Dose | Time of exposure | Parameters investigated for toxicity | Findings | Ref. |
|---|---|---|---|---|---|---|
| Male Wistar-Kyoto rats | **SC:** N/R; **Size:** 10 and 50 nm; **Shape:** Spherical and hexagonal for 10 and 50 nm respectively; **Charge (zeta potential):** N/R | Intraperitoneal; 5 µg Au/rat/day | 3 or 7 days | Animal behaviour; and histopathological examination. | 10 nm AuNPs induced highest toxicity in liver and lung in relation to time exposure. Size-dependent toxicity was noted. | Abdelhalim (2012) |
| Male Wistar-Kyoto rats | **SC:** N/R; **Size:** 10, 20 nm and 50 nm; **Shape:** Spherical for 10 and 20 nm, and Hexagonal for 50 nm; **Charge (zeta potential):** N/R | Intraperitoneal; *(50 or 100 uL)/day | 3 or 7 days | Histopathology of the liver by H&E staining. | Nuclear destruction; alterations in the hepatocytes, portal triads and the sinusoids. | Abdelhalim and Jarrar (2012) |
| Male Wistar-Kyoto rats | **SC:** N/R; **Size:** 10 nm; **Shape:** N/R; **Charge (zeta potential):** N/R | Intraperitoneal; 5 µg Au/rat/day | 7 days | Oxidative stress markers (reduced GSH and MDA). | Lipid peroxidation in the liver, but not in the heart and lungs. | Khan *et al.* (2012) |
| Male Wistar rats | **SC:** N/R; **Size:** 20 nm; **Shape:** N/R; | Intraperitoneal; 20 µg/kg b.w. | 3 days | Oxidative stress parameters (MDA and GPx); DNA damage and | There was induction of oxidative stress, impairment | Siddiqi *et al.* (2012) |

| | | | | | | |
|---|---|---|---|---|---|---|
| | **Charge (zeta potential):** N/R | | | apoptosis markers (8-OHdG, Caspase-3, and Hsp70); neurotransmitters (Serotonin, dopamine, and GABA); inflammation marker (*IFN-γ*) | glutathione peroxidase in rat brain, and decreased dopamine and serotonin levels. | |
| Female Wistar rats | **SC:** Porphyran; **Size:** 14 nm; **Shape:** Spherical; **Charge (zeta potential):** − ve (− 31 mV) | Oral; *375, 750, and 1500 ppm/kg b.w./day | 28 days | Physical examinations; body and organ weights; biochemical parameters (ALT, AST, ALP, CHO, blood GLU, BIL, proteins, urea, CREA, $Na^+$, and $K^+$); haematological parameters (HB, RBC, WBC, DLC, and ESR); tissue histology by H&E staining | Non-toxic and no abnormalities (in body weight, haematology or biochemical parameters) recorded. | Venkatpurwar *et al.* (2012) |
| Male Wistar-Kyoto rats | **SC:** N/R; **Size:** 10 and 50 nm; **Shape:** Spherical for 10 nm, Hexagonal for 50 nm; **Charge (zeta potential):** N/R | Intraperitoneal; 22 µg/kg b.w. | Acute (1 day) and sub-chronic (5 days) | Expressions of proinflammatory cytokines genes (*IL-1β, IL-6,* and *TNF-α*) by qRT-PCR. | Increased proinflammatory cytokines, which returned to normal after repeated exposure. The 50 nm AuNPs produced a | Khan *et al.* (2013) |

| | | | | | | |
|---|---|---|---|---|---|---|
| | | | | | more severe inflammatory response when compared to 10nm AuNPs. | |
| Male Wistar rats | **SC:** N/R; **Size:** 5-10 nm; **Shape:** Spherical; **Charge (zeta potential):** N/R | Intraperitoneal; 5 mL solution containing 5, 10, and 100 µg Au/rat/day | 7 days | Biochemical parameters (BUN, UA, urea, CR); kidney histology by H&E staining. | Damage to the renal tubules. | Doudi and Setorki (2014) |
| Male Wistar rats | **SC:** Citrate, CALNN; **Size:** Citrate-AuNPs: 16.1 ± 2.8 nm, CALNN-AuNPs: 16.3 ± 2.8 nm; **Shape:** Spherical; **Charge (zeta potential):** -ve (Citrate-AuNPs: −49.4 ± 12.8, CALNN-AuNPs: −34.3 ± 12.8mV) | Intravenous; Single injection of ~0.7 mg/kg | Short- and long-term (30 min and 28 days) | Animal behaviour, food and water intake, body and organ weights; haematological analysis (RBC, HB, HCT, WBC, MCV, MCH, MCHC, RDW, PLT, PCT, PDW, and MPV); electrolyte balance ($Na^+$, $K^+$ and $Cl^-$). | Alterations in some haematological parameters, such as significant decreases in HGB, HCT levels, and the number of RBCs, as well as spleen atrophy were observed in rats injected with CALNN-AuNPs. The observed toxicity could be surface chemistry-dependent. | Fraga *et al.* (2014) |
| Male Wistar rats | **SC:** Citrate; **Size:** 10–25 nm; **Shape:** N/R; **Charge (zeta potential):** N/R | Oral; 20 µg/kg/day | 21 days | Body weight; biochemical parameters (ALT and AST for liver damage, urea and BUN | Toxic to the lung, liver and kidney. | Rathore *et al.* (2014) |

| | | | | | | |
|---|---|---|---|---|---|---|
| | | | | for kidney function, CPK-MB for myocardial injury); and tissue histopathology | | |
| Male Wistar rats | **SC:** Citrate, antibody (IgG); **Size:** 20 nm; **Shape:** N/R; **Charge:** – ve **(zeta potential):** –10.4 and –26.4 mV for citrate-AuNP, AuNP-IgG, respectively) | Intravenous; *1 mL 80 µg Au/mL (80 µg/rat) | Up to 2 h after injection | Inflammatory tests (leukocyte-endothelial interactions, neutrophils inflammatory functions by the expression of adhesion molecules, chemotaxis, and oxidative burst). | No toxicity (anti-inflammatory properties were observed). | Uchiyama *et al.* (2014) |
| Male Wistar Kyoto rats | **SC:** N/R; **Size:** 10 nm; **Shape:** Spherical; **Charge (zeta potential):** N/R | Intraperitoneal; #5 µg Au/kg rat /day (50 µL 100 µg/mL/ rat/day). | 3 or 7 days | Oxidative stress markers (GSH, GPx, GR, SOD, TAC, and MDA). | Disturbance in the natural balance between oxidative stress and antioxidant defence, which resulted in pathological effects. | Abdelhalim *et al.* (2015) |

| | | | | | | |
|---|---|---|---|---|---|---|
| Female Sprague Dawley rats | **SC:** Citrate; **Size:** 5 to 15 nm; **Shape:** Spherical; **Charge (zeta potential):** −ve (−3.37 ± 0.28 mV) | Oral; 325, 650 and 1300 µg/kg/day | 14 days | Body and organ weights; haematological parameters (RBC, HB, WBC, LYM, NEU, MON, EOS, BAS, HCT, MCV, MCH, MCHC, RET, PLT, PT, APTT); biochemical parameters (ALT, AST, ALP, ALB, TP, A/G, TBIL, CREA, BUN, TCHOL, TG, GLU, CA, IP, CK, Na, K, Cl); tissue histology by H&E staining. | No detectable toxicity. | Jo *et al.* (2015) |
| Male Wistar rats | **SC:** Silica; **Size:** 100 nm; **Shape:** N/R; **Charge (zeta potential):** N/R | Intraperitoneal; Single injection of 1100 µg/kg and exposure to static magnetic field (1 h/ day for 14 days) | 14 days | Oxidative stress and antioxidant markers (MDA, CAT, SOD, and GPx); tissue (lung) histopathology by H&E staining. | Oxidative damage observed in rat lung treated with AuNPs only, and more damage was observed when co-exposed with static magnetic field. This was due to the accumulation of AuNPs in the lung under magnetic environment. | Ferchichi *et al.* (2016) |

| | | | | | | |
|---|---|---|---|---|---|---|
| Male Sprague Dawley rats | **SC:** Citrate; **Size:** 14 nm; **Shape:** Spherical; **Charge (zeta potential):** −ve (−47 mV) | Intravenous; #0.9, 9 and 90 µg Au/rat (500 µL each) | 8 weeks | Physiological and behavioural indicators; body weight; biochemical assays (ALT, ALP, TBIL, CREA, BUN); tissue histopathology | No observed acute or sub-chronic toxicity. | Rambanapasi *et al.* (2016) |
| Male Wistar rats | **SC:** Citrate; **Size:** 20 nm; **Shape:** Spherical; **Charge (zeta potential):** −ve (− 30 mV) | Intraperitoneal; 2500 µg/kg/day or 2 days | 21 days | Biochemical assays (ALT, ALP, TP, liver and serum cholesterol and TG); oxidative stress markers (SOD, CAT, GPx, DCFH, NO, protein carbonyl, sulfhydryl, and ETC enzymes); tissue histopathology (H&E) | Every 24-h administration produced marked parenchymal changes, necrosis and leukocyte infiltration. No observed toxicity with every 48-h administration. | Muller *et al.* (2017) |

* - information not completed to calculate and report in µg/kg body weight (presented as reported); #exact weight of rat used not supplied to calculate the dose in µg/kg body weight of rat (weight ranges or other units were reported); 8-OHdG (8- hydroxydeoxyguanosine); A/G (Albumin/Globulin ratio); ALB (Albumin); ALT (Alanine aminotransferase); ALP (Alkaline phosphatase); APTT (Activated partial thromboplastin time); AST (Aspartate aminotransferase); BUN (Blood urea nitrogen); CA (Calcium); CALNN (Pentapeptide: cysteine–alanine–leucine–asparagine–asparagine); CAT (Catalase); CHO (Cholesterol); CK (Creatine kinase); $Cl^-$ (Chloride ion); CPK-MB (creatinine phosphokinase-MB); CR (Creatine); CREA (Creatinine); DCFH (Dichlorodihydrofluorescein); DLC (Differential leukocyte count); ESR (Erythrocyte sedimentation rate); ETC (Electron transport chain); GABA (Gamma amino-butyric acid); GPx (Glutathione peroxidase); GLU (Glucose); GR (glutathione reductase); GSH (glutathione); HCT (Haematocrit); H&E (Haematoxylin and eosin); HB (Haemoglobin); Hsp70 (Heat shock protein70); *IFN-γ* (Interferon-γ); *IL-1β* (Interleukin-1β); *IL-6* (Interleukin-6); IP (Inorganic phosphorus); $K^+$ (Potassium ion); MDA (Malondialdehyde); MCH (Mean corpuscular haemoglobin); MCHC (Mean corpuscular haemoglobin concentration); MCV (Mean corpuscular volume); MDA (Malondialdehyde); MPV (Mean platelet volume); $Na^+$ (Sodium ion); NO (Nitric oxide); N/R (Not reported); PCT (Plateletcrit); PDW (Platelet distribution width); PLT (Platelet); PT (Prothrombin time); qRT-PCR (Quantitative real time-polymerase chain reaction); RET (Reticulocyte); RBC (Red blood cells); RDW (Red cell distribution width); SC (Surface coating); SOD (Superoxide dismutase); TAC (Total antioxidant capacity); TP (Total protein); UA (Uric acid); WBC (white blood cells); TBIL (Total bilirubin); TCHOL (Total cholesterol); TG (Triglycerides); *TNF*-α (Tumour necrotic factor-α).

It was observed that citrate-capped AuNPs between 5 nm and 20 nm were non-toxic to rats via intravenous administration at low doses (Table 2.4).

*2.3.2.2.2.4. Studies using rabbits as an in vivo model*

The toxicological evaluation of AuNPs using the rabbit model (Table 2.5) has been reported. Sharma *et al.* (2011) suggested the safe use of polyethylenimine-conjugated AuNPs for the cornea and for corneal gene therapy, because of observed normalcy in rabbit eyes.

**Table 2.5:** Effect of AuNPs in rabbits

| Model used | AuNPs characteristics | Route of administration; Dose | Time of exposure | Parameters investigated for toxicity | Findings | Ref. |
|---|---|---|---|---|---|---|
| New Zealand white rabbits | **SC:** Citrate; **Size:** 5 nm, 25 nm; **Shape:** Spherical; **Charge (zeta potential):** N/R | Intravenous; 1000 µg/kg single dose | 24 h | Animal behaviour; biochemical analysis (ALT, AST, ALP, LDH, BIL, CREA, CK, and lipase); haematology (WBC, NEU, LYM, and PLT); tissue histology by H&E staining. | No morphological or histological evidence of acute toxicity. | Glazer *et al.* (2011) |
| New Zealand white female rabbits | **SC:** PEI2; **Size:** N/R; **Shape:** N/R; **Charge (zeta potential):** +ve (N/R) | Topical; #100 µl 150 mM | 12 h, 72 h, or 7 days | Apoptosis by TUNEL assay; IHC of CD11b antigen specific for activated granulocytes; eye examination with slit-lamp microscope. | No observed inflammation, redness, or oedema in rabbit eyes, indicating lack of toxicity of PEI2-AuNPs in corneal gene therapy. | Sharma *et al.* (2011) |
| New Zealand white male rabbits | **SC:** PEG; **Size:** 7 nm; **Shape:** Spherical; **Charge (zeta potential):** −ve (−12.3 mV) | Intravenous; 300 µg/kg single dose | 7 days | Haematology (RBC, HCT, HB, WBC and differential WBC count, MCV, MCHC); biochemical parameters (ALT, AST, GLU, ALB, GB, TP, CREA, BUN); tissue histology by H&E staining. | No obvious acute toxicity but inflammatory reactions in tissues, such as liver, lungs and kidneys, were observed. Mild to moderate changes in the serum biochemical and haematological parameters were also observed. | Bashandy *et al.* (2015) |

#exact weight of rabbit used not supplied to calculate the dose in µg/kg body weight of rat (weight ranges or other units were reported); ALB (Albumin); ALT (Alanine transaminase); ALP (Alkaline phosphatase); AST (Aspartate transaminase); BIL (Bilirubin); BUN (Blood urea nitrogen); CD11B (Cluster of differentiation molecule 11b); CK (Creatine kinase); CREA (Creatinine); GB (Globulin); GLU (Glucose); HCT (Hematocrit); H&E (Haematoxylin and eosin); HB (Haemoglobin); IHC

(Immunohistochemistry); LDH (Lactate dehydrogenase); LYM (Lymphocytes); MCHC (Mean corpuscular haemoglobin concentration); MCV (Mean corpuscular volume); NEU (Neutrophils); N/R (Not reported); PEG (Polyethylene glycol); PEI2 (polyethylenimine); PLT (Platelets); WBC (White blood cells); RBC (Red blood cells); SC (Surface coating); TP (Total protein); TUNEL (Terminal deoxynucleotidyl transferase dUTP nick end labelling).

It was observed that AuNPs between 5 nm and 25 nm are non-toxic to rabbits via intravenous administration at low doses (Table 2.5).

*2.3.2.2.2.5 Studies using Drosophila melanogaster as an in vivo model of toxicity*

The fruit fly, *Drosophila melanogaster*, is a well-established model for human disease (Auluck *et al.*, 2002; Kazantsev *et al.*, 2002; Pompa *et al.*, 2011), because the genes related to diseases in humans have functional homolog in *Drosophila melanogaster* (Pandey and Nichols, 2011). The effects of 15 nm citrate-capped AuNPs was studied by Pompa *et al.* (2011), using six concentrations (1.9, 3.8, 19, 38, 190, and 380 pmol/L) in the *Drosophila melanogaster* after ingestion. It was found that the AuNPs caused DNA fragmentation, significant over-expression of the stress proteins, as well as significant reduction of their life-span and fertility. This is the only report in this model to explore the toxicity of AuNPs.

2.3.2.2.3 *In ovo* assessment of the toxicity of AuNPs

*2.3.2.2.3.1 Studies using chicken embryo as a model of toxicity*

Chicken embryo has a rapid growth rate, and is independent of the mother (Ribatti, 2010). The embryo is highly sensitive to harmful factors (Heinz *et al.*, 2009) and has therefore been used as a model for cancer therapy research (Luyten *et al.*, 1993) and the development of new drug delivery systems (Vargas *et al.*, 2007). Only a few studies have recently been reported using the *in ovo* model (Table 2.6). The model is easily implemented and cost-effective, as it allows limited use of animals, but impossible to perform pharmacokinetic studies and no possibility of long-term studies when compared to *in vivo* model (Zabielska-Koczywas *et al.*, 2017).

**Table 2.6:** Effect of AuNPs on chicken embryos

| Model used | AuNPs characteristics | Route of administration; Concentration or Dose | Time of exposure | Parameters investigated for toxicity | Findings | Ref. |
|---|---|---|---|---|---|---|
| Chicken embryo (1 day old) | **SC:** AuNPs, HS; **Size:** 5-70 nm; **Shape:** Spherical (as viewed on the TEM image provided); **Charge (zeta potential):** N/R | Injection into egg (air sack); 500 µL 50 µg/mL (Naked); 0.032 µg/mL (HS) | 20 days of incubation | Mortality; body and organ weights; morphology by TEM and SEM; IHC; biochemical parameters and electrolytes (ALT, AST, ALP, LDH, TG, GLU, Chol-VLDL, Mg, Ca, and P); expression of *FGF-2* gene at protein level by PCR. | No effect on mortality and homeostasis of the embryos with AuNPs, but there were increased numbers of myocytes and nuclei in chicken embryo muscles with HS-AuNPs. | Zielinska *et al.* (2011) |
| Chicken embryo (3 days old) | **SC:** AuNPs, Taurine; **Size:** 10-30 nm; **Shape:** Spherical (as viewed on the TEM image provided); **Charge (zeta potential):** N/R | Injection into egg (air sack); 50 mg/L AuNP, 4.32 mg/mL taurine | 3 to 20 days of incubation | Gene expression by RT-qPCR, IHC, and ELISA methods; histology by van Gieson staining | Both naked and taurine-AuNP affected the number of muscle cells during development, though taurine exhibited the most significant effect; no significant interactions between AuNP and taurine were observed. | Zielinska *et al.* (2012) |

ALP (Alkaline phosphatase); ALT (Alanine aminotransferase); AST (Aspartate aminotransferase); Ca (Calcium); Chol-VLDL (Cholesterol-Very low-density lipoprotein); ELISA (Enzyme-linked immunosorbent assay); *FGF-2* (Fibroblast growth factor 2); Glu (Glucose); HS (Heparin sulfate); LDH (Lactate dehydrogenase); Mg (Magnesium); N/R (Not reported); P (Phosphorus); PCR (Polymerase chain reaction); qRT-PCR (Quantitative real time-polymerase chain reaction); SC (Surface coating); SEM (Scanning electron microscope); TEM (Transmission electron microscope); TG (Triglyceride).

Further research was suggested to elucidate the mechanism of muscle fibre enlargement (Zielinska *et al.*, 2011), as this is a model that serves as an intermediate between *in vitro* and *in vivo* studies (due to reduction in number of animals used in *in ovo*) (Zabielska-Koczywas *et al.*, 2017), to investigate the toxicity of AuNPs.

### 2.3.3 Assessment of gold nanoparticle toxicity

To date, there is no standard guideline for the assessment of the *in vivo* toxicity of NPs. This could result from the diverse characteristics and physicochemical properties exhibited by them. Researchers have investigated the *in vivo* toxicity of AuNPs through various methods (Tables 2.2 – 2.5). These include initial basic examinations, such as monitoring the physical and physiological changes, food and water intake, body weights and relative organ weights, biochemical and heamatological evaluations, assessment of oxidative stress and inflammation, as well as tissue histological examinations.

Food and water intake levels could be affected by exposure of animals to AuNPs (Fraga *et al.*, 2014). Changes in body and organ weights are important indices for assessing the effect of foreign substances in animals upon exposure. A significant reduction (more than 10%) in the initial body weight of the animal on exposure to foreign substances, could lead to mortality (Adewale *et al.*, 2016). The spleen plays an important role in immunity and maintenance of healthy blood cells, as it is part of the lymphatic system. Significant increases in the weight of the spleen is an indication of systemic toxicity (El-Nahas *et al.*, 2017). The ratio of heart weight to body weight is an important parameter to examine cardiac structure (Yang *et al.*, 2016). Citrate-AuNPs (14 nm) are distributed and accumulated mainly in the liver, spleen, and at lower concentration in the kidney (Rambanapasi *et al.*, 2016). It is therefore imperative to determine the toxicity of AuNPs in these organs.

Biosafety evaluations for NPs and drugs are determined by the liver and kidney toxicities, as these are the main metabolism and clearance organs (Kupffer cells of the hepatic sinusoid system and the renal glomerular basement membrane), and are fragile to toxic agents (Yang *et al.*, 2017b).

The liver is the primary target of foreign compounds as it is the site where these substances are metabolised and detoxified. It is the largest internal organ in the body, and performs three major functions (storage, metabolism, and biosynthesis). The liver consists of the sinusoidal system, containing specialised cells known as Kupffer cells, which ingest and catabolise toxic matter. These cells are designed to remove toxic substances, such as chemicals, dead cells, drugs, microorganisms and particulate debris from the bloodstream. Kupffer cells recognise NPs as foreign materials, which are internalised via receptor-mediated pathways, such as clathrin-mediated endocytosis, caveolin-mediated endocytosis, macropinocytosis, and additional endocytotic pathways (Zhang *et al.*, 2016).

These functions are affected in liver pathology caused by chemicals or other toxic foreign substances and infections. The integrity of the liver can be assessed by the liver damage markers, such as alanine aminotransferase (ALT), aspartate aminotransferase (AST), LDH, sorbital dehydrogenase (SDH) and glutamate dehydrogenase (GLDH); cholestatic-induction parameters including bilirubin, gamma-glutamyltranspeptidase (GGT), alkaline phosphatase (ALP), and 5′-nucleotidase (5′-NT); and liver function markers, which include albumin, total protein and bilirubin (Ramaiah, 2007).

#### *2.3.3.1 Liver damage markers*

The aminotransferases (ALT and AST) are the most widely used indicators of hepatocellular injury (Ramaiah, 2007; Wang *et al.*, 2016a). The aminotransferases are liver pyridoxal phosphate (PLP) – dependent enzymes, which are important in carbohydrate and amino acid metabolism, as they are involved in the catalysis of intermediary reactions of glucose and metabolism of proteins (Zareei *et al.*, 2017).

Alanine aminotransferase is predominantly found in the liver, localised in the cytosol. It catalyses the transfer of the amino group from alanine to α-ketoglutarate to produce L-glutamate and pyruvate (Reaction 2.1), which is subsequently converted to oxaloacetate by pyruvate decarboxylase or to acetyl coenzyme A by pyruvate dehydrogenase (Wang *et al.*, 2016a; Zareei *et al.*, 2017).

L- alanine + α-ketoglutarate $\xleftrightarrow{\text{ALT}}$ L- glutamate + Pyruvate Reaction 2.1

Aspartate aminotransferase is predominantly found in the liver, kidney, heart, brain and skeletal muscle (Kwo *et al.*, 2017). It is present in both the cytoplasm and mitochondria of cells and catalyses the transfer of the amino group from L-aspartate to α-ketoglutarate (α-oxoglutarate) to produce L-glutamate and oxaloacetate (Reaction 2.2). In a reaction catalysed by malate dehydrogenase (MDH), the oxaloacetate and reduced nicotinamide adenine dinucleotide (NADH) formed in the cytoplasm (transported into the mitochondria) are, respectively, reduced to L-malate, and oxidised to nicotinamide adenine dinucleotide ($NAD^+$) (Siddique *et al.*, 2016; Wang *et al.*, 2016a).

L- aspartate + α-ketoglutarate $\xleftrightarrow{\text{AST}}$ L- glutamate + Oxaloacetate Reaction 2.2

In healthy adults, the concentration of serum ALT and AST ranges from 5 to 35 U/L and 5 to 40 U/L, respectively. Any damage to tissues results in the leakage of these enzymes into the systemic circulation, causing increased serum concentrations (Abou Seif, 2016; Wang *et al.*, 2016a). Elevation in the level of AST without an increase in ALT levels is an indication of possible cardiac or muscle damage (Kwo *et al.*, 2017). Several studies used ALT and AST as markers of liver (tissue) toxicity upon exposure to AuNPs (Tables 2.3 – 2.5) (Venkatpurwar *et al.*, 2012; Zhang *et al.*, 2012; Abdelhalim and Abdelmottaleb Moussa, 2013; Chen *et al.*, 2013a; Chen *et al.*, 2013b; Ghahnavieh *et al.*, 2014; Magaye *et al.*, 2014; Rathore *et al.*, 2014; Jo *et al.*, 2015; Kunjiappan *et al.*, 2015; Berce *et al.*, 2016; Rambanapasi *et al.*, 2016; Wang *et al.*, 2016b).

#### *2.3.3.2 Cholestatic-induction parameters*

Gamma-glutamyltranspeptidase and ALP are commonly used in the detection of impaired bile flow when compared to 5'-NT, but these enzymes show minimal activity in normal liver tissues (Ramaiah, 2007). Gamma-glutamyltranspeptidase is present within the epithelial cells of various tissues, such as the brain, heart, kidney, lung, pancreas and spleen, and in the biliary epithelial cells of the liver, while ALP is located within biliary canaliculi and epithelial cells. Due to the rapidly increased level of serum ALP in rats after food consumption, GGT is considered more suitable indicator of cholestasis, as food consumption and changes in body weights are important parameters to be considered while interpreting ALP in toxicity testing (Ramaiah, 2007).

Alkaline phosphatase is expressed in the liver, bone, placenta and intestine, and this is thus a non-specific marker for liver damage. Increased levels of ALP are commonly used as an indicator for both liver and bone diseases. It is less sensitive than GGT in the detection of intra- and extra-hepatic biliary obstruction (Cuperus *et al.*, 2017). As GGT lacks specificity to liver disease, screening using GGT should be avoided in the absence of other liver damage markers, because elevation of GGT levels can also be associated with diabetes, kidney failure, myocardial infarction, and pancreatic disease, as well as exposure to some medications including barbiturates and phenytoin (Kwo *et al.*, 2017).

#### *2.3.3.3 Liver function markers*

Bilirubin is a metabolic product of haem, which is derived mainly from senescent erythrocytes. After formation, it is transported to the liver, tightly bound to albumin (Cuperus *et al.*, 2017), and the unconjugated form cannot be excreted in the urine (Kwo *et al.*, 2017). Conjugation of bilirubin to glucoronyl moieties in the liver by uridine diphosphate (UDP)-glucuronosyltransferase makes it water-soluble, and allows its excretion in bile. This conjugated bilirubin (direct bilirubin) is hydrolysed by β-glucuronidase to unconjugated bilirubin, and then broken down to urobilinogen and other urobilinoids by the intestinal microflora, which is excreted in the faeces or can be

reabsorbed from the gut into the bloodstream and excreted in the urine (Cuperus *et al.*, 2017; Kwo *et al.*, 2017).

Total serum bilirubin is normally < 1.1 mg/dl, where increased levels of conjugated bilirubin indicates hepatocellular damage or extrahepatic cholestasis. Increase in the levels of serum total bilirubin (hyperbilirubinemia) with elevated levels of unconjugated bilirubin do not suggest hepatocellular dysfunction, but rather increased erythrocyte breakdown. Other liver tests, such as AST, ALT, and ALP should be conducted to validate this (Kwo *et al.*, 2017).

Increased levels of total bilirubin are linked to hepatotoxicity caused by AuNPs. Intravenous injection of 15 nm Tween®20-conjugated AuNPs to mice for 21 days resulted in increased levels of bilirubin, alongside liver enzymes (ALT and AST), which suggested liver damage (Berce *et al.*, 2016). There was no significant difference in the levels of total bilirubin in rats administered intravenously with 14 nm AuNPs for 57 days (Rambanapasi *et al.*, 2016). No significant effect on the levels of bilirubin was observed after 90 days in mice injected intraperitoneally with 3.2 nm positively- and 3.7 nm negatively-charged AuNCs (Wang *et al.*, 2016b).

Total protein and albumin are markers of hepatocellular functions, which are also indicators of renal functions. The liver is responsible for the synthesis of total protein and albumin. There are two groups of blood protein, which are albumin and globulins. Albumin is the most abundant plasma protein synthesised by the liver, with a half-life of 3 weeks (Kwo *et al.*, 2017). It is involved in the transport of substances, such as bilirubin and several drugs, through the circulation (Casarett and Klaassen, 2008), and prevents diffusion from blood capillaries. On the other hand, globulins are synthesised by the liver and the immune system, and play important roles in the immune system. The serum total protein assay measures the total amount of protein present in the blood. Low levels of serum total protein may be an indication of liver damage and/or kidney disorder, while high levels may be seen in chronic inflammation. Low levels of albumin may suggest liver or kidney disorder. Several authors have reported the effect of AuNPs on the levels

of albumin and total proteins (Jo *et al.*, 2015; Kunjiappan *et al.*, 2015; Wang *et al.*, 2016b), and are, therefore, suggested as good indicators of liver and kidney functions.

#### *2.3.3.4 Kidney function markers*

The kidneys play an important role in the filtration and excretion of substances from the body. On exposure of the body to infections, chemical substances or foreign agents, kidney functions may be impaired, thereby causing damage to the glomerulus. Serum urea and creatinine are products of protein metabolism, and are useful in the assessment of kidney integrity, as these substances are readily and rapidly cleared by the kidney under normal physiological conditions (Adewale and Orhue, 2015)..

Urea is a nitrogenous end-product of the catabolism of protein and amino acids. Amino acids are deaminated in the liver, after protein degradation, leading to the production of a toxic substance, ammonia. This is converted to urea (non-toxic) in the urea cycle (an enzymatically-controlled series of reactions) driven by ATP in the presence of aspartate and bicarbonate. The urea formed is transported in the circulation to the kidney, and excreted in the urine. Creatinine on the other hand, is a non-enzymatic and irreversible product of phosphocreatine in muscles, which is rapidly removed from the blood, and excreted in the urine. Creatinine is filtered by the glomerulus at normal levels in the blood, and its clearance is used to measure the glomerular filtrate rate (GFR) (Chatterjea and Shinde, 2011).

Chemical insults or infections causing substantial damage to the glomerulus are known to cause increases in the levels of plasma or serum urea and creatinine (Adewale and Orhue, 2015). Serum or plasma urea (or BUN) and creatinine are used in the assessment of renal function in that both reflect the GFR, as decreased GFR against the normal value (about 125 mL/min) suggests kidney disease. This decrease is accompanied by decreased urinary excretion of urea and creatinine, which results in increased levels in the blood (Higgins, 2016).

#### *2.3.3.5 Haematological parameters*

The haematopoietic system is an important target for toxic substances in the body, and it gives an index of both pathological and physiological conditions. The functionality of this system can be assessed by haematological analysis, which reveals the adverse effect of foreign substances on the blood components, including red blood cells (RBC), haemoglobin, haematocrit (HCT), total white blood cells (WBC) and differential WBC counts, as well as platelets. Blood is responsible for the transport of foreign substances (and most nutrients) to various organs, and any damage to the blood cells by these foreign agents affects the normal function of the body (Adewale *et al.*, 2016; Arika *et al.*, 2016).

The interaction of NPs with the blood should be investigated *in vivo* via haematological parameters including RBC, WBC, HCT and platelets. The interaction of NPs with RBC indicates toxicity through haemolysis, WBC in innate and adaptive immune responses, and with platelets results in inflammation and thrombosis (Shah and Bischof, 2013).

a. Red blood cells

Red blood cells, also known as erythrocytes, are produced in the bone marrow. Red blood cells contain haemoglobin, which gives the blood its red colour, and are responsible for the transport of oxygen from the lungs to other body parts, and make up about 96% of the total blood cells (Shah and Bischof, 2013). The level of RBC is about 4.54-5.78 and 3.85-5.16 million/µL in men and women, respectively, under normal physiological conditions. Elevated levels of RBC are associated with body dehydration, and diseases of the liver, kidney, lung and heart, as well as smoking and alcohol addictions. Low levels of RBC could result from free radical-induced lipid peroxidation upon exposure of the body to toxic agents. This eventually leads to anaemia (Arika *et al.*, 2016).

b. Haemoglobin

Haemoglobin is produced in the bone marrow, and with the RBC, are responsible for the transport of oxygen to tissues from the lungs. Haemoglobin contains haem (formed from the combination of iron with a porphyrin ring) as its prosthetic group, with globin as the apoprotein. Under normal physiological conditions, the concentration in adults ranges from 12.0 to 17.2 g/dL. Haemoglobinemia (elevated level of blood haemoglobin) may result from RBC haemolysis following inflammation and a high number of leucocytes in the blood. Factors such as iron deficiency, haemorrhage and massive RBC destruction could result in low levels of haemoglobin in the blood, ultimately leading to anaemia (Arika *et al.*, 2016).

c. Haematocrit

Haematocrit, also known as packed cell volume (PCV), is a representation of RBC volume in relation to the whole blood volume, which is expressed in percentage. Values of PCV in males and females ranges from 42-52% and 36-48%, respectively. Elevated levels of PCV is seen with increased numbers of WBC, vitamin B12 and B9 deficiencies, chronic alcohol consumption and exposure to toxic agents. Anaemia is associated with a low PCV, resulting from obstruction of haemopoiesis by certain agents, such as toxic substances, gamma radiation, and medications including some antibiotics and sedatives (Arika *et al.*, 2016).

d. White blood cells and differential white blood cell counts

Total WBC and its indices (lymphocytes, neutrophils, eosinophils, monocytes, and basophils) are important to the normal function of the body's defence and immune systems. The WBC are made up of about 3% of the total blood cells, and the differential levels are about 60% neutrophils, 25% lymphocytes, 6% monocytes, 1-4% eosinophils, and < 1% basophils (Shah and Bischof, 2013). These, except the lymphocytes (which are formed from the lymphoid stem cells), are formed in the myeloid (bone marrow) from pluripotent haematopoietic stem cells (Arika *et al.*, 2016). In general, increased WBC counts is an indication of normal inflammatory response to foreign

substances in the blood, while a decrease indicates exposure to infection or high doses of foreign substances (Ghahnavieh *et al.*, 2014).

Lymphocytes (B and T) helps in the defence against infection and other foreign agents. The T lymphocytes are involved in cell-mediated immunity and constitute about 75% of the blood lymphocytes, while B lymphocytes participate in humoral immunity by releasing antibodies against antigens (Shah and Bischof, 2013; Arika *et al.*, 2016). The third group is the natural killer cells, which are responsible for the destruction of normal cells (Shah and Bischof, 2013). In the lymph nodes and spleen (lymphoid tissues), B cells are stimulated by antigens, and are morphologically transformed to immunoblasts, and then to plasma cells. Levels of lymphocytes are higher in infancy and decline in adult stage (Arika *et al.*, 2016).

Neutrophils are responsible for the attack and destruction of foreign substances, bacteria, and waste cell materials (Shah and Bischof, 2013). The neutrophils make up about 60-70% of circulating WBC in humans, with a short half-life of 6-7 h in blood, and a life span of 1-4 days in connective tissues. Increased numbers of neutrophils (neutrophilia) results from bacterial infection, tissue injury or inflammation, metabolic disorders and haemolysis, while decreased numbers (neutropenia) could result from HIV/AIDS, malaria, vitamin deficiencies, toxicity, immune-mediated damage by drugs including antibacterial, oral hypoglycaemic agents, and anti-inflammatory drugs. Low neutrophil counts may occur in reduced WBC production, or in increased utilization and/or destruction (Arika *et al.*, 2016). Monocytes are mononuclear cells that are involved in phagocytotic processes (Shah and Bischof, 2013), with a half-life of 12 to 100 h in the blood (in the connective tissues). They form macrophages and play a role in the immune response against antigens, on interaction with lymphocytes. Abnormal increases or decreases in the number of monocytes may result from chronic bacterial infections or inflammation (Arika *et al.*, 2016).

Eosinophils are polymorphic nuclear cells, which help in the defence against parasitic infection (Shah and Bischof, 2013). The eosinophils are also involved in the detoxification of foreign

proteins from the intestinal tract and lungs, and help in the destruction of foreign substances and regulation of inflammation. Elevated numbers of eosinophils could result from parasitic infection, autoimmune diseases, and allergy, while a significant reduction in the number of eosinophils could occur in alcohol intoxication (Arika *et al.*, 2016). Basophils are also polymorphic nuclear cells that function in antigenic and allergic responses (Shah and Bischof, 2013), as they are involved in the hypersensitivity reactions mediated by the presence of immunoglobulin E (IgE) (Arika *et al.*, 2016).

e. Platelets

Platelets are synthesised from myeloid stem cells in the bone marrow, and are stimulated by thrombopoietin in series of stages involving the development of the myeloid stem cells to the formation of megakaryocyte-colony-forming cells, megakaryoblasts, megakaryocytes, and fragments enclosed by cell membrane (platelets or thrombocytes). They are responsible for blood coagulation during bleeding (Arika *et al.*, 2016). Platelets have a life span of about 10 days, and make up about 1% of the total blood cells (Shah and Bischof, 2013). Under normal physiological conditions, human blood contains 150,000-450,000 platelets/$mm^3$, of which 67% circulate in the blood, while the rest stored in the spleen (Frohlich, 2016). In increased platelet counts, there are increase risk of thromboses in the blood vessels, which may lead to arteriosclerosis. This increase may result from inflammation and blood disease. Low platelet counts may be associated with pregnancy, excessive chemotherapy, anaemia, bone marrow disease, and in cases of enlarged spleen (Arika *et al.*, 2016), may lead to uncontrolled or spontaneous bleeding.

#### *2.3.3.6 Oxidative stress and inflammation markers*

The unique chemical nature of NPs, such as small size, high surface area and reactivity, have a significant effect on the levels of ROS formation. Generation of ROS mediates the formation of oxidative stress in tissues through free-radical mechanism, an important mechanism of NP toxicity. Upon exposure to NPs, there is an interaction with the biological system (Figure 2.7),

which results in conformational changes and oxidative damage to cellular components, such as proteins, lipids, and DNA. These include: 1) conformational changes to protein structures, which might result in oxidative stress through the generation of ROS, such as protein radicals; 2) initiation of lipid peroxidation by radicals generated through reactions with membrane lipids; 3) modification of nucleic acids; and 4) inflammatory response modulation through signal transduction. These processes can ultimately lead to genotoxicity and cell death (Fu *et al.*, 2014).

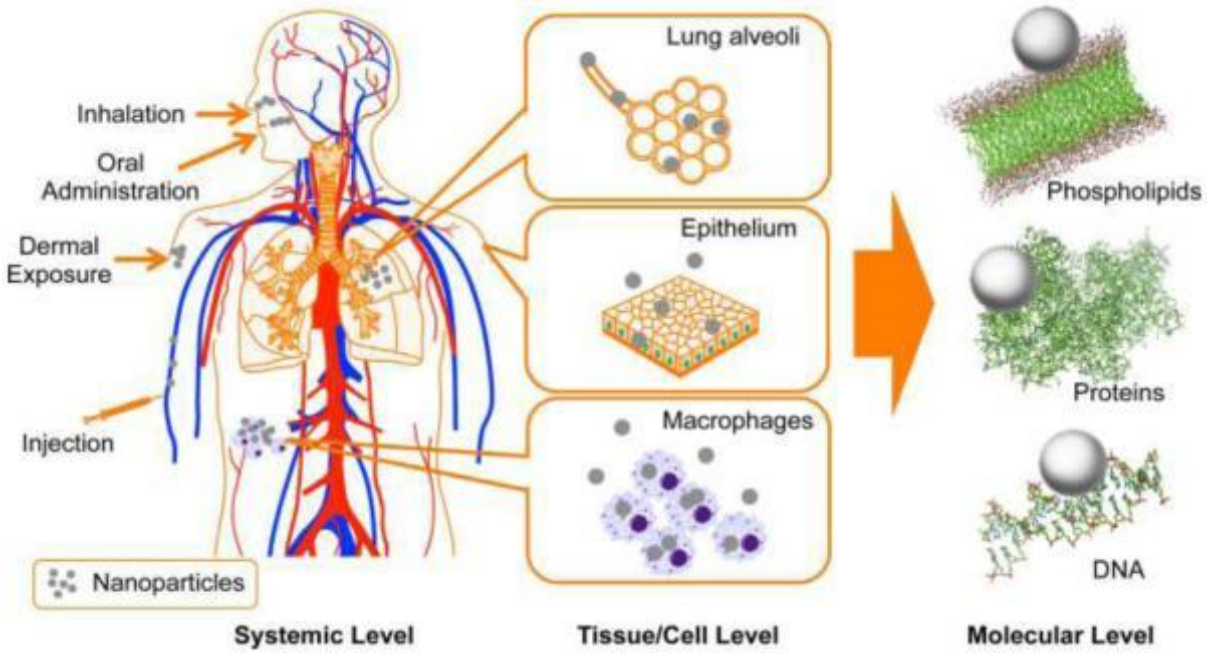


**Figure 2.7:** Schematic diagram illustrating the interactions of nanoparticles with the biological systems at different levels. Adapted from Mu *et al.* (2014).

Free radicals are highly reactive, with a short half-live of about $10^{-9}$ seconds, which makes the free-radical mechanisms of toxicity difficult to be studied at the molecular level. In view of this, biochemical and cell-based methods are employed in determining the acute and chronic toxicity of NPs (Fu *et al.*, 2014). Markers of oxidative stress include malondialdehyde (MDA) and 4-hydroxy-2-nonenal (4-HNE) (markers of lipid peroxidation), protein carbonyls (marker of protein oxidation), and 8-hydroxydeoxyguanosine (8-OHdG) (a marker of oxidative DNA damage) (Santo *et al.*, 2016).

Generally, the major mechanism of cellular injury in oxidatively-stressed aerobic organisms is lipid peroxidation. Lipid peroxidation involves chains of free radical reactions of polyunsaturated fatty acids, which can be categorised into three stages: initiation, propagation, and termination (Gasparovic *et al.*, 2013).

During the initiation stage, there is an abstraction of hydrogen atom by pro-oxidants, resulting in carbon-centred lipid radical (bisallylic radical) ($L^{\bullet}$) (Reaction 2.3) (Gasparovic *et al.*, 2013).

$$LH \longrightarrow L^{\bullet} + H^{\bullet} \qquad \text{Reaction 2.3}$$

The propagation step involves the $L^{\bullet}$ reaction with oxygen ($O_2$) to form a lipid peroxyl radical ($LOO^{\bullet}$) (Reaction 2.4), which abstracts a hydrogen to from another lipid molecule, generating a new $L^{\bullet}$ radical, and continues the chain reaction with lipid hydroperoxide (LOOH) (Reaction 2.5) (Gasparovic *et al.*, 2013).

$$L^{\bullet} + O_2 \longrightarrow LOO^{\bullet} \qquad \text{Reaction 2.4}$$

$$LOO^{\bullet} + LH \longrightarrow LOOH + L^{\bullet} \qquad \text{Reaction 2.5}$$

In the termination step, there is generation of non-radical products (Reactions 2.6, 2.7, 2.8) (Gasparovic *et al.*, 2013), either by radical-radical reactions or reaction with antioxidants, such as vitamin E (Ayala *et al.*, 2014).

$$L^{\bullet} + L^{\bullet} \longrightarrow \text{non-radical products} \qquad \text{Reaction 2.6}$$

$$L^{\bullet} + LOO^{\bullet} \longrightarrow \text{non-radical products} \qquad \text{Reaction 2.7}$$

$$LOO^{\bullet} + LOO^{\bullet} \longrightarrow \text{non-radical products} \qquad \text{Reaction 2.8}$$

These products are conjugated dienes and aldehydes, including MDA, 4-HNE, hexanal, and propanal, which are used to assess the occurrence of oxidative stress. Malondialdehyde is the

most mutagenic product, and the most convenient marker of lipid peroxidation because of its facile reaction with thiobarbituric acid (TBA) (Ayala *et al.*, 2014).

Oxidative protein damage occurs as a result of protein modifications due to ROS generated during oxidative stress. Such modifications include the oxidation of amino acid side chains, fragmentation of the polypeptide chain, and protein-protein cross-linkages. Protein carbonylation is the generation of reactive aldehydes or ketones due to oxidative stress, and is a useful marker for oxidative stress. Oxidative stress-mediated protein oxidation can be assessed by carbonyl content of protein (protein carbonyl) (Santo *et al.*, 2016).

Increased MDA levels and protein carbonyls due to overproduction of ROS (oxidative stress), in the presence of toxic NPs, may activate the transcription of pro-inflammatory mediators, such as tumour necrotic factor-alpha (*TNF-α*), Interleukin 2 (*IL-2*), Interleukin 6 (*IL-6*), Interleukin 18 (*IL-18*), and Interleukin 8 (*IL-8)* genes, through principal cascades including the nuclear factor-kappaB (*NF-kB*), mitogen-activated protein kinase (MAPK) and phosphoinositide 3-kinase (PI3-K) pathways (Khanna *et al.*, 2015).

The NF-kB, in the absence of external stimulus, forms a stable complex with Inhibitor of κB (*IκB*) in the cytoplasm. On exposure to free radicals, oxidative stress, or inflammatory stimuli, *IκB* is phosphorylated by activated *IκB* kinase (IKK), causing the release and activation of NF-*k*B. The activated NF-*k*B translocate to the nucleus and increases the production of inflammatory mediators such as cytokines, chemokines and adhesion molecules (Mu *et al.*, 2014; Liu *et al.*, 2017). These include IL-1, IL-2, IL-18, TNF-α, and intercellular adhesion molecule (ICAM). Interleukin-18 (interferon-γ (IFN-γ) inducing factor) is a pro-inflammatory cytokines produced by antigen-presenting cells (activated macrophages) (Striz *et al.*, 2005).

#### *2.3.3.7 Tissue histopathology*

Histology is the study of cellular organisation or structures of body tissues and cells in relation to physiological functions, with the use of light microscopy (for fine structures) or electron

microscopy (for ultrastructure). This can be achieved by exposing sections of tissues to stains, such as haematoxylin and eosin (H&E) stains. Histopathological examinations are useful in toxicity studies, as it reveals structural integrity of tissues following exposure to toxic agents or infection. These include an indication of renal glomerulus degeneration, brain histology examination, and changes in the structure of the spleen (major immune organ) (Yang *et al.*, 2017b). Histopathological examination of tissues, together with biochemical markers, is the gold standard to assess structural damage of tissues in toxicity (Rambanapasi *et al.*, 2016).

To understand the structural organisation of tissues, histological procedures are performed on harvested tissues. The paraffin method involves several steps before tissue sections can be viewed under microscopy (Section 3.2.3.6.5). Currently, histological staining is divided into H&E staining, immunohistochemistry (IHC), and *in situ* hybridization (Alturkistani *et al.*, 2016).

Haematoxylin and eosin are the two most commonly used histological stains. Haematoxylin is a basic dye, which binds to acidic structures such as nuclei and basophilic granules, and stains blue. Nuclear DNA is the most distinct acid in cells, and the nuclei usually appear blue, as they attract basic stains. Eosin is acidic, and stains basic structures, such as cytoplasm and eosinophilic granules red or pink. The cytoplasm, a slightly basic part of the cell, is stained pink with eosin (Chan, 2014).

Several other types of histological stains are used for examining structural components. These include Oil red O and Sudan black for staining fats; periodic acid–Schiff for carbohydrates; Perls' Prussian blue reaction for iron; and trichrome, picrosirius red, and Martius scarlet blue for connective tissues (Scudamore *et al.*, 2016).

Histochemistry is another technique used in the examination of tissues, linking histology and biochemistry or analytical chemistry. It analyses the identification and localisation of chemical components in cells and tissues, and can be viewed using a microscope (Kalyuzhny, 2016). Immunohistochemistry evolved from histochemistry, and is a powerful tool in the identification, distribution and localisation of cellular components by means of a specific antibody-antibody

reaction (Kim *et al.*, 2016). The antibody is tagged or labelled with fluorescent compound or active enzyme, to give a coloured reaction product visualisation under light microscopy (Taylor *et al.*, 2013). This technique requires the use of special dyes for staining cells or tissue sections, providing information on the location, availability and quantification of target components, which might not be possible with the H&E stains (Kim *et al.*, 2016; Shujalpurkar and Vikey, 2016).

Immunohistochemistry is used to detect various pathological changes in tissues, such as liver fibrosis and inflammation, and in the detection of glomerulosclerosis and collagenous tubule-interstitial matrix in the kidney (Yang *et al.*, 2017b).

## 2.4 RATIONALE AND MOTIVATION

Early detection of CRC can reduce its incidence and mortality rate. The clinical rationale for screening is that CRC usually develops slowly. Progresses showed that the detection and removal of CRC at an early stage (polyps) may prevent CRC and reduce the mortality rate (Zauber *et al.*, 2012). Colonoscopy is invasive, costly and limited by the expertise of the specialist performing the procedure, which is not within the reach of many patients. In view of this, there is a need for safe, non-invasive, cost-effective, and readily-available tools with high specificity and sensitivity that can detect CRC at an early stage.

Peptides are useful in cancers because of their small size, ease of synthesis and modification, good compatibility, specificity, high receptor affinity, and tumour penetrating/targeting abilities (Thundimadathil, 2012; Shapira *et al.*, 2014; Fosgerau and Hoffmann, 2015; Michalska *et al.*, 2016; Marqus *et al.*, 2017). Peptides (p.C, p.L and p.14) were shown to selectively bind to CRC cells *in vitro* (Wang *et al.*, 2012; Mazyambe, 2013), and are hypothesised to be useful *in vivo* diagnosis of CRC. Conjugating these peptides to AuNPs enables tumour specificity and selectivity, because AuNPs may not target CRC without conjugation to CRC specific biomarkers. In the diagnosis of CRC, peptides specific for CRC binds to receptors on the tumour cells and the AuNPs can be viewed by imaging techniques, such as X-ray based CT. The major concern in the successful use of AuNPs in biomedical applications are possible adverse effects, as several conflicting

toxicity results have been reported (Table 2.1 – 2.5). Some researchers reported their safety, while others their toxicity. To date, limited studies have been reported on the long-term toxicological effects of AuNPs (conjugated and unconjugated form) after a single- or repeated-dose administration (Fraga *et al.*, 2014; Rambanapasi, 2015). It is therefore of utmost importance to investigate the short- and long-term effects of a single intravenous dose of these conjugated AuNPs. This will allow examinations that can be performed regularly at shorter intervals between examinations, using imaging techniques, thereby reducing the risk of interval cancers.

## 2.5 RESEARCH AIM AND OBJECTIVES

**Aim:** The aim of this study was to assess the short- and long-term toxicity of a single intravenous injection of peptide-AuNPs in a healthy rat model.

**Objectives**

The aim of this study was achieved via the following objectives:

I. To analyse the effects of AuNPs on food and water consumption, as well as body and organ weights of male Wistar rats.
II. To ascertain the safe use of 14 nm citrate-capped AuNPs for conjugation of biomolecules, thereby facilitating comparison with previously published toxicity studies.
III. To assess the short (2 weeks)- and long (12 weeks)-term effects of a single intravenous injection of AuNPs, using markers of liver and kidney damage (ALT, AST, ALP, total protein, albumin, total and direct bilirubin, as well as creatinine and urea).
IV. To investigate the effects of the AuNPs on the immune response, using haematological parameters.
V. To determine the oxidative stress and inflammatory responses to a single intravenous injection of the AuNPs in rats, using markers of oxidative stress (MDA and protein carbonyls in liver homogenates) and inflammation (p-I*k*B-α, IL-18 and IFN-γ antibodies for immunohistochemistry).

VI. To examine the short- and long-term histopathological changes resulting from a single injection of the AuNPs in the liver, spleen, and kidney (major organs of distribution and toxicity), colon (target organ for the peptide-AuNPs) and pancreas (organ for insulin secretion).

VII. To investigate toxicity of the combination of PEG-OH and PEG-biotin on Wistar rats, to further substantiate its role as stabilising and linking agents for AuNP and peptide.

VIII. To elucidate and compare the acute or persistent toxicities of a single injection of the peptide-AuNPs in male rats 2 weeks and 12 weeks post-intravenous exposure.

IX. To potentiate the safe use of peptide-AuNPs in healthy patients during the diagnosis of CRC.

# CHAPTER THREE

# METHODOLOGY

## 3.1 MATERIALS: CHEMICALS AND SUPPLIERS

The chemicals and kits used in this study, including the suppliers, are listed in Table 3.1, 3.2 and 3.3 respectively.

**Table 3.1:** Chemicals and suppliers

| S/N | Chemicals/Analytical reagents | Supplier |
|---|---|---|
| 1. | Acetone | Sigma-Aldrich, USA |
| 2. | Dipotassium hydrogen phosphate ($K_2HPO_4$) | Sigma-Aldrich, USA |
| 3. | Disodium hydrogen phosphate ($Na_2HPO4$) | Sigma-Aldrich, USA |
| 4. | Diethyl ether | Sigma-Aldrich, USA |
| 5. | Ethanol | Merck, South Africa |
| 6. | Formaldehyde (37%) | Sigma-Aldrich, USA |
| 7. | Gold(III) chloride trihydrate ($HAuCl_4.3H_20$) | Sigma-Aldrich, USA |
| 8. | Hydrochloric acid (HCl) | Sigma-Aldrich, USA |
| 9. | n-Butanol | Sigma-Aldrich, USA |
| 10. | Nitric acid ($HNO_3$) | Sigma-Aldrich, USA |
| 11. | PEG-OH | ProChimia Surfaces, Poland |
| 12. | PEG-Biotin | ProChimia Surfaces, Poland |
| 13. | Peptides (p.L, p.C., p.14) | Mintek, South Africa |
| 14. | Potassium chloride (KCl) | Merck, South Africa |
| 15. | Potassium dihydrogen phosphate ($KH_2PO_4$) | Sigma-Aldrich, USA |
| 16. | Sodium chloride (NaCl) | Merck, South Africa |
| 17. | Sodium dihydrogen phosphate ($NaH_2PO_4$) | Sigma-Aldrich, USA |
| 18. | Sodium hydroxide (NaOH) | Merck, South Africa |
| 19. | Thiobarbituric acid (TBA) | Sigma-Aldrich, USA |

| | | |
|---|---|---|
| 20. | Trichloroacetic acid (TCA) | Sigma-Aldrich, USA |
| 21. | Tris base | Sigma-Aldrich, USA |
| 22. | Trisodium citrate ($Na_3C_6H_5O_7$) | ACS-Reagent |

**Table 3.2:** Biochemical assay kits and suppliers

| S/N | Assay kits | Supplier |
|---|---|---|
| 1. | Albumin | Randox Laboratories, UK |
| 2. | Alanine transaminase | Randox Laboratories, UK |
| 3. | Alkaline phosphatase | Randox Laboratories, UK |
| 4. | Aspartate transaminase | Randox Laboratories, UK |
| 5. | Bilirubin | Randox Laboratories, UK |
| 6. | Creatinine | Randox Laboratories, UK |
| 7. | Protein carbonyl | Sigma-Aldrich, USA |
| 8. | Bicinchoninic acid protein | Thermo Fisher Scientific, USA |
| 9. | Urea | Randox Laboratories, UK |

**Table 3.3:** Antibodies and suppliers

| S/N | Antibody | Type | Host species | Supplier |
|---|---|---|---|---|
| 1. | p-I*k*β-α | Primary | Mouse | Abcam, UK |
| 2. | IFN-γ | Primary | Mouse | Cloud-Clone Corp., USA |
| 3. | IL-18 | Primary | Mouse | eBioscience, USA |
| 4. | Cy3-conjugated F(ab')2 fragment donkey-anti-mouse | Secondary | Donkey | Jackson ImmunoResearch, USA |

IFN-γ (Interferon- γ); IL-18(Interleukin-18); p-I*k*β-α (Anti-IKB alpha (phospho S32 + S36).

## 3.2 METHODS

### 3.2.1 Design of gold nanoparticle conjugate

#### *3.2.1.1 Synthesis of gold nanoparticles*

All glassware used was treated with aqua regia (3:1 HCl:$HNO_3$), and all materials were rinsed with distilled water and Milli-Q water (18.2 MΩ.$cm^{-1}$ at $25^0$C), and oven dried. Colloidal AuNPs were prepared by the reduction of $HAuCl_4.3H_20$ (MW 393.83 g/mol) with trisodium citrate (MW 258.06 g/mol), according to the citrate-reduction method (Turkevich *et al.*, 1951; Frens, 1973). In a 1000-mL beaker containing 500 mL boiling Milli-Q water (300°C), 5 mL of 28.95 mM $HAuCl_4.3H_20$ was added. Into the beaker, 14.5 mL of 38.75 mM trisodium citrate was added rapidly, causing the solution to change colour from grey to purple, and finally to ruby red. The colloidal solution was boiled for 30 min with continuous stirring, and left to cool to room temperature. The solution was centrifuged at 12000 x *g* for 15 min to remove excess citrate, and the citrate-capped AuNP pellet was washed in Milli-Q water. The resulting solution was stored at 4 °C prior to conjugation.

#### *3.2.1.2 Functionalisation of AuNPs with PEG chains and peptides*

The process of functionalisation of the citrate-capped AuNPs with PEG and peptides for biological application was performed according to the method of Sosibo *et al.* (2015), with slight modifications.

3.2.1.2.1 Synthesis of PEG-Biotin gold nanoparticles

Ethanolic solutions of PEG-biotin (8.4 mg/mL, 0.24 µL) and PEG-OH (18.8 mg/mL, 10.53 µL) were added simultaneously to the synthesised citrate-capped AuNPs (2 nM, 20 mL). The reaction mixture was stirred at 4 °C for 3 h, then centrifuged (12000 x *g*, 22 °C, 20 min) and washed twice with PBS (0.01M phosphate buffer, 0.0027 M KCl and 0.137 M NaCl) to obtain 1% PEG-biotin AuNPs containing 99% PEG-OH as a co-stabiliser. This was stored at 4 °C in PBS until needed.

#### 3.2.1.2.2 Functionalisation with Streptavidin

The resultant PEG-AuNPs was functionalised with streptavidin by streptavidin-biotin chemistry. An aqueous solution of streptavidin (1 mg/mL, 25 µL) was added to 800 µL PEG-AuNPs (16 nM), and the volume made up to 2 mL with PBS. The reaction mixture was mixed thoroughly by swirling, followed by an overnight incubation at 4 °C. Excess streptavidin was removed by centrifugation (12000 x *g*, 22 °C, 20 min). The streptavidin-AuNP conjugate was stored at 4 °C in PBS.

#### 3.2.1.2.3 Immobilisation with biotinylated peptides

Biotinylated peptides were immobilised on the streptavidin-AuNP conjugates. Into the streptavidin-AuNP conjugate (12 nM, 5 mL), 20 µL solution of each biotinylated peptide (2.94 µL 170 µg/mL p.C; 7.4 µL 70 µg/mL p.L; 2.54 µL 197 µg/mL p.14) was added separately. Each mixture was gently swirled and then incubated overnight at 4 °C. The resultant peptide-conjugated AuNPs were centrifuged (12000 x *g*, 22 °C, 20 min) in PBS to remove excess peptide. The resultant conjugated AuNPs were stored at 4 °C in PBS until needed.

### 3.2.2 Characterisation of conjugated gold nanoparticles

#### *3.2.2.1 UV-Vis spectroscopy*

The conjugated AuNPs were characterised by UV-Vis spectroscopy using the Nanodrop 2000c spectrophotometer (Thermoscientific, USA), to determine the stability and aggregation levels of the NPs (Section 2.2.2.2.1). The maximum wavelength was measured, and the absorbance was used to calculate the concentrations of the NPs using the Beer Lambert's equation ($A = \varepsilon bc$), where A is the absorbance, ε is the molar extinction coefficient ($M^{-1}cm^{-1}$), b is the path length (cm) of the sample, and c is the concentration (M) of NPs in solution. The absorption coefficient varies with NP size. The concentration of the size of AuNPs obtained in this study was determined using the calculated extinction coefficient of a series of spherical AuNPs with diameters ranging

from 4 nm to 40 nm using the equation (ln ε = 3.32 ln d + 10.8), where ε = molar extinction coefficient ($M^{-1}cm^{-1}$), d = diameter (nm) of AuNPs (Liu *et al.*, 2007; Shang and Gao, 2014).

#### *3.2.2.2 High resolution transmission electron microscopy*

The size distribution and morphology of the AuNPs was determined using HRTEM (JEOL model 1200 $LaB_6$) (Section 2.2.2.2.2). Samples were prepared by dropping solutions of AuNPs onto carbon-coated copper grids, which were allowed to dry at room temperature prior to measurement (Sosibo *et al.*, 2015).

#### *3.2.2.3 Dynamic light scattering and zeta potential measurement*

The zeta potential measurement and the DLS were determined using the Zetasizer Nano ZS, Malvern Instruments (Malvern, UK), with a variable power (5–50mW) He-Ne laser beam at 633 nm. The operating voltage range was 20–200 kV with a resolution of 2.4 A° (Section 2.2.2.2.3) (Fraga *et al.*, 2014). The DLS provides the polydispersity index (PDI) and hydrodynamic size (Z-average size) of the AuNPs, while the zeta potential measurements provides information on the surface charge of the AuNPs. The NPs were dispersed in PBS solution up to a concentration of 2 nM, and the measurements were performed at 25 °C, with a scattering angle of 90° (Rambanapasi, 2015).

#### *3.2.2.4 Fourier transmission infrared spectroscopy*

The PerkinElmer FTIR Spectrometer (Spectrum two) was used to detect the presence of additional functional groups on the surface of the citrate-capped AuNPs (section 2.2.2.2.4). A portion of the AuNPs in solution was centrifuged for 15 min at 12000 x *g* to obtain a pellet. The dried pellet was analysed by FTIR in a wide range (450-4000 $cm^{-1}$) of FTIR spectral analysis at a resolution of 0.5 $cm^{-1}$ (Ghosh *et al.*, 2012).

### 3.2.3 Animal experimentation

#### *3.2.3.1 Animals and Ethics approval*

A total of 72 (12 weeks old) male Wistar rats was used for this research. Thirty-six rats were obtained from the animal house of North West University, South Africa, and were used for phase 1 of the experiment. Due to unavailability of rats at North West University during the start of the phase 2 experiment, the second group of 36 rats was obtained from SA Vaccine Producers (Animal Unit), South Africa. Animal procedures were approved by the Nelson Mandela University Research Ethics Committee: Animal (reference number: **A15-SCI-BCM-002**) (Appendix 1). Animals were housed at 22 °C (± 2 °C), with a 12-hour light-dark cycle. The rats were fed standard commercial rat chow and given distilled water *ad libitum*.

#### *3.2.3.2 Animal grouping*

The experiment was divided into two phases: Phase 1 experiment investigated the acute toxicity of AuNPs 2 weeks (short-term) post-intravenous injection, while the phase 2 study evaluated the long-term (12 weeks) effect of the NPs after a single intravenous injection. The rats in each phase were divided into 6 groups of 6 animals each (Table 3.4). For both phases, group I received 1 X PBS as the vehicle control, while groups 2-6 received a single intravenous injection of 100 µg/kg b.w. citrate-, PEG-, p.C-PEG-, p.L-PEG-, or p.14-PEG-AuNPs, respectively. The concentration was made at 100 µg/ml PBS, and the dose (100 µg/kg) falls within the range of the rat model dose for low and medium doses (∼10 and ∼1000 µg/kg) (Lin *et al.*, 2016a). The dose was used in our laboratory towards targeting CRC tumour in rats (Cairncross, 2015), and is in the range of the safe doses (3-373 µg/kg) used in the toxicity studies of 14 nm citrate-AuNPs (Rambanapasi *et al.*, 2016). As the dose received by each rat was calculated based on the body weight, constant dosing was ensured (OECD, 2012).

**Table 3:4:** Administration protocol for phase 1 and 2 experiments

n=6

| Groups | Treatment |
|---|---|
| Group I | Control |
| Group II | Citrate-AuNPs |
| Group III | PEG-AuNPs |
| Group IV | p.C-PEG-AuNPs |
| Group V | p.L-PEG-AuNPs |
| Group VI | p.14-PEG-AuNPs |

Rats were weighed 24 h after injection, and then weekly throughout the experiment. The rats were observed for the first 4 h, then over a period of 24 h, and thereafter daily throughout the experiment. Observations were performed to assess general health status, symptoms of toxicity, and mortality.

#### *3.2.3.3 Sacrifice of animals*

Phase 1 and phase 2 rats were sacrificed 2 weeks and 12 weeks, respectively, after treatment, following an overnight fast, by quick exposure to diethyl ether. After the loss of sensory reflexes, blood was withdrawn by cardiac puncture.

#### *3.2.3.4 Blood sampling and organ harvesting*

Blood samples were collected into empty vacutainer tubes for collection of the serum and vacutainer tubes containing EDTA, as anti-coagulant, for the collection of plasma. Serum samples were obtained by centrifugation at 3000 x *g* for 10 min, and stored at -80 °C for subsequent biochemical analyses.

Organs including the liver, spleen, colon, kidney, brain, heart, lungs, and pancreas of each animal were removed and rinsed in ice-cold physiological saline (0.9% NaCl), blotted with filter paper

and weighed. Portions of each organ were stored as follows: pieces of organs (3 $mm^2$) were stored in 10% neutral phosphate buffered-formalin at room temperature for histological and immunohistochemical analyses; 1 $mm^2$ of each tissue was stored in a solution of PBS containing 2.5% glutaraldehyde and 2% paraformaldehyde (0.5 mL, pH 7.4) for HRTEM at 4 °C, until processed for analyses; 3 $mm^2$ of each tissue was stored at 4°C in RNAlater (0.5 mL) for gene analyses, and the last portion was divided into separate sections in aluminium foil, snap-frozen in liquid nitrogen, and stored at -80 °C for subsequent biochemical analyses.

#### *3.2.3.5 Preparation of liver homogenate*

A portion (1 g) of the liver was homogenised (20% w/v) with a Potter-Elvehjem homogeniser (LabSource, USA) in ice-cold 1.15% KCl–0.01 M potassium phosphate buffer (pH 7.4). Homogenates were centrifuged at 12000 x *g* at 4 $^0$C for 15 min. The supernatants were stored at -80 °C, and used for biochemical assays.

#### *3.2.3.6 Parameters investigated*

3.2.3.6.1 Relative organ weight

Organs were harvested and weighed. The relative organ weight of each animal was calculated as follows:

$$\text{Relative organ weight (/100g)} = \frac{\text{absolute organ weight (g)} \times 100}{\text{body weight (g) of rat on day of sacrifice}}$$

3.2.3.6.2 Biochemical assays

*3.2.3.6.2.1 Determination of serum alanine aminotransferase activity*

Serum ALT activity was determined following the method described by Reitman and Frankel (1957), using the Randox ALT assay kit.

**Principle**

Alanine aminotransferase was measured by monitoring the concentration of pyruvate hydrazone formed with DNPH. The enzyme catalyzes the transfer of the amino group from L-alanine to α-oxoglutarate to form L-glutamate and pyruvate (Reaction 3.1) (Wang *et al.*, 2016a). The pyruvate formed is then complexed with DNPH to produce an intensely coloured hydrazone on the addition of NaOH. This coloured complex absorbs maximally between 530-550 nm.

α- oxoglutarate + L- alanine $\xrightarrow{\text{ALT}}$ L- glutamate + Pyruvate Reaction 3.1

**Procedure**

Serum sample (0.1 mL) was mixed with phosphate buffer (100 mmol/L, pH 7.4), L-alanine (100 mmol/L), and α- oxoglutarate (2 mmol/L) in test tubes, incubated at 37 $^{o}$C for exactly 30 min. Into the mixture, 0.5 mL DNPH (2 mmol/L) was added, and allowed to stand at 25 $^{o}$C for exactly 20 min. Sodium hydroxide (0.4 mol/L, 5 mL) was added, and left to stand for 5 min at room temperature. Reagent blank was prepared as described, replacing the sample with 0.1 mL distilled water. To obtain the same experimental conditions, 200 µL of each sample was transferred to a 96-well plate, and the absorbance read at 37 $^{o}$C against a reagent blank at 546 nm using the PowerWave HT Microplate reader (Bio-Tek® Instruments, Inc., USA) PowerWave HT microplate reader (Bio-Tek® Instruments, Inc., USA).

The activity of ALT was calculated from the ALT calibration curve plotted with the standard results provided by the Randox AST assay kit (Appendix 2).

*3.2.3.6.2.2 Determination of serum aspartate aminotransferase activity*

Serum AST activity was determined using the Randox AST assay kit, following the method of Reitman and Frankel (1957).

**Principle**

Aspartate aminotransferase was measured by monitoring the concentration of oxaloacetate hydrazone formed with 2,4-dinitrophenylhydrazine (DNPH). The enzyme catalyses the transfer of the amino group from L-aspartate to α-oxoglutarate to form L-glutamate and oxaloacetate (Reaction 3.2) (Wang *et al.*, 2016a). The oxaloacetate formed is unstable and is quantitatively decarboxylated to pyruvate, which is then complexed with DNPH to give an intensely coloured hydrazone on the addition of NaOH, which absorbs maximally between 530-550nm.

α- oxoglutarate + L- aspartate $\xrightarrow{\text{AST}}$ L- glutamate + Oxaloacetate Reaction 3.2

**Procedure**

A serum sample (0.1 mL) was added to phosphate buffer (100 mmol/L, pH 7.4), L-aspartate (100 mmol/L), and α-oxoglutarate (2 mmol/L) in test tubes, mixed and incubated at 37 $^{o}$C for exactly 30 min. This was followed by the addition of 0.5 mL DNPH (2 mmol/L). The mixture was allowed to stand at 25 $^{o}$C for exactly 20 min. Then, 5 mL NaOH (0.4 mol/L) was added, and left to stand for 5 min at room temperature. Reagent blank was prepared as described, replacing the sample with 0.1 mL distilled water. To obtain the same experimental conditions, 200 µL of each sample was transferred to a 96-well plate, and the absorbance read at 37 $^{o}$C against a reagent blank at 546 nm using the PowerWave HT microplate reader (Bio-Tek® Instruments, Inc., USA).

Serum samples were optimised based on the standard results (in the linear range) provided by the Randox AST assay kit and the enzyme (AST) activity was obtained from the AST calibration curve plotted with the standard results (Appendix 2).

*3.2.3.6.2.3 Determination of serum alkaline phosphatase activity*

The activity of ALP was carried out following the recommendations of Deutsche Gesellschaft für Klinische Chemie (DGKC) (Rec. GSCC, 1972), using the Randox ALP assay kit .

**Principle**

Serum ALP hydrolyses colourless P-nitrophenylphosphate to produce phosphate and P-nitrophenol (Reaction 3.3). The product (pink in colour) is photometrically measured at 405 nm.

P-nitrophenylphosphate + $H_2O$ $\xrightarrow{ALP}$ Phosphate + P-nitrophenol Reaction 3.3

**Procedure**

Into a test tube containing 0.01 mL sample, 0.5 mL reagent (a mixture of P-nitrophenylphosphate and diethanolamine buffer) was added, and mixed. The initial absorbance of the mixture was read at 405 nm (25 $^{o}$C) against air immediately after transferring 200 µL sample to a 96-well plate (for uniform assay conditions), then after 1, 2 and 3 min, using the PowerWave HT microplate reader (Bio-Tek® Instruments, Inc., USA).

The activity of serum ALP was calculated using the following formula provided by the Randox ALP assay kit:

U/L of ALP = 2760 x ΔA 405 nm/min

where ΔA = change in absorbance ($A_3$-$A_0$)

*3.2.3.6.2.4 Estimation of total protein concentration*

Total protein concentrations were determined by the bicinchoninic acid (BCA) method as described by Smith *et al.* (1985), using the protocol of the Thermo Scientific™ Pierce™ BCA protein assay kit.

**Principle**

The BCA method combines the biuret method (reduction of $Cu^{2+}$ to $Cu^{+}$ by protein in an alkaline medium) with the highly sensitive and selective colorimetric detection of the cuprous cation

($Cu^{+}$), using a reagent containing BCA. A purple-coloured complex is formed by the chelation between two molecules of BCA and one $Cu^{+}$. The absorbance of this water-soluble complex was read at 562 nm.

**Procedure**

Working reagent (BCA reagent A, consisting of sodium carbonate, sodium bicarbonate, BCA and sodium tartrate in 0.1 M sodium hydroxide, and BCA reagent B, 4% cupric sulphate) (200 µL) was added to 25 µL sample or BSA standard (20-2000 µg/mL) in a 96-well plate, and mixed thoroughly for 30 sec. The plate was covered and incubated at 37 °C for 30 min. A blank was prepared as described, replacing the sample or standard with 25 µL distilled water. The absorbance was read against the blank at 562 nm (25 °C), using the PowerWave HT microplate reader (Bio-Tek® Instruments, Inc., USA).

Total protein concentration (µg/mL) of the sample was calculated from the BSA standard curve derived from the prepared concentrations obtained from stock solution (2mg/mL) of BSA standard provided (Appendix 2).

*3.2.3.6.2.5 Determination of serum albumin concentration*

Serum albumin concentrations were determined by the Bromocresol Green (BCG) method described by Doumas *et al.* (1971), using the Randox albumin assay kit.

**Principle**

Serum albumin binds with BCG to form an albumin-BCG-complex, which absorbs maximally at 600-650 nm.

**Procedure**

Into test tubes containing 10 µL standard (5 g/dL), blank, or sample, 3000 µL of the diluted BCG reagent (13.5 mL 1.7 mmol/L BCG concentrate in 75 mmol/L succinate buffer, pH 4.2 + 87 mL

distilled water) was mixed and incubated at room temperature for 5 min. To obtain the same experimental conditions, 200 µL sample or standard was transferred to a 96-well plate, and the absorbance read at 25 $^{o}$C against the reagent blank at 630 nm using the PowerWave HT microplate reader (Bio-Tek® Instruments, Inc., USA).

The serum albumin concentrations were calculated using the formula provided by the Randox albumin assay kit, as follows:

$$\text{Serum albumin concentration (g/dL)} = \frac{A_{630}\ \text{sample} \times \ \text{concentration of standard}}{A_{630}\ \text{standard}}$$

where $A_{630}$ sample = absorbance of sample at 630 nm, $A_{630}$ standard = absorbance of standard at 630 nm.

*3.2.3.6.2.6 Determination of serum total and direct bilirubin concentrations*

The serum bilirubin assay was performed based on the method of Jendrassik and Gróf (1938), according to the protocol of the Randox bilirubin assay kit.

**Principle**

The bilirubin assay kit measures both total and conjugated (direct) bilirubin. The method is based on the reaction of direct bilirubin with diazotised sulphanilic acid in an alkaline medium, resulting into a blue-coloured complex, proportionate to the bilirubin present in the sample. It is measured colorimetrically at 546 nm. Total bilirubin is determined by the reaction with diazotised sulphanilic acid in the presence of caffeine to release albumin-bound bilirubin, which is measured colorimetrically at 578 nm.

**Procedure**

For total bilirubin, 200 µL sulphanilic acid (29 mmol/L, containing 0.17 N HCl), 50 µL sodium nitrite (38.5 mmol/L), and 1000 µL caffeine (0.26 mol/L, containing 0.52 mol/L sodium benzoate) were

mixed in a test tube containing 200 µL test sample. The mixture was allowed to stand at 25 $^{o}$C for 10 min. Tartrate (1000 µL) was then added to the mixture and left at 25 $^{o}$C for 15 min. The sample blank was prepared by the addition of the reagents to the sample, except for sodium nitrite. For accuracy, the mixtures were transferred into 96-well plate, and the absorbance of the samples read against the sample blank at 578 nm, using the PowerWave HT microplate reader (Bio-Tek® Instruments, Inc., USA).

The concentration of serum total bilirubin (mg/dL) was calculated using the following formula, provided by the Randox bilirubin assay kit:

Serum total bilirubin concentration (mg/dL) = 10.8 x $A_{TB}$

where 10.8 is the conversion factor from µmol/L to mg/dL, $A_{TB}$ = absorbance of total bilirubin = $A_{sample} - A_{sample\ blank}$.

For direct bilirubin, 200 µL sulphanilic acid (29 mmol/L, containing 0.17 N HCl), 50 µL sodium nitrite (38.5 mmol/L), and 2000 µL NaCl (0.9%) were mixed with 200 µL test sample, and incubated at 25 $^{o}$C for 10 min. The sample blank was prepared by the addition of the reagents to the sample, except for sodium nitrite. The mixtures were transferred into 96-well plate, and the absorbance of the samples read against the sample blank at 546 nm, using the PowerWave HT microplate reader (Bio-Tek® Instruments, Inc., USA).

The concentration of serum direct bilirubin (mg/dL) was calculated using the following formula, provided by the Randox bilirubin assay kit:

Serum direct bilirubin concentration (mg/dL) = 14.4 x $A_{DB}$

where 14.4 is the conversion factor from µmol/L to mg/dL, $A_{DB}$ = absorbance of direct bilirubin = $A_{sample} - A_{sample\ blank}$.

*3.2.3.6.2.7 Serum creatinine levels determination*

The serum creatinine assay was performed based on Jaffe's method, as described by Bartels *et al.* (1972), according to the protocol of the Randox Creatinine assay kit.

**Principle**

Creatinine reacts with picric acid to form a coloured complex in alkaline solution due to the formation of a red tautomer of creatinine picrate (Jaffe's reaction).

**Procedure**

An equal mixture (1000 µL) of picric acid (35 mmol/L) and sodium hydroxide (0.32 mol/L) was added to 100 µL serum sample or standard in a test tube. This was mixed and transferred into a 96-well plate. The absorbance ($A_1$) of the sample and standard was read against air at 492 nm (25 $^{o}$C), using the PowerWave HT microplate reader (Bio-Tek® Instruments, Inc., USA), after 30 sec ($A_1$), and exactly 2 min later ($A_2$).

The concentration of serum creatinine was calculated, using the following formula as provided by the Randox Creatinine assay kit:

$$\text{Creatinine concentration (mg/dL)} = \frac{\Delta A_{sample} \times \text{concentration of standard (1.91 mg/dL)}}{\Delta A_{standard}}$$

where $\Delta A_{sample}$ or $\Delta A_{standard}$ = $A_2 - A_1$

*3.2.3.6.2.8 Determination of serum urea levels*

The serum urea assay was performed by the Urease-Barthelot method, following the Randox Urea assay kit specifications.

**Principle**

Hydrolysis of serum urea in the presence of urease produces ammonia (Reaction 3.4), which is measured colorimetrically (Reaction 3.5) by the Berthelot's reaction (Weatherburn, 1967).

$$\text{Urea} + H_2O \xrightarrow{\text{Urease}} 2NH_3 + CO_2 \qquad \text{Reaction 3.4}$$

$$2NH_3 + \text{hypochlorite} + \text{phenol} \longrightarrow \text{indophenol (blue compound)} \qquad \text{Reaction 3.5}$$

**Procedure**

A mixture (100 µL) of sodium nitroprusside (6 mmol/L) and urease (1 g/L) was added to 10 µL serum, standard or distilled water (blank) in a test tube. This was mixed and incubated at 37 $^{o}$C for 10 min. Phenol (2.5 mL, 120 mmol/L) and 2.5 mL hypochlorite (27 mmol/L sodium hypochlorite and 0.14 N sodium hydroxide) was added to the mixture and incubated at 37 $^{o}$C for 15 min. To obtain the same experimental conditions, 200 µL sample was transferred to a 96-well plate, and the absorbance read at 37 $^{o}$C against the reagent blank at 546 nm using the PowerWave HT microplate reader (Bio-Tek® Instruments, Inc., USA).

The concentration of urea in the serum was calculated using the following formula, provided by the Randox urea assay kit, as follows:

$$\text{Urea concentration (mg/dL)} = \frac{A_{sample} \times \text{Concentration of standard (78.43 mg/dL)}}{A_{standard}}$$

3.2.3.6.3 Oxidative stress marker assays

The MDA and protein carbonyl assays were selected, respectively, to evaluate lipid peroxidation (Ayala *et al.*, 2014) and protein oxidation (Santo *et al.*, 2016), which are major indicators of oxidative stress.

*3.2.3.6.3.1 Assessment of lipid peroxidation in tissue homogenate*

Malondialdehyde is one of the end-products for lipid oxidation, which is a widely used marker for lipid peroxidation. Lipid peroxidation was determined by measuring the formation of

thiobarbituric acid reactive substances (TBARS), according to the method of Varshney and Kale (1990), with some modifications.

**Principle**

Under acidic conditions, MDA produced from the peroxidation of fatty acid membranes and food products react with the chromogenic reagent, TBA, to yield a pink coloured-complex with a maximum absorbance of 532 nm. The pink chromophore is readily extractable into organic solvents such as n-butanol.

**Procedure**

An aliquot of 0.4 mL liver homogenate was mixed with 1.6 mL Tris-KCl buffer (0.15 M, pH 7.4) in a screw-capped tube, to which 0.5 mL 30% TCA was added. Then, 0.5 mL 0.75% TBA was added and placed in a water bath at 80 $^{o}$C for 45 min. After cooling on ice for 10 min, 3 mL n-butanol was added, and mixed vigorously to extract the MDA adduct. The mixture was centrifuged at 3000 x *g* at 4 $^{o}$C for 3 min. The clear supernatant was collected in a 96-well plate, and the absorbance read against a reference blank of distilled water at 532 nm, using the PowerWave HT microplate reader (Bio-Tek® Instruments, Inc., USA). The MDA level was calculated according to the method of Ádám-Vizi and Seregi (1982). Lipid peroxidation was calculated with a molar extinction coefficient ($E_{532nm}$) of 1.56 x $10^5$ $M^{-1}Cm^{-1}$, using the formula:

$$\text{MDA (units/mg protein)} = \frac{\text{Absorbance x volume of mixture}}{E_{532nm} \text{ x volume of sample x mg protein of tissue homogenates}}$$

3.2.3.6.3.2 Determination of protein carbonyl content in tissue homogenate

Protein carbonyl is a marker of protein oxidation. This was measured by a colorimetric method, as specified by the Sigma Protein Carbonyl Content Assay kit.

**Principle**

The carbonyl content in a sample is determined by the derivatization of protein carbonyl groups with DNPH, which results in the formation of stable dinitrophenyl (DNP) hydrazone adducts (Figure 3.1). In proportion to the carbonyls present, the DNP hydrazone adducts can be measured spectrophotometrically at 375 nm.

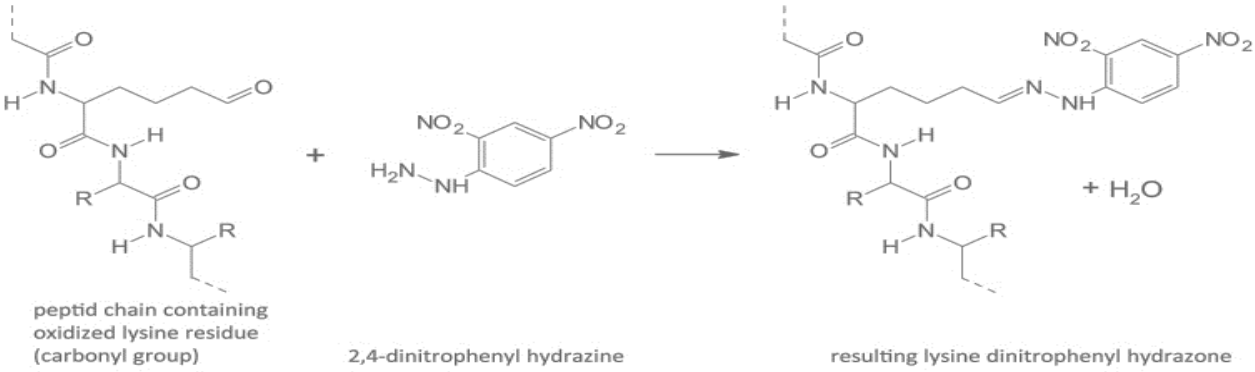


**Figure 3.1:** Formation of stable lysine dinitrophenyl hydrazone. Adapted from Weber *et al.* (2015).

**Procedures**

Liver homogenates were diluted with Milli-Q water to a protein concentration of 10 mg/mL. Into Eppendorf tubes containing 100 µL sample or Milli-Q water (blank), 100 µL DNPH solution was added and the tube vortexed. The mixture was incubated at room temperature for 10 min, after which 30 µL 100% TCA solution was added, vortexed, and then incubated on ice for 5 min. The mixture was centrifuged at 13,000 x *g* for 2 min, and the supernatant carefully removed. Five hundred µL ice-cold acetone was added to the resulting pellet and sonicated for 30 sec. The mixture was incubated at –20 °C for 5 min and then centrifuged at 13,000 x *g* for 2 min. Acetone and free DNPH was carefully aspirated from the tube. To the pellet, 200 µL 6 M guanidine solution was added and sonicated for 10 sec. Into a 96-well plate, 100 µL sample was transferred, and the absorbance read at 25 $^{o}$C against the blank spectrophotometrically at 375 nm, using the PowerWave HT microplate reader (Bio-Tek® Instruments, Inc., USA).

**Protein Assay Reaction**

To determine the amount of protein per sample, 5 µL sample was used, following the total protein BCA procedure (Section 3.2.3.6.2.4 above).

The carbonyl content was calculated using the formula, provided by the Sigma Protein Carbonyl Content Assay kit:

Carbonyl content in sample, C (nmole/well) = ($A_{375}$/6.364) x 100

where 6.364 = Millimolar extinction coefficient ($e^{mM}$ = 22 $mM^{-1}cm^{-1}$) x 0.2893 cm pathlength in a well for enclosed 96 well plate [6.364 = $e^{mM}$ (22 $mM^{-1}cm^{-1}$) x 0.2893 cm]; 100 = total volume (V) in well (µL)

CP = nmole carbonyl/mg protein = (C/P) x 1000 x D

where C = Carbonyl content in sample (nmole/well), P = Amount of protein from standard well x 20 = µg/well, D = dilution factor or concentration of sample, 1000 = conversion factor (µg to mg).

3.2.3.6.4 Haematological parameters

Heamatological parameters, such as total WBC and differential WBC count (neutrophils, lymphocytes, monocytes, eosinophils, and basophils), as well as haemoglobin concentrations were determined on the plasma samples. This was analysed by Ampath Pathologists, Drs Du Buisson, Kramer, Swart, Bouwer Inc, South Africa. The relative WBC counts was calculated from the absolute values as follows:

$$\text{Relative WBC counts (\%)} = \frac{\text{Absolute WBC count } (10^{\wedge 9}/L) \text{ X } 100}{\text{Total WBC } (10^{\wedge 9}/L)}$$

3.2.3.6.5 Tissues histopathology

Tissue sections were fixed in 10% formalin and counter-stained with H&E for examination under light microscopy. Histopathological examinations were conducted in blinded studies (Adesanoye *et al.*, 2016) using the paraffin method of histology at the Department of Medical Laboratory Sciences, Nelson Mandela University, South Africa.

Paraffin method of histology

Tissues were fixed in 10% buffered formalin at room temperature to preserve the cellular integrity. The tissues were then dehydrated with graded alcohol (50%, 70%, 95%, 100%), after which clearing agent (xylene) was added to allow mixing of alcohol and embedding agent (paraffin). The samples were then embedded in paraffin wax.

Sectioning was followed by cutting of tissues with a microtome, and sections of tissues were mounted on microscope slides. The slides were deparaffinised in a hot air oven at 60 °C for 30 min, and was immersed in xylene for 10 min to clear the wax. Then, the sections were rehydrated in graded alcohol (100%, 95%, 70%, 50%). The tissues were stained with haematoxylin for 5 min, then rinsed with distilled water until a blue colouration formed. Eosin was then introduced to the tissue sections for 15 secs, and then dipped in distilled water to remove excess stain. This was followed by dehydration with graded alcohol (50%, 70%, 95%, 100%), and cleared with xylene.

The slides were drained of excess water, and water-soluble mountant was added before covering with cover-slips, for light microscopic examination.

3.2.3.6.6 Immunohistochemistry

Paraffin-embedded tissues were used for immunohistochemical staining with p-I*k*B-α, IFN-γ and IL-18 antibodies, markers of inflammation (Siegmund *et al.*, 2001). Antigen retrieval was performed on the rehydrated tissue sections prior to haematoxylin staining (Section 3.2.3.6.5), by incubating tissue sections with 10 mM Tris buffer and 1 mM EDTA (pH 8.5) in water bath (90

°C) for 5 min. The slides were cooled on ice for 2 min, and tissue sections were incubated in 3% hydrogen peroxide for 10 min to quench endogenous peroxidases. Sections were blocked with 1% BSA and 0.1% Triton X-100 in 1 x PBS (pH 7.4) at room temperature for 10 min. Tissue sections were then incubated at room temperature with a 1:1000 dilution of primary antibodies (p-I*k*B-α, IFN-γ or IL-18), in 1 x PBS (pH 7.4), for 3 hr. Sections were washed 2 times in PBS for 10 min, and further incubated with secondary antibody (Cy3-conjugated F(ab')2 fragment donkey-anti-mouse, 1:500 dilution in PBS), for 1 hr. Excess antibody was removed by washing at room temperature in PBS (2 times for 10 min), and then incubated with Hoechst nucleus staining in the dark for 30 min. The sections were then washed with PBS, and viewed using light microscopy. A positive control (an inflamed tissue sample of high fat diet-fed rat) was used to set the exposure time.

### 3.2.4 Statistical analysis

Statistical analyses were performed following the advice of a statistician at Nelson Mandela University, South Africa. The analyses were completed with the one-way analysis of variance (ANOVA), using SPSS software package for Windows (version 16.0, 2007). Whenever a significant difference was detected, post-hoc testing was performed for inter-group comparisons using Tukey's multiple comparisons test (Alalaiwe *et al.*, 2017). All results are expressed as mean ± standard deviation (SD) for six determinations (n=6). In all instances, p values $< 0.05$ were considered statistically significant.

# CHAPTER FOUR

# RESULTS AND DISCUSSION

## 4.1 CHARACTERISATION OF GOLD NANOPARTICLES

### 4.1.1 Ultraviolet-Visible spectroscopy

The characteristic resonance peaks of the AuNPs obtained by UV-Vis spectroscopy is shown in Figure 4.1a, and are in the wavelength range attributed to 14 nm AuNPs (520-530 nm) (Rambanapasi *et al.*, 2016). There were slight red shifts in the wavelengths of the functionalised-AuNPs when compared to the citrate-AuNPs (520 nm), i.e. 522, 524, 524 and 525 nm for PEG-, p.C-PEG-, p.L-PEG-, and p.14-PEG-AuNPs, respectively (Figure 4.1a). These results are similar to a study by Sosibo *et al.* (2015), where slight shifts were noted in the UV-Vis spectra of AuNPs with the surface plasmon resonance peaks detected at 520, 524, and 525 nm for citrate-, PEG-, and TAT-AuNPs, respectively. The slight red shift in the surface plasmon resonance was caused by PEG and peptides on the surface of citrate-AuNPs, with no broadening of the peaks. This indicates mono-dispersed AuNPs, with no aggregation on functionalisation (Sosibo *et al.*, 2015).

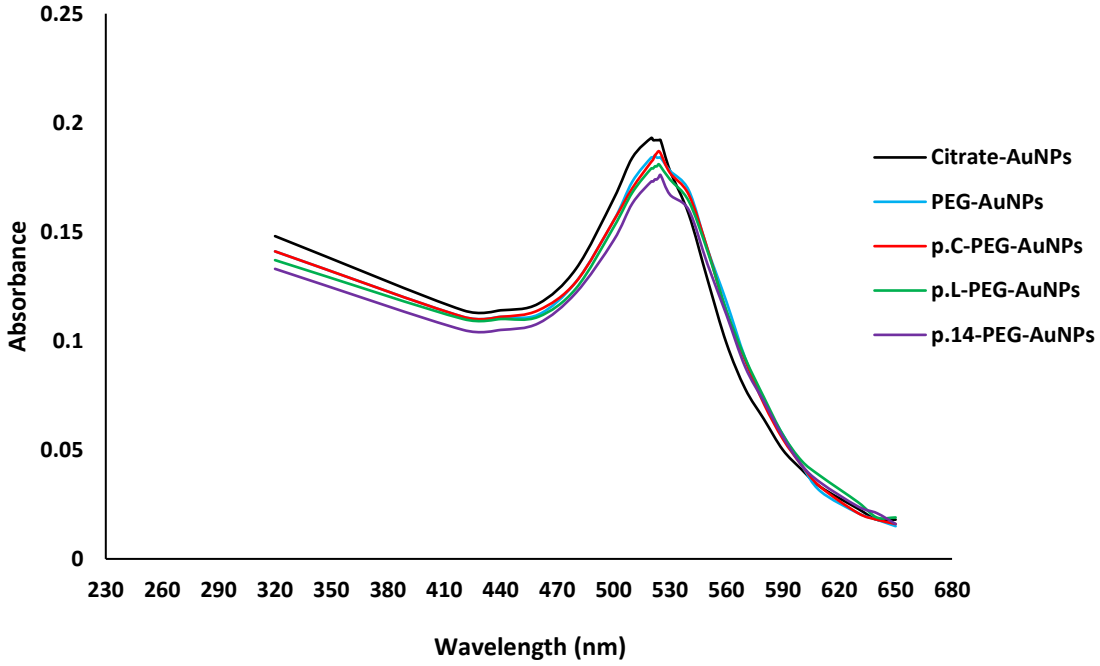


**Figure 4.1:** UV-Vis spectra of AuNPs showing the surface plasmon resonance shifts.

### 4.1.2 High resolution transmission electron microscopy

The HRTEM micrographs of all the AuNPs showed uniform spherical particles with average diameters of 14 ± 1 nm (Figure 4.2a-e). There were no changes in the shape or size of the NPs on conjugation, and no signs of aggregation were observed. A thin film (arrow) surrounding the citrate-AuNPs (Figure 4.3a) was observed in all the conjugated AuNPs (Figure 4.3b-e), suggesting the presence of peptide on the surface of the AuNPs. A similar result was reported by Thi Ha Lien *et al.* (2012), where a film was observed around citrate-AuNPs, indicating the presence of a BSA protein layer on the surface of AuNPs.

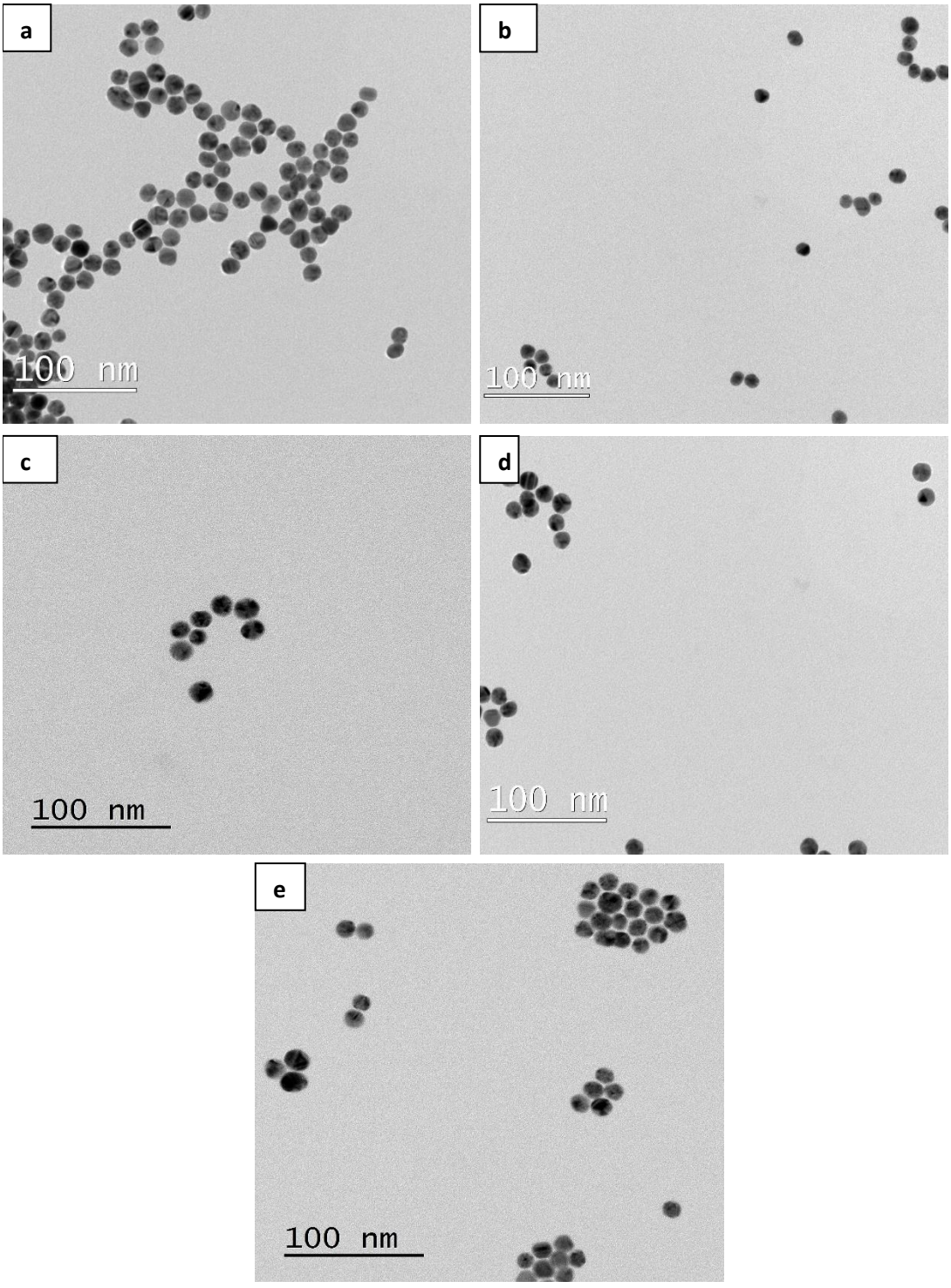


**Figure 4.2:** Transmission electron micrograph of a) citrate-AuNPs (*scale bar 100 nm*), b) PEG-AuNPs (*Scale bar 100 nm*), c) p.C-PEG-AuNPs (*Scale bar 100 nm*), d) p.L-PEG-AuNPs (*Scale bar 100 nm*), e) p.14-PEG-AuNPs (*Scale bar 100 nm*).

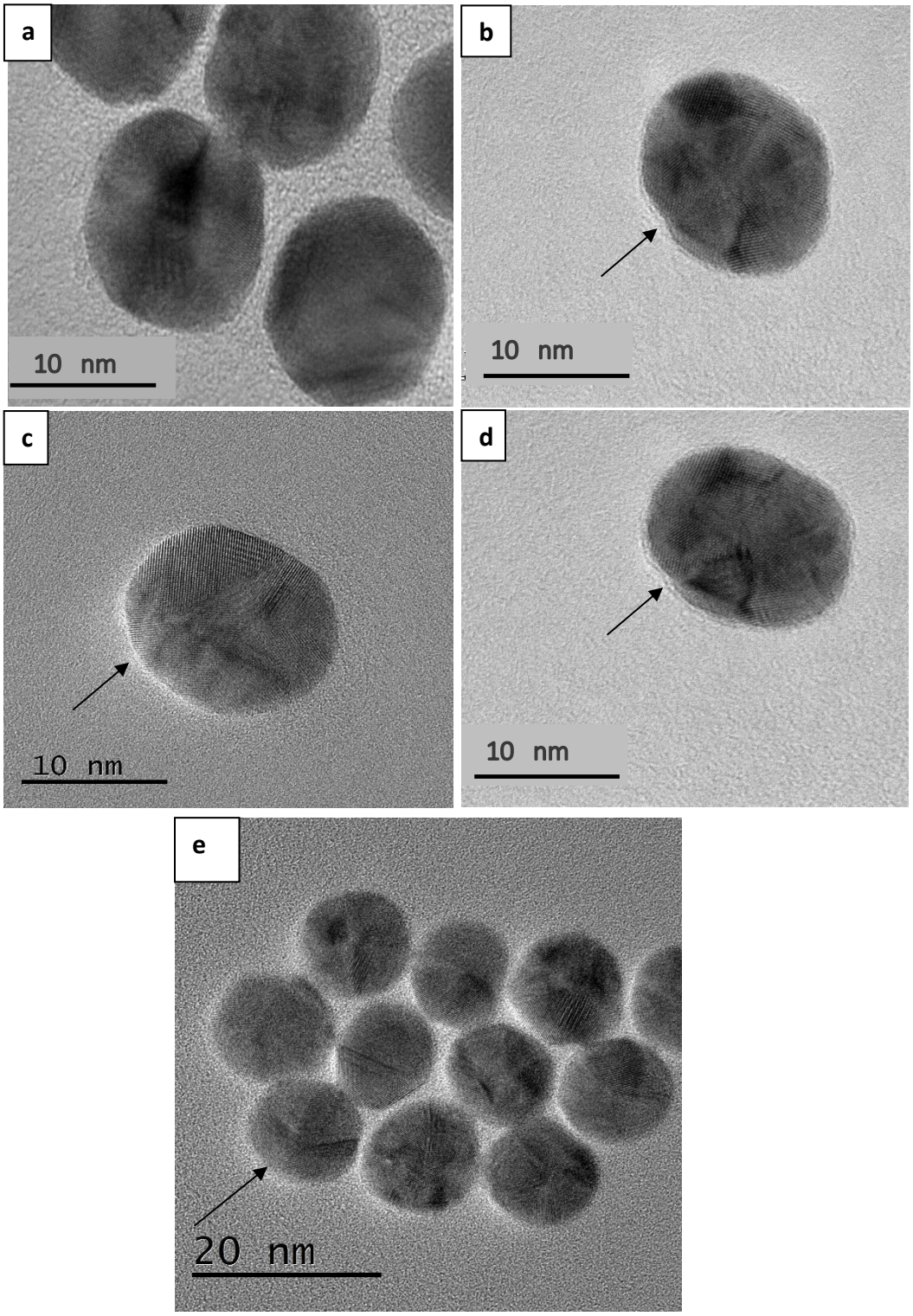


**Figure 4.3:** Transmission electron micrograph of a) citrate-AuNPs (*scale bar 10 nm*), b) PEG-AuNPs (*Scale bar 10 nm*), c) p.C-PEG-AuNPs (*Scale bar 10 nm*), d) p.L-PEG-AuNPs (*Scale bar 10 nm*), e) p.14-PEG-AuNPs (*Scale bar 20 nm*).

### 4.1.3 Zeta potential and dynamic light scattering measurements

The zeta potential measurement showed a negative value for the surface potential of citrate-capped AuNPs, indicating the presence of negatively-charged citrate (Table 4.1). On conjugation, there was an increase in the zeta potential of the conjugated-AuNPs. This indicates the presence of additional functional groups on the citrate-capped AuNPs (Verissimo *et al.*, 2016), causing a reduction in the negativity of citrate. The slight reduction in the negativity of PEG-AuNPs when compared to citrate-AuNPs could suggest the presence of polar hydroxyl group on PEG-OH and biotin on PEG-biotin. The presence of $NH_3^+$ groups on the peptides could explain the sharp reduction in the zeta potential values towards neutral (Table 4.1). In addition, the terminal amino acid in p.14-PEG-AuNPs (methionine) is more hydrophobic when compared to glycine of p.C-PEG-AuNPs and tyrosine of p.L-PEG-AuNPs (Section 2.2.3.2.1). This could suggest the decreased negativity when compared to p.C- and p.L-PEG-AuNPs (Table 4.1). The presence of additional functional groups was confirmed by increases in the hydrodynamic size of the conjugated-AuNPs with the DLS measurements. An increase in the hydrodynamic size of conjugated-AuNPs (Table 4.1) could result from the presence of PEG and peptides on the surface of citrate-AuNPs. This agrees with studies by Kalmodia *et al.* (2016) and Leopold *et al.* (2017), where significant increases were observed in size distributions upon coating of AuNPs with BSA and Pep-A, respectively. Increased sizes of the AuNPs obtained with the DLS measurement when compared to the size obtained using HRTEM (Figure 4.2) could be linked to the hydration of the AuNPs during DLS measurements. The polydispersity results showed that the AuNPs were well-dispersed in aqueous media, as all the values were less than 0.7 (no agglomeration), which are in the acceptable range described by Jiang *et al.* (2013) and Akrami *et al.* (2016). The AuNPs were stable in the respective suspension solutions (no change of colour in the solution) at 4 $^0$C up to 2 months (Figure 4.4). Citrate-AuNPs were stable in milli-Q water, while the conjugated AuNPs were unstable and aggregated in water on addition of streptavidin to the PEGylated AuNPs, but were stable in PBS.

**Table 4.1:** Zeta potential and DLS measurements of AuNPs, and the suspension media

| AuNPs | Zeta potential (mV) | DLS (nm) | Polydispersity | Suspension solution |
|---|---|---|---|---|
| Cit-AuNP | -31.34±2.37 | 17.94± 0.12 | 0.37±0.01 | Milli-Q water |
| PEG-AuNP | -25.60±1.15 | 19.70±0.20 | 0.19±0.00 | PBS |
| p.C-PEG-AuNP | -10.90±0.62 | 21.22±0.93 | 0.24±0.01 | PBS |
| p.L-PEG-AuNP | -9.22±1.22 | 20.93±0.12 | 0.10±0.01 | PBS |
| p.14-PEG-AuNP | -6.34±1.25 | 22.37±0.29 | 0.25±0.00 | PBS |

AuNPs – Gold nanoparticles; TEM – Transmission electron microscopy; Cit – Citrate; PBS – Phosphate-buffered saline; PEG – Polyethylene glycol. Values are reported as Mean ± SD.

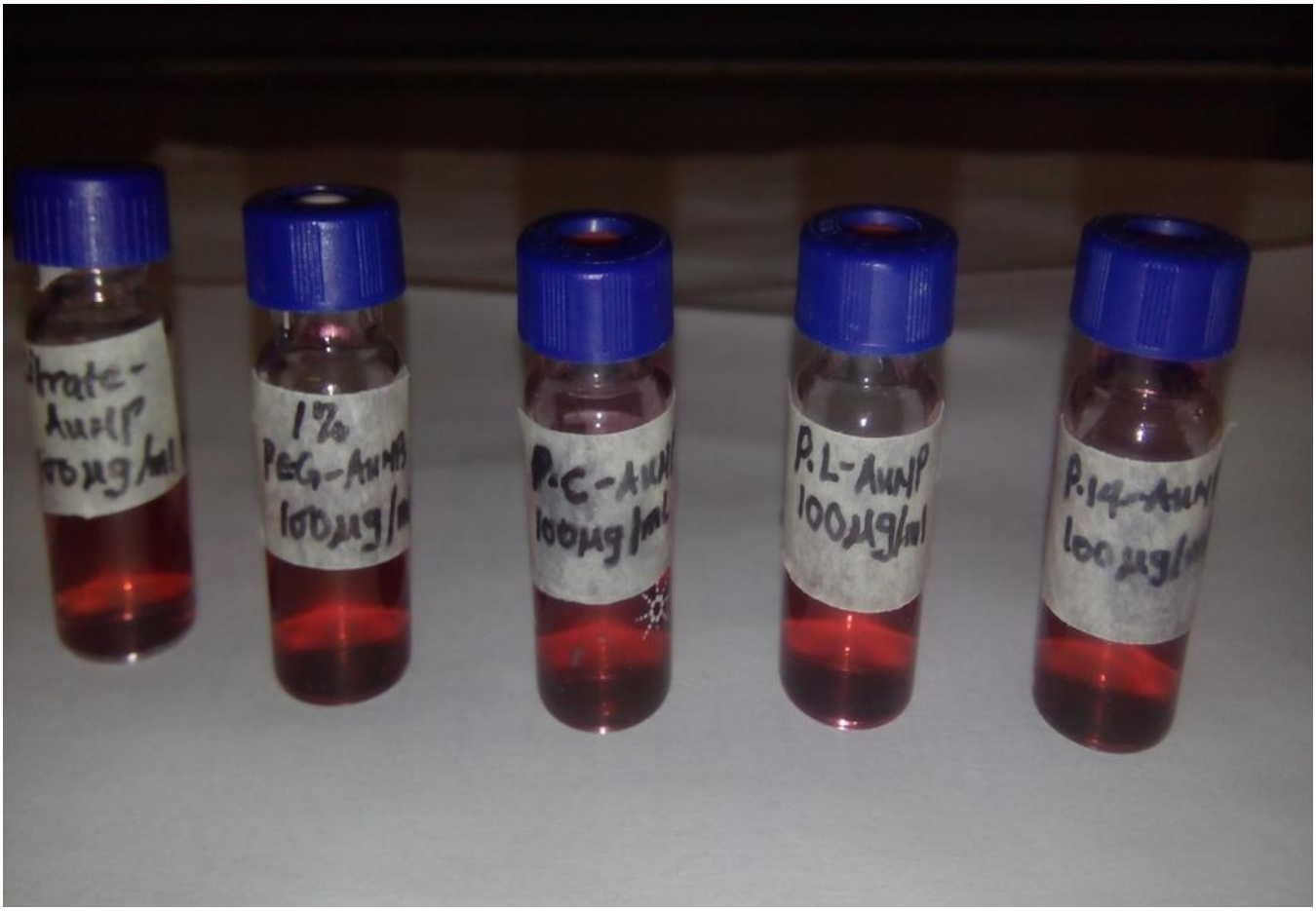


**Figure 4.4:** Physical appearance of gold nanoparticles (Citrate-AuNPs in milliQ water, conjugated-AuNPs in PBS)

### 4.1.4 Fourier transmission Infrared spectroscopy

Spectroscopic analysis of the AuNPs by FTIR is shown in Figure 4.5. The spectra revealed the presence of additional groups in the functionalised-AuNPs when compared to the citrate-AuNPs.

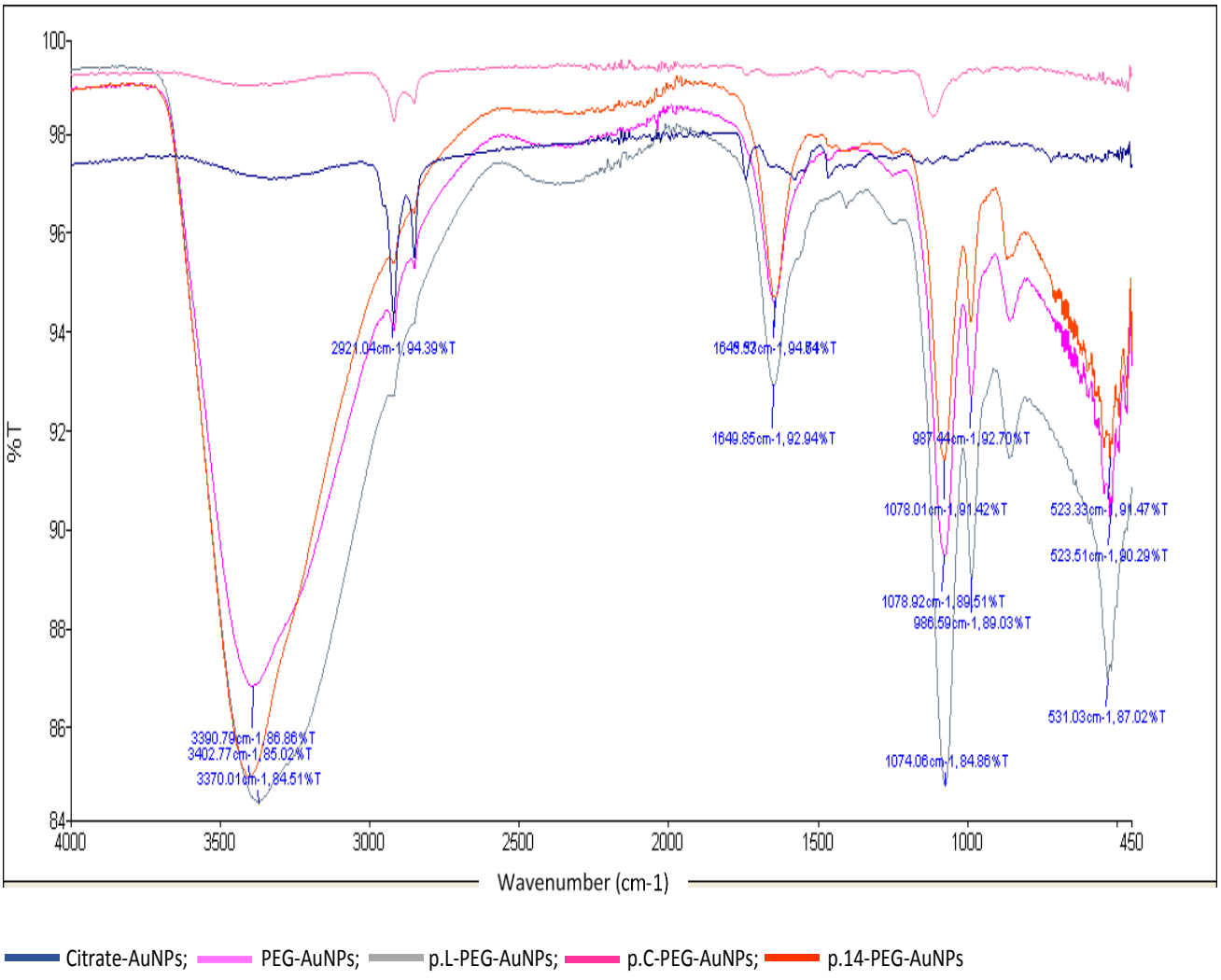


**Figure 4.5:** Fourier transmission infrared spectroscopy of gold nanoparticles.

The FTIR spectra of the AuNPs were recorded in the frequency range between 450 and 4000 $cm^{-1}$ in the % transmittance (%T) mode. The two characteristic peaks shown at 2985 and 2921 $cm^{-1}$ can be assigned to the presence of alkyl groups ($CH_2$ and $CH_3$) or stretching modes on the AuNPs,

as described by Kalmodia *et al.* (2016). These are more pronounced on citrate-AuNPs, followed by PEG-AuNPs and then the peptide-AuNPs. It is suggested that this is due to the loss of the alkyl groups by the washing steps during the synthesis of the peptide-conjugated AuNPs. The intense band at 1078 $cm^{-1}$ on PEG- and peptide-PEG-AuNPs was caused by the C-O stretching vibrations, which demonstrates the attachment of PEG on citrate-AuNPs. This is in the range of the intense C-O absorption band of PEG (1000–1290 $cm^{-1}$) (Leopold *et al.*, 2017), and near the stretching of ether bonds on PEG as indicated at the 1117 $cm^{-1}$ band (Cho *et al.*, 2009a; Cho *et al.*, 2010). The attachment of the peptides to PEG-AuNPs and citrate-capped AuNPs was seen with additional characteristic vibrational bands at 1645, 1645 and 1649 $cm^{-1}$, for p.C-, p.14 and p.L-PEG-AuNPs, respectively. This corresponds to the presence of amide bonds in the characteristic vibrational features of proteins (1500-1700 cm-1) (Kalmodia *et al.*, 2016; Leopold *et al.*, 2017). Absorption bands of 3370, 3390 and 3402 $cm^{-1}$ correspond to the presence of $NH_3^+$ on the amino acids make-up of p.L, p.C and p.14, respectively, which are in the previously described range of 3000–3500 $cm^{-1}$ (Kalmodia *et al.*, 2016).

## 4.2 PHASE 1 *IN VIVO* EXPERIMENT

The phase 1 study investigated the acute toxicity (2 weeks after administration) of a single intravenous administration of 14 nm AuNPs (100 µg/kg b.w.) in rats. An acute toxicity study is important to provide first-line information about the direct effect of AuNPs on tissues *in vivo*. Guidelines for the *in vivo* testing of chemicals are periodically updated (OECD, 2008), a single exposure to a substance, even at low dose, could cause long-lasting damage to an organism, and therefore toxicity studies are important. Nanoparticles have unique properties such as small size, large surface area, easy penetration of cells and ability to react with various biological components, and their general behaviour *in vivo* (Schmid *et al.*, 2017).

Acute toxicity studies include observations done within the first 48 h (OECD, 2008), up to studies within 2 weeks. Interference with vital physiological processes or severe activation of the immune system can be observed within the first 24 h post-exposure to a substance. Physiological

responses which affect homeostatic regulation, for instance, liver function or inflammation, will be better observed after two weeks.

An acute study up to 48 h was not done, since a previous pilot study with the peptide-AuNPs showed no obvious side-effects (Cairncross, 2015). In this current study, various parameters were investigated to provide insight to possible toxic effects of AuNPs two weeks after a single intravenous injection to rats.

### 4.2.1 Assessment of general body signs

Animals were monitored during the first four hours after injection with the AuNPs for signs of adverse reactions. This was followed by daily monitoring for the duration of the study. The rats did not show any signs of adverse reactions or observable toxicity. No change in the behaviour of the animals was noted, and no mortalities occurred. The results of this study contrast the acute and chronic exposure study of Sengupta *et al.* (2013), where there were physical and morphological changes in mice injected intraperitoneally with 50 nm AuNPs (2 mg/kg/day) after 8 days, and 1 mg/kg b.w. after 15 days. These differences could be due to the size, dose, and animal model used in the study.

### 4.2.2 Effect on food intake and water consumption

During the 2-week period, there were no significant changes in either the food or water intake in all the NP-treated rats when compared to the control group ($p>0.05$) (Table 4.2).

**Table 4.2:** Effect of AuNPs on food intake and water consumption

| Treatment | Average food intake (g/day/rat) | Average water intake (mL/day/rat) |
|---|---|---|
| PBS control | 7.30±0.67 | 37.56±0.77 |
| Cit-AuNPs | 7.03±0.53 | 36.67±0.26 |
| PEG-AuNPs | 7.12±0.49 | 39.17±0.83 |
| p.C-PEG-AuNPs | 6.93±0.29 | 35.61±0.03 |
| p.L-PEG-AuNPs | 6.90±0.17 | 37.42±0.06 |
| p.14-PEG-AuNPs | 6.80±0.31 | 36.35±0.96 |

Cit - Citrate; PBS – Phosphate-buffered saline; AuNPs – Gold nanoparticles
Values are expressed as Mean ± SD, n=6

In another study, up to 8 weeks, there were also no signs of toxicity as revealed by the feeding habits of rats injected intravenously with 14 nm citrate-capped AuNPs (3–375 µg/kg b.w.) (Rambanapasi *et al.*, 2016).

### 4.2.3 Effect of AuNPs on body weights

The effect of the AuNPs on the weights of the rats is shown in Figure 4.6. A single intravenous injection of AuNPs (100 µg/kg b.w.) did not affect the body weights of AuNP-treated rats when compared to the control group ($p>0.05$), or inter-group comparison ($p>0.05$), during the 2-week study period (Figure 4.6). There was, however, a non-significant reduction ($p>0.05$) in the body weight of the AuNP-injected rats 1 week post-injection. It is suggested that the weight loss results from exposure to foreign agents, although there was a recovery to normalcy at 2 weeks. This indicated that the rats were healthy. These results are similar to a study by Ghahnavieh *et al.* (2014), where no significant difference in the body weights of mice was observed 2 weeks after intraperitoneal injection of 10 nm citrate-capped AuNPs.

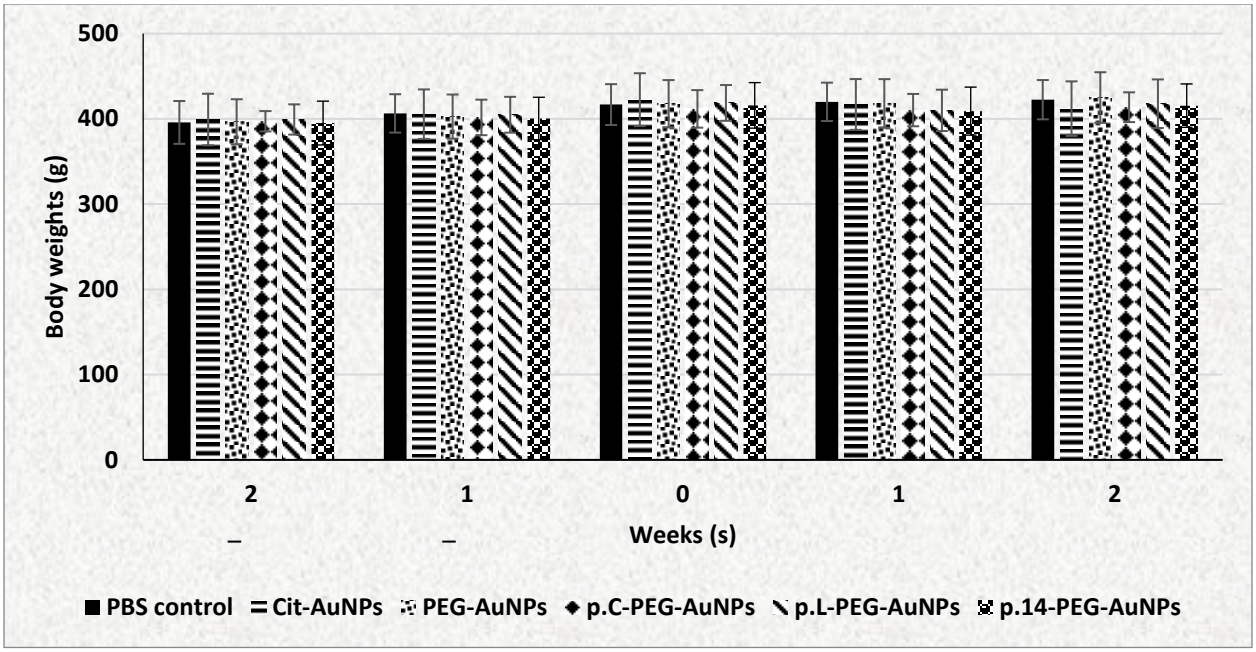


**Figure 4.6:** Body weights (g) of rats 2 weeks pre- and post-injection of AuNPs.
Cit - Citrate; PBS – Phosphate-buffered saline; AuNPs – Gold nanoparticles
Values are expressed as Mean ± SD, n=6

### 4.2.4 Effect on organ weights

Significant changes in organ weights are regarded as indices of toxicity in animals, which is determined by toxicity tests (Adewale *et al.*, 2016). A single intravenous injection of AuNPs did not affect the organ weights of the rats after 2 weeks, except the liver, where a significant decrease ($p=0.016$) was observed in p.L-PEG-AuNP-treated rats when compared to the control group (Figure 4.7). The weights of the spleen and colon of p.C-PEG-AuNP-treated rats were significantly increased when compared to the citrate-AuNP-injected rats and the control group, respectively ($p<0.05$). The increased spleen weight might be an indication of systemic toxicity, as described by El-Nahas *et al.* (2017), and needs further investigation. The unchanged weights of some organs in this study is similar to the findings of Zhang *et al.* (2011), where no significant changes in organ weights (liver, lungs, kidneys, heart, and spleen) were noted 4 weeks post-injection with 5, 10, 30, and 60 nm PEG-AuNPs (4000 µg/kg) to mice.

Overall, the unchanged organ weights of rats in the AuNPs groups when compared to the control group suggest that there was no toxicity to the vital organs. Biochemical and histopathological examinations of the liver, kidney, spleen and colon are, however, required to validate these observations.

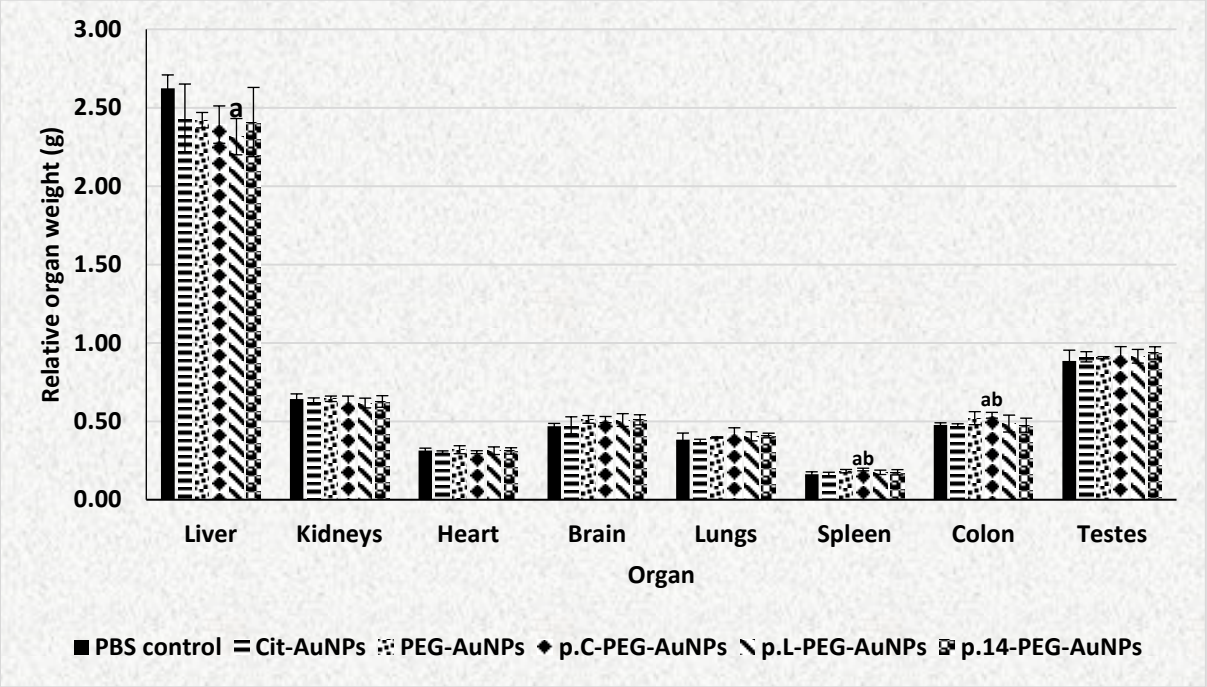


**Figure 4.7:** Relative organ weights of rats 2 weeks post-injection of AuNPs (per 100 g body weight).
Cit - Citrate; PBS – Phosphate-buffered saline; AuNPs – Gold nanoparticles
Values are expressed as Mean ± SD, n=6
[a]p<0.05 when compared to the PBS control group; [b]p<0.05 when compared to Cit-AuNP group

### 4.2.5 Biochemical analyses in the serum

#### *4.2.5.1 Serum marker enzymes*

Alanine aminotransferase and AST are important enzymes used to assess the hepatocellular integrity of the liver. ALT is predominantly found in the liver, while AST is found in equal concentrations in the liver, heart, muscle, kidney and brain (Dollah *et al.*, 2013). ALP is a marker of liver or hepatobiliary damage (non-specific) and bone disease, as is commonly found on the canalicular membrane of the hepatocytes and in the bone (Kwo *et al.*, 2017). As these enzymes

are present within the hepatocytes, any damage to the hepatocytes would cause leakage of these enzymes from the liver (Abou Seif, 2016; Hanafy *et al.*, 2016).

Elevated levels of ALT, AST, and ALP in the blood thus indicate liver damage, and some other organs. In this study, no significant differences in the concentrations of ALT and AST ($p>0.05$) were noted after a single injection of AuNPs to rats when compared to the control group (Figure 4.8). The levels of AST in the p.L-PEG-AuNPs group showed a significant increase ($p<0.05$) when compared to the p.C-PEG-AuNPs group, but this is only because p.L-PEG-AuNP and p.C-PEG-AuNP have opposite effects due to differences in the amino acid sequence, and therefore is not regarded to have any clinical value. The non-significant change is similar to a study by Rambanapasi *et al.* (2016), where no significant changes in the levels of liver damage markers in 14 nm citrate-AuNPs-treated rats were noted, even with repeated doses (3 – 375 µg/kg b.w.) for 7 weeks.

Alkaline phosphatase activity was decreased in all the treated rats, however, was only significantly reduced ($p<0.05$) in the PEG-, p.C-PEG-, and p.L-PEG-AuNPs-treated rats when compared to the control group. The predominant isoform of ALP in circulation (in mature rats) originates from the intestine, and are responsive to food intake, i.e. decreased total ALP is an indicator of decreased food intake (Ramaiah, 2007; York, 2013). The observed reduction in ALP levels do not directly correlate with the food intake (Table 4.2), and can therefore not be linked to food intake in this study. Since neither ALT nor AST, except for increased level in p.L-PEG when compared to the citrate-AuNPs, were significantly affected by AuNP injections, it is expected that the significant changes of ALP were derived from either bone or hepatobiliary (though not specific) sources.

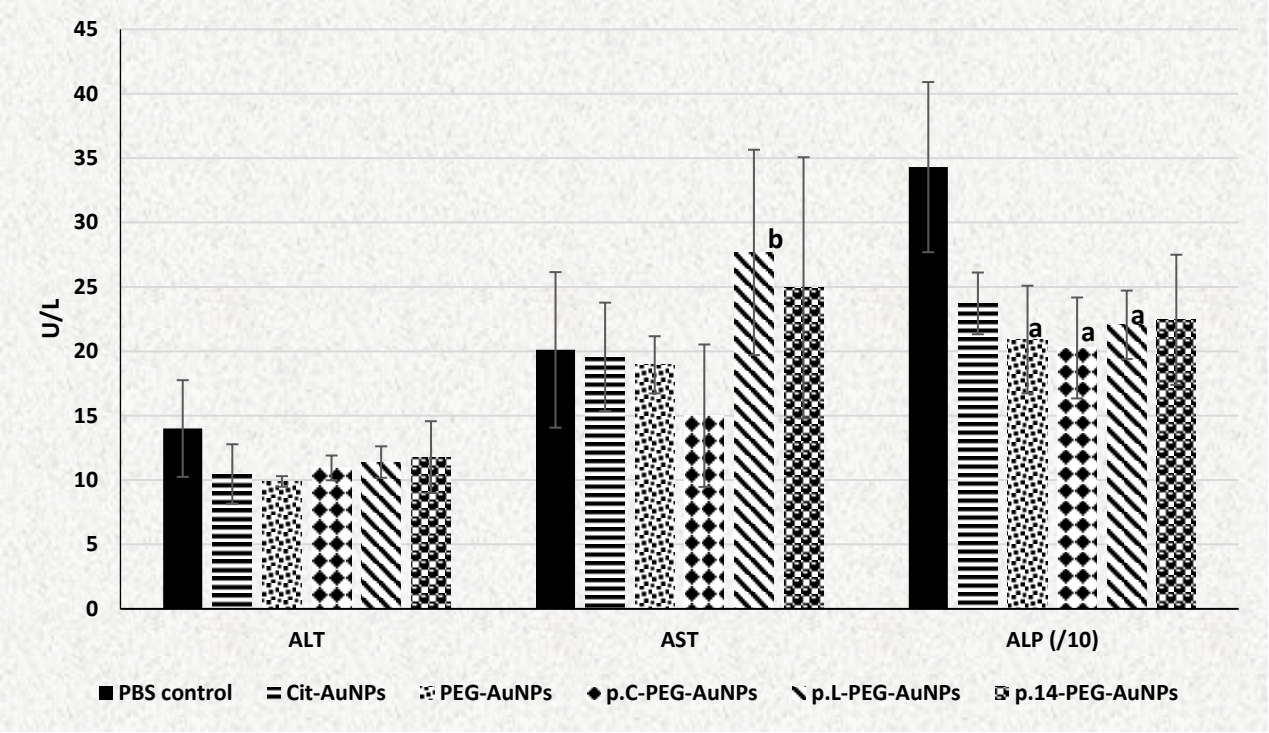


**Figure 4.8:** Effect of a single intravenous injection of AuNPs on serum marker enzymes
Cit - Citrate; PBS – Phosphate-buffered saline; AuNPs – Gold nanoparticles; (/10) – Actual values divided by 10
Values are expressed as Mean ± SD, n=6. [a]p<0.05, when compared to PBS control group [b]p<0.05, when compared to p.C-PEG-AuNPs group.

### *4.2.5.2 Hepatic function markers*

The effect of a single intravenous injection of AuNPs on hepatocellular function markers, including albumin, total protein, and bilirubin (direct and total), is shown in Figure 4.9 and Table 4.3. Albumin, a major component of total protein, is an indicator of hepatocellular function (Kwo *et al.*, 2017). Any marked reduction in serum albumin levels indicates an impairment of liver function. Here, no significant difference in the levels of albumin and total protein ($p>0.05$) were noted in all the treatment groups when compared to the control group (Figure 4.9). This suggests normal synthesis of proteins by the liver, as described by Hanafy *et al.* (2016). In p.L-PEG-AuNP-treated rats, the level of total protein was significantly reduced when compared to citrate-, PEG-, and p.14-PEG-AuNPs groups ($p<0.05$). P.L-PEG-AuNP was the only AuNP that showed a trend towards reduced protein synthesis. It was also noted that the liver weight and ALP were

significantly reduced in rats treated with p.L-PEG-AuNP, with a trend towards increased serum AST.

Bilirubin is a product of haemoglobin breakdown, which is normally excreted via the bile and urine. As a marker of hepatocellular function, elevation in the levels of total and direct bilirubin in the serum indicates hepatobiliary and hepatic function disorders (Okokon *et al.*, 2017). This increase may result from over-production of bilirubin through haemolysis and decreased liver uptake (Sefi *et al.*, 2014; Kunjiappan *et al.*, 2015). Elevations in both direct and total bilirubin could also result from decreased conjugation and reduced secretion from the liver, or as a result of blockage of bile ducts (Hussein and Khalifa, 2014). In this study, no significant changes to direct and total bilirubin were noted (Table 4.3).

These results are similar to a study by Rambanapasi *et al.* (2016), where no significant changes in the level of total bilirubin in 14 nm citrate-AuNPs-treated rats were noted when compared to the control group ($p<0.05$). The dose (100 µg/kg b.w.) used in the current study falls within the range of the doses (3 - 375 µg/kg b.w.) of 14 nm citrate-AuNPs administered by Rambanapasi *et al.* (2016).

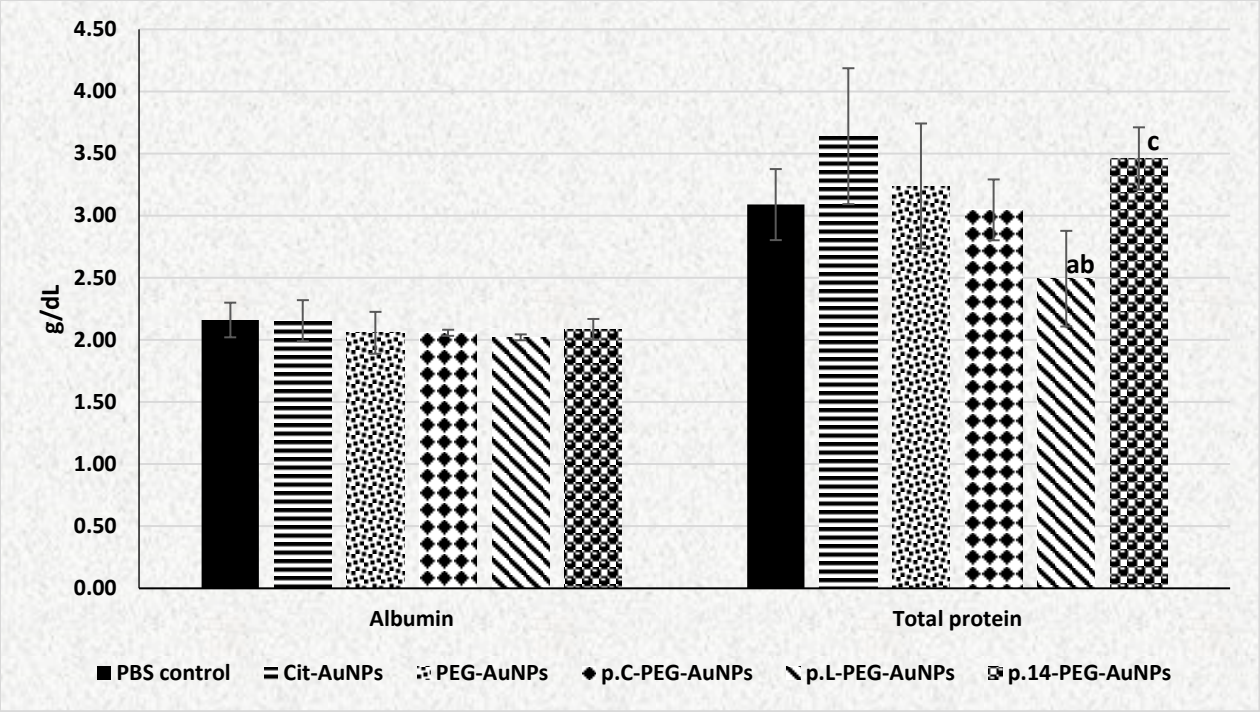


**Figure 4.9:** Effect of AuNPs on the levels of albumin and total protein
Cit - Citrate; PBS – Phosphate-buffered saline; AuNPs – Gold nanoparticles
Values are expressed as Mean ± SD, n=6. [a]p<0.05 when compared to Cit-AuNP group; [b]p<0.05 when compared to PEG-AuNPs group; [c]p<0.05 when compared to p.L-AuNPs group

**Table 4.3:** Effect of AuNPs on bilirubin levels in rats

| Treatment | Direct bilirubin (mg/dL) | Total bilirubin (mg/dL) |
|---|---|---|
| PBS control | 0.06±0.03 | 0.19±0.15 |
| Cit-AuNPs | 0.04±0.02 | 0.14±0.10 |
| PEG-AuNPs | 0.04±0.02 | 0.16±0.09 |
| p.C-PEG-AuNPs | 0.07±0.03 | 0.12±0.06 |
| p.L-PEG-AuNPs | 0.06±0.02 | 0.12±0.10 |
| p.14-PEG-AuNPs | 0.06±0.04 | 0.11±0.08 |

Cit - Citrate; PBS – Phosphate-buffered saline; AuNPs – Gold nanoparticles
Values are expressed as Mean ± SD

#### *4.2.5.3 Kidney function markers*

Elevation in the levels of serum urea and creatinine are indicative of renal impairment or kidney damage (Adewale *et al.*, 2016). In this study, there was no significant difference ($p>0.05$) in the level of these parameters when compared to the control group (Table 4.4). This is similar to the study by Rambanapasi *et al.* (2016), where no nephrotoxicity was observed after weekly intravenous administration of 14 nm citrate-capped AuNPs (3 – 375 µg/kg b.w.) for 7 weeks. This, however, contradicts the findings of Rathore *et al.* (2014), where significant differences in urea and creatinine levels were noted after oral administration of 10 nm citrate-capped AuNPs (20 µg/kg b.w.) to rats for 21 days when compared to the control group. The contradiction could result from differences in size, dose, exposure time, route of administration, as well as surface chemistry of the AuNPs used.

A significant increase in the levels of creatinine was noted in p.L-PEG-AuNP-treated rats when compared to the citrate-AuNP group. This significant difference was probably due to lower creatinine levels in the citrate-AuNP group. Increased creatinine levels result normally from increased damage to muscle tissues and creatinine leaking into the interstitial fluid. Lower muscle mass will be expected for clear signs of inflammation at two weeks post-injection. Increased levels of urea would also be expected (Higgins, 2016). There were no significant changes in the urea levels, and in the relative heart weights of these treatment groups (citrate-AuNPs and p.L-PEG-AuNPs) when compared to the control group, which indicates no significant effects on the kidneys and muscle mass. Since there was no significant difference when compared to the control group, the tendency of increased creatinine in the p.L-PEG-AuNP treated group was only noted.

**Table 4.4:** Effect of AuNPs on kidney function markers

| Treatment | Urea (mg/dL) | Creatinine (mg/dL) |
|---|---|---|
| PBS control | 39.85±3.87 | 1.02±0.18 |
| Cit-AuNPs | 36.58±2.70 | 0.82±0.18 |
| PEG-AuNPs | 39.25±2.42 | 1.06±0.19 |
| p.C-PEG-AuNPs | 37.64±3.40 | 0.85±0.23 |
| p.L-PEG-AuNPs | 35.80±1.66 | 1.25±0.14[a] |
| p.14-PEG-AuNPs | 37.07±4.09 | 1.17±0.32 |

Cit - Citrate; PBS – Phosphate-buffered saline; AuNPs – Gold nanoparticles
Values are expressed as Mean + SD, n=6. [a]$p<0.05$ when compared to Cit-AuNP group

### 4.2.6 Haematological analyses

Blood and its components give an index of the pathological and physiological status of animal health (Adewale *et al.*, 2016). This is because the circulatory system is the major medium of transport for nutrients and foreign substances. The haematopoietic system (the most sensitive target of toxic substances), may be affected on exposure to foreign substances. White blood cells play a major role in the immune system as it provides immunity against antigen exposure (Arika *et al.*, 2016).

In this study, the pathological and physiological indices were investigated via the haematological analysis in rats injected with AuNPs (Table 4.5a and b). Differential WBC counts, and haemoglobin tests were performed to determine the effect of the AuNPs on the haematological parameters. Although the AuNPs did not affect some of these parameters, significant reductions were observed in the absolute values of neutrophils in the AuNP-treated rats ($p<0.05$) when compared to the control (Table 4.5a). This reduction could be linked to increased interaction with neutrophils after exposure to toxic substances (such as toxic NPs), or the reduced production of neutrophils (Arika *et al.*, 2016). In p.C- and p.L-PEG-AuNP groups, there was a significant reduction in the relative values of neutrophils when compared to the control group ($p<0.05$) (Table 4.5b). This could be related to increases in the relative values of lymphocytes due to

increased production of antibodies against the NPs (Dykman and Khlebtsov, 2011). Further, a significant reduction in total WBC count and lymphocytes was observed in the p.L-PEG-AuNPs rats when compared to the control group ($p<0.05$) (Table 4.5a). This suggests impaired function of the haematopoietic system following exposure to p.L-PEG-AuNPs, as 10 nm AuNPs reportedly caused an adverse effect on the haematopoietic system (Ghahnavieh *et al.*, 2014). Haemopoiesis takes place in the red bone marrow, and it can be recalled that there was a significant change in the ALP level in the p.L-PEG-AuNP group when compared to the control group. No signs of anaemia were observed in this study, as indicated by the constant levels of haemoglobin (Arika *et al.*, 2016).

After acute and chronic exposure of 50 nm AuNPs (1, 2 and 10 mg/kg) to mice, a significant increase in WBC and lymphocyte numbers, as well as haemoglobin (except for 1 mg/kg) were noted (Sengupta *et al.*, 2013). This contrasts with the present study, and could be due to differences in the size and dose of injected AuNPs, and animal model used.

**Table 4.5a:** Effect on haematological parameters with absolute values of the differential white blood cell counts

| Treatment | Hb (g/dL) | WBC ($10^{\wedge 9}$/L) | Lym ($10^{\wedge 9}$/L) | Neu ($10^{\wedge 9}$/L) | Mon ($10^{\wedge 9}$/L) | Eos ($10^{\wedge 9}$/L) | Bas ($10^{\wedge 9}$/L) |
|---|---|---|---|---|---|---|---|
| PBS control | 15.50±0.68 | 9.99±0.48 | 5.87±0.63 | 3.22±0.75 | 0.58±0.21 | 0.13±0.05 | 0.01±0.05 |
| PEG-AuNPs | 15.32±0.66 | 9.90±2.98 | 6.11±2.22 | 2.68±0.93[a] | 0.69±0.31 | 0.21±0.08 | 0.01±0.01 |
| p.C-PEG-AuNPs | 15.58±0.42 | 8.83±1.29 | 6.47±0.93 | 1.39±0.06[a] | 0.60±0.21 | 0.14±0.00 | 0.01±0.00 |
| p.L-PEG-AuNPs | 15.32±0.77 | 6.68±1.69[a] | 4.13±0.94[a] | 1.80±0.49[a] | 0.43±0.25 | 0.15±0.10 | 0.01±0.01 |
| p.14-PEG-AuNPs | 15.52±0.93 | 6.73±2.24 | 4.47±1.63 | 1.45±0.49[a] | 0.54±0.21 | 0.13±0.06 | 0.01±0.01 |

PBS – Phosphate-buffered saline; AuNPs – Gold nanoparticles; Hb – Haemoglobin; WBC – White blood cells; Lym - Lymphocytes; Neu - Neutrophils; Mon - Monocytes; Eos – Eosinophils; Bas – Basophils

Values are expressed as Mean ± SD, n=6

[a]$p<0.05$ when compared with the PBS group

**Table 4.5b:** Effect on haematological parameters with relative values (%) of the differential white blood cell counts

| Treatment | Lym (%) | Neu (%) | Mon (%) | Eos (%) | Bas (%) |
|---|---|---|---|---|---|
| PBS control | 58.88±6.95 | 32.02±5.92 | 5.93±2.26 | 1.32±0.52 | 0.05±0.05 |
| PEG-AuNPs | 60.97±6.44 | 27.12±6.39 | 6.80±1.65 | 2.04±0.40 | 0.10±0.06 |
| p.C-PEG-AuNPs | 73.38±2.54[ab] | 17.63±3.56[a] | 6.68±1.26 | 1.70±0.10 | 0.13±0.05 |
| p.L-PEG-AuNPs | 62.37±5.95 | 27.48±6.39 | 6.13±2.42 | 2.28±1.01 | 0.07±0.08 |
| p.14-PEG-AuNPs | 66.15±6.18 | 22.15±5.07[a] | 8.13±1.52 | 1.94±0.62 | 0.05±0.05 |

PBS – Phosphate-buffered saline; AuNPs – Gold nanoparticles; Lym - Lymphocytes; Neu - Neutrophils; Mon - Monocytes; Eos – Eosinophils; Bas – Basophils
Values are expressed as Mean ± SD, n=6
[a]$p<0.05$ when compared with the PBS group; [b]$p<0.05$ when compared with PEG-AuNPs group

### 4.2.7 Oxidative stress markers

Oxidative stress occurs when the body's defence mechanism (antioxidative system) is unable to neutralise an oxidative attack on cells and tissues, and could result from over-production of free radicals and ROS. This leads to damage to cellular components, including lipids, proteins, and DNA, and thus, cellular dysfunction (Rani *et al.*, 2016). Oxidative stress can be assessed by biomarkers, such as MDA (an index of lipid peroxidation), and protein carbonyls (an index of protein oxidation).

Peroxidation of lipids, mediated by free radicals, as a result of xenobiotics and environmental pollutants or during pathology, causes cellular damage and disrupts the biological membrane, leading to the leakage of liver marker enzymes into the extracellular fluid (Hanafy *et al.*, 2016). Treatment of rats with AuNPs in this study did not induce the expression of oxidative stress markers, as determined by levels of MDA and protein carbonyls, except in p.L-PEG-AuNPs-treated rats, where a significant increase in MDA levels ($p<0.05$) was noted (Table 4.6) when compared to the control, citrate-AuNPs and p.14-PEG-AuNPs groups ($p<0.05$). This indicates an increased potential of cellular damage by p.L-PEG-AuNPs. There was, however, no significant increase in the levels of protein carbonyl, and therefore only minor cellular damage is expected. It is thus suggested that care should be taken in the development of tools for CRC diagnosis using p.L-PEG-AuNPs.

The result of the study contrasts that of Abdelhalim *et al.* (2015), where significant differences in the oxidative stress markers in rats treated intraperitoneally with naked AuNPs were observed when compared to the control group. These disparities could be linked to differences in the size of AuNPs (10 nm), route of administration, and the duration of exposure (3 or 7 days), as well as surface chemistry (unconjugated AuNPs).

**Table 4.6:** Levels of oxidative stress markers in liver homogenates

| Treatment | MDA (µmol/mg protein) | Protein carbonyl (nmol/mg protein) |
|---|---|---|
| PBS control | 0.16±0.02 | 2.27±1.01 |
| Cit-AuNPs | 0.21±0.04 | 3.15±0.52 |
| PEG-AuNPs | 0.22±0.04 | 3.12±1.30 |
| p.C-PEG-AuNPs | 0.23±0.03 | 3.92±0.92 |
| p.L-PEG-AuNPs | 0.30±0.08[ab] | 2.96±0.80 |
| p.14-PEG-AuNPs | 0.20±0.04[c] | 2.54±0.70 |

Cit - Citrate; PBS – Phosphate-buffered saline; AuNPs – Gold nanoparticles
Values are expressed as Mean ± SD, n=6. [a]$p<0.05$ when compared to the PBS control group; [b]$p<0.05$ when compared to Cit-AuNPs group; [c]$p<0.05$ when compared to p.L-AuNPs group

### 4.2.8 Histopathological analysis

Photomicrographs showing various tissue (liver, kidney, spleen, colon, and pancreas) morphology of the treatment groups are shown in Figures 4.10 to 4.14.

a) Liver

The hepatic histology is congruent with age-matched healthy Wistar rats (Figure 4.10). There was no significant gross histopathology indicative of any pervasive adverse impact of the AuNPs. No fatty degeneration was observed. In all the groups, there was congestion of the central vein (CV) and sinusoidal spaces (arrow head), which could suggest intrahepatic haemodynamic forces prevalent at necropsy. Minimal bile duct (thick arrow) hyperplasia is noted in all groups. Little changes were noted in the architectural pattern of p.L-PEG-AuNP-treated rats. Further testing (over a longer exposure time) could elucidate the exact nature of these changes.

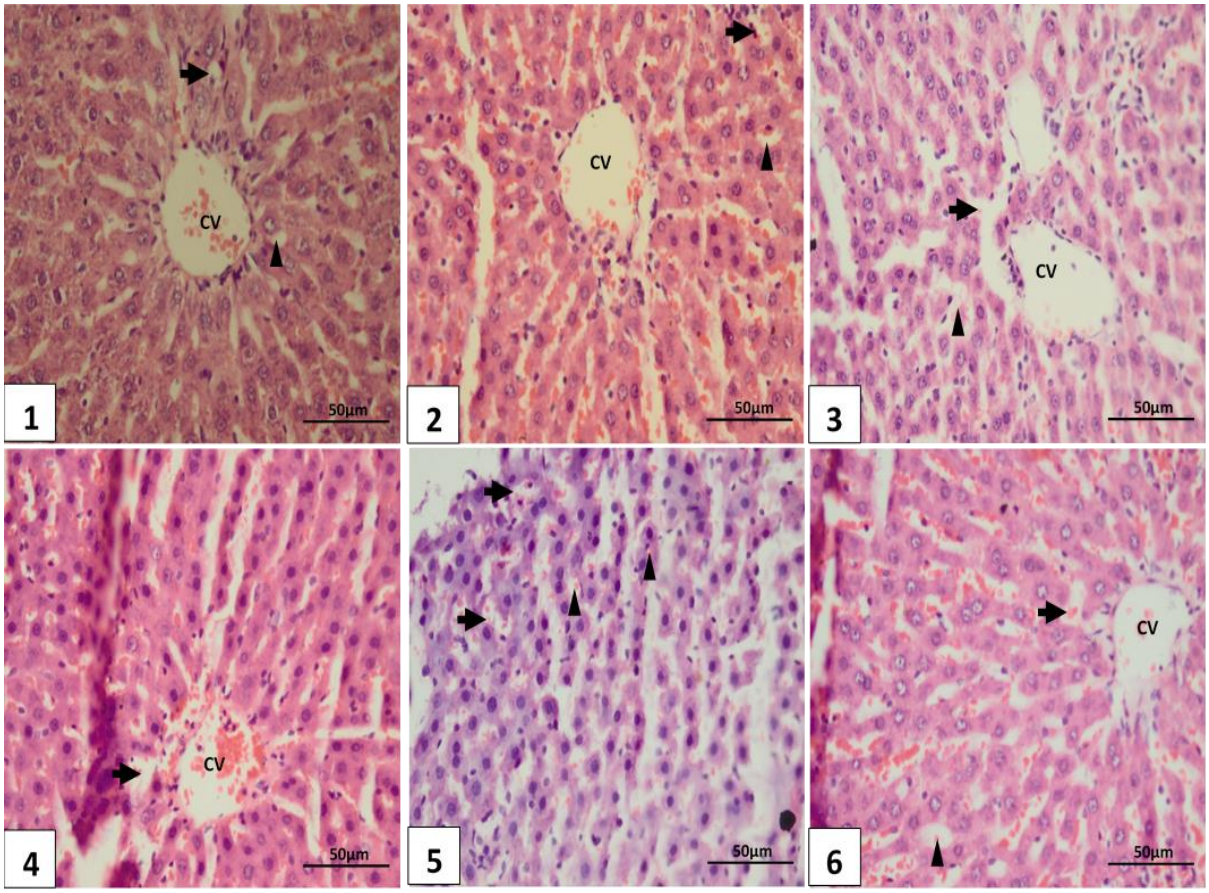


**Figure 4.10:** Histology of the liver 2 weeks after treatment with AuNPs *(Haematoxylin & Eosin, x400 original magnification, Scale bar = 50 µm)*
Key: 1 = PBS control; 2 = Citrate-AuNPs; 3 = PEG-AuNPs; 4 = p.C-PEG-AuNPs; 5 = p.L-PEG-AuNPs; 6 = p.14-PEG-AuNPs; CV = Central vein; thick arrow- Bile ducts; arrow head – Sinusoidal spaces.

b. Kidney

The glomerulus, being a high-pressured filtration structure under enormous physiological demand, is uniquely suited for toxicity-focused histomorphometrically assessment. Due to the inexorable high pressures over protracted times, the glomerulus inevitably reflects any cumulative deleterious changes associated with toxic metabolites (Carton *et al.*, 2007). Two important and physiologically inseparable micro-anatomical regions assessed were the glomerular filtration barrier (GFB), and the mesangial cells (thick arrow) (Figure 4.11). Figure 4.11 represents the histopathological analysis of kidney tissue sections of rats treated with AuNPs 2 weeks post-injection. In all groups, renal tubular integrity was intact, with no tubular specific changes noted. The histological integrity of the glomerular filtration membrane (arrow) and the Bowman's capsule (*) appeared normal in all groups. In addition, no

glomerulonephritis-associated changes in capillary patency and mesangial cellularity were noted.

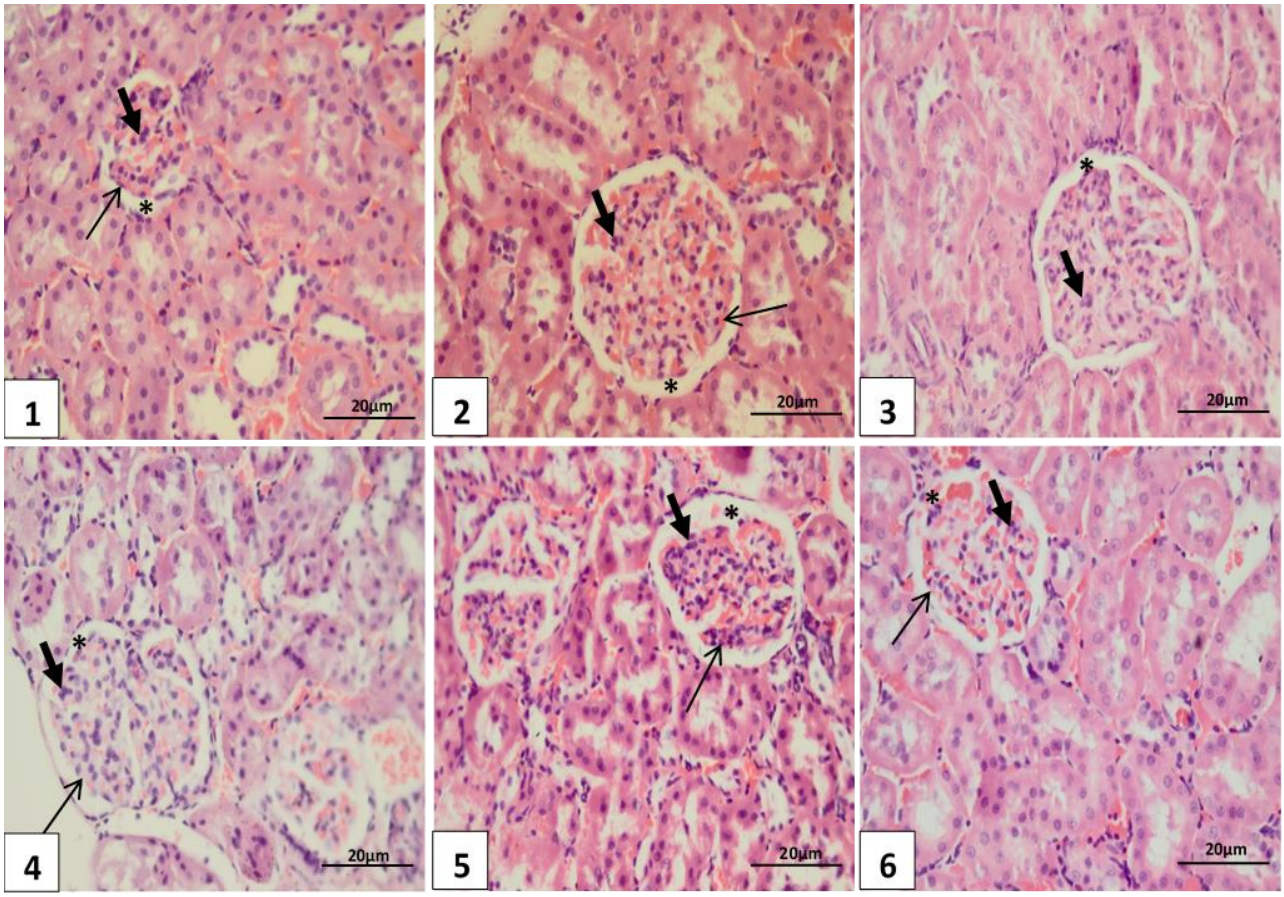


**Figure 4.11:** Histology of the kidney sections of rats 2 weeks after exposure to AuNPs (*Haematoxylin & Eosin, x400 original magnification, Scale bar = 20 µm*)
Key: 1 = PBS control group; 2 = Citrate-AuNPs; 3 = PEG-AuNPs; 4 = p.C-PEG-AuNPs; 5 = p.L-PEG-AuNPs; p.14-PEG-AuNPs. Arrow = filtration membrane; thick arrow = mesangial cells; * = Bowman's space

c. Spleen

The spleen is the largest secondary immune or lymphoid organ in the body. It is an important organ to investigate treatment-related lesions, as it is considered the draining and filtering site for intravenously-administered substances. Its main functions are to initiate immune reactions to blood-borne antigens, and filter the blood of old or damaged RBC, as well as foreign substances. These functions are performed by the splenic pulp, which has two major compartments; the red pulp (RP) and the white pulp (WP). The red pulp, composed of the splenic cords and sinusoids, is responsible for the blood filtering of old or damaged RBC and foreign substances, while the white pulp, composed of the periarteriolar lymphoid sheath

(PALS), follicles, and marginal zones, initiates immune reactions to blood-borne antigens (Cesta, 2006).

In this study, there was no salient spleen-specific pathological processes evident in any of the samples (Figure 4.12). Extramedullary haematopoiesis (EMH) shows marked reductions by four months of age in rat populations (Elmore, 2012). It consists of erythroid precursors, myeloid precursors and/or megakaryocytes. Although there is a degree of EMH in rodents, increased EMH can result from exposure to haematotoxin, infections, and systemic anaemia (Suttie, 2006).

There were no significant changes in the central artery (arrow) and marginal sinus (arrow head) in the spleen of rats treated with AuNPs (Figure 4.12). In the RP, small niches of erythroid-dominant precursors were seen in the control, citrate-, PEG-, and p.14-PEG-AuNPs groups. Of these, p.14-PEG-AuNPs group, although showing smaller niches had the majority. Hemosiderin laden macrophages (a potential sign of increased breakdown of red cells), was lowest in citrate-AuNPs group and peaked in p.L- and p.14-PEG-AuNPs.

Compensatory erythropoiesis may explain the significantly decreased numbers of neutrophils and lymphocytes in p.L-PEG-AuNP-treated rats, and the significantly decreased neutrophils in the p.14-PEG-AuNP-treated rats.

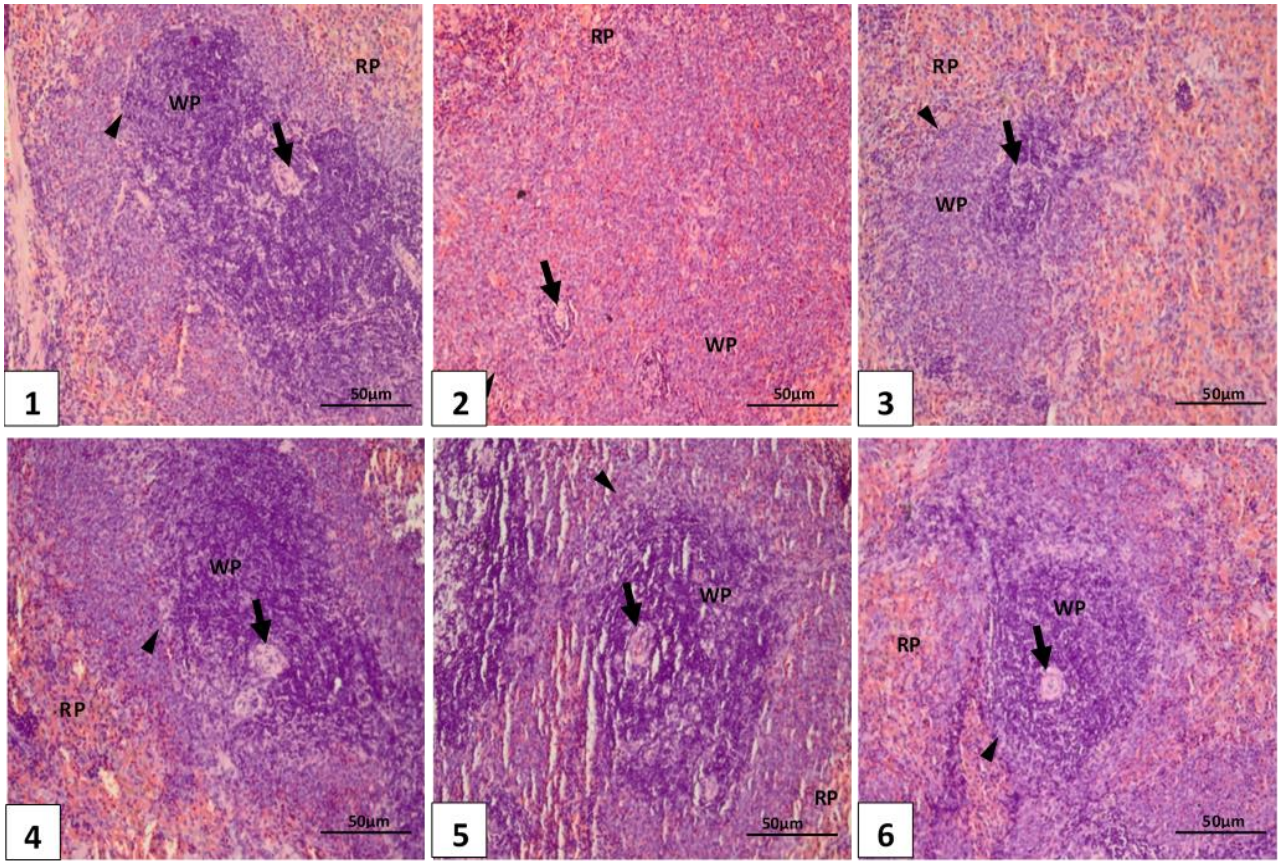


**Figure 4.12:** Histology of the spleen 2 weeks post-injection of rats with AuNPs (*Haematoxylin & Eosin, x100 original magnification, Scale bar = 50 µm*)
Key: 1 = PBS control group; 2 = Citrate-AuNPs; 3 = PEG-AuNPs; 4 = p.C-PEG-AuNPs; 5 = p.L-PEG-AuNPs; p.14-PEG-AuNPs. WP = White pulp; RP = Red pulp; arrow = central artery; arrow head = marginal sinus

d. Colon

Histomorphological examination was described to be effectively used in the assessment of the gastrointestinal tract following intestinal inflammation, such as leukocyte infiltrating, mucosal and epithelial cell proliferation (Erben *et al.*, 2014). In this study, no histopathological changes were observed in the colon of all the groups (Figure 4.13), as there were no changes in the basement membrane of lining epithelium (arrow) and the crypts (C) of the colon.

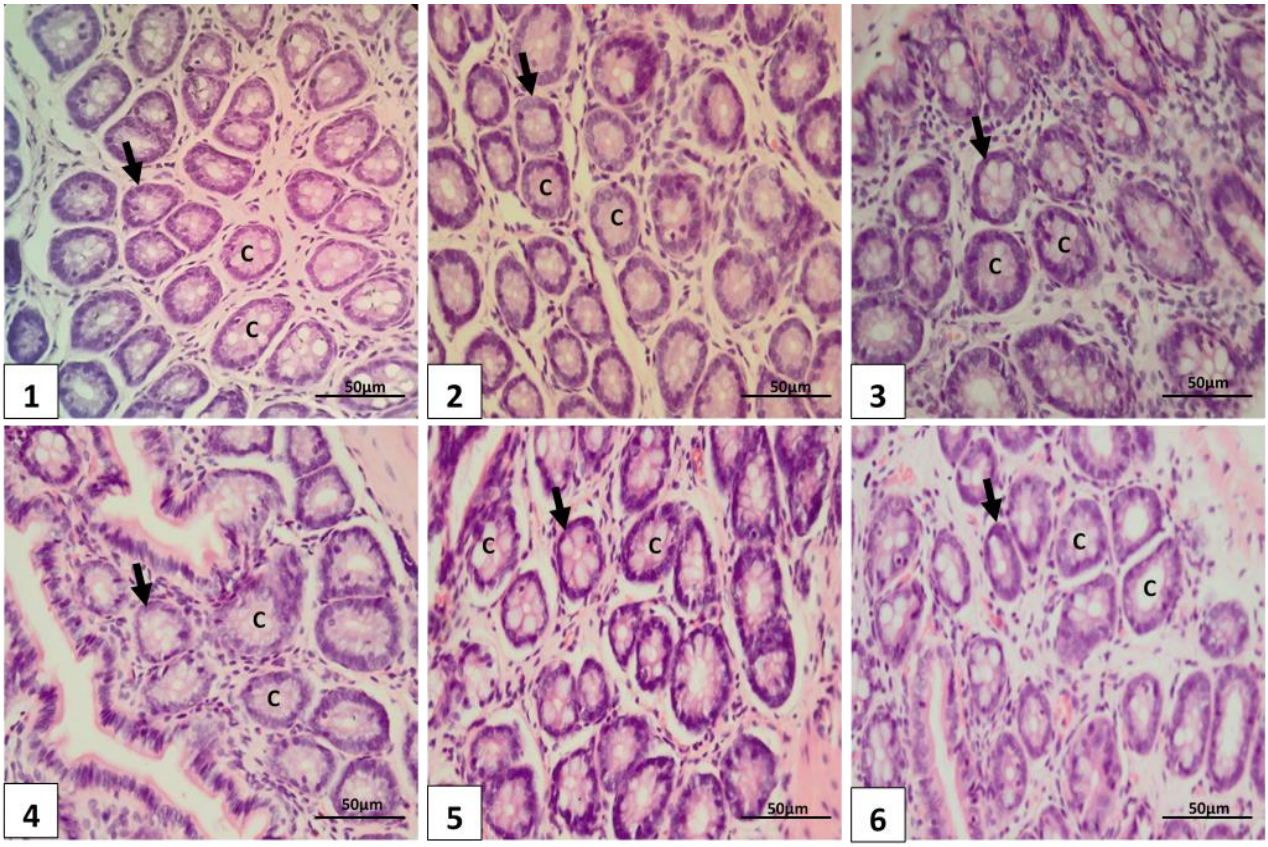


**Figure 4.13:** Histology of the colon 2 weeks after treatment (Haematoxylin & Eosin, x400 original magnification, Scale bar = 50 µm)
Key: 1 = PBS control group; 2 = Citrate-AuNPs; 3 = PEG-AuNPs; 4 = p.C-PEG-AuNPs; 5 = p.L-PEG-AuNPs; p.14-PEG-AuNPs. C = Crypts; arrow = epithelium

e. Pancreas

Histological examination of the Islets of Langerhans of the pancreas is used to access the integrity of the pancreatic endocrine functions making up about 1-2% of the pancreatic mass. The Islets of Langerhans consist of α-cells which secrete glucagon; β-cells that secrete insulin; delta-cells that secrete somatostatin; and pancreatic polypeptide cells that secrete pancreatic polypeptide (Longnecker, 2014). In this study, no histopathological changes were observed in the pancreas of all the groups (Figure 4.14), as the normal structures of the Islets of Langerhans (IL) with no loss of β-cells were seen. This suggests no impairment in the metabolism of glucose after AuNP administration.

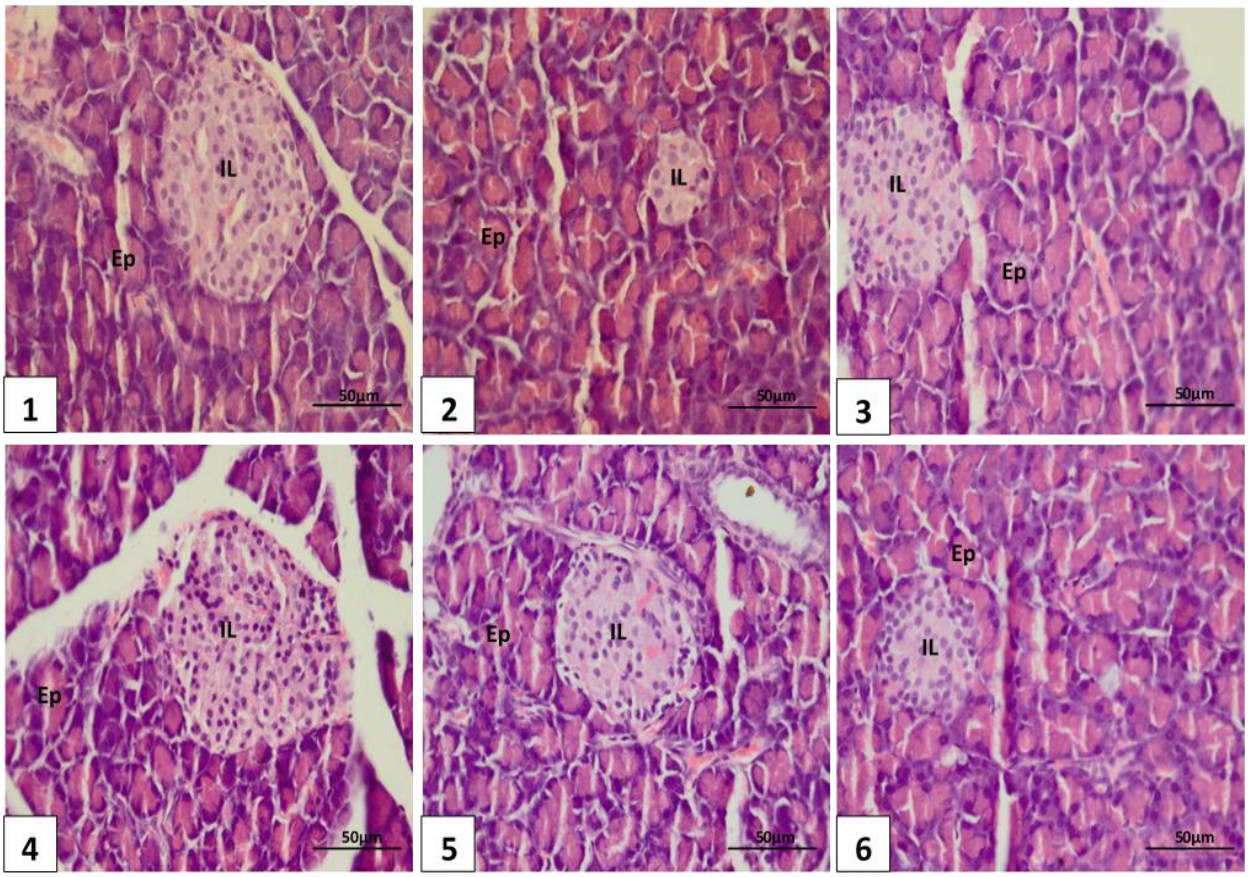


**Figure 4.14:** Histology of the pancreas 2 weeks post-injection of AuNPs to rats (*Haematoxylin & Eosin, x400 original magnification, Scale bar = 50 µm*)
Key: 1 = PBS control group; 2 = Citrate-AuNPs; 3 = PEG-AuNPs; 4 = p.C-PEG-AuNPs; 5 = p.L-PEG-AuNPs; p.14-PEG-AuNPs. IL = Islets of Langerhans; Ep = exocrine parenchyma

### 4.2.9 Inflammation markers

To better understand the significant changes noted after intravenous injection of p.C-PEG-AuNPs (spleen and colon weights, and neutrophil levels) and p.L-PEG-AuNPs (liver weight, MDA and haematological parameters) to rats two weeks post-injection, immunohistochemistry was performed to investigate the presence of pro-inflammation markers (p-I*k*B-α, IL-18 and IFN-γ), following possible inflammation in the liver, spleen, kidney and colon.

Phosphorylated I*k*B-α, produced by the phosphorylation of I*k*B-α by IKK on exposure to inflammatory stimuli, is involved in the activation of NF-*k*B, leading to the translocation into the nucleus and increase the production of pro-inflammatory factors including IFN-γ and IL-18 (Liu *et al.*, 2017).

There was no induction of inflammation as the markers of inflammation were not present in tissue sections (Figure 4.15a, b, c), but a few p-I*k*B-α (Figure 4.15a) and *IL-18* (Figure 4.15b) was noted in the liver of rats treated with p.L-PEG-AuNPs. This further provides information on the physiological and biochemical changes noted in p.L-PEG-AuNP-treated rats.

In a study by Cho *et al.* (2009a), the levels of IL-1β, IL-6, IL-10, and TNF-α were significantly increased 30 min post-injection of mice with 13 nm PEG-AuNPs when compared to the control, but the TNF-α and IL-12β persisted up to 4 h in Kupffer cells and hepatocytes, as indicated by immunohistochemical staining of liver sections. It was suggested that the transient acute inflammation was due to acute response of PEG-AuNPs after injection to mice.

The expression of pro-inflammatory cytokines (IL-1 β, IL-6 and TNF-α) was induced by 10 and 50 nm unconjugated AuNPs (with more severe effects with 10 nm AuNPs) in the liver 24 hr after intraperitoneal injection, but reduced after 5 days. In the kidney, there was no expression of IL-1 β, IL-6 and TNF-α with 10 nm AuNPs, but the 50 nm NPs increased levels of IL-6 and TNF-α 24 hr after injection, which was reversed after 5 days (Khan *et al.*, 2013). This contrasts with the results of this study, and can be linked to differences in size, surface chemistry (unconjugated), and dose (22 μg/kg body weight) of AuNPs, as well as route of administration, exposure time, as well as pro-inflammatory markers and procedure (quantitative real-time polymerase chain reaction) tested.

The inflammation marker proteins were not found in the kidney (Figure 4.16a, b, c), spleen (Figure 4.17a, b, c) and colon (Figure 4.18a, b, c) of rats in all the groups, except very few IL-18 (Figure 4.18b) and IFN-γ (Figure 4.18c) found in the colon of p.C-PEG-AuNP-treated rats. This is in consistent with the increased colon weights noted in p.C-PEG-AuNP-treated rats.

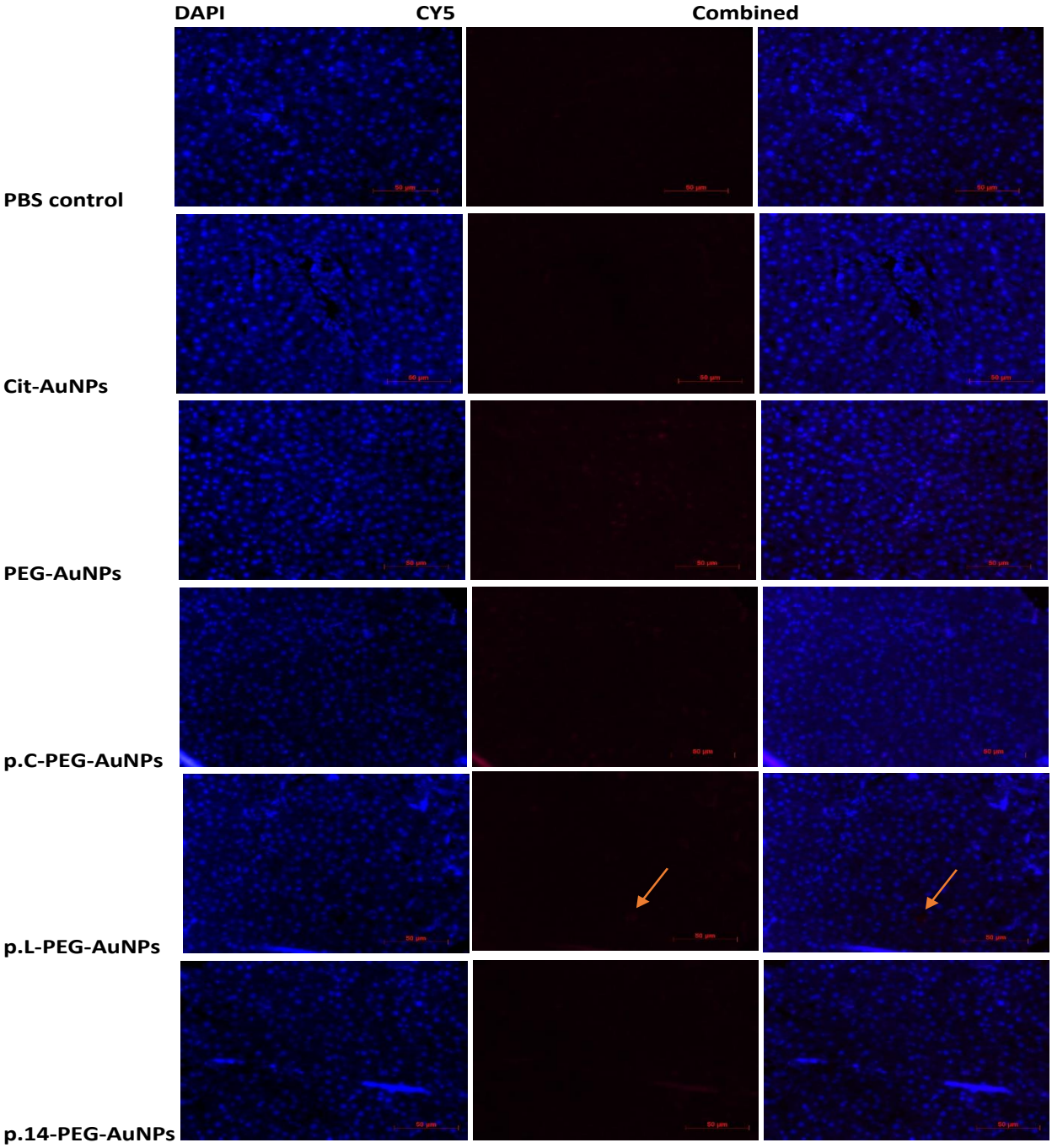


**Figure 4.15a:** Representative photomicrographs from one of six different liver sections of rats stained for the presence of p-I*k*B-α protein 2 weeks post-injection of AuNPs. (*Immunohistochemical staining x40 original magnification, Scale bar = 50 µm)*

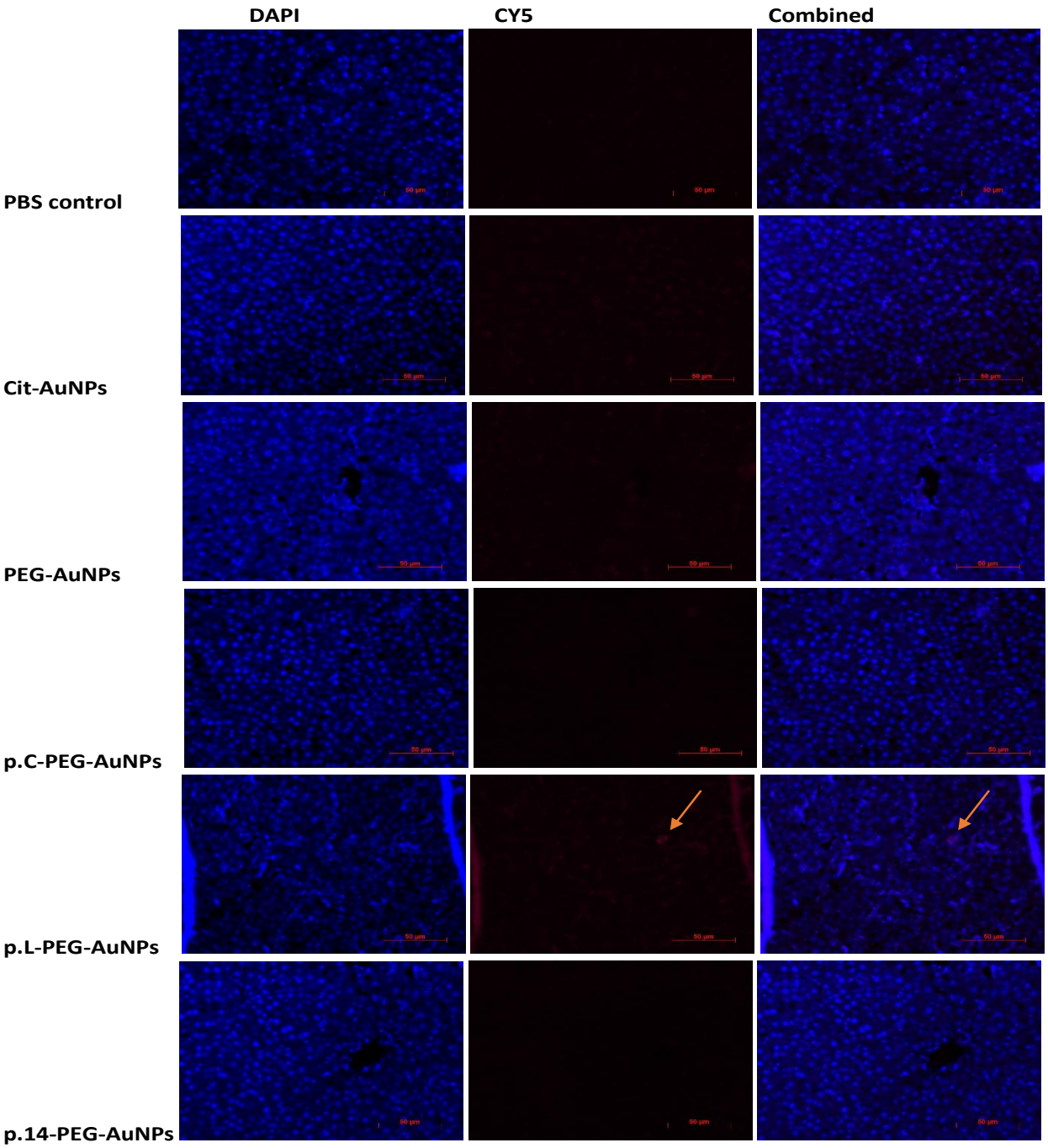


**Figure 4.15b:** Representative photomicrographs from one of six different liver sections of rats stained for the presence of IL-18 protein 2 weeks post-injection of AuNPs. (*Immunohistochemical staining x40 original magnification, Scale bar = 50 µm)*

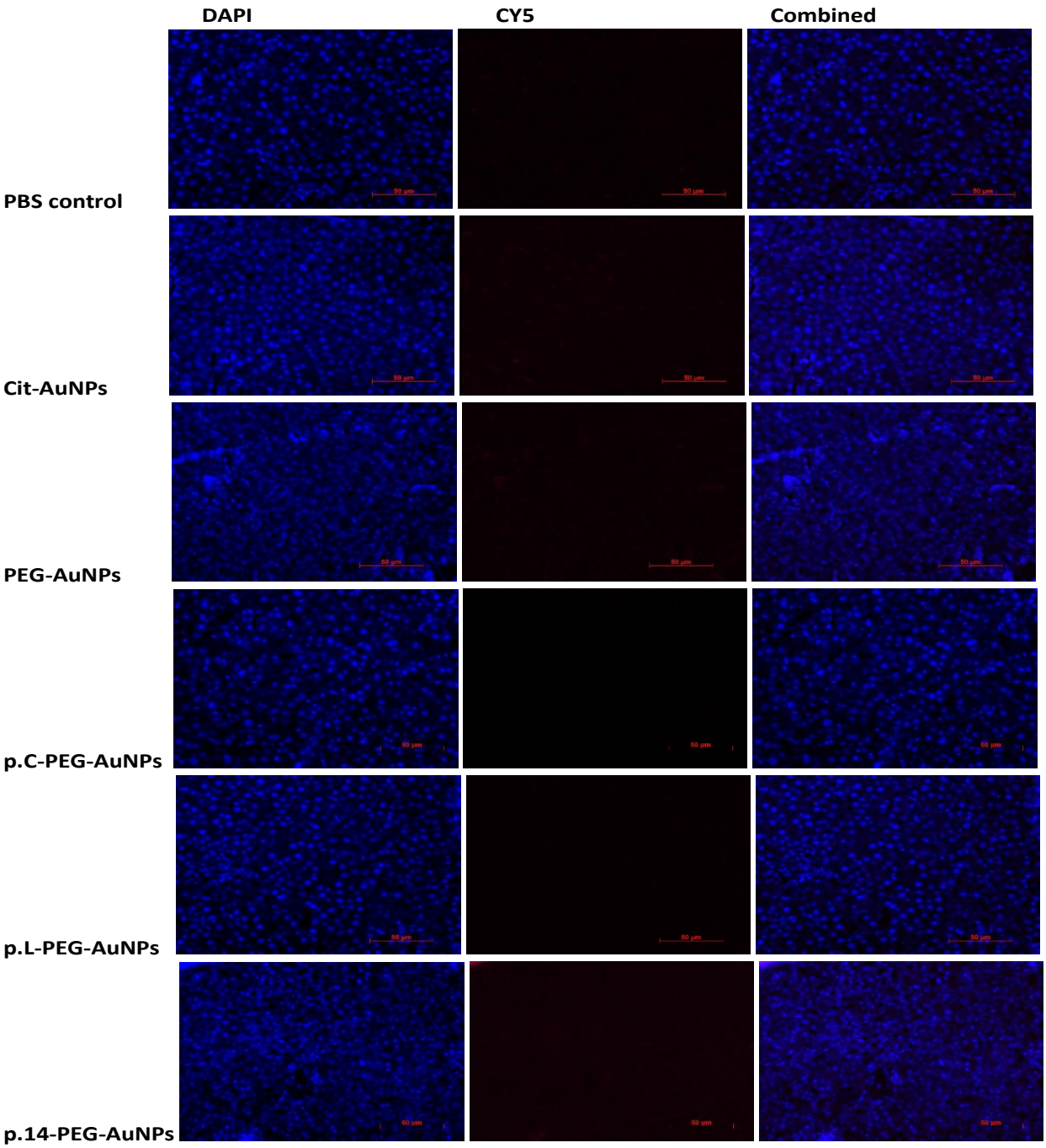


**Figure 4.15c:** Representative photomicrographs from one of six different liver sections of rats stained for the presence of IFN-γ protein 2 weeks post-injection of AuNPs. (*Immunohistochemical staining x40 original magnification, Scale bar = 50 µm)*

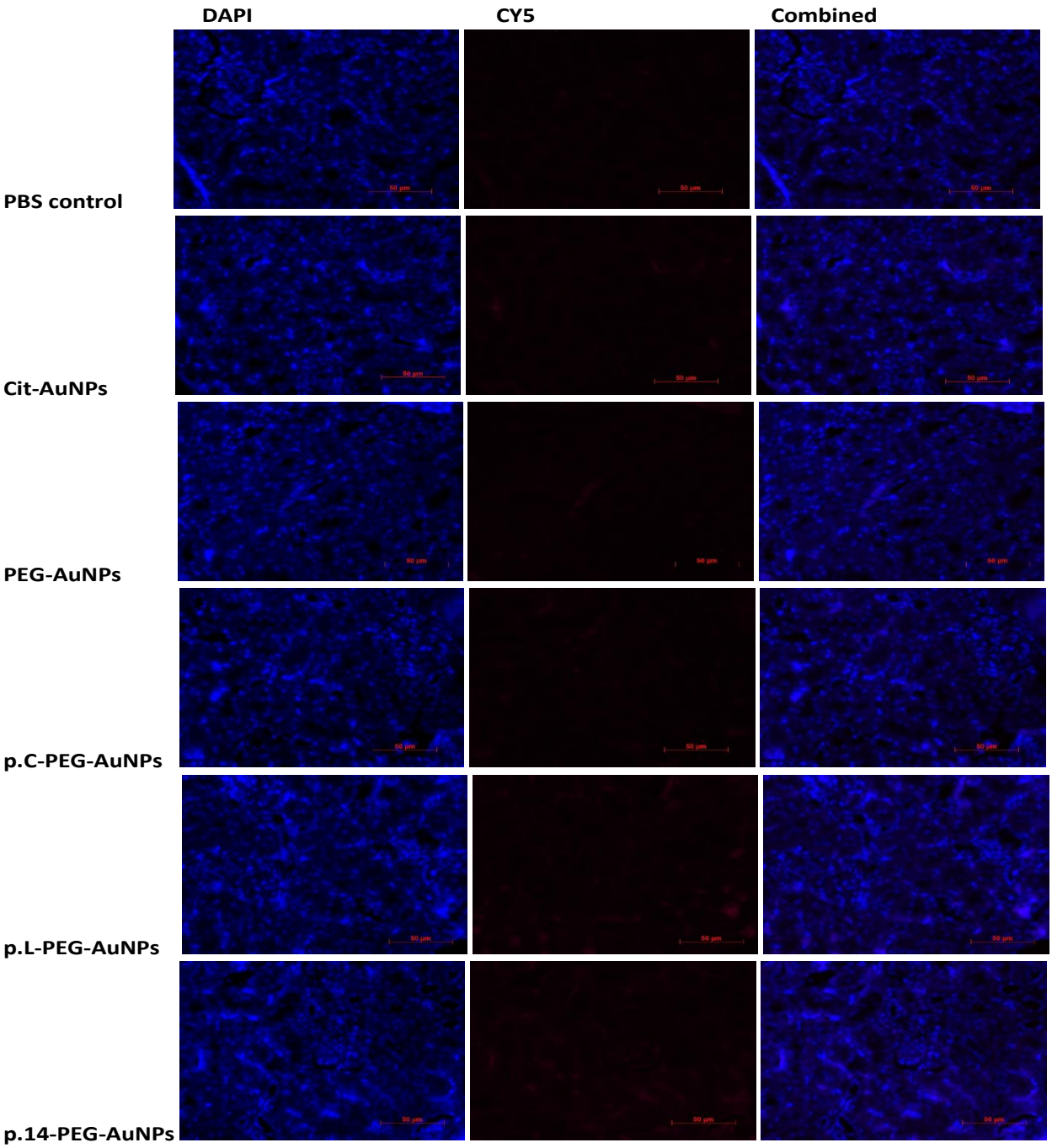


**Figure 4.16a:** Representative photomicrographs from one of six different rat kidney sections stained for the presence of p-I*k*B-α protein 2 weeks post-injection of AuNPs. (*Immunohistochemical staining x40 original magnification, Scale bar = 50 µm)*

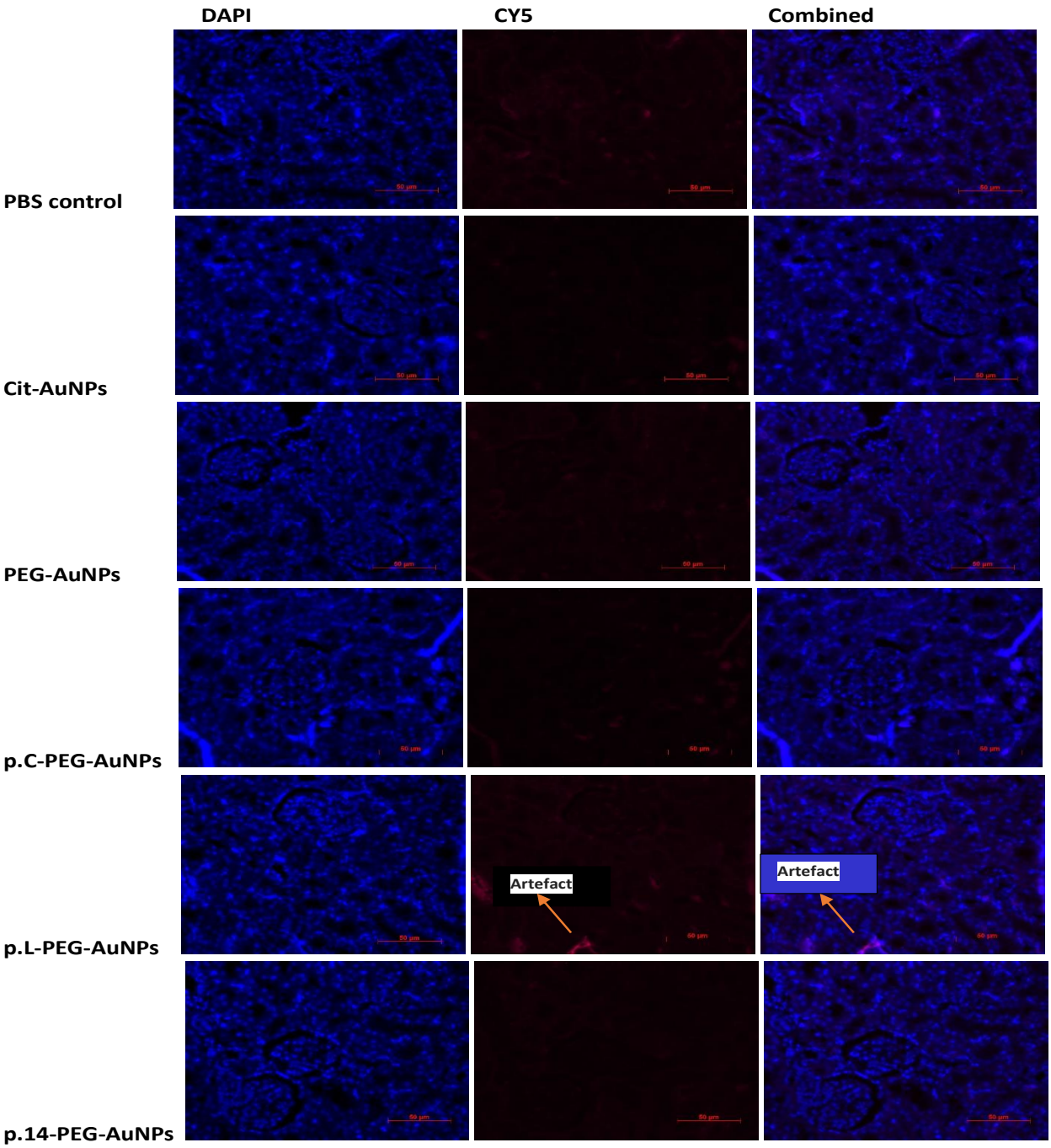


**Figure 4.16b:** Representative photomicrographs from one of six different kidney sections of rats stained for the presence of IL-18 protein 2 weeks post-injection of AuNPs. (*Immunohistochemical staining x40 original magnification, Scale bar = 50 µm)*

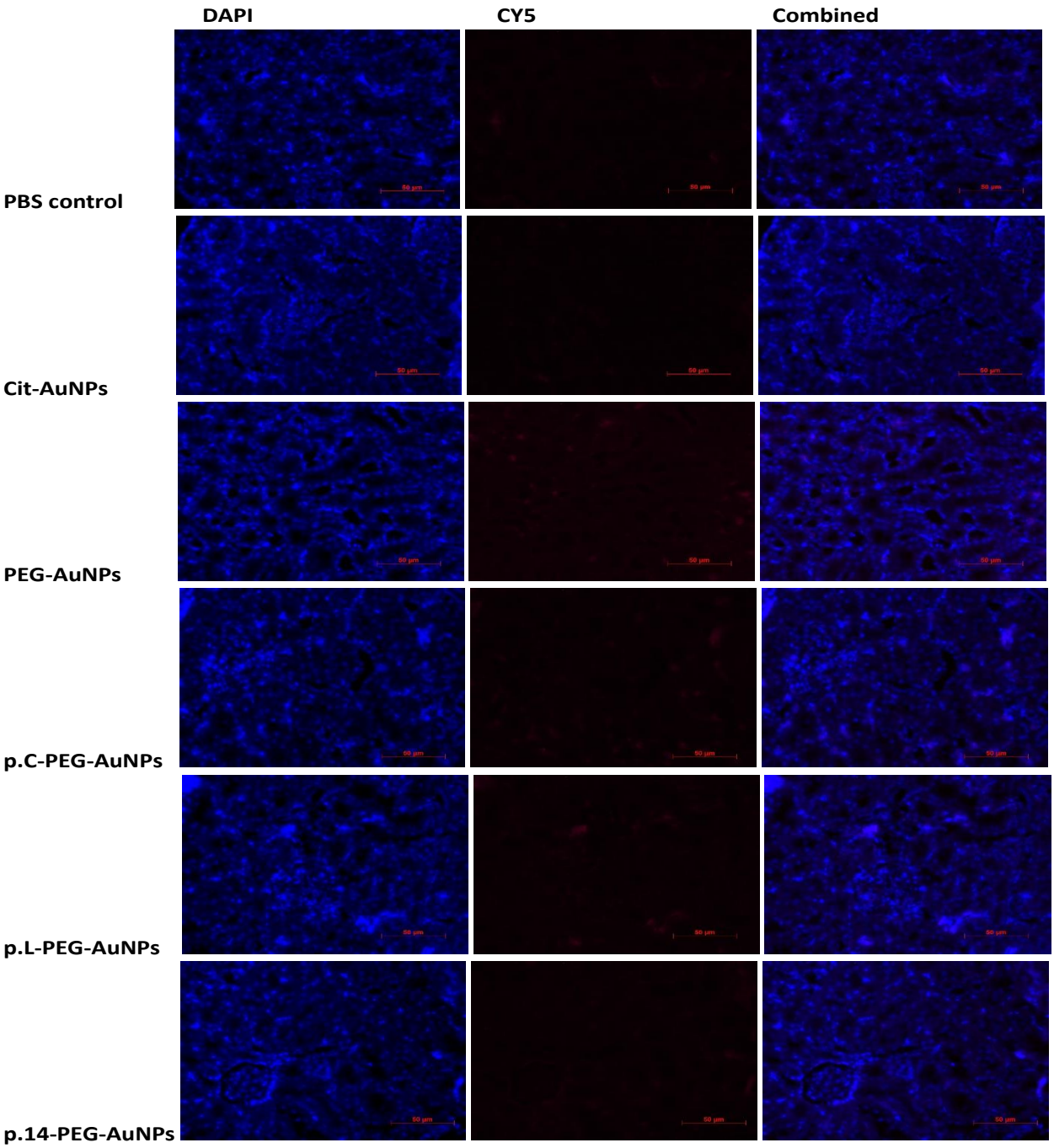


**Figure 4.16c:** Representative photomicrographs from one of six different kidney sections of rats stained for the presence of IFN-γ protein 2 weeks post-injection of AuNPs. (*Immunohistochemical staining x40 original magnification, Scale bar = 50 µm)*

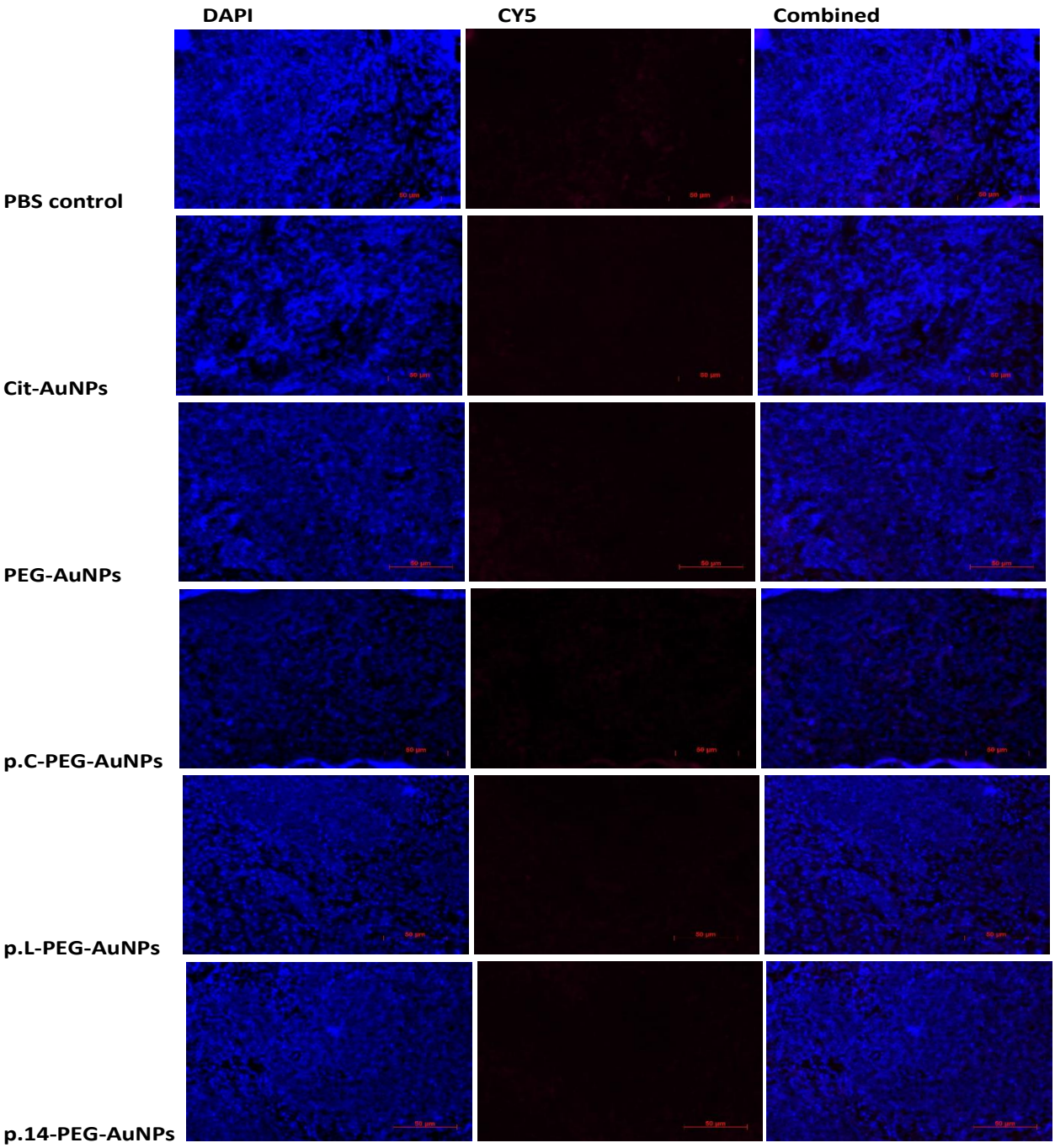


**Figure 4.17a:** Representative photomicrographs from one of six different rat splenic sections stained for the presence of p-I*k*B-α protein 2 weeks post-injection of AuNPs. (*Immunohistochemical staining x40 original magnification, Scale bar = 50 µm)*

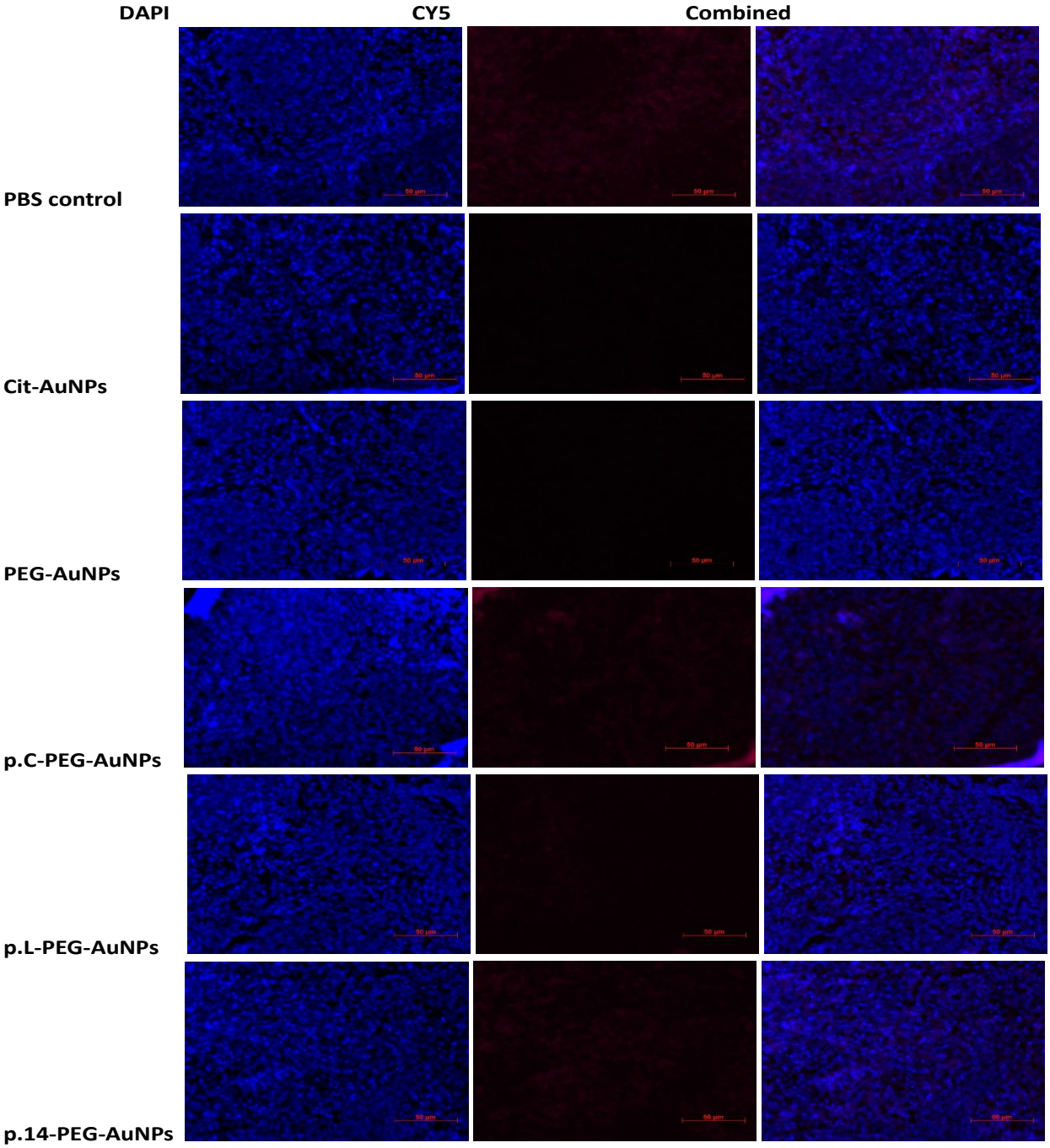


**Figure 4.17b:** Representative photomicrographs from one of six different splenic sections of rats stained for the presence of IL-18 protein 2 weeks post-injection of AuNPs. (*Immunohistochemical staining x40 original magnification, Scale bar = 50 µm)*

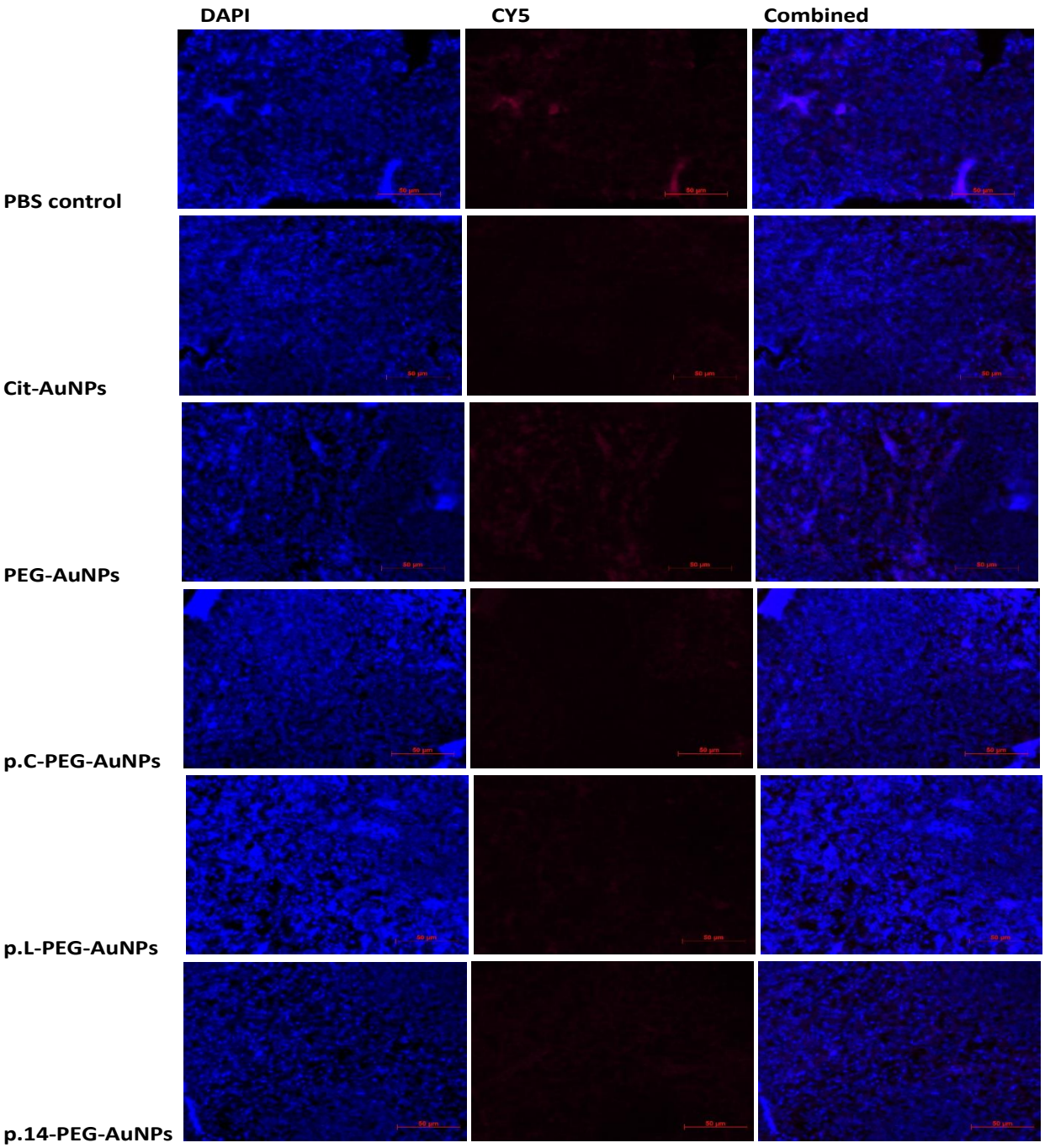


**Figure 4.17c:** Representative photomicrographs from one of six different splenic sections of rats stained for the presence of IFN-γ protein 2 weeks post-injection of AuNPs. (*Immunohistochemical staining x40 original magnification, Scale bar = 50 µm)*

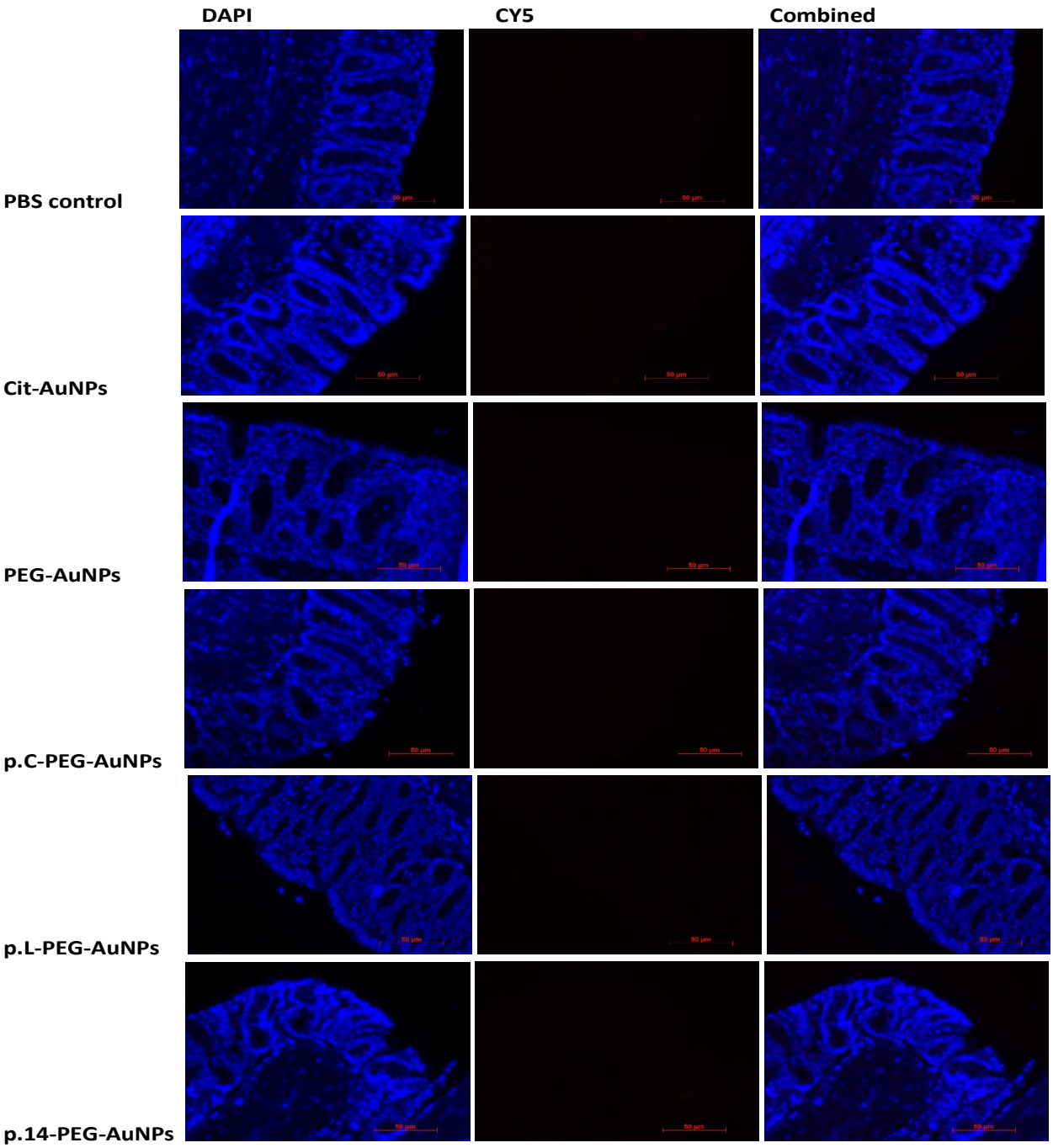


**Figure 4.18a:** Representative photomicrographs from one of six different rat colonic sections stained for the presence of p-I*k*B-α protein 2 weeks post-injection of AuNPs. (*Immunohistochemical staining x40 original magnification, Scale bar = 50 µm)*

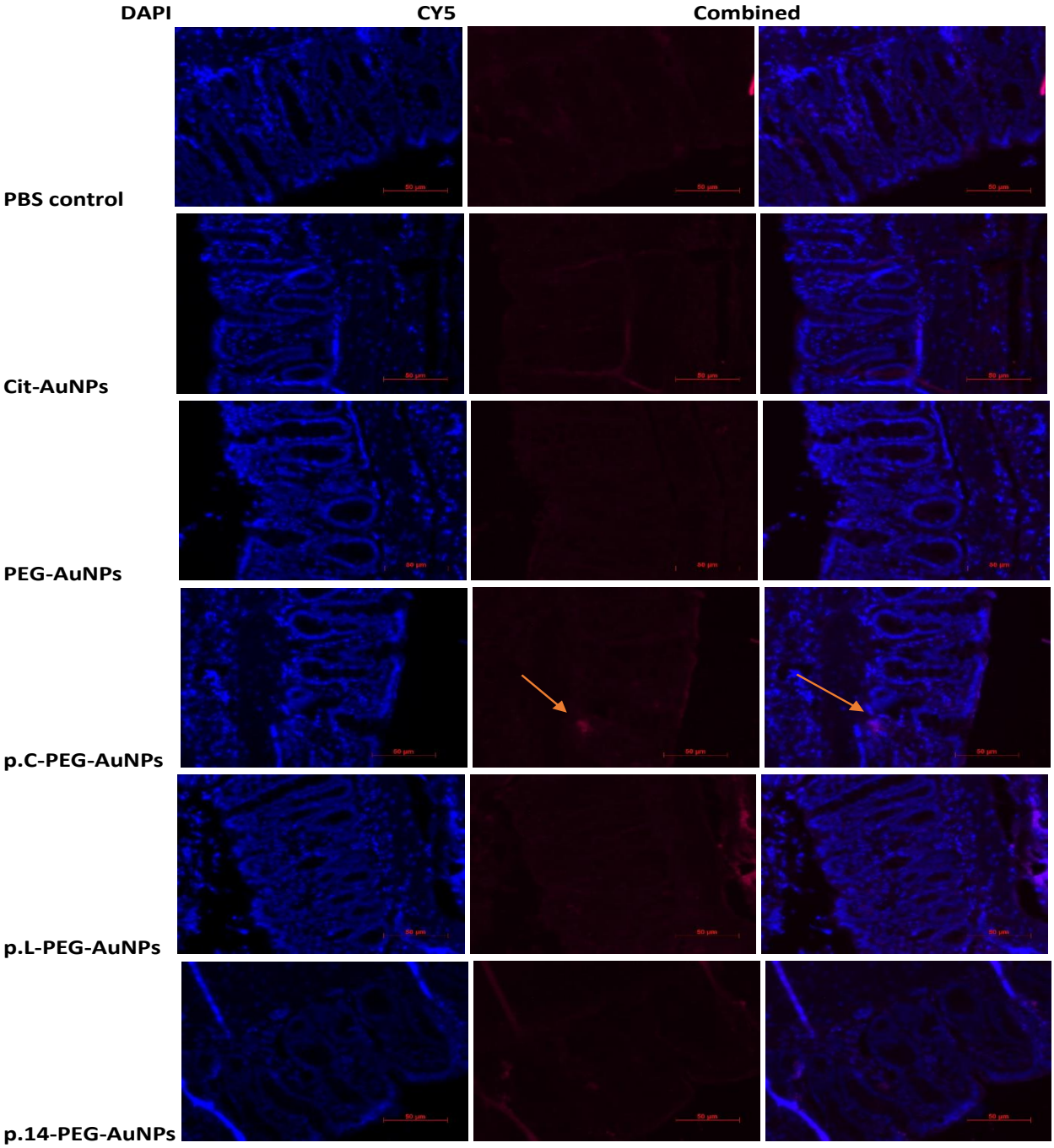


**Figure 4.18b:** Representative photomicrographs from one of six different colonic sections of rats stained for the presence of IL-18 protein 2 weeks post-injection of AuNPs. (*Immunohistochemical staining x40 original magnification, Scale bar = 50 µm)*

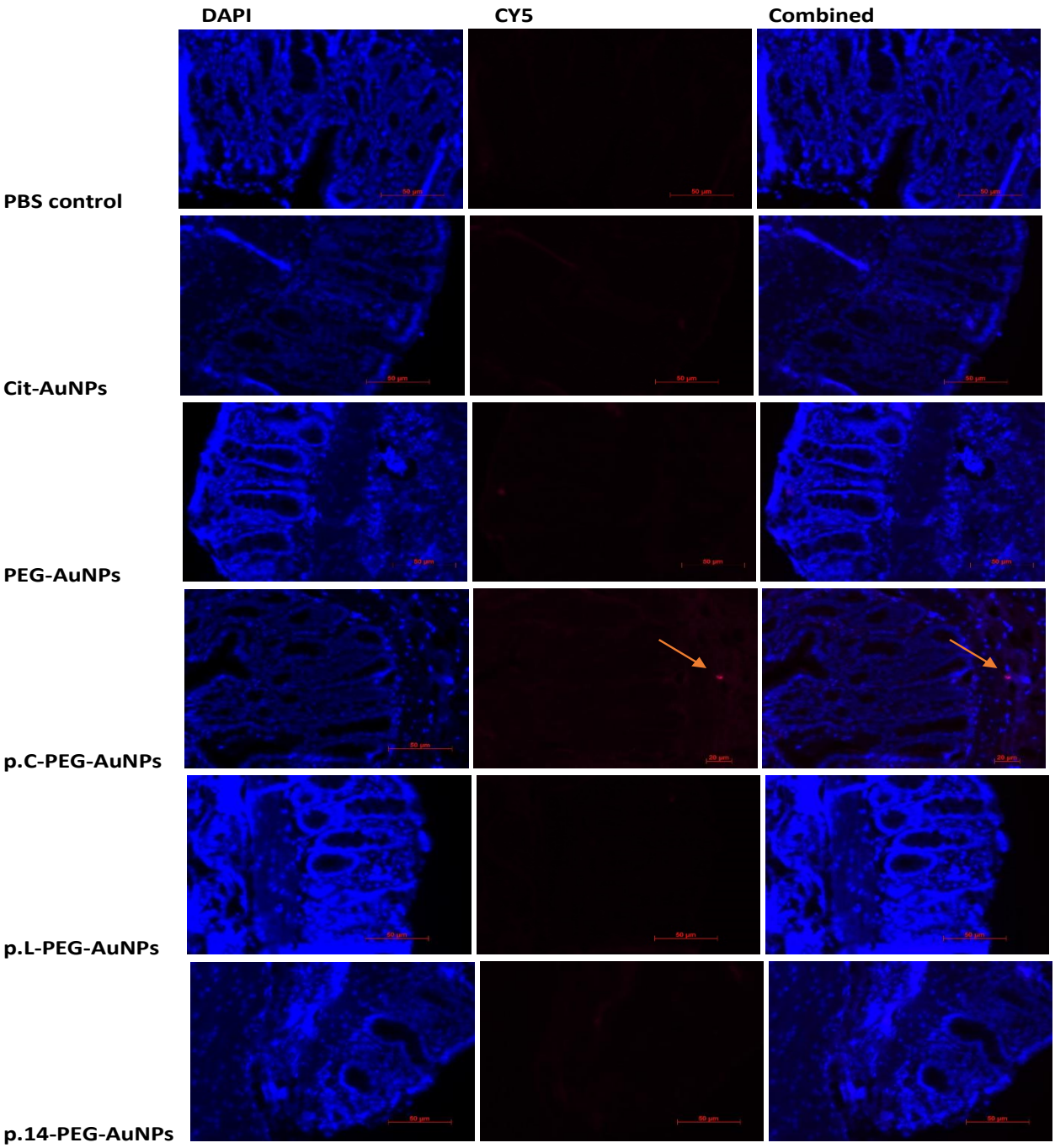


**Figure 4.18c:** Representative photomicrographs from one of six different colonic sections of rats stained for the presence of IFN-γ protein 2 weeks post-injection of AuNPs. (*Immunohistochemical staining x40 original magnification, Scale bar = 50 µm)*.

The toxicity study of 14 nm AuNPs 14 days after a single intravenous injection to rats suggests that p.C- and p.14-PEG-AuNPs are potential agents for diagnosing CRC *in vivo*, with caution for the use of p.L-PEG-AuNPs. In many of the parameters investigated, there were significant changes in relative liver weight, ALP, the haematopoiesis system, and MDA in p.L-PEG-AuNPs-

treated rats when compared to the control group ($p<0.05$). These changes suggest possible low degree of tissue damage since there were increased trend of AST and creatinine levels and decreased total protein, as well as indications of inflammation in the liver. Immunohistochemical staining of the colon revealed the presence of IL-18 and IFN-γ, which could be linked to the increased colon weight noted in p.C-PEG-AuNPs. There were, however, no significant changes in the biochemical and physiological parameters investigated, as well as colon and spleen histology.

In conclusion, from the results of the short-term study, it seems that neither the citrate capping nor the PEG (stabilizing molecule) would contribute towards toxicity of the AuNP, and should be considered in the synthesis and functionalization of AuNP. The three peptides investigated in this study showed a preliminary safety pattern in the following order: p.14 > p.C > p.L.

Acute toxicity studies should provide information on the nature of toxicity, if sudden, delayed, time-limited, or continuous (National Research Council, 2006). Long-term (12 weeks) *in vivo* toxicity studies (Chapter 5) after a single injection of these AuNPs is therefore necessary to provide further insight to the changes noted 2 weeks post-exposure. This was considered because the interaction of the AuNPs with the biological system was inconclusive within 2 weeks of exposure, which might be the reason for the inconsistency of the results from the toxicity parameters previously reported.

# CHAPTER FIVE

# PHASE 2 *IN VIVO* EXPERIMENT

## 5.1 INTRODUCTION

This phase investigated the long-term (12 weeks) effects of a single intravenous injection of AuNPs in rats. It was designed to reveal delayed, persistent or continuous toxicity of these NPs *in vivo.* This was necessary because of the small size, easy tissue penetration, tissue bioaccumulation of AuNPs over a prolonged period could increase the risk of toxicity (Balasubramanian *et al.*, 2010; Zhang *et al.*, 2011).

In a study by Zhang *et al.* (2012), alterations in the liver and kidney functions, as well as immune response were observed 24 h after intraperitoneal injection of AuNCs (7.55 mg/kg) to mice. These changes returned to normal in mice injected with 2.1 nm GSH-AuNCs 4 weeks post-injection, but the 8.2 nm BSA-AuNCs-treated mice showed no recovery. Toxicity studies 4 weeks after a single intravenous injection of 20 nm citrate-capped and pentapeptide (CALNN)-coated AuNPs (0.7 mg/kg) to rats was investigated. Haematological alterations, including significant changes in HCT, RBC, and Hb were noted in the CALNN-AuNP-injected rats, although in both AuNPs, WBC counts did not change when compared to the control. It was suggested that the AuNPs did not cause significant inflammatory responses (as measured by haematology) and that the elicited inflammatory responses were reversed during the 4 week period (Fraga *et al.*, 2014).

In this chapter, the effect of a single intravenous injection of AuNPs to rats was investigated using the standard toxicity biochemical parameters, such as measurement of ALT, AST and ALP activities, as well as levels of total protein, albumin, bilirubin, urea and creatinine. In addition, oxidative stress markers, haematological parameters, and tissue histopathology were investigated. These parameters were in-line with several reported toxicological studies of NPs (Rambanapasi, 2015; Rambanapasi *et al.*, 2016; Yang *et al.*, 2017b).

Several authors have suggested both short- and long-term toxicological studies of AuNPs (Yah, 2013; Fraga *et al.*, 2014; Jia *et al.*, 2017) due to inconclusive results from short-term study, as

in the case of this study (Chapter four). This will enable researchers to focus on areas for further studies. If there are delayed or persistent toxicities noted from these parameters long-term post-exposure, genotoxicity studies are suggested.

## 5.2 RESULTS AND DISCUSSION

### 5.2.1 General morphology, behaviour and physiology of rats

The rats did not show any sign of toxicity over the 12 weeks following injection with the AuNPs. There were no changes in the behaviour or skin colour of the rats. No mortalities were recorded, and no premature animal sacrifice was needed due to distress or other ethical considerations. All animals maintained a normal intake of food and water, as well as a steady weight gain during the 12 week-period of the study (Figure 5.1); all indications of healthy growth. These results are similar to studies by Fraga *et al.* (2014) and Rambanapasi (2015), where rats were monitored for 4 and 8 weeks, respectively, after a single intravenous injection of citrate- or CALNN-AuNPs. No abnormalities, including behavioural changes, food and water intake, and body weight, were recorded throughout the period of the studies, except for the CALNN-AuNP group that showed a significant relative spleen weight 4 weeks post-exposure when compared to the control (Fraga *et al.*, 2014).

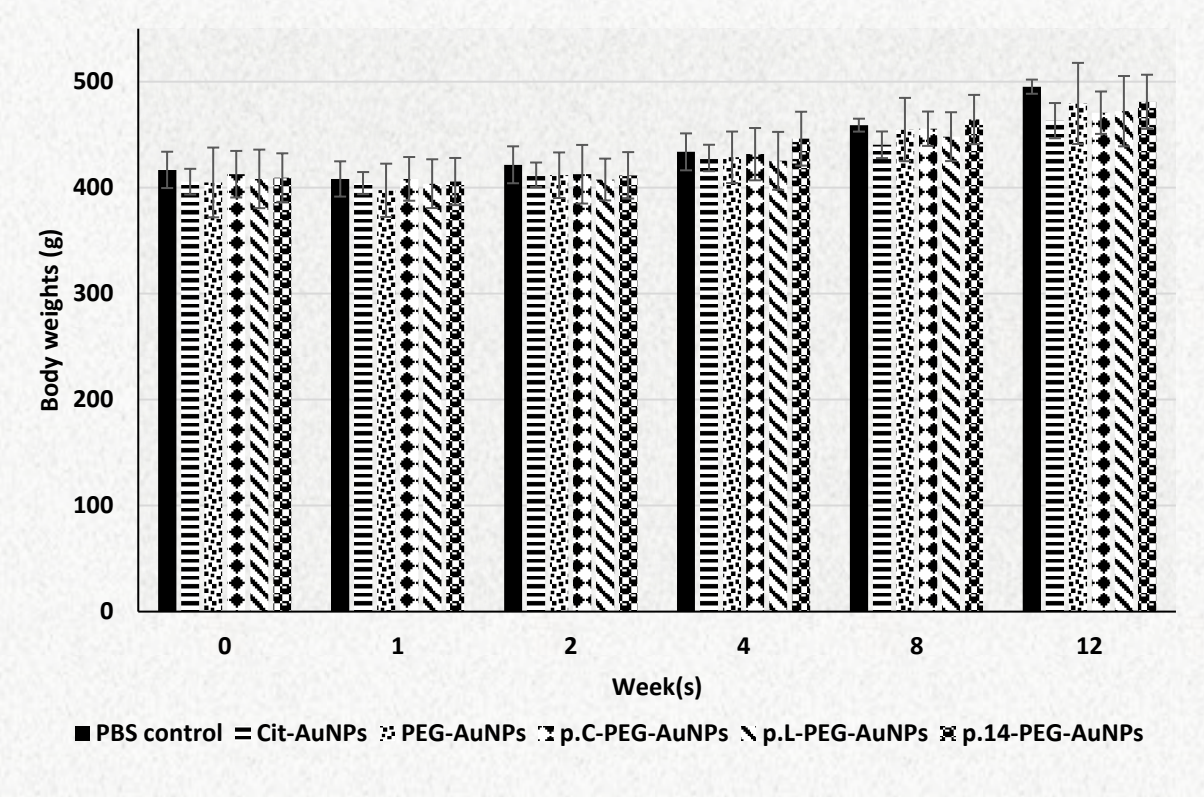


**Figure 5.1:** Body weights (g) of rats over a 12 week period post-injection with AuNPs.
Cit - Citrate; PBS – Phosphate-buffered saline; AuNPs – Gold nanoparticles
Values are expressed as Mean ± SD, n=6

Over the first 2 weeks, the weights of the rats remained relatively constant in all the groups, but picked up weight over the next 10 weeks. There was no significant change ($p>0.05$) in percentage (%) increase in the body weights (0 week to 12 weeks) of rats when compared to the control group. The % increase results are: 16.97±5.63, 13.13±2.48, 18.50±4.47, 14.21±5.27, 15.73±4.62, and 17.58±5.33 for PBS control, citrate-, PEG-, p.C-PEG-, p.L-PEG-, and p.14-PEG-AuNPs, respectively.

### 5.2.2 Effect on relative organ weights

A single intravenous injection of AuNPs did not cause any significant effects ($p>0.05$) on the relative organ weights of rats in all the AuNPs-treatment groups when compared to the control group (Figure 5.2). This shows no sign of macrotoxicity in all the organs investigated 12 weeks post-injection. In a study by Zhang *et al.* (2011), no significant changes in organ

weights were noted after 4 weeks injection with PEG-AuNPs (4000 µg/kg) of different sizes (5, 10, 30, and 60 nm) in mice. These results are echoed in this study.

The acute effect of p.L-PEG-AuNP showed, however, a significant increase in the weights of the spleen and colon and a decrease in liver weight, compared to control rats (Figure 4.5). This means that it was a transient effect on the relevant organs weights. These results suggest a low degree of inflammation at 2 weeks in the relevant organs, which caused interstitial fluid accumulation, but it was reversed after 12 weeks. It needs to be emphasized that it would only be a low degree of inflammation because the p.L-PEG-AuNP-treated rats did not show significant increases in inflammatory markers measured in this study at two weeks.

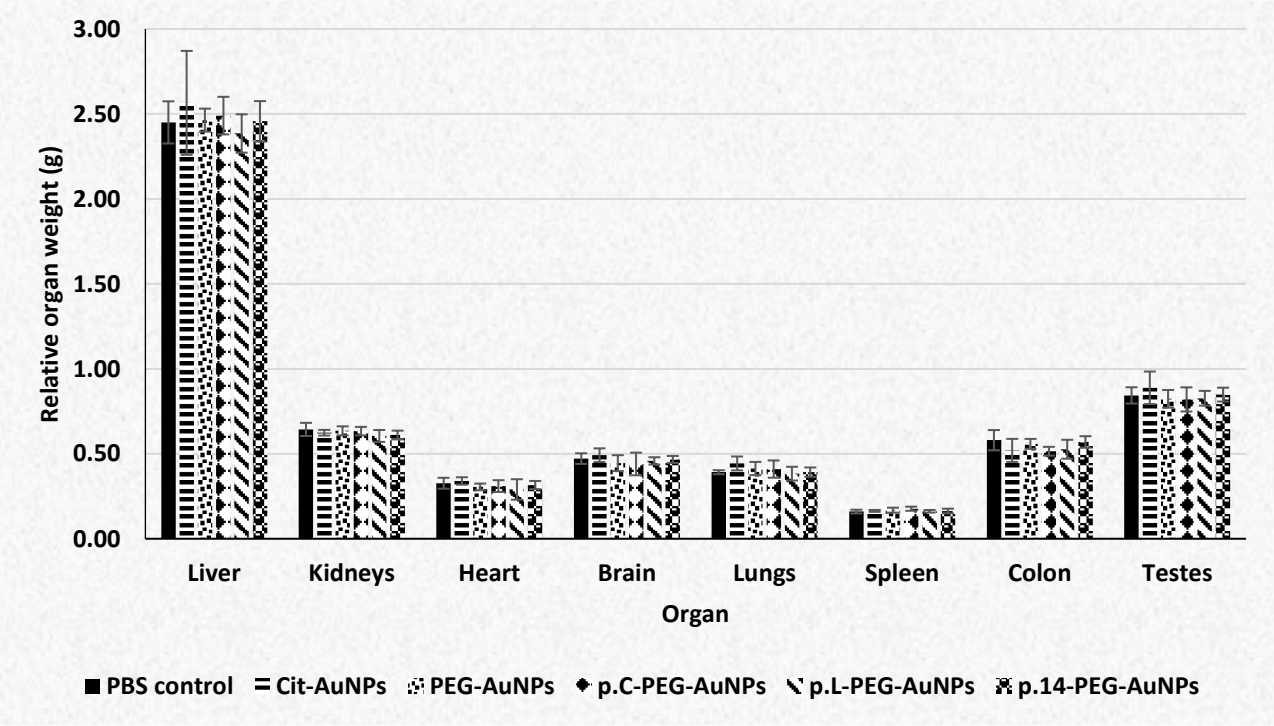


**Figure 5.2:** Effect on organ weight relative to 100 g body weight of rats at 12 weeks.
Cit - Citrate; PBS – Phosphate-buffered saline; AuNPs – Gold nanoparticles
Values are expressed as Mean ± SD, n=6

### 5.2.3 Biochemical analyses in the serum

#### *5.2.3.1 Effect on serum marker enzymes*

No significant differences ($p > 0.05$) in the levels of serum ALT, AST and ALP were noted when compared to the control group (Figure 5.3). This indicates that there was no long-term damage to or loss of functional integrity of body organs. Liver damage was measured by the levels of ALT and AST; kidney, heart, brain, and skeletal muscle integrity was assessed by AST activities; bone, intestinal, and hepatic injury was measured by ALP levels (Cuperus *et al.*, 2017). This is similar to the findings by Rambanapasi (2015), where no significant difference in the levels of these parameters was noted when compared to the control group 8 weeks after a single intravenous injection of 14 nm citrate-AuNPs to rats.

A significant increase in the levels of ALP in rats injected with p.14-PEG-AuNPs was observed when compared to the p.C-PEG-AuNPs-injected group. This suggests differences in the effects of the AuNPs *in vivo*, which can be linked to the amino acid composition of the peptides. It was noted that at two weeks there was a decreased trend in ALP in all the rats treated with AuNPs when compared to the control. At 12 weeks, there was no clear trend. The increased trend in AST in the p.L- PEG-AuNP-treated group at 2 weeks did not persist till 12 weeks.

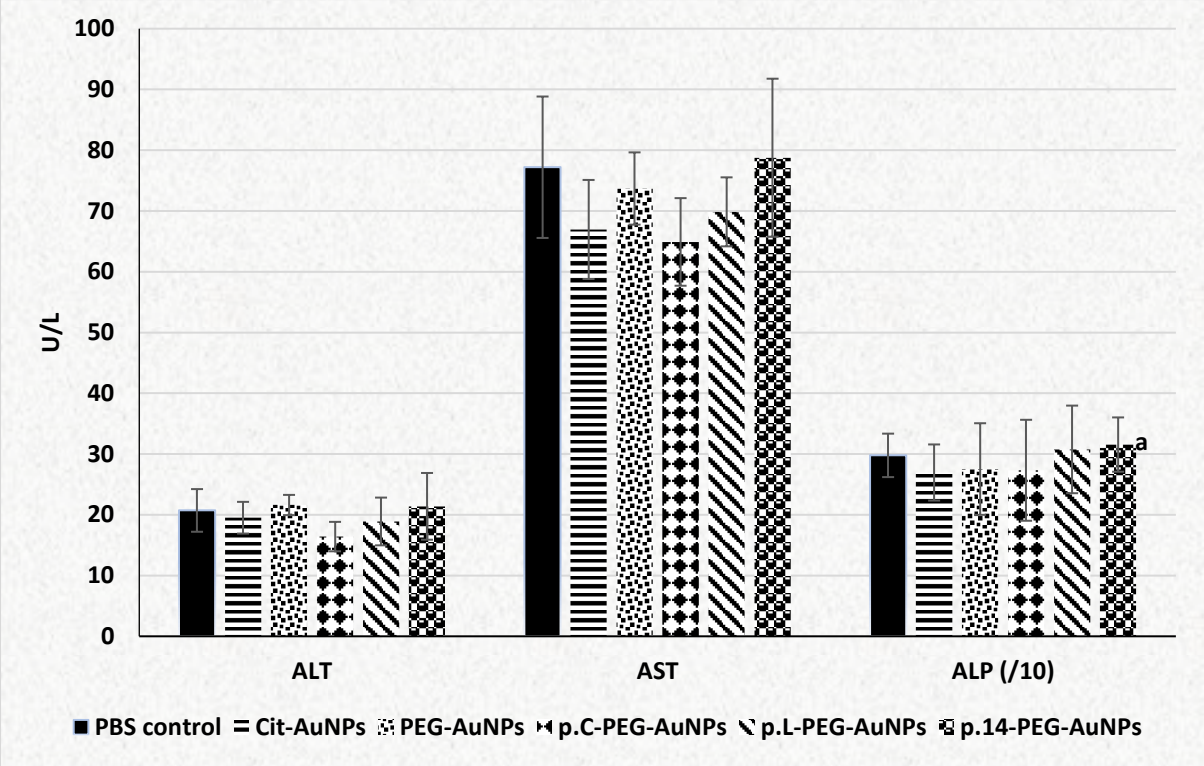


**Figure 5.3:** Effect on serum markers enzymes.
Cit - Citrate; PBS – Phosphate-buffered saline; AuNPs – Gold nanoparticles; (/10) – Actual values divided by 10
Values are expressed as Mean ± SD, n=6. [a]p<0.05, when compared to p.C-PEG-AuNPs group

### *5.2.3.2 Effect on hepatocellular function markers*

Liver function was investigated by determining the concentrations of serum total protein and albumin, while the hepatobiliary function or the presence of cholestasis was measured by serum bilirubin (total and direct) levels (Kwo *et al.*, 2017).

Treatment of rats with AuNPs showed no significant effect ($p > 0.05$) on the levels of these parameters 12 weeks post-injection when compared to the control group (Figures 5.4 and Table 5.1). This indicates that the AuNPs were well-tolerated by the rats and did not cause any significant alterations to the functions of the liver. Further, there was no evidence of biliary obstruction up to 12 weeks after of a single intravenous injection.

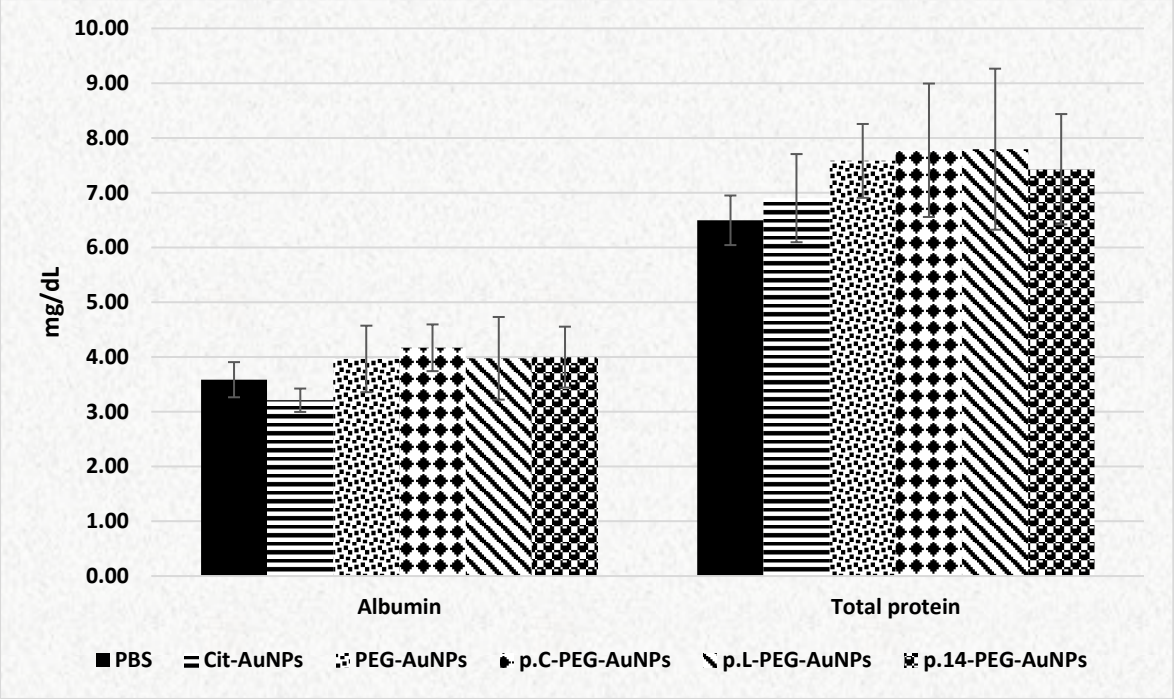


**Figure 5.4:** Effect of AuNPs on the levels of albumin and total protein.
Cit - Citrate; PBS – Phosphate-buffered saline; AuNPs – Gold nanoparticles
Values are expressed as Mean ± SD, n=6.

**Table 5.1:** Effect of AuNPs on bilirubin levels

| Treatment | Direct bilirubin (mg/dL) | Total bilirubin (mg/dL) |
|---|---|---|
| PBS control | 0.05±0.02 | 0.34±0.06 |
| Cit-AuNPs | 0.08±0.02 | 0.22±0.08 |
| PEG-AuNPs | 0.06±0.02 | 0.30±0.03 |
| p.C-PEG-AuNPs | 0.06±0.02 | 0.32±0.04 |
| p.L-PEG-AuNPs | 0.07±0.02 | 0.32±0.02 |
| p.14-PEG-AuNPs | 0.05±0.01 | 0.28±0.01 |

Cit - Citrate; PBS – Phosphate-buffered saline; AuNPs – Gold nanoparticles
Values are expressed as Mean ± SD, n=6.

#### *5.2.3.3 Effect on renal function markers*

A single injection of AuNPs to rats did not cause a significant difference ($p > 0.05$) in the levels of serum urea and creatinine when compared to the control group (Table 5.2). This shows that no impairment to the functional integrity of the kidney occurred with AuNP-treatment 12 weeks after a single intravenous injection. A similar result was reported by Rambanapasi (2015), where no significant increase in these parameters was noted 8 weeks after a single injection with 14 nm citrate-capped AuNPs to rats.

**Table 5.2:** Effect of AuNPs on markers of kidney function

| Treatment | Urea (mg/dL) | Creatinine (mg/dL) |
|---|---|---|
| PBS control | 26.79±2.86 | 1.34±0.09 |
| Cit-AuNPs | 26.99±1.57 | 1.40±0.05 |
| PEG-AuNPs | 24.38±4.96 | 1.37±0.06 |
| p.C-PEG-AuNPs | 31.24±1.78 | 1.30±0.07 |
| p.L-PEG-AuNPs | 25.70±1.81 | 1.37±0.03 |
| p.14-PEG-AuNPs | 25.76±0.88 | 1.32±0.05 |

Cit - Citrate; PBS – Phosphate-buffered saline; AuNPs – Gold nanoparticles
Values are expressed as Mean ± SD, n=6.

### 5.2.4 Haematological investigations

Haematological analysis of plasma samples of rats injected with AuNPs showed no significant difference ($p>0.05$) when compared to the control group (Table 5.3a and b). No significant difference in haematological parameters, at various time points, after a single injection of AuNPs to experimental animals were previously reported (Ivanov *et al.*, 2012; Zhang *et al.*, 2012; Fraga *et al.*, 2014; Wang *et al.*, 2016b), which is similar to the results of this study.

There is however, a difference between this study and that of Zhang *et al.* (2012), where mice injected with 8.2 nm BSA-AuNCs showed a significant increase in some haematological parameters (WBC and Hb) when compared to the control mice 4 weeks after a single intraperitoneal injection, indicating inflammatory response following exposure to the NPs. This difference could be linked to different size and shape (8.2 nm and NCs), surface chemistry

(BSA), exposure time (4 weeks), and experimental animal (mice) and route of administration used.

The decreased numbers in neutrophil and lymphocytes observed in the p.L-PEG-AuNP group 2 weeks post-injection was not sustained at 12 weeks post-injection. This means that the compensatory erythropoiesis proposed in chapter 4 was not sustained on the long-term.

**Table 5.3a:** Effect on haematological parameters with absolute values of the differential white cell counts

| Treatment | Plat ($10^{\wedge 9}$/L) | HCT (%) | Hb (g/dL) | WBC ($10^{\wedge 9}$/L) | Lym ($10^{\wedge 9}$/L) | Neu ($10^{\wedge 9}$/L) | Mon ($10^{\wedge 9}$/L) | Eos ($10^{\wedge 9}$/L) | Bas ($10^{\wedge 9}$/L) |
|---|---|---|---|---|---|---|---|---|---|
| PBS control | 1225.60±148.62 | 43.06±1.23 | 15.50±0.69 | 10.51±3.48 | 6.59±1.31 | 1.97±0.11 | 0.58±0.36 | 0.20±0.09 | 0.01±0.00 |
| Cit-AuNPs | 1126.80±145.97 | 43.52±0.51 | 15.30±0.48 | 7.89±2.12 | 5.18±1.36 | 2.09±0.61 | 0.46±0.19 | 0.16±0.06 | 0.01±0.01 |
| PEG-AuNPs | 1291.70±174.93 | 43.55±1.18 | 15.32±0.50 | 9.25±1.39 | 6.08±0.94 | 2.31±0.16 | 0.56±0.16 | 0.15±0.07 | 0.00±0.01 |
| p.C-PEG-AuNPs | 1265.80±90.39 | 43.32±0.95 | 15.23±0.30 | 9.86±1.88 | 5.81±1.27 | 3.20±0.96 | 0.63±0.26 | 0.20±0.08 | 0.01±0.01 |
| p.L-PEG-AuNPs | 1228.30±58.51 | 43.15±1.25 | 15.33±0.42 | 8.14±2.55 | 5.13±1.89 | 2.42±0.51 | 0.38±0.22 | 0.20±0.06 | 0.01±0.01 |
| p.14-PEG-AuNPs | 1231.40± 81.42 | 43.22±1.10 | 15.32±0.32 | 8.66±0.99 | 5.34±0.47 | 2.49±0.67 | 0.62±0.07 | 0.17±0.12 | 0.01±0.01 |

PBS – Phosphate-buffered saline; AuNPs – Gold nanoparticles; Cit – Citrate; WBC – White blood cells; Lym - Lymphocytes; Neu - Neutrophils; Mon - Monocytes; Eos – Eosinophils; Bas – Basophils; Hb – Haemoglobin; Plat = Platelet; HCT = Haematocrit.
Values are expressed as Mean ± SD, n=6

**Table 5.3b:** Effect on haematological parameters with relative values (%) of the differential white cell counts

| Treatment | Lym (%) | Neu (%) | Mon (%) | Eos (%) | Bas (%) |
|---|---|---|---|---|---|
| PBS control | 64.64±8.93 | 28.14±8.03 | 5.24±2.23 | 1.90±0.70 | 0.10±0.00 |
| Cit-AuNPs | 65.76±2.87 | 26.52±3.11 | 5.65±1.29 | 1.72±0.23 | 0.06±0.07 |
| PEG-AuNPs | 65.72±2.29 | 26.71±2.82 | 6.48±0.10 | 1.63±0.67 | 0.04±0.06 |
| p.C-PEG-AuNPs | 60.19±6.75 | 32.17±8.35 | 5.67±2.22 | 1.94±0.91 | 0.04±0.04 |
| p.L-PEG-AuNPs | 62.49±3.10 | 30.51±3.84 | 4.47±1.67 | 2.46±0.54 | 0.07±0.07 |
| p.14-PEG-AuNPs | 64.12±0.71 | 28.46±5.10 | 7.18±1.21 | 1.95±1.22 | 0.07±0.06 |

PBS – Phosphate-buffered saline; AuNPs – Gold nanoparticles; Cit – Citrate; Lym - Lymphocytes; Neu - Neutrophils; Mon - Monocytes; Eos – Eosinophils; Bas – Basophils.
Values are expressed as Mean ± SD, n=6

### 5.2.5 Oxidative stress markers

Effect of a single exposure to AuNPs 12 weeks post-injection on MDA and protein carbonyls is shown in Table 5.4. No long-term effects on the levels of MDA and protein carbonyl were noted in all the AuNP-treatment groups when compared to the control group ($p>0.05$). This suggests that oxidative stress was not induced by the presence of AuNPs in the liver, the major organ of metabolism and detoxification, 12 weeks post-injection.

**Table 5.4:** Levels of oxidative stress markers in liver homogenates

| Treatment | MDA (µmol/mg protein) | Protein carbonyl (nmol/mg protein) |
|---|---|---|
| PBS control | 0.19±0.06 | 2.31±0.80 |
| Cit-AuNPs | 0.27±0.10 | 2.98±1.30 |
| PEG-AuNPs | 0.18±0.04 | 2.50±1.36 |
| p.C-PEG-AuNPs | 0.29±0.08 | 2.93±0.81 |
| p.L-PEG-AuNPs | 0.23±0.06 | 2.70±0.83 |
| p.14-PEG-AuNPs | 0.22±0.04 | 2.75±0.20 |

Cit - Citrate; PBS – Phosphate-buffered saline; AuNPs – Gold nanoparticles
Values are expressed as Mean ± SD, n=6.

### 5.2.6 Tissue histopathological analysis

a. Liver

The histopathological examinations of liver sections of rats treated with AuNPs is shown in Figure 5.5. In the control rat liver (Figure 5.5.1), there is congestion of the central vein (CV) and sinusoidal spaces (arrow heads), which has no pathological basis, and simply reflects the local intrahepatic hemodynamic forces prevalent at necropsy. Centrilobular hepatocytes are normal in staining pattern and morphology in all the groups. The hepatocytes are large polygonal cells (dotted circle) with ample light pink stained cytoplasm, and a centrally located large nucleus with dispersed chromatin material (thick arrow). Rats treated with PEG-, p.C-PEG- and p.14-PEG-

AuNPs presented no significant histopathological features when compared to the control rat. In rats exposed to p.L-PEG-AuNPs (Figure 5.5.5), there was mild periductal (around bile ducts (BD)), perivascular (around portal vein (PV)) and mononuclear cell infiltration (light arrow) noted in the portal triad configuration, with bile duct hyperplasia (many bile ducts). This is, however, a common non-neoplastic spontaneous lesion of the Wistar rat. The aetiology of this finding is not significant. This is because it occurs in non-treated rats as well (Greaves, 2011). The histopathological examinations of the liver in the AuNP-treated rats are consistent with the biochemical analyses (Figure 5.3, 5.4 and Table 5.1), as no significant biochemical changes were noted when compared to the control group ($p>0.05$). The oxidative stress markers investigated is consistent with the histological assessment (Table 5.4). It can, therefore be suggested that the AuNPs did not induce liver damage 12 weeks post-injection.

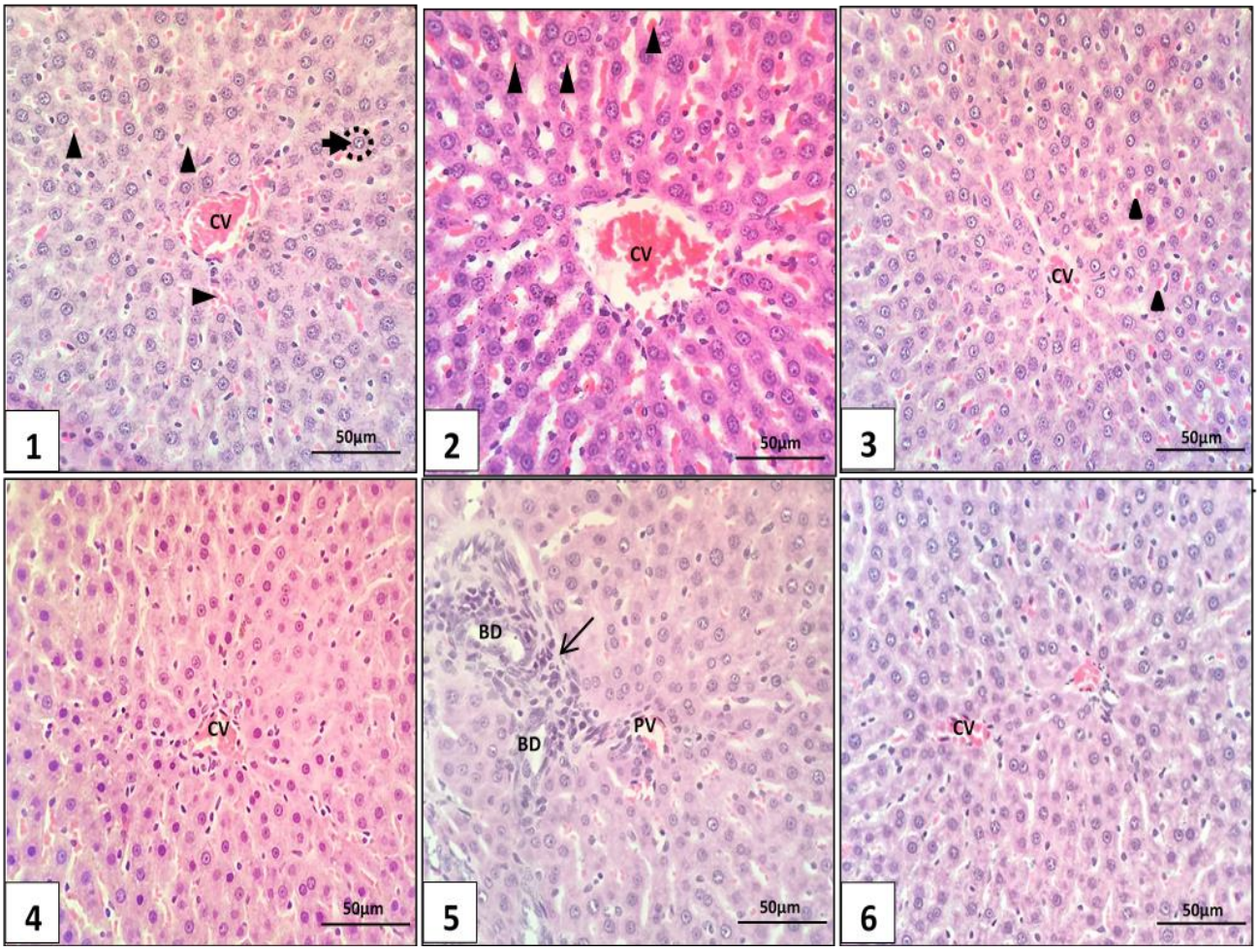


**Figure 5.5:** Histopathological analysis of the liver 12 weeks post-injection. *(Haematoxylin & Eosin, x400 original magnification*)
Key: 1 = PBS control; 2 = Citrate-AuNPs; 3 = PEG-AuNPs; 4 = p.C-PEG-AuNPs; 5 = p.L-PEG-AuNPs; 6 = p.14-PEG-AuNPs. CV = Central vein; arrow heads = Sinusoidal spaces; thick arrow = Chromatin material; BD = Bile ducts; PV = Portal vein.

b. Kidney

Histopathological examinations of kidney sections of rats injected with AuNPs 12 weeks post-exposure is presented in Figure 5.6. Glomerular histology is unremarkable in all groups (Figure 5.6). No overt histopathology is noted, with clear architectural markers of normality. These features are shown as patent glomerular capillaries with uncluttered luminal diameter, and free movement of intra-capillary erythrocytes (arrows). There were no changes in the glomeruli, and no glomerulonephritis in capillary patency or mesangial cellularity noted. The Bowman's capsular

space (asterisk) is open, and both visceral and parietal epithelial profiles are devoid of degenerative changes. This correlates with the biochemical kidney function investigation (Table 5.2), which reveals no nephrotoxicity following exposure to the AuNPs.

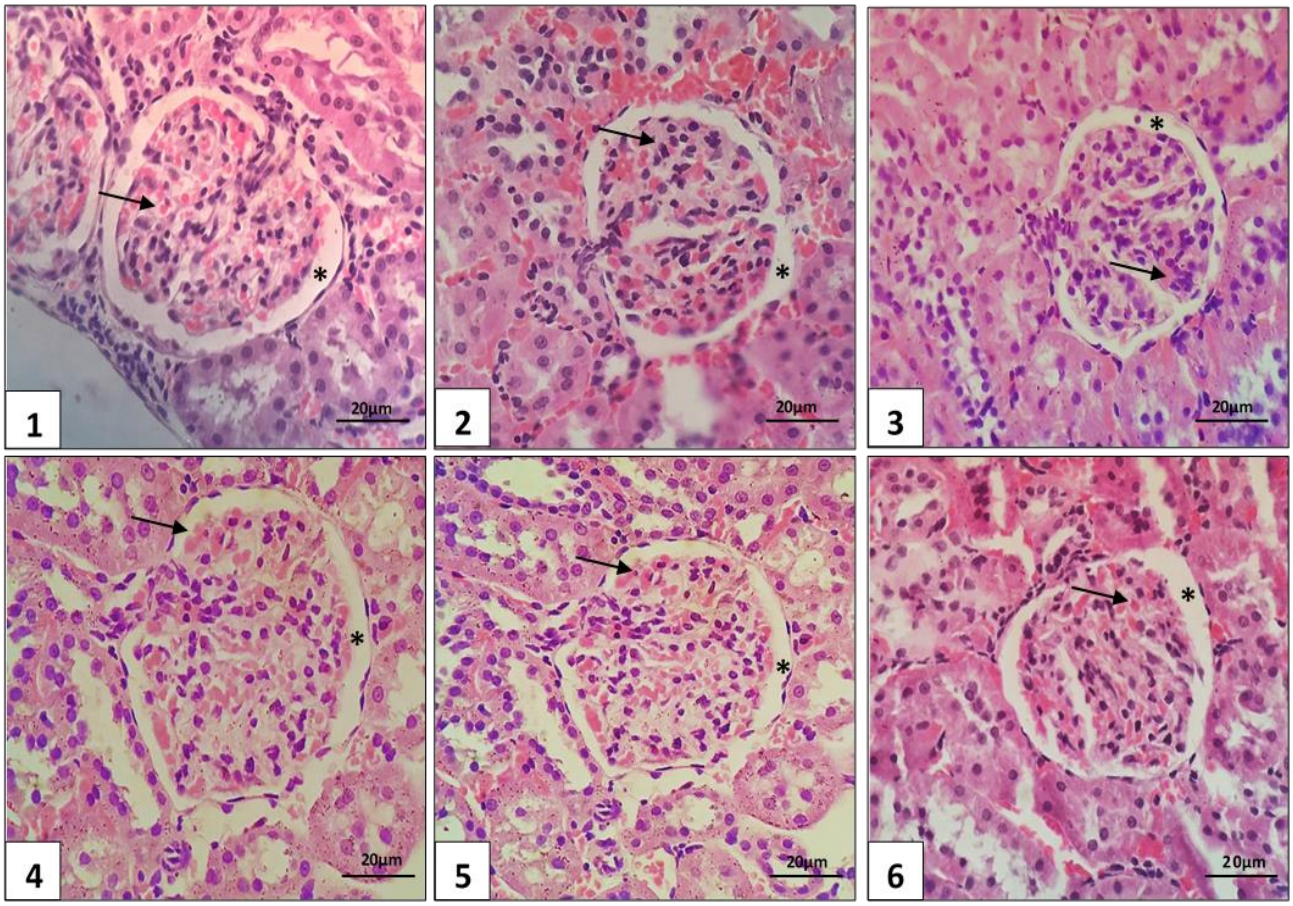


**Figure 5.6:** Photomicrograph of kidney sections of rats 12 weeks post-injection with AuNPs. *(Haematoxylin & Eosin, x400 original magnification, Scale Bar = 20 µm*)
Key: 1 = PBS control; 2 = Citrate-AuNPs; 3 = PEG-AuNPs; 4 = p.C-PEG-AuNPs; 5 = p.L-PEG-AuNPs; 6 = p.14-PEG-AuNPs.
* = Bowman's capsular space; arrow = intra-capillary erythrocytes.

c. Spleen

Histopathological analysis of splenic tissue sections of rats 12 weeks after injection with AuNPs is presented in Figure 5.7. The spleen is one the major organs of AuNPs distribution and accumulation (Balasubramanian *et al.*, 2010; Shi *et al.*, 2016). Consequently, a review of splenic histology can elucidate any negative effect of AuNPs on the immune system (Yang *et al.*, 2017b).

No negative impact on the splenic filtration capacity of old or damaged RBCs, as well as the administered AuNPs over the 12-week occurred. There were no significant changes in the red pulp (RP) and white pulp (WP) in all the AuNPs-treated rats when compared to the control. No significant changes in the marginal sinus (arrow head) and central artery (arrow) were noted in splenic sections of rats treated with AuNPs when compared to the control. These results are similar to studies by Yang *et al.* (2017a) and Rambanapasi (2015), where no significant pathological changes in the spleen was noted after 8 weeks in mice intravenously injected with 6 nm AuNPs, and 8 weeks post-intravenous injection of rats with 14 nm citrate-AuNPs, respectively.

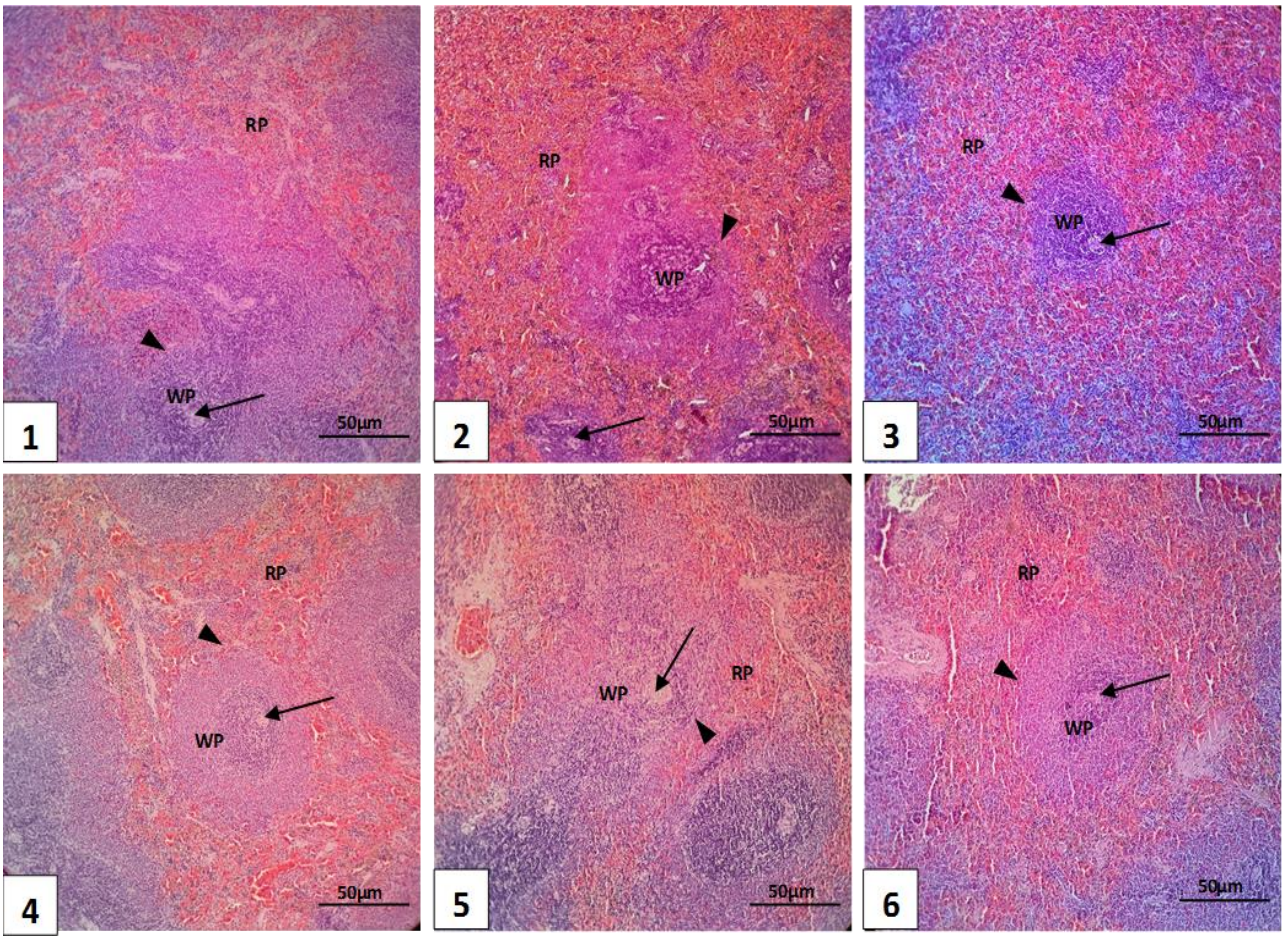


**Figure 5.7:** Histology of the spleen 12 weeks post-injection. (Haematoxylin & Eosin, x100 original magnification, Scale Bar = 50 µm)
Key: 1 = PBS control; 2 = Citrate-AuNPs; 3 = PEG-AuNPs; 4 = p.C-PEG-AuNPs; 5 = p.L-PEG-AuNPs; 6 = p.14-PEG-AuNPs. WP = White pulp; RP = Red pulp; arrow = Central artery; arrow head = marginal sinus.

d. Colon

The major target of the peptide-PEG-AuNPs in this study is the colon, i.e. the potential for the diagnosis of CRC. It was therefore necessary to examine any histopathological changes that could result from the long-term exposure of the AuNPs intensively. Histological analysis of rats intravenously injected with 14 nm AuNPs after 12 weeks is shown on Figure 5.8. All treatments showed normal histology of rat colon. The crypts (C) of all groups were intact, with no disruption to the basement membrane of lining epithelium (arrow).

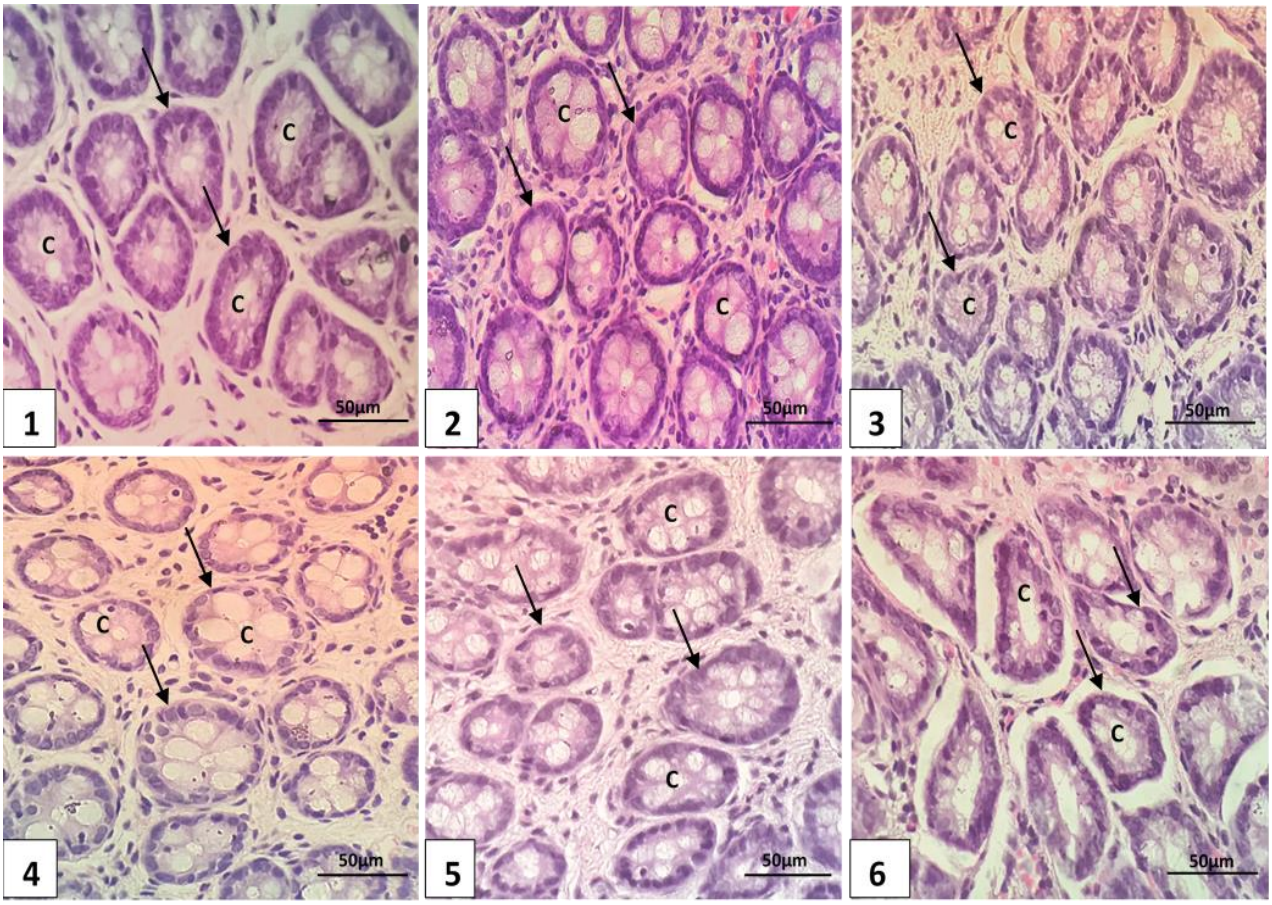


**Figure 5.8:** Histology of the colon 12 weeks post-injection. (Haematoxylin & Eosin, x400 original magnification, Scale Bar = 50 µm)
Key: 1 = PBS control; 2 = Citrate-AuNPs; 3 = PEG-AuNPs; 4 = p.C-PEG-AuNPs; 5 = p.L-PEG-AuNPs; 6 = p.14-PEG-AuNPs.
Arrow = epithelium; C = crypts

e. Pancreas

The two functional parts of the pancreas are the endocrine portion (Islets of Langerhans) and the exocrine portion. The Islets of Langerhans (IL) is the site for the secretion of hormones including insulin, glucagon, somatostatin and pancreatic polypeptide, while the exocrine parenchyma (Ep), which constitutes about 95% of the pancreatic mass, is the site for the secretion of digestive enzyme or pancreatic juice (Longnecker, 2014). The histology of the pancreas sections of rats injected with AuNPs is presented in Figure 5.9. The examinations revealed no change in the morphology of both the IL and the Ep of the pancreas in all the groups, 12 weeks after injection. This suggests that glucose metabolism was not affected up to 12 weeks post-injection of AuNPs to rats.

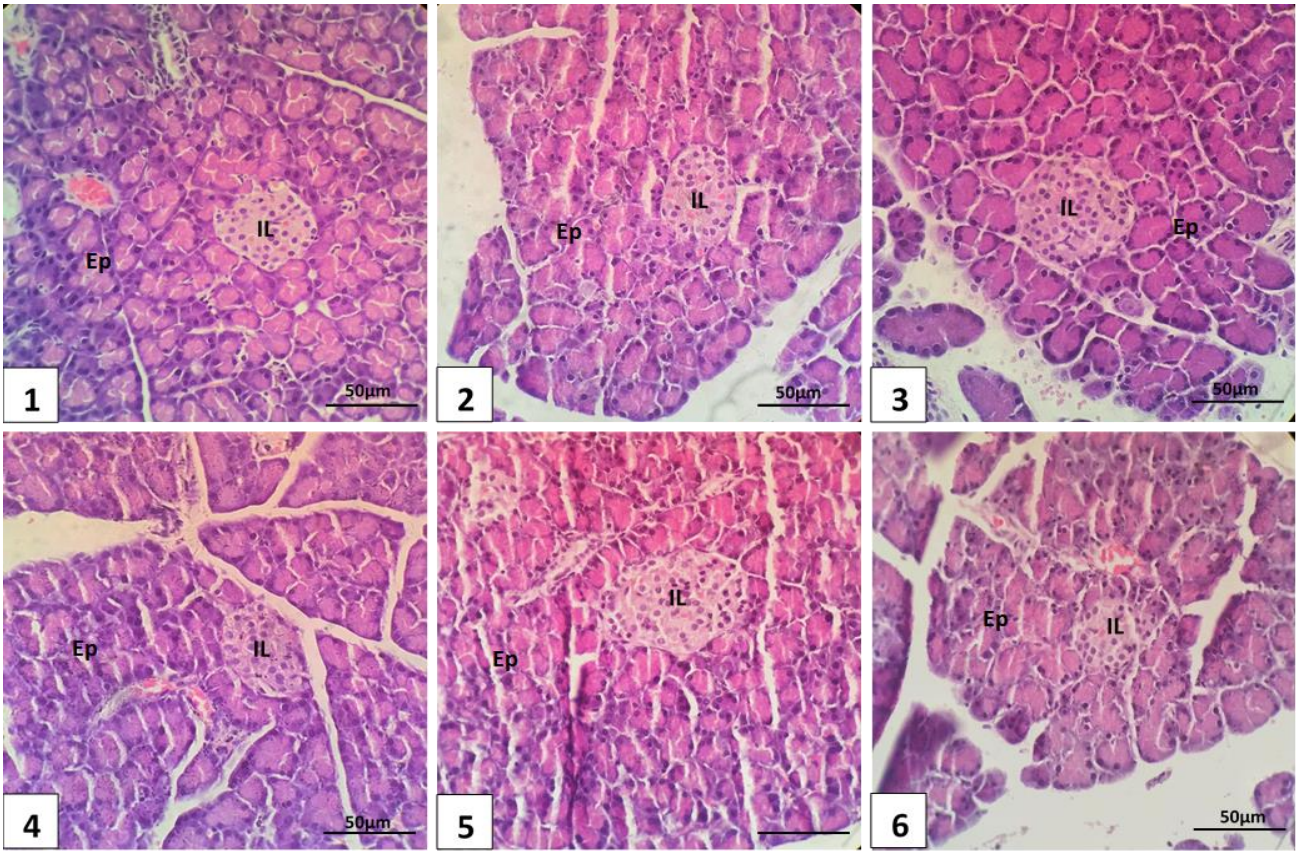


**Figure 5.9:** Histology of the pancreas 12 weeks post-injection. (Haematoxylin & Eosin, x400 original magnification, Scale Bar = 50 µm)
Key: 1 = PBS control; 2 = Citrate-AuNPs; 3 = PEG-AuNPs; 4 = p.C-PEG-AuNPs; 5 = p.L-PEG-AuNPs; 6 = p.14-PEG-AuNPs. Ep = exocrine parenchyma; IL = islets of Langerhans

It can be concluded, based on the results of the investigated physiological (body and organ weights), biochemical (serum marker enzymes, liver and kidney function markers, and cholestatic indicators), haematological (full blood count), oxidative stress (MDA and protein carbonyl), and histological parameters, that all the AuNPs (14 nm, 100 µg/kg b.w.) were not toxic 12 weeks post-injection. In addition, none of the histology slides showed any lesions of previous tissue damage, and no streaks of connective tissue. The results of the tested parameters therefore, suggest that there was no delayed or continuous toxicity noted after a single intravenous injection of healthy rats with 14 nm citrate-capped AuNPs, PEG- or peptide-PEG-AuNPs at 100 µg/kg b.w.

Although, there was acute toxicity noted with p.L-PEG-AuNPs at 100 µg/kg b.w. 2 weeks post injection, this was reversed 12 weeks post injection. Chapter six therefore focuses on comprehensive comparison between the two time-point studies, thereby providing further insight to the immediate, acute, delayed or continuous toxicity of the AuNPs.

# CHAPTER SIX

# GENERAL DISCUSSION, CONCLUSION AND FUTURE STUDIES

## 6.1 GENERAL DISCUSSION

Gold NPs have several potential applications in biomedicine, ranging from diagnosis of disease to treatment. One of the major concerns for the use of AuNPs in humans is the biodegradability and long-term toxicity (Zhu *et al.*, 2017). This is because NPs may accumulate in various organs for long periods (> 3 months), thereby causing damage to such organs (Zhang *et al.*, 2011; Gunduz *et al.*, 2017). The Au concentration following intravenous injection of AuNPs has highest accumulation in the liver and the spleen (even up to 6 months post-exposure) (Sadauskas *et al.*, 2009; Rambanapasi *et al.*, 2016), indicating that the major clearance of AuNPs is the hepatobiliary system (Rambanapasi *et al.*, 2016). It is therefore imperative to investigate the short- and long-term effects of these NPs after exposure to normal, healthy or target tissues before development for biomedical applications.

One of the major challenges in the clinical applicability of AuNPs is the *in vivo* effects after exposure, ranging from immediate to delayed, and persistent toxicity. Several researchers have reported *in vivo* short-term acute toxicity studies of AuNPs after a single exposure (Cho *et al.*, 2009a; Chen *et al.*, 2013a; Khan *et al.*, 2013; Fraga *et al.*, 2014). Toxic effects of these NPs were reported in studies ranging from 1 h to 28 days post-exposure, and further long-term studies were suggested. Limited studies have, however, considered both the short- and long-term effects *in vivo* after a single exposure (Zhang *et al.*, 2012; Sengupta *et al.*, 2013; Fraga *et al.*, 2014; Rambanapasi, 2015).

In this study, biotinylated peptides (p.L, p.C and p.14), which specifically bind to CRC cells *in vitro*, were conjugated to PEGylated citrate-capped AuNPs by streptavidin-biotin chemistry for potential application in the diagnosis of CRC *in vivo*. The short- and long-term effects of these AuNPs (14 nm, 100 µg/kg b.w.) injected intravenously to rats, was investigated. This was

necessary because of several conflicting reports on AuNPs (unconjugated and conjugated) in various *in vitro, in ovo* and *in vivo* models, which can be linked to differences in the protocols and properties of AuNPs used. These include the following:

a. Method of synthesis: The method used in the synthesis of AuNPs greatly influences the toxic effect of AuNPs (Yah, 2013) and its characteristics, such as size and shape. There are different methods used in the synthesis of AuNPs, including the physical, chemical or biological methods (Section 2.2.2.1). The toxicity of the commonly used chemical method, Tukevish-Frens method, can be controlled by reducing the amount of sodium citrate added during the synthesis of the AuNPs, as an increase in sodium citrate concentration, with reduced $HAuCl_4$, increases toxicity (Freese *et al.*, 2012). The Tukevish-Frens method was used in this study for the synthesis of negatively and spherically-shaped 14 nm AuNPs - no toxic effects have been reported in literature and is confirmed by this acute and long-term *in vivo* studies.

b. Surface chemistry: Surface chemistry plays an important role in the functionalisation of AuNPs (Section 2.3.2.1.3). The choice of ligands or biomolecules depends on the potential application of the synthesised AuNPs. Surface-dependent toxicity has been reported in literature (Fraga *et al.*, 2014). The toxicity (Cho *et al.*, 2009a; Bashandy *et al.*, 2015) and safety of PEGs (Yang *et al.*, 2016; Jia *et al.*, 2017), the commonly used ligands, have been reported.

   Combination of two PEGs (PEG-OH and PEG-biotin) used in this study was based on the use as both stabilisation agent (PEG-OH) and linking agent (PEG-biotin). The biotin of the PEG binds to the affinity site on streptavidin, and allows for the binding of biotinylated peptides (p.C, p.L and p.14). No literature has been reported on the safety of this design for functionalising AuNPs. Several studies have reported both the toxicity and safety (either mild or acute) of peptide-AuNPs (Simpson *et al.*, 2013; Fraga *et al.*, 2014). Mild alterations in some haematological parameters were noted with rats intravenously-

injected with a single dose of 20 nm pentapeptide conjugated to AuNPs, but the citrate-capped AuNPs did not show toxicity 4 weeks post-exposure (Fraga *et al.*, 2014). The combination of PEG-OH and PEG-biotin, used in this study, proofed to be safe in both acute and in the long-term studies, as no side effects were observed, except for a decrease in total serum protein in p.L-PEG-AuNP-treated rats 2 weeks post injections, but was reversed at 12 weeks.

c. Model used and route of administration of AuNPs: Toxicity studies on various *in vitro*, *in ovo* and *in vivo* models have been reported (Section 2.3.2.2). The *in vitro* model provides preliminary information on the effects of AuNPs, which may not correspond to *in vivo* results. The *in vivo* models provides the complexity of the organism, in terms of the administration, distribution, metabolism and excretion of the AuNPs (Jia *et al.*, 2017). The rat model was considered in this study because of the various similarities shared with humans, which include sinusoidal spleen capillaries (Cesta, 2006), physiological parameters, such as organ weight fraction of body weight and plasma volume fraction of body weight (Lin *et al.*, 2016a). Intravenous injection was used in this study to mimic intravenous exposure during CRC diagnosis. Lowest toxicity of AuNPs via intravenous exposure (compared to intraperitoneal and oral) have been reported (Zhang *et al.*, 2010).

d. Dose and duration of exposure: Dose is another crucial factor to be considered prior to exposure of AuNPs to experimental animals. Dose(s) should be selected based on previous information of the AuNPs and/or dose that mimics biomedical applications. High doses with prolonged exposure of AuNPs could result in toxicity to major organs. These factors were taken into consideration when designing this study. A diagnostic dose that falls within the low and medium range, as described by Lin *et al.* (2016a), which was previously used in a pilot study by Cairncross (2015) towards targeting CRC tumour in rats, was used in this study. Equally, short- and long-term effects of a single dose of AuNPs (100 µg/kg b.w.), were investigated in rats, to provide information on the immediate, delayed or persistent toxicity.

### 6.1.1 Comparison of the two time-point studies

#### *6.1.1.1 General morphology, behaviour and physiology of rats*

No observable changes in the general behaviour, and body weights were noted in rats injected with AuNPs. Generally, no change in the organ weights were noted, with the following exceptions: a significant decrease ($p<0.05$) in the liver weights of rats treated with p.L-PEG-AuNPs, as well as a significant increase ($p<0.05$) in the spleen and colon weights of rats treated with p.C-PEG-AuNPs were noted (Figure 4.7), 2 weeks post-injection. These changes, however, returned to normalcy 12 weeks post-injection (Figure 5.2). This indicates that the general morphology and physiology of the rats were not affected after intravenous exposure of 14 nm AuNPs 12 weeks post-injection.

#### *6.1.1.2 Changes in liver damage and function parameters*

6.1.1.2.1 Serum marker enzymes

The increase (though not significant compared to the control group) in the levels of AST in p.L-PEG-AuNP-treated rats 2 weeks post-injection (Figure 4.8) was reversed by 12 weeks when compared to the control (Figure 5.3). The observed reduction in ALP levels after exposure to the AuNPs in all the treatment groups 2 weeks post-injection (Figure 4.8) returned to normal at 12 weeks when compared to the control (Figure 5.3). This suggests that any toxicity induced by the NPs does not persist at long-term. There was no evidence of cellular damage or loss of architectural/functional integrity of the membrane of the liver as indicated by the concentrations of ALT or the histology of the liver at 12 weeks.

6.1.1.2.2 Liver function markers

The liver is responsible for various functions, including 1) synthesis of proteins, such as albumin and antibodies; 2) production of bile; 3) detoxification of foreign toxic substances, and conversion

of waste products to excretable materials; 4) metabolism and storage of carbohydrates; 5) filtration of blood; and 6) production of immune factors (Zhang *et al.*, 2016). Serum albumin, the most abundant plasma protein, transports substances, such as bilirubin, metals, and drugs in circulation. Albumin maintains colloid osmotic pressure, and plays a role in the detoxification of exogenous and endogenous substances (Bernardi *et al.*, 2012; Cuperus *et al.*, 2017). These functions are impaired in liver pathology, and can be measured by the levels of albumin, total protein, and bilirubin in the serum (Ramaiah, 2007).

Similar results were noted in the concentrations of total protein, albumin, as well as total and direct bilirubin during the two time-points of this study in all the treatment groups. In rats injected with p.L-PEG-AuNPs, decreased total protein, though not significant, was noted when compared to the control 2 weeks post-injection (Figure 4.9), returned to normal at 12 weeks (Figure 5.4). A significant reduction ($p<0.05$) in the levels of total protein in p.L-PEG-AuNP-treated rats when compared to the citrate- and PEG-AuNP groups suggests reduction in the protein synthesis by the liver, which returned to normal 12 weeks post-exposure.

The results of the serum bilirubin assays (Table 4.3 and 5.1) indicate no obstruction to the free flow of bile in rats, with no effect on the excretory function of the liver short- and long-term after exposure to the AuNPs.

It is, therefore, suggested that there was no significant effect on the biosynthetic function of the liver and hepatobiliary system 12 weeks post-exposure of rats to the AuNPs.

#### *6.1.1.3 Changes in kidney function parameters*

The kidneys perform the crucial role of filtration and excretion of toxic substances from the body. These functions are impaired in kidney pathology, and are accessed by changes in the concentrations of two zero-threshold substances, urea and creatinine, which are readily and rapidly cleared by the functional kidney (Adewale and Orhue, 2015). Gold NPs can cause

substantial impairment of the highly-coordinated process of glomerular filtration, thereby resulting in increased concentrations of serum urea and creatinine (Zhang *et al.*, 2011).

The concentrations of urea and creatinine, as well as the histology of the kidney were normal in rats injected with the AuNPs, compared to the control group, during the two time-points of this study (Table 4.4; 5.2). These, in addition to the concentrations of albumin and total protein, where no significant changes were noted, provide no evidence of renal dysfunction, or damage to the structural and functional integrity of the kidney by the AuNPs.

#### *6.1.1.4 Changes in immune response*

A significant decrease in the number of WBCs followed exposure to p.L-PEG-AuNPs 2 weeks post-injection, but returned to normal at 12 weeks (Table 4.5a; 5.3a). A significant decrease in the absolute and relative values of neutrophils was noted 2 weeks post-injection, which also returned to normal 12 weeks post-injection (Table 4.5a, b; 5.3a, b).

#### *6.1.1.5 Oxidative stress markers*

Common oxidative stress markers, MDA and protein carbonyls, were investigated in the liver homogenate, as the liver (major organ for detoxification) is the most vulnerable to damage induced by foreign agents (Sefi *et al.*, 2014). Further, the liver is a major accumulation site for AuNPs after intravenous injection (Fraga *et al.*, 2014; Rambanapasi *et al.*, 2016; Yang *et al.*, 2017a). In this study, no significant changes in the levels of MDA and protein carbonyls were noted at either 2 or 12-week post-injection with AuNPs when compared to the control group, except for p.L-PEG-AuNPs (Table 4.6), which returned to normal at 12 weeks (Table 5.4). This suggests that oxidative stress or inflammation induced by p.L-PEG-AuNPs at a low dose (100 µg/kg) can be overcome in the long-term.

#### *6.1.1.6 Changes in the histology of the tissues*

Results from the tissue histopathological studies are consistent with the biochemical and haematological parameters. No significant damage was noted in tissues under histological examination during the two time-points post-injection when compared to the control. The histology of the spleen showed possible low-grade breakdown of RBCs at 2 weeks post-injection of p.L-PEG-AuNP (Figure 4.12), and was reversed at 12 weeks. From these two studies, this effect seems to be peptide linked.

#### *6.1.1.7 Inflammatory response*

There was no evidence of inflammation in the liver, spleen, kidney and colon of rats 2 weeks post-injection with AuNPs, as there was no inflammatory marker (p-I*k*B-α, IL-18 and IFN-γ) proteins found. Few exceptions were noted in liver sections of rats injected with p.L-PEG-AuNPs, where a very few p-I*k*B-α and IFN-γ proteins was seen in liver sections, and the presence of few IL-18 and IFN-γ in the colon of p.C-PEG-AuNP-treated rats on immunohistochemical staining. The significant changes noted in liver weight, MDA and haematological parameters in p.L-PEG-AuNP-treated rats, and a significant increase in spleen and colon weights in rats treated with p.C-PEG-AuNPs 2 weeks post-injection, did not persist 12 weeks post-exposure to the AuNPs. This prevents further inflammatory investigations. It is suggested that no inflammatory response was elicited by the AuNPs at 100 µg/kg b.w. 12 weeks post-exposure.

### 6.1.2 General effect of gold nanoparticles on rat

#### *6.1.2.1 Citrate-capped gold nanoparticles*

No evidence of toxicity was noted with citrate-capped AuNP (14 nm) at 100 µg/kg b.w. during the two time-points of this study. Similar results have been reported (Table 2.3 and 2.4) during *in vivo* short-term (Lasagna-Reeves *et al.*, 2010; Zhang *et al.*, 2010; Glazer *et al.*, 2011; Chen *et al.*, 2013a; Uchiyama *et al.*, 2014; Jo *et al.*, 2015; Muller *et al.*, 2017); long-term (Rambanapasi *et*

*al.*, 2016); or both exposure periods (Fraga *et al.*, 2014; Rambanapasi, 2015) using AuNPs in the same size range (5 to 25 nm).

Of interest, no toxicity has been reported with 14 nm citrate-capped AuNPs *in vivo* after short- and long-term exposure at a dose range of 3 to 375 µg/kg (Rambanapasi, 2015; Rambanapasi *et al.*, 2016). The dose used in our study falls within this range. Researchers have reported the *in vivo* toxicity of citrate-AuNPs at various time-points (Zhang *et al.*, 2010; Sengupta *et al.*, 2013; Ghahnavieh *et al.*, 2014; Rathore *et al.*, 2014; Muller *et al.*, 2017), which were in contrast with this study. The disparities could be linked to differences in the size (14 nm), dose (100 µg/kg), as well as exposure period (single exposure during 2 and 12 weeks) and route of administration (intravenous). Fourteen (14) nm AuNPs, at 100 µg/kg, falls within the non-toxic size (Rambanapasi, 2015; Rambanapasi *et al.*, 2016) and dose range (Rambanapasi, 2015; Lin *et al.*, 2016a; Rambanapasi *et al.*, 2016) reported.

#### *6.1.2.2 PEGylated gold nanoparticles*

Polyethylene glycol is a hydrophilic polymer that prevents and reduces non-specific interactions of AuNPs with serum proteins and the immune system, respectively; thus, increasing blood circulation of the NPs (Leopold *et al.*, 2017). Polyethylene glycol is used in coating AuNPs to enhance stability, and prevents aggregation and toxicity of NPs (Yang *et al.*, 2016). Polyethylene glycol-(PEGylated) AuNPs do, however, induce toxicity in experimental animals (Cho *et al.*, 2009a; Cho *et al.*, 2009b; Zhang *et al.*, 2011; Hwang *et al.*, 2012; Bashandy *et al.*, 2015). These discrepancies could result from differences in the type of PEG used, and the size, shape and charge of AuNPs, as well as the experimental model and administration route used.

To date, no toxicity studies have been reported on the combination of PEG (PEG-OH and PEG-biotin) used in this study. The toxicity of the combinational PEGs on the surface of AuNPs for enhanced stability in aqueous solution was, therefore investigated in rats short- and long-term post-exposure.

The combination of PEG-OH (99%) and PEG-Biotin (1%) on the surface of 14 nm AuNPs did not induce toxicity 2 weeks and 12 weeks post-intravenous injection to rats at 100 µg/kg b.w. The dose of PEG-AuNPs used in this study is lower than the reported toxic doses used in previous studies (Cho *et al.*, 2009a; Zhang *et al.*, 2011; Bashandy *et al.*, 2015). Also, many of these studies did not compare the toxicity of citrate-capped AuNPs with the PEG-coated AuNPs, making it difficult to determine the effect of PEG on the AuNPs. For example, the size (13 nm) and dose (0.17, 0.85 or 4.26 mg/kg), type of PEG (HS-PEG, MW 5000) and animal model used by Cho *et al.* (2009a) were different from our study.

#### *6.1.2.3 Peptide-conjugated gold nanoparticles*

Peptides (p.C, p.L and p.14) specifically bind to CRC cells *in vitro*, potentiating the use in the diagnosis of CRC *in* vivo, when conjugated to AuNPs. It is therefore important to investigate the toxicity profile of these peptides before considering them as diagnostic tools in biomedicine. From the results obtained, these peptides appear to be non-toxic 12 weeks after intravenous exposure. The p.L-PEG-AuNPs showed toxicity, as revealed by changes in liver weight, WBCs, and MDA levels, 2 weeks post-injection, but this was reversed at 12 weeks. This explains the ability of the body to fight against toxicity or inflammatory response induced by foreign agents (Zhang *et al.*, 2011). It must be noted that the toxicity of p.L-PEG-AuNPs 2 weeks after a single intravenous injection to rats was not influenced by capping with citrate or PEGs, as these did not induce toxic effects in the rats at the two time-points of this study. The 2-week study revealed a safety pattern followed the order p.14 > p.C > p.L.

The amino acid sequence of the peptides could be a factor in this safety pattern, as terminal amino acids could influence the toxic effects of functionalised-AuNPs (Harper *et al.*, 2014; Zong *et al.*, 2017). The transient toxicity noted in p.L-PEG-AuNPs could be linked to the presence of an aromatic amino acid (tyrosine) at the terminal (free) end of the peptide, interacting with the cellular membrane (Zong *et al.*, 2017). It is interesting that all the signs associated with the toxicity of p.L-PEG-AuNP can be linked to a compromised cell membrane: a) increased weights of

liver – known sites for AuNP accumulation, if p.L-PEG-AuNP bound to cell membranes and caused damage to cells, it could lead to small increase in interstitial fluid, which could increase organ weight (Scallan *et al.*, 2010; Openstax, 2013); b) increased MDA indicates disruption of lipids in the cellular membranes (lipid peroxidation) (Casarett and Klaassen, 2008). This aspect, however, warrants further investigations before any conclusion can be made.

Glycine is the terminal amino acid in the amino acid sequence of p.C. Although p.C has more amino acids (11) in its sequence relative to p.L (7) and p.14 (7), the interaction of glycine with the biological membrane is minimised due to its hydrophobic nature, but can readily permeate the membrane by passive diffusion (Casarett and Klaassen, 2008).

Methionine, the terminal amino acid in p.14, minimises biological interactions due to its hydrophobic nature, and can enhance internalisation of the AuNPs with arginine (within the sequence), a cationic amino acid (Kalmodia *et al.*, 2016). The role of the terminal amino acid (methionine) in minimising biological interactions (Harper *et al.*, 2014) may contribute to its lack of toxicity. Any interaction of the peptides with the membrane can be suggested non-persistent, as indicated by the toxicity results of the parameters investigated.

Interestingly, the hydropathy indices of the terminal amino acids in p.14 (methionine), p.C (glycine), and p.L (tyrosine) are 1.9, -0.4 and -1.3, respectively (Nelson and Cox, 2005), relating to the safety pattern of the peptides as indicated by this study, as larger values indicate more hydrophobicity and hence reduced membrane interaction.

## 6.2 CONCLUSION

To affirm the safe use of AuNPs in cancer diagnosis, both short- and long-term toxicity studies are of utmost importance. Acute toxicity studies provide immediate and preliminary information about the effect of these NPs *in vivo*, while the long-term study provides insight on the delayed or continuous toxic effect. To mimic potential CRC diagnostic application, where a single injection

of AuNPs would be administered, a single intravenous injection of these conjugated AuNPs in rats was performed to investigate the short- and long-term post-exposure effects.

Citrate-capped AuNPs were investigated in this study to confirm its possible role in the toxicity of the peptides under investigation, because of the various contradictory toxicity results previously reported. Based on the findings of this study, it is suggested that spherically-shaped 14 nm citrate-capped AuNPs do not induce acute or long-term toxicity at 100 µg/kg b.w. after a single intravenous injection to rats. This supports the use of negatively-charged, spherical AuNPs in nanomedicine, and as suitable carrier for diagnostic and/or therapeutic molecules such as peptides. The intravenous route can be suggested as a better route for AuNPs exposure in clinical applications, as suggested by Zhang *et al.* (2010).

Based on the results of this study, it can be concluded that the combination of 99% PEG-OH and 1% PEG-biotin would not potentiate toxicity of either citrate-capped AuNPs or the peptides investigated, as no toxicity was noted in rats up to 12 weeks post-exposure. This combination can thus be considered an appropriate option for conjugating secondary diagnostic or therapeutic biomolecules or agents to AuNPs. The PEG-OH molecule is mainly responsible for stabilising AuNPs in an aqueous environment, thereby preventing aggregation, while the PEG-biotin serves as a co-stabiliser and a linker between streptavidin and biotinylated peptides. This prevents direct attachment of the peptides to the AuNPs' surface, resulting in strong non-covalent bonding between the peptides and the citrate-capped AuNPs.

Gold NPs are conjugated with biomolecules or markers of cancer cells for enhanced permeability and accumulation in tumour tissues, thereby reducing accumulations in normal tissues and enhancing X-ray attenuation in tumour tissues (Popovtzer *et al.*, 2008). The peptides conjugated to AuNPs (14 nm) via streptavidin-biotin chemistry can be considered non-toxic long-term (12 weeks) after intravenous exposure to rats at 100 µg/kg b.w. This was based on the physiological, biochemical, haematological, and histological parameters, as well as inflammation markers

investigated. Two peptides, p.C and p.14 are considered most suitable for the development into a diagnostic tool for CRC *in vivo*.

## 6.3 LIMITATIONS TO THIS STUDY

Several challenges were encountered during this study, which include:

1. Unavailability of X-ray imaging machine to view the behaviour of the AuNPs in rats. This resulted in two separate groups of rats for the two time-points of this study.

## 6.4 RECOMMENDATIONS AND FUTURE PERSPECTIVES

### 6.4.1 Recommendations

The following recommendations were drawn for future studies:

1. Researchers are encouraged to focus and fully characterise the AuNPs investigated for biomedical applications. This will prevent other researchers from repeating experiments, rather than to explore other areas.
2. Spherically-shaped, 14 nm-sized citrate-capped AuNPs is recommended as a starting material for conjugation of biomolecules or ligands for clinical applicability.
3. Combination of PEG-OH (99%) and PEG-Biotin (1%) is recommended as possible stabilising and linking agents for AuNPs and other biomolecules, such as peptides. Increased PEG-biotin (10%) resulted in aggregation, which limits its single use. The use of PEG-biotin (100%) as both stabilising and linking agent (Sosibo *et al.*, 2015), and 90% PEG-OH and 10% PEG-biotin as stabilising and linking agent, respectively (previously used in this study), resulted in aggregation of the AuNPs. This further supports the use of 99% PEG-OH and 1% PEG-biotin.
4. Quantification of Au in various tissues to ascertain the distribution and accumulation of the AuNPs in healthy rats should be performed. The high cost per sample was a great concern in this current study, but since biodistribution and accumulation of AuNPs does

not have a direct link to toxicity (Fraga *et al.*, 2014; Tiwari *et al.*, 2014; Rambanapasi *et al.*, 2016; Shi *et al.*, 2016; Zong *et al.*, 2017), this was not investigated, as it is outside the scope of this study. It is therefore recommended to investigate detailed biodistribution and accumulation of AuNPs to provide further insight to other applications *in vivo*. As liver is the major organ of AuNP distribution, a sample from citrate-AuNPs group was prepared following the protocol of Yang *et al.* (2017a), and analysed with ICP-OES to confirm the presence of gold in the tissue. The result indicated that 17.95 µg Au/g liver was present 2 weeks post-injection of citrate-AuNPs to rat.

### 6.4.2 Future perspectives

The results from this study clearly indicates that 14 nm AuNPs (100 µg/kg b.w.) are non-toxic to healthy rats, though care with p.L-PEG-AuNPs. It is therefore worthwhile to perform further studies on the peptide-AuNPs. These include, but are not limited to:

1. Biodistribution and bioaccumulation, as well as tissue localisation studies of the peptide-AuNPs at various time points (0 to 12 hr) in cancer (CRC)-induced rats, and healthy rat tissues as control. This is necessary to investigate the selectivity and specificity of the peptides to CRC cells. The time points suggested is to mimic its application in diagnosis, as patients should be examined within 12 hr of intravenous injection. Further, the receptors on the CRC tumours responsible for the specificity need investigation.
2. Evaluate *in vivo* toxicity (sub-acute, chronic and sub-chronic) studies involving repeated intravenous injections, using 100 µg/kg b.w. as a reference.
3. Investigate *in vivo* toxicity (acute, sub-acute, chronic and sub-chronic) studies with different doses and/or repeated intravenous injections of AuNPs, to potentiate therapeutic applications.
4. Investigate the possible therapeutic application of these AuNPs in cancer treatment.

## REFERENCES


Abadeer, N. S. and Murphy, C. J. 2016. Recent progress in cancer thermal therapy using gold nanoparticles. *Journal of Physical Chemistry C,* 120**,** 4691-4716.

Abdelhalim, M. and Jarrar, B. M. 2012. Histological alterations in the liver of rats induced by different gold nanoparticle sizes, doses and exposure duration. *Journal of Nanobiotechnology,* 10**,** 1-9.

Abdelhalim, M. A. 2012. The Influence of size and exposure duration of gold nanoparticles on gold nanoparticles levels in several rat organs in vivo. *Journal of Cell Science and Therapy,* 3**,** 129.

Abdelhalim, M. A. and Abdelmottaleb Moussa, S. A. 2013. The gold nanoparticle size and exposure duration effect on the liver and kidney function of rats: In vivo. *Saudi Journal of Biological Sciences,* 20**,** 177-181.

Abdelhalim, M. A., Al-Ayed, M. S. and Moussa, S. A. 2015. The effects of intraperitoneal administration of gold nanoparticles size and exposure duration on oxidative and antioxidants levels in various rat organs. *Pakistan Journal of Pharmaceutical Sciences,* 28**,** 705-712.

Abdelhalim, M. A., Mady, M. M. and Ghannam, M. M. 2012. Physical properties of different gold nanoparticles: Ultraviolet-visible and fluorescence measurements. *Journal of Nanomedicine and Nanotechnology,* 3**,** 178-194.

Abou Seif, H. S. 2016. Physiological changes due to hepatotoxicity and the protective role of some medicinal plants. *Beni-Suef University Journal of Basic and Applied Sciences,* 5**,** 134-146.

Ádám-Vizi, V. and Seregi, A. 1982. Receptor independent stimulatory effect of noradrenaline on Na,K-ATPase in rat brain homogenate. *Biochemical Pharmacology,* 31**,** 2231-2236.

Adesanoye, O. A., Adekunle, A. E., Adewale, O. B., Mbagwu, A. E., Delima, A. A., Adefegha, S. A., Molehin, O. R. and Farombi, E. O. 2016. Chemoprotective effect of Vernonia amygdalina Del. (Astereacea) against 2-acetylaminofluorene-induced hepatotoxicity in rats. *Toxicology and Industrial Health,* 32**,** 47-58.

Adewale, O. B., Onasanya, A., Anadozie, S. O., Abu, M. F., Akintan, I. A., Ogbole, C. J., Olayide, I. I., Afolabi, O. B., Jaiyesimi, K. F., Ajiboye, B. O. and Fadaka, A. O. 2016. Evaluation of acute and subacute toxicity of aqueous extract of Crassocephalum rubens leaves in rats. *Journal of Ethnopharmacology,* 188**,** 153-158.

Adewale, O. B. and Orhue, N. E. J. 2015. Protective effect of aqueous extract of Xylopia aethiopica fruits on carbon tetrachloride-induced nephrotoxicity in rats. *Journal of Experimental and Integrative Medicine,* 5**,** 105-109.

Ahmed, T. A. and Aljaeid, B. M. 2016. Preparation, characterization, and potential application of chitosan, chitosan derivatives, and chitosan metal nanoparticles in pharmaceutical drug delivery. *Drug Design, Development and Therapy,* 10**,** 483-507.

Ahn, S., Jung, S. Y. and Lee, S. J. 2013. Gold nanoparticle contrast agents in advanced X-ray imaging technologies. *Molecules,* 18**,** 5858-5890.

Akrami, M., Balalaie, S., Hosseinkhani, S., Alipour, M., Salehi, F., Bahador, A. and Haririan, I. 2016. Tuning the anticancer activity of a novel pro-apoptotic peptide using gold nanoparticle platforms. *Scientific Reports,* 6**,** 31030.

Al-Azawi, M. A. and Bidin, N. 2015. Gold nanoparticles synthesized by laser ablation in deionized water. *Chinese Journal of Physics,* 53**,** 201-209.

Alalaiwe, A., Roberts, G., Carpinone, P., Munson, J. and Roberts, S. 2017. Influence of PEG coating on the oral bioavailability of gold nanoparticles in rats. *Drug Delivery,* 24**,** 591-598.

Albrethsen, J., Møller, C. H., Olsen, J., Raskov, H. and Gammeltoft, S. 2006. Human neutrophil peptides 1, 2 and 3 are biochemical markers for metastatic colorectal cancer. *European Journal of Cancer,* 42**,** 3057-3064.

Alizadeh, A., Parsafar, S. and Khodaei, M. M. 2017. Biosynthesis of spherical and highly stable gold nanoparticles using Ferulago angulata aqueous extract: Dual role of extract. *Materials Research Express,* 4**,** 035029.

Alkilany, A. M., Abulateefeh, S. R., Mills, K. K., Bani Yaseen, A. I., Hamaly, M. A., Alkhatib, H. S., Aiedeh, K. M. and Stone, J. W. 2014. Colloidal stability of citrate and mercaptoacetic acid capped gold nanoparticles upon lyophilization: Effect of capping ligand attachment and type of cryoprotectants. *Langmuir,* 30**,** 13799-13808.

Alkilany, A. M. and Murphy, C. J. 2010. Toxicity and cellular uptake of gold nanoparticles: What we have learned so far? *Journal of Nanoparticle Research,* 12**,** 2313-2333.

Alkilany, A. M., Nagaria, P. K., Hexel, C. R., Shaw, T. J., Murphy, C. J. and Wyatt, M. D. 2009. Cellular uptake and cytotoxicity of gold nanorods: Molecular origin of cytotoxicity and surface effects. *Small,* 5**,** 701-708.

Almeida, A. C. C. 2014. *Gold Nanoparticles for Plasmid Delivery.* M.Sc Biochemistry, Universidade Nova de Lisboa.

Alturkistani, H. A., Tashkandi, F. M. and Mohammedsaleh, Z. M. 2016. Histological stains: A literature review and case study. *Global Journal of Health Science,* 8**,** 72-79.

Amendola, V., Meneghetti, M., Stener, M., Guo, Y., Chen, S., Crespo, P., García, M. A., Hernando, A., Pengo, P. and Pasquato, L. 2014. Physico-chemical characteristics of gold nanoparticles. *In:* MIGUEL, V. & ÁNGELA, I. L.-L. (eds.) *Comprehensive Analytical Chemistry.* Elsevier.

American Cancer Society 2014. Colorectal cancer facts & figures. Atlanta: American Cancer Society.

American Cancer Society 2015. Global cancer facts and figures. 3rd ed. Atlanta: American Cancer Society.

American Cancer Society 2016. Cancer Facts & Figures 2016. Atlanta: American Cancer Society.

American Cancer Society 2017. Colorectal cancer facts & figures 2017-2019. Atlanta: American Cancer Society.

Andre, N. and Schmiegel, W. 2005. Chemoradiotherapy for colorectal cancer. *Gut,* 54**,** 1194–1202.

Arika, W., Nyamai, D., Musila, M., Ngugi, M. and Njagi, E. 2016. Hematological markers of in vivo toxicity. *Journal of Hematology and Thromboembolic Diseases,* 4**,** 236.

Arnida, Malugin, A. and Ghandehari, H. 2010. Cellular uptake and toxicity of gold nanoparticles in prostate cancer cells: A comparative study of rods and spheres. *Journal of Applied Toxicology,* 30**,** 212-217.

Arnold, M., Sierra, M. S., Laversanne, M., Soerjomataram, I., Jemal, A. and Bray, F. 2017. Global patterns and trends in colorectal cancer incidence and mortality. *Gut,* 66**,** 683-691.

Auluck, P. K., Chan, H. Y., Trojanowski, J. Q., Lee, V. M. and Bonini, N. M. 2002. Chaperone suppression of alpha-synuclein toxicity in a Drosophila model for Parkinson's disease. *Science,* 295**,** 865-868.

Ayala, A., Munoz, M. F. and Arguelles, S. 2014. Lipid peroxidation: Production, metabolism, and signaling mechanisms of malondialdehyde and 4-hydroxy-2-nonenal. *Oxidative Medicine and Cellular Longevity,* 2014**,** 360438.

Balasubramanian, S. K., Jittiwat, J., Manikandan, J., Ong, C. N., Yu, L. E. and Ong, W. Y. 2010. Biodistribution of gold nanoparticles and gene expression changes in the liver and spleen after intravenous administration in rats. *Biomaterials,* 31**,** 2034-2042.

Barbazuk, W. B., Korf, I., Kadavi, C., Heyen, J., Tate, S., Wun, E., Bedell, J. A., Mcpherson, J. D. and Johnson, S. L. 2000. The syntenic relationship of the zebrafish and human genomes. *Genome Research,* 10**,** 1351-1358.

Bartczak, D. and Kanaras, A. G. 2011. Preparation of peptide-functionalized gold nanoparticles using one pot EDC/sulfo-NHS coupling. *Langmuir,* 27**,** 10119-10123.

Bartczak, D., Muskens, O. L., Sanchez-Elsner, T., Kanaras, A. G. and Millar, T. M. 2013. Manipulation of in vitro angiogenesis using peptide-coated gold nanoparticles. *ACS nano,* 7**,** 5628-5636.

Bartels, H., Bohmer, M. and Heierli, C. 1972. Serum creatinine determination without protein precipitation. *Clinica Chimica Acta,* 37**,** 193-197.

Bashandy, M. M., Ahmed, A. R., El-Gaffary, M. and Abd El-Rahman, S. S. 2015. Gold nanoparticle: Synthesis, characterization, clinico-pathological, pathological, and bio-distribution studies in rabbits. *International Journal of Biological, Biomolecular, Agricultural, Food and Biotechnological Engineering,* 9**,** 1092-1099.

Basu, S., Ghosh, S. K., Kundu, S., Panigrahi, S., Praharaj, S., Pande, S., Jana, S. and Pal, T. 2007. Biomolecule induced nanoparticle aggregation: Effect of particle size on interparticle coupling. *Journal of Colloid and Interface Science,* 313**,** 724-734.

Belliraj, T. S., Nanda, A. and Ragunathan, R. 2015. In-vitro hepatoprotective activity of Moringa oleifera mediated synthesis of gold nanoparticles. *Journal of Chemical and Pharmaceutical Research,* 7**,** 781-788.

Bensebaa, F. 2012. *Nanoparticle Technologies: Chapter 1. Nanoparticle fundamentals,* Britain, Elsevier Inc. Chapters.

Berce, C., Lucan, C., Petrushev, B., Boca, S., Miclean, M., Sarpataki, O., Astilean, S., Buzoianu, A., Tomuleasa, C. and Bojan, A. 2016. In vivo assessment of bone marrow toxicity by gold nanoparticle-based bioconjugates in Crl:CD1(ICR) mice. *International Journal of Nanomedicine,* 11**,** 4261-4273.

Bernardi, M., Maggioli, C. and Zaccherini, G. 2012. Human albumin in the management of complications of liver cirrhosis. *Critical Care,* 16**,** 211.

Bhatia, S. 2016. Nanoparticles types, classification, characterization, fabrication methods and drug delivery applications. *Natural Polymer Drug Delivery Systems: Nanoparticles, Plants, and Algae.* Cham: Springer International Publishing.

Bhattacharjee, S. 2016. DLS and zeta potential – What they are and what they are not? *Journal of Controlled Release,* 235**,** 337-351.

Bloch, M., Kam, Y., Yavin, E., Moradov, D., Nissan, A., Ariel, I. and Rubinstein, A. 2012. The relative roles of charge and a recognition peptide in luminal targeting of colorectal cancer by fluorescent polyacrylamide. *European Journal of Pharmaceutical Sciences,* 47**,** 904-913.

Bogdanov, A. A., Gupta, S., Koshkina, N., Corr, S. J., Zhang, S., Curley, S. A. and Han, G. 2015. Gold nanoparticles stabilized with MPEG-grafted poly(l-lysine): In vitro and in vivo evaluation of a potential theranostic agent. *Bioconjugate Chemistry,* 26**,** 39-50.

Bohl Kullberg, E., Bergstrand, N., Carlsson, J., Edwards, K., Johnsson, M., Sjoberg, S. and Gedda, L. 2002. Development of EGF-conjugated liposomes for targeted delivery of boronated DNA-binding agents. *Bioconjugate Chemistry,* 13**,** 737-743.

Boisselier, E. and Astruc, D. 2009. Gold nanoparticles in nanomedicine: Preparations, imaging, diagnostics, therapies and toxicity. *Chemical Society Reviews,* 38**,** 1759-1782.

Borglin, J., Selegard, R., Aili, D. and Ericson, M. B. 2017. Peptide functionalized gold nanoparticles as a stimuli responsive contrast medium in multiphoton microscopy. *Nano Letters,* 17**,** 2102-2108.

Botha, T. L., James, T. E. and Wepener, V. 2015. Comparative aquatic toxicity of gold nanoparticles and ionic gold using a species sensitivity distribution approach. *Journal of Nanomaterials,* 2015**,** 16.

Boyles, M. S. P., Kristl, T., Andosch, A., Zimmermann, M., Tran, N., Casals, E., Himly, M., Puntes, V., Huber, C. G., Lütz-Meindl, U. and Duschl, A. 2015. Chitosan functionalisation of gold nanoparticles encourages particle uptake and induces cytotoxicity and pro-inflammatory conditions in phagocytic cells, as well as enhancing particle interactions with serum components. *Journal of Nanobiotechnology,* 13**,** 84.

Boyoglu, C., He, Q., Willing, G., Boyoglu-Barnum, S., Dennis, V. A., Pillai, S. and Singh, S. R. 2013. Microscopic studies of various sizes of gold nanoparticles and their cellular localizations. *ISRN Nanotechnology,* 2013**,** 13.

Bozich, J. S., Lohse, S. E., Torelli, M. D., Murphy, C. J., Hamers, R. J. and Klaper, R. D. 2014. Surface chemistry, charge and ligand type impact the toxicity of gold nanoparticles to Daphnia magna. *Environmental Science-Nano,* 1**,** 260-270.

Braet, F. and Wisse, E. 2002. Structural and functional aspects of liver sinusoidal endothelial cell fenestrae: A review. *Comparative Hepatology,* 1**,** 1-17.

Brandenberger, C., Muhlfeld, C., Ali, Z., Lenz, A. G., Schmid, O., Parak, W. J., Gehr, P. and Rothen-Rutishauser, B. 2010. Quantitative evaluation of cellular uptake and trafficking of plain and polyethylene glycol-coated gold nanoparticles. *Small,* 6**,** 1669-1678.

Brennan, J. L., Hatzakis, N. S., Tshikhudo, T. R., Dirvianskyte, N., Razumas, V., Patkar, S., Vind, J., Svendsen, A., Nolte, R. J., Rowan, A. E. and Brust, M. 2006. Bionanoconjugation via click chemistry: The creation of functional hybrids of lipases and gold nanoparticles. *Bioconjugate Chemistry,* 17**,** 1373-1375.

Brown, S. D., Nativo, P., Smith, J.-A., Stirling, D., Edwards, P. R., Venugopal, B., Flint, D. J., Plumb, J. A., Graham, D. and Wheate, N. J. 2010. Gold nanoparticles for the improved anticancer drug delivery of the active component of oxaliplatin. *Journal of the American Chemical Society,* 132**,** 4678-4684.

Brust, M., Walker, M., Bethell, D., Schiffrin, D. J. and Whyman, R. 1994. Synthesis of thiol-derivatised gold nanoparticles in a two-phase Liquid-Liquid system. *Journal of the Chemical Society, Chemical Communications,* 0**,** 801-802.

Buzea, C., Pacheco, I. I. and Robbie, K. 2007. Nanomaterials and nanoparticles: Sources and toxicity. *Biointerphases,* 2**,** MR17-MR71.

Cairncross, L. C. 2015. *An investigation into the localisation of peptide-gold nanoparticles in an in vitro and in vivo colorectal cancer model.* M.Sc, Nelson Mandela Metropolitan University.

Capehart, S. L., Elsohly, A. M., Obermeyer, A. C. and Francis, M. B. 2014. Bioconjugation of gold nanoparticles through the oxidative coupling of ortho-aminophenols and anilines. *Bioconjugate Chemistry,* 25**,** 1888-1892.

Carbo-Argibay, E. and Rodriguez-Gonzalez, B. 2016. Controlled growth of colloidal gold nanoparticles: Single-crystalline versus multiply-twinned particles. *Israel Journal of Chemistry,* 56**,** 214-226.

Carton, J., Daly, R. and Ramani, P. 2007. *Clinical Pathology*, Oxford University Press.

Casarett, L. J. and Klaassen, C. D. 2008. *Casarett and Doull's Toxicology: The Basic Science of Poisons,* United States, New York: McGraw-Hill Medical.

Casarett, L. J., Klaassen, C. D., Amdur, M. O. and Doull, J. 1996. *Casarett and Doull's toxicology: The basic science of poisons,* New York, McGraw-Hill, Health Professions Division.

Cesta, M. F. 2006. Normal structure, function, and histology of the spleen. *Toxicologic Pathology,* 34**,** 455-465.

Chan, J. K. C. 2014. The wonderful colors of the hematoxylin–eosin stain in diagnostic surgical pathology. *International Journal of Surgical Pathology,* 22**,** 12-32.

Chanda, N., Kattumuri, V., Shukla, R., Zambre, A., Katti, K., Upendran, A., Kulkarni, R. R., Kan, P., Fent, G. M., Casteel, S. W., Smith, C. J., Boote, E., Robertson, J. D., Cutler, C., Lever, J. R., Katti, K. V. and Kannan, R. 2010. Bombesin functionalized gold nanoparticles show in vitro and in vivo cancer receptor specificity. *Proceedings of the National Academy of Sciences of the United States of America,* 107**,** 8760-8765.

Chatterjea, M. and Shinde, R. 2011. *Textbook of medical biochemistry,* New Delhi, India, JP Medical Ltd.

Chen, H.-J. and Wen, D. 2011. Ultrasonic-aided fabrication of gold nanofluids. *Nanoscale Research Letters,* 6**,** 198.

Chen, H., Dorrigan, A., Saad, S., Hare, D. J., Cortie, M. B. and Valenzuela, S. M. 2013a. In vivo study of spherical gold nanoparticles: Inflammatory effects and distribution in mice. *PLoS One,* 8**,** e58208.

Chen, J., Deng, L., Dreymüller, D., Jiang, X., Long, J., Duan, Y., Wang, Y., Luo, M., Lin, F., Mao, L., Müller, B., Koller, G. and Bartsch, J. W. 2016. A novel peptide ADAM8 inhibitor attenuates

bronchial hyperresponsiveness and Th2 cytokine mediated inflammation of murine asthmatic models. *Scientific Reports,* 6**,** 30451.

Chen, J., Wang, H., Long, W., Shen, X., Wu, D., Song, S.-S., Sun, Y.-M., Liu, P.-X., Fan, S., Fan, F. and Zhang, X.-D. 2013b. Sex differences in the toxicity of polyethylene glycol-coated gold nanoparticles in mice. *International Journal of Nanomedicine,* 8**,** 2409-2419.

Chen, W.-H., Chen, J.-X., Cheng, H., Chen, C.-S., Yang, J., Xu, X.-D., Wang, Y., Zhuo, R.-X. and Zhang, X.-Z. 2013c. A new anti-cancer strategy of damaging mitochondria by pro-apoptotic peptide functionalized gold nanoparticles. *Chemical Communications,* 49**,** 6403-6405.

Chen, Y. S., Hung, Y. C., Liau, I. and Huang, G. S. 2009. Assessment of the in vivo toxicity of gold nanoparticles. *Nanoscale Research Letters,* 4**,** 858-864.

Chinedu, E., Arome, D. and Ameh, F. S. 2013. A new method for determining acute toxicity in animal models. *Toxicology International,* 20**,** 224-226.

Chithrani, B. D., Ghazani, A. A. and Chan, W. C. W. 2006. Determining the size and shape dependence of gold nanoparticle uptake into mammalian cells. *Nano Letters,* 6**,** 662-668.

Cho, W.-S., Cho, M., Jeong, J., Choi, M., Cho, H.-Y., Han, B. S., Kim, S. H., Kim, H. O., Lim, Y. T., Chung, B. H. and Jeong, J. 2009a. Acute toxicity and pharmacokinetics of 13 nm-sized PEG-coated gold nanoparticles. *Toxicology and Applied Pharmacology,* 236**,** 16-24.

Cho, W.-S., Cho, M., Jeong, J., Choi, M., Han, B. S., Shin, H.-S., Hong, J., Chung, B. H., Jeong, J. and Cho, M.-H. 2010. Size-dependent tissue kinetics of PEG-coated gold nanoparticles. *Toxicology and Applied Pharmacology,* 245**,** 116-123.

Cho, W.-S., Kim, S., Han, B. S., Son, W. C. and Jeong, J. 2009b. Comparison of gene expression profiles in mice liver following intravenous injection of 4 and 100 nm-sized PEG-coated gold nanoparticles. *Toxicology Letters,* 191**,** 96-102.

Choi, H. S., Liu, W., Misra, P., Tanaka, E., Zimmer, J. P., Itty Ipe, B., Bawendi, M. G. and Frangioni, J. V. 2007. Renal clearance of quantum dots. *Nature Biotechnology,* 25**,** 1165-1170.

Clichici, S. and Filip, A. 2015. In vivo assessment of nanomaterials toxicity. *In:* LARRAMENDY, P. M. (ed.) *Nanomaterials - Toxicity and risk assessment.* InTech.

Comstock, S. S., Xu, D., Hortos, K., Kovan, B., Mccaskey, S., Pathak, D. R. and Fenton, J. I. 2014. Association of insulin-related serum factors with colorectal polyp number and type in adult males. *Cancer Epidemiology and Prevention Biomarkers,* 23**,** 1843-1851.

Conde, J., Dias, J. T., Grazú, V., Moros, M., Baptista, P. V. and De La Fuente, J. M. 2014. Revisiting 30 years of biofunctionalization and surface chemistry of inorganic nanoparticles for nanomedicine. *Frontiers in Chemistry,* 2**,** 48.

Coradeghini, R., Gioria, S., García, C. P., Nativo, P., Franchini, F., Gilliland, D., Ponti, J. and Rossi, F. 2013. Size-dependent toxicity and cell interaction mechanisms of gold nanoparticles on mouse fibroblasts. *Toxicology Letters,* 217**,** 205-216.

Correard, F., Maximova, K., Estève, M.-A., Villard, C., Roy, M., Al-Kattan, A., Sentis, M., Gingras, M., Kabashin, A. V. and Braguer, D. 2014. Gold nanoparticles prepared by laser ablation in aqueous biocompatible solutions: Assessment of safety and biological identity for nanomedicine applications. *International Journal of Nanomedicine,* 9**,** 5415-5430.

Crawford, A. D., Esguerra, C. V. and De Witte, P. a. M. 2008. Fishing for drugs from nature: Zebrafish as a technology platform for natural product discovery. *Planta Medica,* 74**,** 624-632.

Cuperus, F. J. C., Drenth, J. P. H. and Tjwa, E. T. 2017. Mistakes in liver function test abnormalities and how to avoid them. *United European Gastroenterology Education,* 17**,** 1–5.

D'agata, R., Palladino, P. and Spoto, G. 2017. Streptavidin-coated gold nanoparticles: Critical role of oligonucleotides on stability and fractal aggregation. *Beilstein Journal of Nanotechnology,* 8**,** 1-11.

Daniel, M. C. and Astruc, D. 2004. Gold nanoparticles: Assembly, supramolecular chemistry, quantum-size-related properties, and applications toward biology, catalysis, and nanotechnology. *Chemical Reviews,* 104**,** 293-346.

Dauthal, P. and Mukhopadhyay, M. 2016. Noble metal nanoparticles: Plant-mediated synthesis, mechanistic aspects of synthesis, and applications. *Industrial and Engineering Chemistry Research,* 55**,** 9557-9577.

De Jong, M. C., Pulitano, C., Ribero, D., Strub, J., Mentha, G., Schulick, R. D., Choti, M. A., Aldrighetti, L., Capussotti, L. and Pawlik, T. M. 2009. Rates and patterns of recurrence following curative intent surgery for colorectal liver metastasis: An international multi-institutional analysis of 1669 patients. *Annals of Surgery,* 250**,** 440-448.

De Jong, W. H., Hagens, W. I., Krystek, P., Burger, M. C., Sips, A. J. and Geertsma, R. E. 2008. Particle size-dependent organ distribution of gold nanoparticles after intravenous administration. *Biomaterials,* 29**,** 1912-1919.

De La Fuente, J. M. and Berry, C. C. 2005. Tat peptide as an efficient molecule to translocate gold nanoparticles into the cell nucleus. *Bioconjugate Chemistry,* 16**,** 1176-1180.

De Sa, D. D. and Chen, H. H. 2008. The role of natriuretic peptides in heart failure. *Current Cardiology Reports,* 10**,** 182-189.

Dedeh, A., Ciutat, A., Treguer-Delapierre, M. and Bourdineaud, J.-P. 2015. Impact of gold nanoparticles on zebrafish exposed to a spiked sediment. *Nanotoxicology,* 9**,** 71-80.

Deng, Z. J., Liang, M., Monteiro, M., Toth, I. and Minchin, R. F. 2011. Nanoparticle-induced unfolding of fibrinogen promotes Mac-1 receptor activation and inflammation. *Nature Nanotechnology,* 6**,** 39-44.

Dhawan, A. and Sharma, V. 2010. Toxicity assessment of nanomaterials: Methods and challenges. *Analytical and Bioanalytical Chemistry,* 398**,** 589-605.

Dobrowolska, P., Krajewska, A., Gajda-Rączka, M., Bartosewicz, B., Nyga, P. and Jankiewicz, B. 2015. Application of Turkevich method for gold nanoparticles synthesis to fabrication of SiO2@Au and TiO2@Au core-shell nanostructures. *Materials,* 8**,** 2849-2862.

Dollah, M. A., Parhizkar, S., Latiff, L. A. and Bin Hassan, M. H. 2013. Toxicity effect of Nigella sativa on the liver function of rats. *Advanced Pharmaceutical Bulletin,* 3**,** 97-102.

Doudi, M. and Setorki, M. 2014. The effect of gold nanoparticle on renal function in rats. *Nanomedicine Journal,* 1**,** 171-179.

Doumas, B. T., Watson, W. A. and Biggs, H. G. 1971. Albumin standards and the measurement of serum albumin with bromcresol green. *Clinica Chimica Acta,* 31**,** 87-96.

Dreaden, E. C., Alkilany, A. M., Huang, X., Murphy, C. J. and El-Sayed, M. A. 2012a. The golden age: Gold nanoparticles for biomedicine. *Chemical Society Reviews,* 41**,** 2740-2779.

Dreaden, E. C., Austin, L. A., Mackey, M. A. and El-Sayed, M. A. 2012b. Size matters: Gold nanoparticles in targeted cancer drug delivery. *Therapeutic delivery,* 3**,** 457-478.

Duque, M. A., Tiozon, R. N. and Nueva Espana, R. C. 2016. Chitosan from Portunus pelagicus in the synthesis of reduced gold nanoparticle as potential carrier for the delivery of erythropoietin. *BioRxiv*.

Dykman, L. A. and Khlebtsov, N. G. 2011. Gold nanoparticles in biology and medicine: Recent advances and prospects. *Acta Naturae,* 3**,** 34-55.

Edwards, B. K., Ward, E., Kohler, B. A., Eheman, C., Zauber, A. G., Anderson, R. N., Jemal, A., Schymura, M. J., Lansdorp-Vogelaar, I., Seeff, L. C., Van Ballegooijen, M., Goede, S. L. and Ries, L. A. 2010. Annual report to the nation on the status of cancer, 1975-2006, featuring colorectal cancer trends and impact of interventions (risk factors, screening, and treatment) to reduce future rates. *Cancer,* 116**,** 544-573.

Eissa, S., Shawky, S. M., Matboli, M., Mohamed, S. and Azzazy, H. M. E. 2014. Direct detection of unamplified hepatoma upregulated protein RNA in urine using gold nanoparticles for bladder cancer diagnosis. *Clinical Biochemistry,* 47**,** 104-110.

El-Nahas, A. E., Allam, A. N., Abdelmonsif, D. A. and El-Kamel, A. H. 2017. Silymarin-loaded eudragit nanoparticles: Formulation, characterization, and hepatoprotective and toxicity evaluation. *Journal of the American Association of Pharmaceutical Scientists,* 18**,** 3076-3086.

Elci, S. G., Jiang, Y., Yan, B., Kim, S. T., Saha, K., Moyano, D. F., Yesilbag Tonga, G., Jackson, L. C., Rotello, V. M. and Vachet, R. W. 2016. Surface charge controls the suborgan biodistributions of gold nanoparticles. *ACS Nano,* 10**,** 5536-5542.

Elia, P., Zach, R., Hazan, S., Kolusheva, S., Porat, Z. E. and Zeiri, Y. 2014. Green synthesis of gold nanoparticles using plant extracts as reducing agents. *International Journal of Nanomedicine,* 9**,** 4007-4021.

Elmore, S. A. 2012. Enhanced histopathology of the immune system: A review and update. *Toxicologic Pathology,* 40**,** 148-56.

Elsayed, K. A., Imam, H., Ahmed, M. A. and Ramadan, R. 2013. Effect of focusing conditions and laser parameters on the fabrication of gold nanoparticles via laser ablation in liquid. *Optics and Laser Technology,* 45**,** 495-502.

Erben, U., Loddenkemper, C., Doerfel, K., Spieckermann, S., Haller, D., Heimesaat, M. M., Zeitz, M., Siegmund, B. and Kühl, A. A. 2014. A guide to histomorphological evaluation of intestinal inflammation in mouse models. *International Journal of Clinical and Experimental Pathology,* 7**,** 4557-4576.

Escudero-Francos, M. A., Cepas, V., González-Menéndez, P., Badía-Laíño, R., Díaz-García, M. E., Sainz, R. M., Mayo, J. C. and Hevia, D. 2017. Cellular uptake and tissue biodistribution of functionalized gold nanoparticles and nanoclusters. *Journal of Biomedical Nanotechnology,* 13**,** 167-179.

Fadeel, B. and Garcia-Bennett, A. E. 2010. Better safe than sorry: Understanding the toxicological properties of inorganic nanoparticles manufactured for biomedical applications. *Advanced Drug Delivery Reviews,* 62**,** 362-374.

FDA 1996. United States Food and Drug Administration guidance for industry on single dose acute toxicity testing for pharmaceuticals. 61**,** 43934-43935.

Ferchichi, S., Trabelsi, H., Azzouz, I., Hanini, A., Rejeb, A., Tebourbi, O., Sakly, M. and Abdelmelek, H. 2016. Evaluation of oxidative response and tissular damage in rat lungs exposed to silica-coated gold nanoparticles under static magnetic fields. *International Journal of Nanomedicine,* 11**,** 2711-2719.

Ferreira, G. K., Cardoso, E., Vuolo, F. S., Michels, M., Zanoni, E. T., Carvalho-Silva, M., Gomes, L. M., Dal-Pizzol, F., Rezin, G. T., Streck, E. L. and Da Silva Paula, M. M. 2015. Gold nanoparticles alter parameters of oxidative stress and energy metabolism in organs of adult rats. *Biochemistry and Cell Biology,* 93**,** 548-557.

Fosgerau, K. and Hoffmann, T. 2015. Peptide therapeutics: Current status and future directions. *Drug Discovery Today,* 20**,** 122-128.

Fraga, S., Brandão, A., Soares, M. E., Morais, T., Duarte, J. A., Pereira, L., Soares, L., Neves, C., Pereira, E., Bastos, M. D. L. and Carmo, H. 2014. Short- and long-term distribution and toxicity of gold nanoparticles in the rat after a single-dose intravenous administration. *Nanomedicine: Nanotechnology, Biology and Medicine,* 10**,** 1757-1766.

Fraga, S., Faria, H., Soares, M. E., Duarte, J. A., Soares, L., Pereira, E., Costa-Pereira, C., Teixeira, J. P., De Lourdes Bastos, M. and Carmo, H. 2013. Influence of the surface coating on the cytotoxicity, genotoxicity and uptake of gold nanoparticles in human HepG2 cells. *Journal of Applied Toxicology,* 33**,** 1111-1119.

Fratoddi, I., Venditti, I., Cametti, C. and Russo, M. V. 2015. How toxic are gold nanoparticles? The state-of-the-art. *Nano Research,* 8**,** 1771-1799.

Freese, C., Uboldi, C., Gibson, M. I., Unger, R. E., Weksler, B. B., Romero, I. A., Couraud, P. O. and Kirkpatrick, C. J. 2012. Uptake and cytotoxicity of citrate-coated gold nanospheres: Comparative studies on human endothelial and epithelial cells. *Particle and Fibre Toxicology,* 9**,** 23.

Frens, G. 1973. Controlled nucleation for the regulation of the particle size in monodisperse gold suspensions. *Nature Physical Science,* 241**,** 20-22.

Frohlich, E. 2016. Action of nanoparticles on platelet activation and plasmatic coagulation. *Current Medicinal Chemistry,* 23**,** 408-430.

Fu, P. P., Xia, Q., Hwang, H.-M., Ray, P. C. and Yu, H. 2014. Mechanisms of nanotoxicity: Generation of reactive oxygen species. *Journal of Food and Drug Analysis,* 22**,** 64-75.

Gao, N., Sun, H., Dong, K., Ren, J. and Qu, X. 2015. Gold-nanoparticle-based multifunctional amyloid-β inhibitor against Alzheimer's disease. *Chemistry – A European Journal,* 21**,** 829-835.

Gasparovic, A. C., Jaganjac, M., Mihaljevic, B., Sunjic, S. B. and Zarkovic, N. 2013. Assays for the measurement of lipid peroxidation. *In:* GALLUZZI, L., VITALE, I., KEPP, O. & KROEMER, G. (eds.) *Cell Senescence: Methods and Protocols.* Totowa, NJ: Humana Press.

Ghahnavieh, M. Z., Ajdary, M., Ghahnavieh, M. Z. and Naghsh, N. 2014. Effects of intraperitoneal injection of gold nanoparticles in male mice. *Nanomedicine Journal,* 1**,** 121-127.

Ghodake, G. and Lee, D. S. 2011. Biological synthesis of gold nanoparticles using the aqueous extract of the brown algae Laminaria japonica. *Journal of Nanoelectronics and Optoelectronics,* 6**,** 268-271.

Ghosh, S., Patil, S., Ahire, M., Kitture, R., Gurav, D. D., Jabgunde, A. M., Kale, S., Pardesi, K., Shinde, V., Bellare, J., Dhavale, D. D. and Chopade, B. A. 2012. Gnidia glauca flower extract mediated synthesis of gold nanoparticles and evaluation of its chemocatalytic potential. *Journal of Nanobiotechnology,* 10**,** 1-9.

Glazer, E. S., Zhu, C., Hamir, A. N., Borne, A., Thompson, C. S. and Curley, S. A. 2011. Biodistribution and acute toxicity of naked gold nanoparticles in a rabbit hepatic tumor model. *Nanotoxicology,* 5**,** 459-468.

Goede, S. L., Rabeneck, L., Van Ballegooijen, M., Zauber, A. G., Paszat, L. F., Hoch, J. S., Yong, J. H. E., Kroep, S., Tinmouth, J. and Lansdorp-Vogelaar, I. 2017. Harms, benefits and costs of fecal immunochemical testing versus guaiac fecal occult blood testing for colorectal cancer screening. *PLoS One,* 12**,** e0172864.

Goodman, C. M., Mccusker, C. D., Yilmaz, T. and Rotello, V. M. 2004. Toxicity of gold nanoparticles functionalized with cationic and anionic side chains. *Bioconjugate Chemistry,* 15**,** 897-900.

Graham, A., Adeloye, D., Grant, L., Theodoratou, E. and Campbell, H. 2012. Estimating the incidence of colorectal cancer in Sub–Saharan Africa: A systematic analysis. *Journal of Global Health,* 2**,** 020404.

Greaves, P. 2011. *Histopathology of preclinical toxicity studies: Interpretation and relevance in drug safety evaluation,* Amsterdam, Netherlands, Academic Press.

Gu, Y.-J., Cheng, J., Lin, C.-C., Lam, Y. W., Cheng, S. H. and Wong, W.-T. 2009. Nuclear penetration of surface functionalized gold nanoparticles. *Toxicology and Applied Pharmacology,* 237**,** 196-204.

Gunduz, N., Ceylan, H., Guler, M. O. and Tekinay, A. B. 2017. Intracellular accumulation of gold nanoparticles leads to inhibition of macropinocytosis to reduce the endoplasmic reticulum stress. *Scientific Reports,* 7**,** 40493.

Häfner, M. F. and Debus, J. 2016. Radiotherapy for colorectal cancer: Current standards and future perspectives. *Visceral Medicine,* 32**,** 172-177.

Hagan, S., Orr, M. C. M. and Doyle, B. 2013. Targeted therapies in colorectal cancer—an integrative view by PPPM. *European Association for Predictive Preventive and Personalized Medicine Journal,* 4**,** 3.

Haggag, Y. A., Matchett, K. B., Dakir, E.-H., Buchanan, P., Osman, M. A., Elgizawy, S. A., El-Tanani, M., Faheem, A. M. and Mccarron, P. A. 2017. Nano-encapsulation of a novel anti-Ran-GTPase peptide for blockade of regulator of chromosome condensation 1 (RCC1) function in MDA-MB-231 breast cancer cells. *International Journal of Pharmaceutics,* 521**,** 40-53.

Hainfeld, J. F., Slatkin, D. N., Focella, T. M. and Smilowitz, H. M. 2006. Gold nanoparticles: A new X-ray contrast agent. *British Journal of Radiology,* 79**,** 248-453.

Han, Z., Zhou, Z., Shi, X., Wang, J., Wu, X., Sun, D., Chen, Y., Zhu, H., Magi-Galluzzi, C. and Lu, Z.-R. 2015. EDB fibronectin specific peptide for prostate cancer targeting. *Bioconjugate Chemistry,* 26**,** 830-838.

Hanafy, A., Aldawsari, H. M., Badr, J. M., Ibrahim, A. K. and Abdel-Hady, S. E.-S. 2016. Evaluation of hepatoprotective activity of Adansonia digitata extract on acetaminophen-induced hepatotoxicity in rats. *Evidence-Based Complementary and Alternative Medicine,* 2016**,** 4579149.

Harper, B., Sinche, F., Ho Wu, R., Gowrishankar, M., Marquart, G., Mackiewicz, M. and Harper, S. L. 2014. The impact of surface ligands and synthesis method on the toxicity of glutathione-coated gold nanoparticles. *Nanomaterials,* 4**,** 355-371.

Heinz, G. H., Hoffman, D. J., Klimstra, J. D., Stebbins, K. R., Kondrad, S. L. and Erwin, C. A. 2009. Species differences in the sensitivity of avian embryos to methylmercury. *Archives of Environmental Contamination and Toxicology,* 56**,** 129-138.

Herbst, M. C. 2017. *Fact sheet on colorectal cancer. National cancer registry 2012* [Online]. Cancer Association of South Africa (CANSA).

Higgins, C. 2016. *Urea and creatinine concentration, the urea: creatinine ratio* [Online]. Denmark: Radiometer Medical ApS.

Horikoshi, S. and Serpone, N. 2013. Introduction to Nanoparticles. *Microwaves in Nanoparticle Synthesis.* Wiley-VCH Verlag GmbH & Co. KGaA.

Hornos Carneiro, M. F. and Barbosa, F. 2016. Gold nanoparticles: A critical review of therapeutic applications and toxicological aspects. *Journal of Toxicology and Environmental Health, Part B,* 19**,** 129-148.

Hou, K. K., Pan, H., Ratner, L., Schlesinger, P. H. and Wickline, S. A. 2013. Mechanisms of nanoparticle-mediated siRNA transfection by melittin-derived peptides. *ACS Nano,* 7**,** 8605-8615.

Hung, M. W., Zhang, Z. J., Li, S., Lei, B., Yuan, S., Cui, G. Z., Man Hoi, P., Chan, K. and Lee, S. M. 2012. From omics to drug metabolism and high content screen of natural product in zebrafish: a new model for discovery of neuroactive compound. *Evidence-Based Complementary and Alternative Medicine,* 2012**,** 605303.

Hussain, M. M., Samir, T. M. and Azzazy, H. M. E. 2013. Unmodified gold nanoparticles for direct and rapid detection of Mycobacterium tuberculosis complex. *Clinical Biochemistry,* 46**,** 633-637.

Hussein, R. H. and Khalifa, F. K. 2014. The protective role of ellagitannins flavonoids pretreatment against N-nitrosodiethylamine induced-hepatocellular carcinoma. *Saudi Journal of Biological Sciences,* 21**,** 589-596.

Hwang, J. H., Kim, S. J., Kim, Y.-H., Noh, J.-R., Gang, G.-T., Chung, B. H., Song, N. W. and Lee, C.-H. 2012. Susceptibility to gold nanoparticle-induced hepatotoxicity is enhanced in a mouse model of nonalcoholic steatohepatitis. *Toxicology,* 294**,** 27-35.

Irabor, D. 2017. Emergence of colorectal cancer in West Africa : accepting the inevitable. *South African Gastroenterology Review,* 15**,** 11-16.

Ivanov, S., Zhuravsky, S., Yukina, G., Tomson, V., Korolev, D. and Galagudza, M. 2012. In vivo toxicity of intravenously administered silica and silicon nanoparticles. *Materials,* 5**,** 1873-1889.

Iversen, T.-G., Skotland, T. and Sandvig, K. 2011. Endocytosis and intracellular transport of nanoparticles: present knowledge and need for future studies. *Nano Today,* 6**,** 176-185.

Jazayeri, M. H., Amani, H., Pourfatollah, A. A., Pazoki-Toroudi, H. and Sedighimoghaddam, B. 2016. Various methods of gold nanoparticles (GNPs) conjugation to antibodies. *Sensing and Bio-Sensing Research,* 9**,** 17-22.

Jendrassik, L. and Gróf, P. 1938. Simplified photometric methods for the determination of blood bilirubin. *Biochemical Journal,* 297**,** 82-89.

Jia, Y. P., Ma, B. Y., Wei, X. W. and Qian, Z. Y. 2017. The in vitro and in vivo toxicity of gold nanoparticles. *Chinese Chemical Letters,* 28**,** 691-702.

Jiang, W., Hibbert, D. B., Moran, G., Herrmann, J., Jamting, A. K. and Coleman, V. A. 2013. Characterisation of gold agglomerates: Size distribution, shape and optical properties. *RSC Advances,* 3**,** 7367-7374.

Jin, E., Zhang, B., Sun, X., Zhou, Z., Ma, X., Sun, Q., Tang, J., Shen, Y., Van Kirk, E. and Murdoch, W. J. 2013. Acid-active cell-penetrating peptides for in vivo tumor-targeted drug delivery. *Journal of the American Chemical Society,* 135**,** 933-940.

Jo, M. R., Bae, S. H., Go, M. R., Kim, H. J., Hwang, Y. G. and Choi, S. J. 2015. Toxicity and biokinetics of colloidal gold nanoparticles. *Nanomaterials,* 5**,** 835-850.

Joubert, Y., Pan, J.-F., Buffet, P.-E., Pilet, P., Gilliland, D., Valsami-Jones, E., Mouneyrac, C. and Amiard-Triquet, C. 2013. Subcellular localization of gold nanoparticles in the estuarine bivalve Scrobicularia plana after exposure through the water. *Gold Bulletin,* 46**,** 47-56.

Jung, T., Kamm, W., Breitenbach, A., Kaiserling, E., Xiao, J. X. and Kissel, T. 2000. Biodegradable nanoparticles for oral delivery of peptides: Is there a role for polymers to affect mucosal uptake? *European Journal of Pharmaceutics and Biopharmaceutics,* 50**,** 147-160.

Jyoti, K., Baunthiyal, M. and Singh, A. 2016. Characterization of silver nanoparticles synthesized using Urtica dioica Linn. leaves and their synergistic effects with antibiotics. *Journal of Radiation Research and Applied Sciences,* 9**,** 217-227.

Kalia, J. and Raines, R. T. 2010. Advances in bioconjugation. *Current Organic Chemistry,* 14**,** 138-147.

Kalishwaralal, K., Deepak, V., Ram Kumar Pandian, S., Kottaisamy, M., Barathmanikanth, S., Kartikeyan, B. and Gurunathan, S. 2010. Biosynthesis of silver and gold nanoparticles using Brevibacterium casei. *Colloids and Surfaces B: Biointerfaces,* 77**,** 257-262.

Kalmodia, S., Vandhana, S., Tejaswini Rama, B. R., Jayashree, B., Sreenivasan Seethalakshmi, T., Umashankar, V., Yang, W., Barrow, C. J., Krishnakumar, S. and Elchuri, S. V. 2016. Bio-conjugation of antioxidant peptide on surface-modified gold nanoparticles: a novel approach to enhance the radical scavenging property in cancer cell. *Cancer Nanotechnology,* 7**,** 1.

Kalyuzhny, A. E. 2016. *Immunohistochemistry: Essential elements and beyond. Techniques in life science and biomedicine for the non-expert,* Switzerland, Springer Nature.

Karthick, V., Kumar, V. G., Dhas, T. S., Singaravelu, G., Sadiq, A. M. and Govindaraju, K. 2014. Effect of biologically synthesized gold nanoparticles on alloxan-induced diabetic rats—An in vivo approach. *Colloids and Surfaces B: Biointerfaces,* 122**,** 505-511.

Kazantsev, A., Walker, H. A., Slepko, N., Bear, J. E., Preisinger, E., Steffan, J. S., Zhu, Y. Z., Gertler, F. B., Housman, D. E., Marsh, J. L. and Thompson, L. M. 2002. A bivalent Huntingtin binding peptide suppresses polyglutamine aggregation and pathogenesis in Drosophila. *Nature Genetics,* 30**,** 367-376.

Kettiger, H., Schipanski, A., Wick, P. and Huwyler, J. 2013. Engineered nanomaterial uptake and tissue distribution: From cell to organism. *International Journal of Nanomedicine,* 8**,** 3255-3269.

Khan, A. K., Rashid, R., Murtaza, G. and Zahra, A. 2014. Gold nanoparticles: Synthesis and applications in drug delivery. *Tropical Journal of Pharmaceutical Research,* 13**,** 1169-1177.

Khan, H. A., Abdelhalim, M. a. K., Al-Ayed, M. S. and Alhomida, A. S. 2012. Effect of gold nanoparticles on glutathione and malondialdehyde levels in liver, lung and heart of rats. *Saudi Journal of Biological Sciences,* 19**,** 461-464.

Khan, H. A., Abdelhalim, M. a. K., Alhomida, A. S. and Al-Ayed, M. S. 2013. Effects of naked gold nanoparticles on proinflammatory cytokines mRNA expression in rat liver and kidney. *BioMed Research International,* 2013**,** 590730.

Khanna, P., Ong, C., Bay, B. H. and Baeg, G. H. 2015. Nanotoxicity: An interplay of oxidative stress, inflammation and cell death. *Nanomaterials (Basel),* 5**,** 1163-1180.

Kim, H.-J., Yu, M.-H., Kim, H., Byun, J. and Lee, C. 2008. Noninvasive molecular biomarkers for the detection of colorectal cancer. *BMB Reports,* 41**,** 685-692.

Kim, J. H., Kim, J. H., Kim, K.-W., Kim, M. H. and Yu, Y. S. 2009. Intravenously administered gold nanoparticles pass through the blood–retinal barrier depending on the particle size, and induce no retinal toxicity. *Nanotechnology,* 20**,** 505101.

Kim, K.-T., Zaikova, T., Hutchison, J. E. and Tanguay, R. L. 2013. Gold nanoparticles disrupt zebrafish eye development and pigmentation. *Toxicological Sciences,* 133**,** 275-288.

Kim, S.-W., Roh, J. and Park, C.-S. 2016. Immunohistochemistry for pathologists: Protocols, pitfalls, and tips. *Journal of Pathology and Translational Medicine,* 50**,** 411-418.

Kobayashi, H. and Sugihara, K. 2012. Surveillance and Characteristics of Recurrence After Curative Resection for Colorectal Cancer. *In:* HO, Y.-H. (ed.). INTECH Open Access Publisher.

Kong, F. Y., Zhang, J. W., Li, R. F., Wang, Z. X., Wang, W. J. and Wang, W. 2017. Unique Roles of gold nanoparticles in drug delivery, targeting and imaging applications. *Molecules,* 22.

Koniev, O. and Wagner, A. 2015. Developments and recent advancements in the field of endogenous amino acid selective bond forming reactions for bioconjugation. *Chemical Society Reviews,* 44**,** 5495-5551.

Kroll, A., Pillukat, M. H., Hahn, D. and Schnekenburger, J. 2009. Current in vitro methods in nanoparticle risk assessment: Limitations and challenges. *European Journal of Pharmaceutics and Biopharmaceutics,* 72**,** 370-377.

Kulkarni, S. A. and Feng, S. S. 2013. Effects of particle size and surface modification on cellular uptake and biodistribution of polymeric nanoparticles for drug delivery. *Pharmaceutical research,* 30**,** 2512-22.

Kumar, A., Ma, H., Zhang, X., Huang, K., Jin, S., Liu, J., Wei, T., Cao, W., Zou, G. and Liang, X. J. 2012. Gold nanoparticles functionalized with therapeutic and targeted peptides for cancer treatment. *Biomaterials,* 33**,** 1180-1189.

Kunjiappan, S., Bhattacharjee, C. and Chowdhury, R. 2015. Hepatoprotective and antioxidant effects of Azolla microphylla based gold nanoparticles against acetaminophen induced toxicity in a fresh water common carp fish (Cyprinus carpio L.). *Nanomedicine Journal,* 2**,** 88-110.

Kwo, P. Y., Cohen, S. M. and Lim, J. K. 2017. ACG clinical guideline: Evaluation of abnormal liver chemistries. *The American Journal of Gastroenterology,* 112**,** 18-35.

Lam, S. H., Wu, Y. L., Vinsensius, B. V., Lance, D. M., Jan, S., Tong, Y., Zhan, H., Kunde, R. G., Lee, S., Sinnakarupan, M., Karuturi, R. K. M., Donald, R., Buhler , Liu, E. T. and Gong, Z. 2006. Conservation of gene expression signatures between zebrafish and human liver tumors and tumor progression. *Nature Biotechnology,* 24**,** 73-75.

Lan, M.-Y., Hsu, Y.-B., Hsu, C.-H., Ho, C.-Y., Lin, J.-C. and Lee, S.-W. 2013. Induction of apoptosis by high-dose gold nanoparticles in nasopharyngeal carcinoma cells. *Auris Nasus Larynx,* 40**,** 563-568.

Lansdorp-Vogelaar, I., Kuntz, K. M., Knudsen, A. B., Van Ballegooijen, M., Zauber, A. G. and Jemal, A. 2012. Contribution of screening and survival differences to racial disparities in colorectal cancer rates. *Cancer Epidemiology, Biomarkers and Prevention,* 21**,** 728-736.

Lasagna-Reeves, C., Gonzalez-Romero, D., Barria, M. A., Olmedo, I., Clos, A., Sadagopa Ramanujam, V. M., Urayama, A., Vergara, L., Kogan, M. J. and Soto, C. 2010. Bioaccumulation and toxicity of gold nanoparticles after repeated administration in mice. *Biochemical and Biophysical Research Communications,* 393**,** 649-655.

Lee, H., Lee, M.-Y., Bhang, S. H., Kim, B.-S., Kim, Y. S., Ju, J. H., Kim, K. S. and Hahn, S. K. 2014. Hyaluronate–gold nanoparticle/tocilizumab complex for the treatment of rheumatoid arthritis. *ACS Nano,* 8**,** 4790-4798.

Lee, M.-Y., Yang, J.-A., Jung, H. S., Beack, S., Choi, J. E., Hur, W., Koo, H., Kim, K., Yoon, S. K. and Hahn, S. K. 2012. Hyaluronic acid–gold nanoparticle/interferon α complex for targeted treatment of hepatitis C virus infection. *ACS Nano,* 6**,** 9522-9531.

Leopold, L. F., Todor, I. S., Diaconeasa, Z., Rugina, D., Stefancu, A., Leopold, N. and Coman, C. 2017. Assessment of PEG and BSA-PEG gold nanoparticles cellular interaction. *Colloids and Surfaces A-Physicochemical and Engineering Aspects,* 532**,** 70-76.

Li, J. J., Hartono, D., Ong, C. N., Bay, B. H. and Yung, L. Y. 2010. Autophagy and oxidative stress associated with gold nanoparticles. *Biomaterials,* 31**,** 5996-6003.

Libutti, S. K., Paciotti, G. F., Byrnes, A. A., Alexander, H. R., Jr., Gannon, W. E., Walker, M., Seidel, G. D., Yuldasheva, N. and Tamarkin, L. 2010. Phase I and pharmacokinetic studies of CYT-

6091, a novel PEGylated colloidal gold-rhTNF nanomedicine. *Clinical Cancer Research,* 16**,** 6139-6149.

Lieschke, G. J. and Currie, P. D. 2007. Animal models of human disease: Zebrafish swim into view. *Nature Reviews Genetics,* 8**,** 353-367.

Lin, Z., Monteiro-Riviere, N. A., Kannan, R. and Riviere, J. E. 2016a. A computational framework for interspecies pharmacokinetics, exposure and toxicity assessment of gold nanoparticles. *Nanomedicine (Lond),* 11**,** 107-119.

Lin, Z., Monteiro-Riviere, N. A. and Riviere, J. E. 2015. Pharmacokinetics of metallic nanoparticles. *Wiley Interdisciplinary Reviews: Nanomedicine and Nanobiotechnology,* 7**,** 189-217.

Lin, Z., Monteiro-Riviere, N. A. and Riviere, J. E. 2016b. A physiologically based pharmacokinetic model for polyethylene glycol-coated gold nanoparticles of different sizes in adult mice. *Nanotoxicology,* 10**,** 162-172.

Liss, D. T., Petit-Homme, A., Feinglass, J., Buchanan, D. R. and Baker, D. W. 2013. Adherence to repeat fecal occult blood testing in an urban community health center network. *Journal of Community Health,* 38**,** 829-833.

Liu, T., Zhang, L., Joo, D. and Sun, S.-C. 2017. NF-κB signaling in inflammation. *Signal Transduction and Targeted Therapy,* 2**,** 17023.

Liu, X., Atwater, M., Wang, J. and Huo, Q. 2007. Extinction coefficient of gold nanoparticles with different sizes and different capping ligands. *Colloids and Surfaces B: Biointerfaces,* 58**,** 3-7.

Longmire, M., Choyke, P. L. and Kobayashi, H. 2008. Clearance properties of nano-sized particles and molecules as imaging agents: Considerations and caveats. *Nanomedicine (London, England),* 3**,** 703-717.

Longnecker, D. 2014. Anatomy and histology of the pancreas. *The Pancreapedia: Exocrine Pancreas Knowledge Base*.

Lu, W., Huang, Q., Ku, G., Wen, X., Zhou, M., Guzatov, D., Brecht, P., Su, R., Oraevsky, A., Wang, L. V. and Li, C. 2010. Photoacoustic imaging of living mouse brain vasculature using hollow gold nanospheres. *Biomaterials,* 31**,** 2617-2626.

Lu, Y. and Barron, A. 2010. Transmission electron microscopy. *OpenStax-CNX Web site,* m34523.

Luo, W., Su, K., Li, K., Liao, G., Hu, N. and Jia, M. 2012. Substrate effect on the melting temperature of gold nanoparticles. *Journal of Chemical Physics,* 136**,** 234704.

Luyten, G. P., Mooy, C. M., De Jong, P. T., Hoogeveen, A. T. and Luider, T. M. 1993. A chicken embryo model to study the growth of human uveal melanoma. *Biochemical and Biophysical Research Communications,* 192**,** 22-29.

Ma, X., Wu, Y., Jin, S., Tian, Y., Zhang, X., Zhao, Y., Yu, L. and Liang, X.-J. 2011. Gold nanoparticles induce autophagosome accumulation through size-dependent nanoparticle uptake and lysosome impairment. *ACS Nano,* 5**,** 8629-8639.

Magaye, R. R., Yue, X., Zou, B., Shi, H., Yu, H., Liu, K., Lin, X., Xu, J., Yang, C., Wu, A. and Zhao, J. 2014. Acute toxicity of nickel nanoparticles in rats after intravenous injection. *International Journal of Nanomedicine,* 9**,** 1393-1402.

Makkouk, A. R. and Madsen, S. J. 2013. Nanoparticle-mediated photothermal therapy of brain tumors. *In:* MADSEN, S. J. (ed.) *Optical methods and instrumentation in brain imaging and therapy.* New York: Springer.

Malathi, S., Balakumaran, M. D., Kalaichelvan, P. T. and Balasubramanian, S. 2013. Green synthesis of gold nanoparticles for controlled delivery. *Advanced Materials Letters,* 4**,** 933-940.

Marqus, S., Pirogova, E. and Piva, T. J. 2017. Evaluation of the use of therapeutic peptides for cancer treatment. *Journal of Biomedical Science,* 24**,** 21.

Mazyambe, M. K. 2013. *Evaluating the specificity of cancer cell targeting peptides for applications in cancer diagnostics.* M.Sc, University of the Western Cape.

Michalska, M., Florczak, A., Dams-Kozlowska, H., Gapinski, J., Jurga, S. and Schneider, R. 2016. Peptide-functionalized ZCIS QDs as fluorescent nanoprobe for targeted HER2-positive breast cancer cells imaging. *Acta Biomaterialia,* 35**,** 293-304.

Mody, V. V., Siwale, R., Singh, A. and Mody, H. R. 2010. Introduction to metallic nanoparticles. *Journal of Pharmacy and Bioallied Sciences,* 2**,** 282-289.

Moore, T. L., Rodriguez-Lorenzo, L., Hirsch, V., Balog, S., Urban, D., Jud, C., Rothen-Rutishauser, B., Lattuada, M. and Petri-Fink, A. 2015. Nanoparticle colloidal stability in cell culture media and impact on cellular interactions. *Chemical Society Reviews,* 44**,** 6287-6305.

Morhason-Bello, I. O., Odedina, F., Rebbeck, T. R., Harford, J., Dangou, J. M., Denny, L. and Adewole, I. F. 2013. Challenges and opportunities in cancer control in Africa: A perspective from the African Organisation for Research and Training in Cancer. *The Lancet Oncology,* 14**,** e142-51.

Mu, Q., Jiang, G., Chen, L., Zhou, H., Fourches, D., Tropsha, A. and Yan, B. 2014. Chemical basis of interactions between engineered nanoparticles and biological systems. *Chemical reviews,* 114**,** 7740-7781.

Mukherjee, P., Ahmad, A., Mandal, D., Senapati, S., Sainkar, S. R., Khan, M. I., Ramani, R., Parischa, R., Ajayakumar, P. V., Alam, M., Sastry, M. and Kumar, R. 2001. Bioreduction of AuCl4− Ions by the fungus, Verticillium sp. and surface trapping of the gold nanoparticles Formed. *Angewandte Chemie International Edition,* 40**,** 3585-3588.

Muller, A. P., Ferreira, G. K., Da Silva, S., Nesi, R. T., De Bem Silveira, G., Mendes, C., Pinho, R. A., Da Silva Paula, M. M. and Silveira, P. C. L. 2017. Safety protocol for the gold nanoparticles administration in rats. *Materials Science and Engineering: C,* 77**,** 1145-1150.

Murphy, C. J., Gole, A. M., Stone, J. W., Sisco, P. N., Alkilany, A. M., Goldsmith, E. C. and Baxter, S. C. 2008. Gold nanoparticles in biology: Beyond toxicity to cellular imaging. *Accounts of Chemical Research,* 41**,** 1721-1730.

Murphy, N., Strickler, H. D., Stanczyk, F. Z., Xue, X., Wassertheil-Smoller, S., Rohan, T. E., Ho, G. Y. F., Anderson, G. L., Potter, J. D. and Gunter, M. J. 2015. A prospective evaluation of endogenous sex hormone levels and colorectal cancer risk in postmenopausal women. *Journal of the National Cancer Institute,* 107.

National Research Council 2006. Toxicity testing for assessment of environmental agents: Interim report. Washington, DC: The National Academies Press.

Nelson, C. E., Kintzing, J. R., Hanna, A., Shannon, J. M., Gupta, M. K. and Duvall, C. L. 2013. Balancing cationic and hydrophobic content of PEGylated siRNA polyplexes enhances endosome escape, stability, blood circulation time, and bioactivity in vivo. *ACS Nano,* 7**,** 8870-8880.

Nelson, D. and Cox, M. M. 2005. *Lehninger principles of biochemistry*, WH Freeman and Company-New York.

Ng, B. Y. C., Xiao, W., West, N. P., Wee, E. J. H., Wang, Y. and Trau, M. 2015. Rapid, single-cell electrochemical detection of Mycobacterium tuberculosis using colloidal gold nanoparticles. *Analytical Chemistry,* 87**,** 10613-10618.

Nicol, J. R., Dixon, D. and Coulter, J. A. 2015. Gold nanoparticle surface functionalization: a necessary requirement in the development of novel nanotherapeutics. *Nanomedicine (Lond),* 10**,** 1315-1326.

Niidome, T., Yamagata, M., Okamoto, Y., Akiyama, Y., Takahashi, H., Kawano, T., Katayama, Y. and Niidome, Y. 2006. PEG-modified gold nanorods with a stealth character for in vivo applications. *Journal of Controlled Release,* 114**,** 343-347.

OECD 2008. *Test No. 425: Acute Oral Toxicity: Up-and-Down Procedure*, OECD Publishing.

OECD 2012. Guidance on sample preparation and dosimetry for the safety testing of manufactured nanomaterials. *OECD Environment, Health and Safety Publications,* ENV/JM/MONO(2012)40.

Oh, E., Susumu, K., Blanco-Canosa, J. B., Medintz, I. L., Dawson, P. E. and Mattoussi, H. 2010. Preparation of stable maleimide-functionalized Au nanoparticles and their use in counting surface ligands. *Small,* 6**,** 1273-1278.

Oh, M. H., Yu, J. H., Kim, I. and Nam, Y. S. 2015. Genetically programmed clusters of gold nanoparticles for cancer cell-targeted photothermal therapy. *ACS Applied Materials and Interfaces,* 7**,** 22578-22586.

Okokon, J. E., Simeon, J. O. and Umoh, E. E. 2017. Hepatoprotective activity of the extract of Homalium letestui stem against paracetamol-induced liver injury. *Avicenna Journal of Phytomedicine,* 7**,** 27-36.

Oni, Y., Hao, K., Dozie-Nwachukwu, S., Obayemi, J. D., Odusanya, O. S., Anuku, N. and Soboyejo, W. O. 2014. Gold nanoparticles for cancer detection and treatment: The role of adhesion. *Journal of Applied Physics,* 115**,** 1-8.

Openstax 2013. The digestive system. *Anatomy and Physiology.* Rice University: OpenStax.

Oyelere, A. K., Chen, P. C., Huang, X., El-Sayed, I. H. and El-Sayed, M. A. 2007. Peptide-conjugated gold nanorods for nuclear targeting. *Bioconjugate Chemistry,* 18**,** 1490-1497.

Pan-Bartneck, Y. 2010. *Assessing the toxicity of gold nanoparticles in vitro and in vivo.* PhD, RWTH Aachen University.

Pan, Y., Leifert, A., Ruau, D., Neuss, S., Bornemann, J., Schmid, G., Brandau, W., Simon, U. and Jahnen-Dechent, W. 2009. Gold nanoparticles of diameter 1.4 nm trigger necrosis by oxidative stress and mitochondrial damage. *Small,* 5**,** 2067-2076.

Pandey, U. B. and Nichols, C. D. 2011. Human disease models in Drosophila melanogaster and the role of the fly in therapeutic drug discovery. *Pharmacological Reviews,* 63**,** 411-436.

Patra, J. K. and Baek, K.-H. 2014. Green nanobiotechnology: Factors affecting synthesis and characterization techniques. *Journal of Nanomaterials,* 2014**,** 12.

Peng, G., Hakim, M., Broza, Y. Y., Billan, S., Abdah-Bortnyak, R., Kuten, A., Tisch, U. and Haick, H. 2010. Detection of lung, breast, colorectal, and prostate cancers from exhaled breath using a single array of nanosensors. *British Journal of Cancer,* 103**,** 542-551.

Peng, G., Tisch, U., Adams, O., Hakim, M., Shehada, N., Broza, Y. Y., Billan, S., Abdah-Bortnyak, R., Kuten, A. and Haick, H. 2009. Diagnosing lung cancer in exhaled breath using gold nanoparticles. *Nature Nanotechnology,* 4**,** 669-673.

Perrault, S. D., Walkey, C., Jennings, T., Fischer, H. C. and Chan, W. C. 2009. Mediating tumor targeting efficiency of nanoparticles through design. *Nano Letters,* 9**,** 1909-1915.

Pfeiffer, C., Rehbock, C., Hühn, D., Carrillo-Carrion, C., De Aberasturi, D. J., Merk, V., Barcikowski, S. and Parak, W. J. 2014. Interaction of colloidal nanoparticles with their local environment: The (ionic) nanoenvironment around nanoparticles is different from bulk and determines the physico-chemical properties of the nanoparticles. *Journal of the Royal Society Interface,* 11**,** 20130931.

Phuoc, T. X. 2014. Complete green synthesis of gold nanoparticles using laser ablation in deionized water containing chitosan and starch. *Journal of Materials Science and Nanotechnology,* 2**,** 202.

Pissuwan, D., Niidome, T. and Cortie, M. B. 2011. The forthcoming applications of gold nanoparticles in drug and gene delivery systems. *Journal of Controlled Release,* 149**,** 65-71.

Pompa, P. P., Vecchio, G., Galeone, A., Brunetti, V., Sabella, S., Maiorano, G., Falqui, A., Bertoni, G. and Cingolani, R. 2011. In vivo toxicity assessment of gold nanoparticles in Drosophila melanogaster. *Nano Research,* 4**,** 405-413.

Ponti, J., Colognato, R., Rauscher, H., Gioria, S., Broggi, F., Franchini, F., Pascual, C., Giudetti, G. and Rossi, F. 2010. Colony forming efficiency and microscopy analysis of multi-wall carbon nanotubes cell interaction. *Toxicology Letters,* 197**,** 29-37.

Ponti, J., Kinsner-Ovaskainen, A., Norlén, H., Altmeyer, S., Andreoli, C., Bogni, A., Chevillard, S., De Angelis, I., Chung, S.-T., Eom, I., Fujita, K., Gilliland, D., Grollino, M. G., Gulumian, M., Hirsch, C., Ichiraku, K., Igarashi, T., Jeong, J., Jo, E., Kim, D.-Y., Kaiser, J.-P., Lagache, D., La Spina, R., Lee, J. K., Lee, J., Lovera, A., Mäder-Althaus, X., Nesslany, F., Jimenez, I. O., Pacchierotti, F., Pianella, F., Paget, V., Kim, T. R., Roszak, J., Rosenkranz, P., Simar, S., Stępnik, M., Vetten, M., Song, N. W., Yang, J.-Y. and Rossi, F. 2014. Interlaboratory comparison study of the colony forming efficiency assay for assessing cytotoxicity of nanomaterials. *In:* KINSNER-OVASKAINEN, A. & PONTI, J. (eds.). Luxembourg: Joint Research Centre – Institute for Health and Consumer Protection.

Popovtzer, R., Agrawal, A., Kotov, N. A., Popovtzer, A., Balter, J., Carey, T. E. and Kopelman, R. 2008. Targeted gold nanoparticles enable molecular CT imaging of cancer. *Nano Letters,* 8**,** 4593-4596.

Qu, Y. and Lu, X. 2009. Aqueous synthesis of gold nanoparticles and their cytotoxicity in human dermal fibroblasts-fetal. *Biomedical Materials,* 4**,** 025007.

Rabinsky, E. F., Joshi, B. P., Pant, A., Zhou, J., Duan, X., Smith, A., Kuick, R., Fan, S., Nusrat, A., Owens, S. R., Appelman, H. D. and Wang, T. D. 2016. Overexpressed Claudin-1 can be visualized endoscopically in colonic adenomas in vivo. *Cellular and Molecular Gastroenterology and Hepatology,* 2**,** 222-237.

Ramaiah, S. K. 2007. A toxicologist guide to the diagnostic interpretation of hepatic biochemical parameters. *Food and Chemical Toxicology,* 45**,** 1551-1557.

Ramakrishna, M., Babu, D. R., Gengan, R. M., Chandra, S. and Rao, G. N. 2016. Green synthesis of gold nanoparticles using marine algae and evaluation of their catalytic activity. *Journal of Nanostructure in Chemistry,* 6**,** 1-13.

Rambanapasi, C. 2015. *An assessment of the biodistribution, biopersistence and toxicity of gold nanoparticles.* PhD (Pharmaceutics), North-West University (South Africa) , Potchefstroom Campus.

Rambanapasi, C., Zeevaart, J. R., Buntting, H., Bester, C., Kotze, D., Hayeshi, R. and Grobler, A. 2016. Bioaccumulation and subchronic toxicity of 14 nm gold nanoparticles in rats. *Molecules,* 21.

Ramesh, A., Sundari, M. T. and Thirugnanam, P. E. 2015. Microbial molecular mechanisms in biosynthesis of nanoparticles. *In:* SINGH, O. V. (ed.) *Bio-nanoparticles: Biosynthesis and sustainable biotechnological implications.* Hoboken, NJ: John Wiley & Sons, Inc.

Rani, V., Deep, G., Singh, R. K., Palle, K. and Yadav, U. C. S. 2016. Oxidative stress and metabolic disorders: Pathogenesis and therapeutic strategies. *Life Sciences,* 148**,** 183-193.

Raskov, H., Pommergaard, H. C., Burcharth, J. and Rosenberg, J. 2014. Colorectal carcinogenesis--update and perspectives. *World Journal of Gastroenterology,* 20**,** 18151-18164.

Rathore, M., Mohanty, I., Maheswari, U., Dayal, N., Suman, R. and Joshi, D. 2014. Comparative in vivo assessment of the subacute toxicity of gold and silver nanoparticles. *Journal of Nanoparticle Research,* 16**,** 1-12.

Rec. GSCC, D. 1972. Optimised standard colorimetric methods. *Journal of Clinical Chemistry and Clinical Biochemistry,* 10**,** 182.

Rehbock, C., Jakobi, J., Gamrad, L., Van Der Meer, S., Tiedemann, D., Taylor, U., Kues, W., Rath, D. and Barcikowski, S. 2014. Current state of laser synthesis of metal and alloy nanoparticles as ligand-free reference materials for nano-toxicological assays. *Beilstein Journal of Nanotechnology,* 5**,** 1523-1541.

Reitman, S. and Frankel, S. 1957. A colorimetric method for the determination of serum glutamic oxalacetic and glutamic pyruvic transaminases. *American Journal of Clinical Pathology,* 28**,** 56-63.

Ribatti, D. 2010. *The chick embryo chorioallantoic membrane in the study of angiogenesis and metastasis,* New York, Springer Science+Business Media B.V.

Richter, J. M., Campbell, E. J. and Chung, D. C. 2015. Interval colorectal cancer after colonoscopy. *Clinical Colorectal Cancer,* 14**,** 46-51.

Rizzo, L. Y., Golombek, S. K., Mertens, M. E., Pan, Y., Laaf, D., Broda, J., Jayapaul, J., Mockel, D., Subr, V., Hennink, W. E., Storm, G., Simon, U., Jahnen-Dechent, W., Kiessling, F. and Lammers, T. 2013. In vivo nanotoxicity testing using the zebrafish embryo assay. *Journal of Materials Chemistry. B, Materials for Biology and Medicine,* 1**,** 3918-3925.

Roberts, E., Ludman, A. J., Dworzynski, K., Al-Mohammad, A., Cowie, M. R., Mcmurray, J. J. V. and Mant, J. 2015a. The diagnostic accuracy of the natriuretic peptides in heart failure: Systematic review and diagnostic meta-analysis in the acute care setting. *British Medical Journal,* 350.

Roberts, S. M., Williams, P. L. and James, R. C. 2015b. *Principles of toxicology: Environmental and industrial applications*, John Wiley & Sons.

Rockey, D. C., Paulson, E., Niedzwiecki, D., Davis, W., Bosworth, H. B., Sanders, L., Yee, J., Henderson, J., Hatten, P., Burdick, S., Sanyal, A., Rubin, D. T., Sterling, M., Akerkar, G., Bhutani, M. S., Binmoeller, K., Garvie, J., Bini, E. J., Mcquaid, K., Foster, W. L., Thompson, W. M., Dachman, A. and Halvorsen, R. 2005. Analysis of air contrast barium enema, computed tomographic colonography, and colonoscopy: Prospective comparison. *Lancet,* 365**,** 305-311.

Roma-Rodrigues, C., Heuer-Jungemann, A., Fernandes, A. R., Kanaras, A. G. and Baptista, P. V. 2016. Peptide-coated gold nanoparticles for modulation of angiogenesis in vivo. *International Journal of Nanomedicine,* 11**,** 2633-2639.

Roy, R., Zurakowski, D., Wischhusen, J., Frauenhoffer, C., Hooshmand, S., Kulke, M. and Moses, M. A. 2014. Urinary TIMP-1 and MMP-2 levels detect the presence of pancreatic malignancies. *British Journal of Cancer,* 111**,** 1772-1779.

Sadauskas, E., Danscher, G., Stoltenberg, M., Vogel, U., Larsen, A. and Wallin, H. 2009. Protracted elimination of gold nanoparticles from mouse liver. *Nanomedicine: Nanotechnology, Biology and Medicine,* 5**,** 162-169.

Sadhasivam, S., Shanmugam, P., Veerapandian, M., Subbiah, R. and Yun, K. 2012. Biogenic synthesis of multidimensional gold nanoparticles assisted by Streptomyces hygroscopicus and its electrochemical and antibacterial properties. *BioMetals,* 25**,** 351-360.

Salvati, A., Pitek, A. S., Monopoli, M. P., Prapainop, K., Bombelli, F. B., Hristov, D. R., Kelly, P. M., Aberg, C., Mahon, E. and Dawson, K. A. 2013. Transferrin-functionalized nanoparticles lose their targeting capabilities when a biomolecule corona adsorbs on the surface. *Nature Nanotechnology,* 8**,** 137-143.

Sangabathuni, S., Murthy, R. V., Chaudhary, P. M., Subramani, B., Toraskar, S. and Kikkeri, R. 2017. Mapping the glyco-gold nanoparticles of different shapes toxicity, biodistribution and sequestration in adult zebrafish. *Scientific Reports,* 7**,** 4239.

Santo, A., Zhu, H. and Li, Y. R. 2016. Free radicals: From health to disease. *Reactive Oxygen Species,* 2**,** 245-263.

Sau, T. K. and Goia, D. V. 2012. Biomedical applications of gold nanoparticles. *In:* MATIJEVIĆ, E. (ed.) *Fine Particles in Medicine and Pharmacy.* Springer Science+Business Media.

Saxena, V. K., Deb, R., Shrivastava, S., Kantaraja, C., Kumar, A. and Kumar, S. 2012. Functionalizing gold nanoparticles with bluetongue virus multiple peptide antigens utilizing gold–thiol interaction: A novel approach to develop pen side test. *Research in Veterinary Science,* 93**,** 1531-1536.

Scallan, J., Huxley, V. H. and Korthuis, R. J. Capillary fluid exchange: regulation, functions, and pathology. Colloquium lectures on integrated systems physiology: From molecules to function, 2010. Morgan & Claypool Publishers, 1-94.

Schaeublin, N. M., Braydich-Stolle, L. K., Maurer, E. I., Park, K., Maccuspie, R. I., Afrooz, A. R. M. N., Vaia, R. A., Saleh, N. B. and Hussain, S. M. 2012. Does shape matter? Bioeffects of gold nanomaterials in a human skin cell model. *Langmuir,* 28**,** 3248-3258.

Schmid, G., Kreyling, W. G. and Simon, U. 2017. Toxic effects and biodistribution of ultrasmall gold nanoparticles. *Archives of Toxicology,* 91**,** 3011-3037.

Schreuders, E. H., Grobbee, E. J., Spaander, M. C. W. and Kuipers, E. J. 2016. Advances in fecal tests for colorectal cancer screening. *Current Treatment Options in Gastroenterology,* 14**,** 152-162.

Schulz, M., Ma-Hock, L., Brill, S., Strauss, V., Treumann, S., Gröters, S., Van Ravenzwaay, B. and Landsiedel, R. 2012. Investigation on the genotoxicity of different sizes of gold nanoparticles administered to the lungs of rats. *Mutation Research/Genetic Toxicology and Environmental Mutagenesis,* 745**,** 51-57.

Schwartz, J. B. 2003. The influence of sex on pharmacokinetics. *Clinical Pharmacokinetics,* 42**,** 107-121.

Scudamore, C. L., Soilleux, E. J., Karp, N. A., Smith, K., Poulsom, R., Herrington, C. S., Day, M. J., Brayton, C. F., Bolon, B., Whitelaw, B., White, E. S., Everitt, J. I. and Arends, M. J. 2016. Recommendations for minimum information for publication of experimental pathology data: MINPEPA guidelines. *The Journal of Pathology,* 238**,** 359-367.

Sefi, M., Ben Amara, I., Troudi, A., Soudani, N., Hakim, A., Zeghal, K. M., Boudawara, T. and Zeghal, N. 2014. Effect of selenium on methimazole-induced liver damage and oxidative stress in adult rats and their offspring. *Toxicology and Industrial Health* 30**,** 653-669.

Sengupta, J., Datta, P., Patra, H. K., Dasgupta, A. K. and Gomes, A. 2013. In vivo interaction of gold nanoparticles after acute and chronic exposures in experimental animal models. *Journal of Nanoscience and Nanotechnology,* 13**,** 1660-1670.

Senut, M.-C., Zhang, Y., Liu, F., Sen, A., Ruden, D. M. and Mao, G. 2016. Size-dependent toxicity of gold nanoparticles on human embryonic stem cells and their neural derivatives. *Small,* 12**,** 631-646.

Shadidi, M. and Sioud, M. 2003a. Identification of novel carrier peptides for the specific delivery of therapeutics into cancer cells. *Federation of American Societies for Experimental Biology Journal,* 17**,** 256-258.

Shadidi, M. and Sioud, M. 2003b. Selective targeting of cancer cells using synthetic peptides. *Drug Resistance Updates,* 6**,** 363-371.

Shah, M., Badwaik, V., Kherde, Y., Waghwani, H. K., Modi, T., Aguilar, Z. P., Rodgers, H., Hamilton, W., Marutharaj, T., Webb, C., Lawrenz, M. B. and Dakshinamurthy, R. 2014a. Gold nanoparticles: Various methods of synthesis and antibacterial applications. *Frontiers in Bioscience,* 19**,** 1320-1344.

Shah, N. B. and Bischof, J. C. 2013. Blood protein and blood cell interactions with gold nanoparticles: The need for in vivo studies. *BioNanoMaterials,* 14**,** 65-79.

Shah, R., Jones, E., Vidart, V., Kuppen, P. J., Conti, J. A. and Francis, N. K. 2014b. Biomarkers for early detection of colorectal cancer and polyps: Systematic review. *Cancer Epidemiology, Biomarkers and Prevention,* 23**,** 1712-1728.

Shamaila, S., Zafar, N., Riaz, S., Sharif, R., Nazir, J. and Naseem, S. 2016. Gold nanoparticles: An efficient antimicrobial agent against enteric bacterial human pathogen. *Nanomaterials,* 6**,** 71.

Shang, J. and Gao, X. 2014. Nanoparticle counting: Towards accurate determination of the molar concentration. *Chemical Society Reviews,* 43**,** 7267-7278.

Shang, L., Nienhaus, K. and Nienhaus, G. U. 2014. Engineered nanoparticles interacting with cells: Size matters. *Journal of Nanobiotechnology,* 12**,** 1-11.

Shapira, S., Fokra, A., Arber, N. and Kraus, S. 2014. Peptides for diagnosis and treatment of colorectal cancer. *Current medicinal chemistry,* 21**,** 2410-2416.

Sharma, A., Tandon, A., Tovey, J. C., Gupta, R., Robertson, J. D., Fortune, J. A., Klibanov, A. M., Cowden, J. W., Rieger, F. G. and Mohan, R. R. 2011. Polyethylenimine-conjugated gold nanoparticles: Gene transfer potential and low toxicity in the cornea. *Nanomedicine,* 7**,** 505-513.

Shawky, S. M., Bald, D. and Azzazy, H. M. E. 2010. Direct detection of unamplified hepatitis C virus RNA using unmodified gold nanoparticles. *Clinical Biochemistry,* 43**,** 1163-1168.

Shetty, T., Dayal, N., Thakur, M., Dhar, R. and Tambekar, M. 2015. Assessments of safety and toxicity levels of gold nanoparticles using zebra fish (Danio rerio) as a vertebrate model. *4th International Conference and Exhibition on Pathology.* New Orleans, USA.

Shi, X. L., Zhu, Y. T., Hua, W. D., Ji, Y. L., Ha, Q., Han, X. X., Liu, Y., Gao, J. W., Zhang, Q., Liu, S. D., Ren, K. L., Wu, X. C., Li, H. Y. and Han, D. 2016. An in vivo study of the biodistribution of gold nanoparticles after intervaginal space injection in the tarsal tunnel. *Nano Research,* 9**,** 2097-2109.

Shin, S. W., Song, I. H. and Um, S. H. 2015. Role of physicochemical properties in nanoparticle toxicity. *Nanomaterials,* 5**,** 1351-1365.

Shujalpurkar, A. and Vikey, A. 2016. Basics of Immunohistochemical procedure. *International Journal of Advanced Research,* 2**,** 883-886.

Siddiqi, N. J., Abdelhalim, M. a. K., El-Ansary, A. K., Alhomida, A. S. and Ong, W. Y. 2012. Identification of potential biomarkers of gold nanoparticle toxicity in rat brains. *Journal of Neuroinflammation,* 9**,** 123-123.

Siddique, S., Panchmal, G. and Pullishery, F. 2016. Aspartate aminotransferase as a biomarker in periodontal disease: A comparative in vitro study. *Saudi Journal of Oral Sciences,* 3**,** 21-24.

Siegmund, B., Fantuzzi, G., Rieder, F., Gamboni-Robertson, F., Lehr, H. A., Hartmann, G., Dinarello, C. A., Endres, S. and Eigler, A. 2001. Neutralization of interleukin-18 reduces severity in murine colitis and intestinal IFN-gamma and TNF-alpha production. *American Journal of Physiology - Regulatory, Integrative and Comparative Physiology,* 281**,** 1264-1273.

Simpson, C. A., Agrawal, A. C., Balinski, A., Harkness, K. M. and Cliffel, D. E. 2011. Short-chain PEG mixed monolayer protected gold clusters increase clearance and red blood cell counts. *ACS Nano,* 5**,** 3577-3584.

Simpson, C. A., Salleng, K. J., Cliffel, D. E. and Feldheim, D. L. 2013. In vivo toxicity, biodistribution, and clearance of glutathione-coated gold nanoparticles. *Nanomedicine: Nanotechnology, Biology and Medicine,* 9**,** 257-263.

Smith, C. A., Simpson, C. A., Kim, G., Carter, C. J. and Feldheim, D. L. 2013. Gastrointestinal bioavailability of 2.0 nm diameter gold nanoparticles. *ACS Nano,* 7**,** 3991-3996.

Smith, D. J. 2015. Characterization of nanomaterials using transmission electron microscopy. *In:* KIRKLAND, A. I. & HAIGH, S. J. (eds.) *Nanocharacterisation (2).* 2nd ed.: The Royal Society of Chemistry Nanoscience & Nanotechnology.

Smith, P. K., Krohn, R. I., Hermanson, G. T., Mallia, A. K., Gartner, F. H., Provenzano, M. D., Fujimoto, E. K., Goeke, N. M., Olson, B. J. and Klenk, D. C. 1985. Measurement of protein using bicinchoninic acid. *Analytical Biochemistry,* 150**,** 76-85.

Society of Toxicology 1999. The importance of animals in the science of toxicology. *SOT Animals in Research Public Policy Statement.* Reston, VA.

Solé, X., Crous-Bou, M., Cordero, D., Olivares, D., Guinó, E., Sanz-Pamplona, R., Rodriguez-Moranta, F., Sanjuan, X., De Oca, J., Salazar, R. and Moreno, V. 2014. Discovery and validation of new potential biomarkers for early detection of colon cancer. *PLoS One,* 9**,** e106748.

Sonavane, G., Tomoda, K. and Makino, K. 2008. Biodistribution of colloidal gold nanoparticles after intravenous administration: Effect of particle size. *Colloids and Surfaces B: Biointerfaces,* 66**,** 274-280.

Sorenson, A. E., Askin, S. P. and Schaeffer, P. M. 2015. In-gel detection of biotin-protein conjugates with a green fluorescent streptavidin probe. *Analytical Methods,* 7**,** 2087-2092.

Sosibo, N., Keter, F., Skepu, A., Tshikhudo, R. and Revaprasadu, N. 2015. Facile attachment of TAT peptide on gold monolayer protected clusters: Synthesis and characterization. *Nanomaterials,* 5**,** 1211-1222.

Sperling, R. A., Rivera Gil, P., Zhang, F., Zanella, M. and Parak, W. J. 2008. Biological applications of gold nanoparticles. *Chemical Society Reviews,* 37**,** 1896-1908.

Spivak, M. Y., Bubnov, R. V., Yemets, I. M., Lazarenko, L. M., Tymoshok, N. O. and Ulberg, Z. R. 2013. Development and testing of gold nanoparticles for drug delivery and treatment of heart failure: A theranostic potential for PPP cardiology. *European Association for Predictive Preventive & Personalized Medicine Journal,* 4**,** 20.

Sreeprasad, T. S. and Pradeep, T. 2013. Noble metal nanoparticles. *In:* VAJTAI, R. (ed.) *Springer Handbook of Nanomaterials.* Berlin, Heidelberg: Springer Berlin Heidelberg.

Striz, I., Eliska, K., Eva, H., Jiri, L., Katerina, P., Marcela, J., Alena, L., Radka, B., Sarka, V., Antonij, S. and Stefan, V. 2005. Interleukin 18 (IL-18) upregulation in acute rejection of kidney allograft. *Immunology Letters,* 99**,** 30-35.

Sujitha, M. V. and Kannan, S. 2013. Green synthesis of gold nanoparticles using Citrus fruits (Citrus limon, Citrus reticulata and Citrus sinensis) aqueous extract and its characterization. *Spectrochimica Acta Part A: Molecular and Biomolecular Spectroscopy,* 102**,** 15-23.

Suttie, A. W. 2006. Histopathology of the spleen. *Toxicologic Pathology,* 34**,** 466-503.

Takahashi, H., Niidome, Y., Niidome, T., Kaneko, K., Kawasaki, H. and Yamada, S. 2006. Modification of gold nanorods using phosphatidylcholine to reduce cytotoxicity. *Langmuir,* 22**,** 2-5.

Tauran, Y., Brioude, A., Coleman, A. W., Rhimi, M. and Kim, B. 2013. Molecular recognition by gold, silver and copper nanoparticles. *World Journal of Biological Chemistry,* 4**,** 35-63.

Taylor, C. R., Shi, S.-R., Barr, N. and Dabbs, D. 2013. Techniques of immunohistochemistry: Principles, pitfalls, and standardization. *Diagnostic immunohistochemistry,* 2**,** 1-42.

Thakor, A. S., Jokerst, J., Zavaleta, C., Massoud, T. F. and Gambhir, S. S. 2011. Gold nanoparticles: A revival in precious metal administration to patients. *Nano Letters,* 11**,** 4029-4036.

Thi Ha Lien, N., Thi Tuyen, N., Emmanuel, F., Thanh Phuong, N., Thi My Nhung, H., Thi Quy, N. and Hong Nhung, T. 2012. Capping and in vivo toxicity studies of gold nanoparticles. *Advances in Natural Sciences: Nanoscience and Nanotechnology,* 3**,** 015002.

Thundimadathil, J. 2012. Cancer treatment using peptides: Current therapies and future prospects. *Journal of Amino Acids,* 2012**,** 13.

Tian, F., Clift, M. J. D., Casey, A., Del Pino, P., Pelaz, B., Conde, J., Byrne, H. J., Rothen-Rutishauser, B., Estrada, G., De La Fuente, J. M. and Stoeger, T. 2015. Investigating the role of shape on the biological impact of gold nanoparticles in vitro. *Nanomedicine,* 10**,** 2643-2657.

Tiedemann, D., Taylor, U., Rehbock, C., Jakobi, J., Klein, S., Kues, W. A., Barcikowski, S. and Rath, D. 2014. Reprotoxicity of gold, silver, and gold-silver alloy nanoparticles on mammalian gametes. *Analyst,* 139**,** 931-942.

Tiwari, J. N., Tiwari, R. N. and Kim, K. S. 2012. Zero-dimensional, one-dimensional, two-dimensional and three-dimensional nanostructured materials for advanced electrochemical energy devices. *Progress in Materials Science,* 57**,** 724-803.

Tiwari, P. M., Eroglu, E., Bawage, S. S., Vig, K., Miller, M. E., Pillai, S., Dennis, V. A. and Singh, S. R. 2014. Enhanced intracellular translocation and biodistribution of gold nanoparticles functionalized with a cell-penetrating peptide (VG-21) from vesicular stomatitis virus. *Biomaterials,* 35**,** 9484-9494.

Tiwari, P. M., Vig, K., Dennis, V. A. and Singh, S. R. 2011. Functionalized Gold Nanoparticles and Their Biomedical Applications. *Nanomaterials (Basel),* 1**,** 31-63.

Toroz, D. and Corni, S. 2011. Peptide synthesis of gold nanoparticles: The early steps of gold reduction investigated by density functional theory. *Nano letters,* 11**,** 1313-1318.

Torre, L. A., Bray, F., Siegel, R. L., Ferlay, J., Lortet-Tieulent, J. and Jemal, A. 2015. Global cancer statistics, 2012. *CA: A Cancer Journal for Clinicians,* 65**,** 87-108.

Torres-Mendieta, R., Ventura-Espinosa, D., Sabater, S., Lancis, J., Mínguez-Vega, G. and Mata, J. A. 2016. In situ decoration of graphene sheets with gold nanoparticles synthetized by pulsed laser ablation in liquids. *Scientific Reports,* 6**,** 30478.

Tripathi, A., Kumari, S. and Kumar, A. 2016. Toxicity evaluation of pH dependent stable Achyranthes aspera herbal gold nanoparticles. *Applied Nanoscience,* 6**,** 61-69.

Truong, L., Saili, K. S., Miller, J. M., Hutchison, J. E. and Tanguay, R. L. 2012. Persistent adult zebrafish behavioral deficits results from acute embryonic exposure to gold nanoparticles. *Comparative Biochemistry and Physiology,* 155**,** 269-274.

Truong, L., Tilton, S. C., Zaikova, T., Richman, E., Waters, K. M., Hutchison, J. E. and Tanguay, R. L. 2013. Surface functionalities of gold nanoparticles impact embryonic gene expression responses. *Nanotoxicology,* 7**,** 192-201.

Tsung-Ting, T., Shu-Wei, S., Chao-Min, C. and Chien-Fu, C. 2013. Paper-based tuberculosis diagnostic devices with colorimetric gold nanoparticles. *Science and Technology of Advanced Materials,* 14**,** 044404.

Turkevich, J., Stevenson, P. C. and Hillier, J. 1951. A study of the nucleation and growth processes in the synthesis of colloidal gold. *Discussions of the Faraday Society,* 11**,** 55-75.

Uboldi, C., Giudetti, G., Broggi, F., Gilliland, D., Ponti, J. and Rossi, F. 2012. Amorphous silica nanoparticles do not induce cytotoxicity, cell transformation or genotoxicity in Balb/3T3 mouse fibroblasts. *Mutation Research/Genetic Toxicology and Environmental Mutagenesis,* 745**,** 11-20.

Uchiyama, M. K., Deda, D. K., Rodrigues, S. F., Drewes, C. C., Bolonheis, S. M., Kiyohara, P. K., Toledo, S. P., Colli, W., Araki, K. and Farsky, S. H. 2014. In vivo and in vitro toxicity and anti-inflammatory properties of gold nanoparticle bioconjugates to the vascular system. *Toxicological Sciences,* 142**,** 497-507.

Vargas, A., Zeisser-Labouebe, M., Lange, N., Gurny, R. and Delie, F. 2007. The chick embryo and its chorioallantoic membrane (CAM) for the in vivo evaluation of drug delivery systems. *Advanced drug delivery reviews,* 59**,** 1162-1176.

Varshney, R. and Kale, R. K. 1990. Effects of calmodulin antagonists on radiation-induced lipid peroxidation in microsomes. *International Journal of Radiation Biology,* 58**,** 733-743.

Venkatpurwar, V., Mali, V., Bodhankar, S. and Pokharkar, V. 2012. In vitro cytotoxicity and in vivo sub-acute oral toxicity assessment of porphyran reduced gold nanoparticles. *Toxicological and Environmental Chemistry,* 94**,** 1357-1367.

Verissimo, T. V., Santos, N. T., Silva, J. R., Azevedo, R. B., Gomes, A. J. and Lunardi, C. N. 2016. In vitro cytotoxicity and phototoxicity of surface-modified gold nanoparticles associated with neutral red as a potential drug delivery system in phototherapy. *Materials Science and Engineering: C,* 65**,** 199-204.

Verkerk, A. O. and Remme, C. A. 2012. Zebrafish: A novel research tool for cardiac (patho) electrophysiology and ion channel disorders. *Frontiers in Physiology,* 3**,** 255.

Vesaratchanon, S., Nikolov, A. and Wasan, D. T. 2007. Sedimentation in nano-colloidal dispersions: Effects of collective interactions and particle charge. *Advances in Colloid and Interface Science,* 134–135**,** 268-278.

Vetten, M. A., Tlotleng, N., Tanner Rascher, D., Skepu, A., Keter, F. K., Boodhia, K., Koekemoer, L. A., Andraos, C., Tshikhudo, R. and Gulumian, M. 2013. Label-free in vitro toxicity and uptake assessment of citrate stabilised gold nanoparticles in three cell lines. *Particle and fibre toxicology,* 10**,** 50.

Vijayakumar, S. and Ganesan, S. 2012. In vitro cytotoxicity assay on gold nanoparticles with different stabilizing agents. *Journal of Nanomaterials,* 2012**,** 9.

Vijayakumar, S. and Ganesan, S. 2013. Size-dependent in vitro cytotoxicity assay of gold nanoparticles. *Toxicological & Environmental Chemistry,* 95**,** 277-287.

Villiers, C., Freitas, H., Couderc, R., Villiers, M.-B. and Marche, P. 2010. Analysis of the toxicity of gold nano particles on the immune system: Effect on dendritic cell functions. *Journal of Nanoparticle Research,* 12**,** 55-60.

Vliegenthart, A. D. B., Tucker, C. S., Del Pozo, J. and Dear, J. W. 2014. Zebrafish as model organisms for studying drug-induced liver injury. *British Journal of Clinical Pharmacology,* 78**,** 1217-1227.

Wang, C., Wang, J., Liu, D. and Wang, Z. 2010. Gold nanoparticle-based colorimetric sensor for studying the interactions of β-amyloid peptide with metallic ions. *Talanta,* 80**,** 1626-1631.

Wang, H.-L., Chu, C.-H., Tsai, S.-J. and Yang, R.-J. 2016a. Aspartate aminotransferase and alanine aminotransferase detection on paper-based analytical devices with inkjet printer-sprayed reagents. *Micromachines,* 7**,** 9.

Wang, J.-J., Liu, Y., Zheng, Y., Liao, K.-X., Lin, F., Wu, C.-T., Cai, G.-F. and Yao, X.-Q. 2012. Screening peptides binding specifically to colorectal cancer cells from a phage random peptide library. *Asian Pacific Journal of Cancer Prevention,* 13**,** 377-381.

Wang, J.-Y., Chen, J., Yang, J., Wang, H., Shen, X., Sun, Y.-M., Guo, M. and Zhang, X.-D. 2016b. Effects of surface charges of gold nanoclusters on long-term in vivo biodistribution, toxicity, and cancer radiation therapy. *International Journal of Nanomedicine,* 11**,** 3475-3485.

Wang, P., Wang, X., Wang, L., Hou, X., Liu, W. and Chen, C. 2015. Interaction of gold nanoparticles with proteins and cells. *Science and Technology of Advanced Materials,* 16**,** 034610.

Wang, W., Guan, S., Sun, S., Jin, Y., Lee, K.-H., Chen, Y. and Wei, J. 2014a. Detection of circulating antibodies to linear peptide antigens derived from ANXA1 and DDX53 in lung cancer. *Tumor Biology,* 35**,** 4901-4905.

Wang, X., Gobbo, P., Suchy, M., Workentin, M. S. and Hudson, R. H. E. 2014b. Peptide-decorated gold nanoparticles via strain-promoted azide-alkyne cycloaddition and post assembly deprotection. *Royal Society of Chemistry Advances,* 4**,** 43087-43091.

Wang, Z., Xie, D., Liu, H., Bao, Z. and Wang, Y. 2016c. Toxicity assessment of precise engineered gold nanoparticles with different shapes in zebrafish embryos. *RSC Advances,* 6**,** 33009-33013.

Weatherburn, M. 1967. Phenol-hypochlorite reaction for determination of ammonia. *Analytical chemistry,* 39**,** 971-974.

Weber, D., Davies, M. J. and Grune, T. 2015. Determination of protein carbonyls in plasma, cell extracts, tissue homogenates, isolated proteins: Focus on sample preparation and derivatization conditions. *Redox Biology,* 5**,** 367-380.

Wu, P., Leinonen, J., Koivunen, E., Lankinen, H. and Stenman, U. H. 2000. Identification of novel prostate-specific antigen-binding peptides modulating its enzyme activity. *European Journal of Biochemistry,* 267**,** 6212-6220.

Xia, E. Q., Zhu, S. S., He, M. J., Luo, F., Fu, C. Z. and Zou, T. B. 2017. Marine peptides as potential agents for the management of Type 2 Diabetes mellitus-A prospect. *Marine Drugs,* 15**,** 88.

Xiao, Y.-F., Jie, M.-M., Li, B.-S., Hu, C.-J., Xie, R., Tang, B. and Yang, S.-M. 2015. Peptide-based treatment: A promising cancer therapy. *Journal of Immunology Research,* 2015**,** 761820.

Xue, C., Xue, Y., Dai, L., Urbas, A. and Li, Q. 2013. Size- and shape-dependent fluorescence quenching of gold nanoparticles on perylene dye. *Advanced Optical Materials,* 1**,** 581-587.

Yah, C. S. 2013. The toxicity of gold nanoparticles in relation to their physiochemical properties. *Biomedical Research,* 24**,** 400-413.

Yang, C., Tian, A. and Li, Z. 2016. Reversible cardiac hypertrophy induced by PEG-coated gold nanoparticles in mice. *Scientific Reports,* 6**,** 20203.

Yang, J. A., Lohse, S. E. and Murphy, C. J. 2014. Tuning cellular response to nanoparticles via surface chemistry and aggregation. *Small,* 10**,** 1642-1651.

Yang, L., Kuang, H., Zhang, W., Aguilar, Z. P., Wei, H. and Xu, H. 2017a. Comparisons of the biodistribution and toxicological examinations after repeated intravenous administration of silver and gold nanoparticles in mice. *Scientific Reports,* 7**,** 3303.

Yang, Y., Matsubara, S., Nogami, M. and Shi, J. 2007. Controlling the aggregation behavior of gold nanoparticles. *Materials Science and Engineering: B,* 140**,** 172-176.

Yang, Y., Qina, Z., Zeng, W., Yang, T., Cao, Y. B., Mei, C. R. and Kuang, Y. 2017b. Toxicity assessment of nanoparticles in various systems and organs. *Nanotechnology Reviews,* 6**,** 279-289.

Yeh, Y.-C., Creran, B. and Rotello, V. M. 2012. Gold nanoparticles: Preparation, properties, and applications in bionanotechnology. *Nanoscale,* 4**,** 1871-1880.

York, M. J. 2013. Clinical pathology. *In:* FAQI, A. S. (ed.) *A comprehensive guide to toxicology in preclinical drug development.* 1st ed. USA: Academic Press.

You, J., Zhang, G. and Li, C. 2010. Exceptionally high payload of doxorubicin in hollow gold nanospheres for near-infrared light-triggered drug release. *ACS Nano,* 4**,** 1033-1041.

Yu, M. and Zheng, J. 2015. Clearance pathways and tumor targeting of imaging nanoparticles. *ACS Nano,* 9**,** 6655-6674.

Zabielska-Koczywas, K., Dolka, I., Krol, M., Zbikowski, A., Lewandowski, W., Mieczkowski, J., Wojcik, M. and Lechowski, R. 2017. Doxorubicin conjugated to glutathione stabilized gold nanoparticles (Au-GSH-Dox) as an effective therapeutic agent for feline injection-site sarcomas-chick embryo chorioallantoic membrane study. *Molecules,* 22**,** 253.

Zagainova, E. V., Bugrova, M. L., Snopova, L. B., Elagin, V. V., Sirotkina, M. A., Shirmanova, M. V., Denisov, N. N. and Nadtochenko, V. A. 2010. Investigation of biodistribution of gold nanoparticles in healthy animals. *Nanotechnologies in Russia,* 5**,** 409-416.

Zareei, S., Boojar, M. M. A. and Amanlou, M. 2017. Inhibition of liver alanine aminotransferase and aspartate aminotransferase by hesperidin and its aglycone hesperetin: An in vitro and in silico study. *Life Sciences,* 178**,** 49-55.

Zauber, A. G., Winawer, S. J., O'brien, M. J., Lansdorp-Vogelaar, I., Van Ballegooijen, M., Hankey, B. F., Shi, W., Bond, J. H., Schapiro, M. and Panish, J. F. 2012. Colonoscopic polypectomy and long-term prevention of colorectal-cancer deaths. *New England Journal of Medicine,* 366**,** 687-696.

Zhai, J., Hinton, T. M., Waddington, L. J., Fong, C., Tran, N., Mulet, X., Drummond, C. J. and Muir, B. W. 2015. Lipid-PEG conjugates sterically stabilize and reduce the toxicity of phytantriol-based lyotropic liquid crystalline nanoparticles. *Langmuir,* 31**,** 10871-10880.

Zhang, G., Yang, Z., Lu, W., Zhang, R., Huang, Q., Tian, M., Li, L., Liang, D. and Li, C. 2009. Influence of anchoring ligands and particle size on the colloidal stability and in vivo biodistribution of polyethylene glycol-coated gold nanoparticles in tumor-xenografted mice. *Biomaterials,* 30**,** 1928-1936.

Zhang, M., Li, X., Zhang, X., Yang, Y., Feng, Z. and Liu, X. 2014. Association of serum hemoglobin A1c, C-peptide and insulin-like growth factor-1 levels with the occurrence and development of lung cancer. *Molecular and clinical oncology,* 2**,** 506-508.

Zhang, X.-D., Wu, D., Shen, X., Liu, P.-X., Yang, N., Zhao, B., Zhang, H., Sun, Y.-M., Zhang, L.-A. and Fan, F.-Y. 2011. Size-dependent in vivo toxicity of PEG-coated gold nanoparticles. *International Journal of Nanomedicine,* 6**,** 2071-2081.

Zhang, X.-D., Wu, H.-Y., Wu, D., Wang, Y.-Y., Chang, J.-H., Zhai, Z.-B., Meng, A.-M., Liu, P.-X., Zhang, L.-A. and Fan, F.-Y. 2010. Toxicologic effects of gold nanoparticles in vivo by different administration routes. *International Journal of Nanomedicine,* 5**,** 771-781.

Zhang, X. 2015. Gold nanoparticles: Recent advances in the biomedical applications. *Cell Biochemistry and Biophysics,* 72**,** 771-775.

Zhang, X. D., Wu, D., Shen, X., Liu, P. X., Fan, F. Y. and Fan, S. J. 2012. In vivo renal clearance, biodistribution, toxicity of gold nanoclusters. *Biomaterials,* 33**,** 4628-4638.

Zhang, Y. 2013. *Study on gold nanoparticles for biological applications.* Ph.D, University of Strathclyde.

Zhang, Y. N., Poon, W., Tavares, A. J., Mcgilvray, I. D. and Chan, W. C. 2016. Nanoparticle-liver interactions: Cellular uptake and hepatobiliary elimination. *Journal of Controlled Release,* 240**,** 332-348.

Zheng, Y., Hong, Y., Wu, W., Sun, D., Wang, Y., Huang, J. and Li, Q. 2015. Separation of different shape biosynthesized gold nanoparticles via agarose gel electrophoresis. *Separation and Purification Technology,* 151**,** 332-337.

Zhi-Juan, Z., Chun-Xia, W., Yong, W., Shu-Hua, N., Chang-Gui, L. and De-Gang, F. 2007. Fluorescent property of gold nanoparticles with different surface structures. *Chinese Journal of Chemical Physics,* 20**,** 796.

Zhou, W., Gao, X., Liu, D. and Chen, X. 2015. Gold nanoparticles for in vitro diagnostics. *Chemical reviews,* 115**,** 10575-10636.

Zhu, L., Yang, L. and Zhou, Z. 2017. Nanomaterials in cancer theranostics. *In:* BING YAN, HONGYU ZHOU & GARDEA-TORRESDEY, J. L. (eds.) *Bioactivity of Engineered Nanoparticles.* Singapore: Springer Nature.

Zielinska, M., Sawosz, E., Grodzik, M., Balcerak, M., Wierzbicki, M., Skomial, J., Sawosz, F. and Chwalibog, A. 2012. Effect of taurine and gold nanoparticles on the morphological and molecular characteristics of muscle development during chicken embryogenesis. *Archives of Animal Nutrition,* 66**,** 1-13.

Zielinska, M., Sawosz, E., Grodzik, M., Wierzbicki, M., Gromadka, M., Hotowy, A., Sawosz, F., Lozicki, A. and Chwalibog, A. 2011. Effect of heparan sulfate and gold nanoparticles on muscle development during embryogenesis. *International Journal of Nanomedicine,* 6**,** 3163-3172.

Zong, J., Cobb, S. L. and Cameron, N. R. 2017. Peptide-functionalized gold nanoparticles: Versatile biomaterials for diagnostic and therapeutic applications. *Biomaterials Science,* 5**,** 872-886.

**APPENDIX 1**

• PO Box 77000 • Nelson Mandela Metropolitan University
• Port Elizabeth • 6031 • South Africa • www.nmmu.ac.za

Nelson Mandela Metropolitan University
*for tomorrow*

**Chairperson of the Research Ethics Committee (Animal)**
**NMMU**
Tel . +27 (0)41 504-4273 Fax. +27 (0)41 504-2814

**Ref: [A15-SCI-BCM-002 / Approval]**

**Contact person: Mrs U Spies**

27 October 2015

Prof S Roux
NMMU
Faculty: Science
Department of Biochemistry and Microbiology
South Campus

Dear Prof Roux

**ASSESSMENTS OF THE POSSIBLE SIDE-EFFECTS OF PEPTIDE-GOLD NANOPARTICLES USED IN THE DIAGNOSIS OF COLORECTAL CANCER**

PRP: Prof S Roux
PI: Mr O Adewale

We take pleasure in informing you that the above-mentioned application submitted to the Research Ethics Committee (Animal) for ethics approval, was approved by the Committee.

The ethics clearance reference number is **A15-SCI-BCM-002**

Ethics approval remains **valid for three years**, provided that the approved protocols and conditions remain unchanged and that the applicant agrees to regular monitoring (video recordings if necessary where field work is involved) by the RECA for the duration of the project. At the end of the third year, you will have to affirm that the project is complete, or reapply for ethics approval. You will receive the appropriate reminder and documentation each year well in time for any applicable deadline.

Please inform your co-investigators of the outcome. We wish you well with the project.

Yours sincerely

**Prof G Dealtry**
**Chairperson: Research Ethics Committee (Animal)**

cc: Department of Research Capacity Development
Faculty Officer: Science

/us

## APPENDIX 2

### 1. Determination of serum alanine aminotransferase activity

**Table 1:** Calibration of alanine aminotransferase standard curve

| Absorbance | U/l | Absorbance | U/l |
|---|---|---|---|
| 0.025 | 4 | 0.275 | 48 |
| 0.050 | 8 | 0.300 | 52 |
| 0.075 | 12 | 0.325 | 57 |
| 0.100 | 17 | 0.350 | 62 |
| 0.125 | 21 | 0.375 | 67 |
| 0.150 | 25 | 0.400 | 72 |
| 0.175 | 29 | 0.425 | 77 |
| 0.200 | 34 | 0.450 | 83 |
| 0.225 | 39 | 0.475 | 88 |
| 0.250 | 43 | 0.500 | 94 |

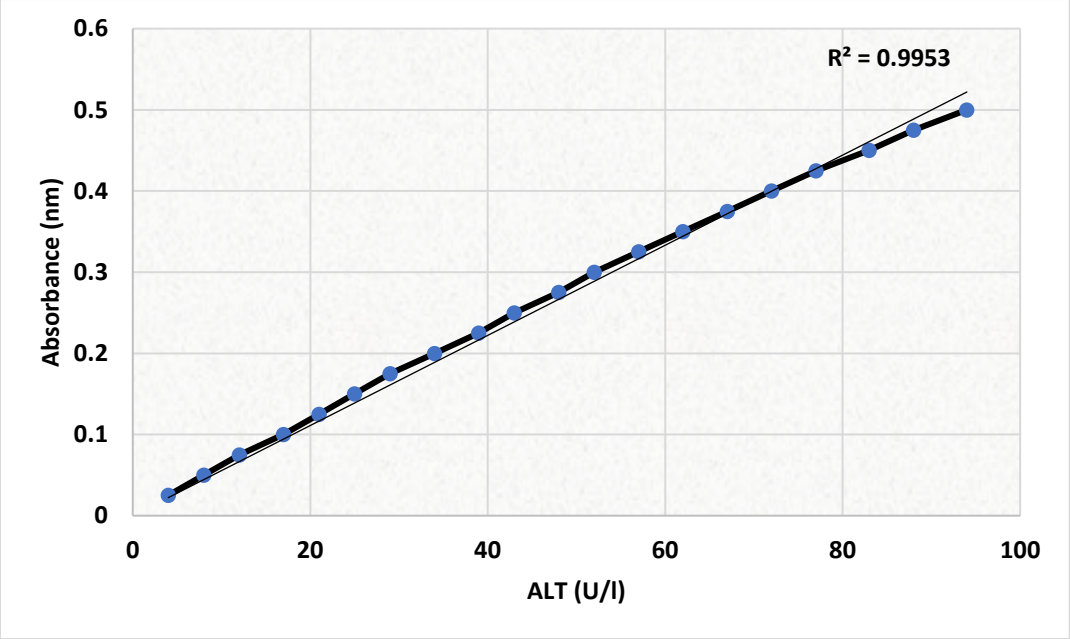


**Figure 1:** Standard curve for the determination of alanine aminotransferase.

## 2. Determination of serum aspartate aminotransferase activity

**Table 2:** Calibration of aspartate aminotransferase standard curve

| Absorbance | U/l | Absorbance | U/l |
|---|---|---|---|
| 0.020 | 7 | 0.100 | 36 |
| 0.030 | 10 | 0.110 | 41 |
| 0.040 | 13 | 0.120 | 47 |
| 0.050 | 16 | 0.130 | 52 |
| 0.060 | 19 | 0.140 | 59 |
| 0.070 | 23 | 0.150 | 67 |
| 0.080 | 27 | 0.160 | 76 |
| 0.090 | 31 | 0.170 | 89 |

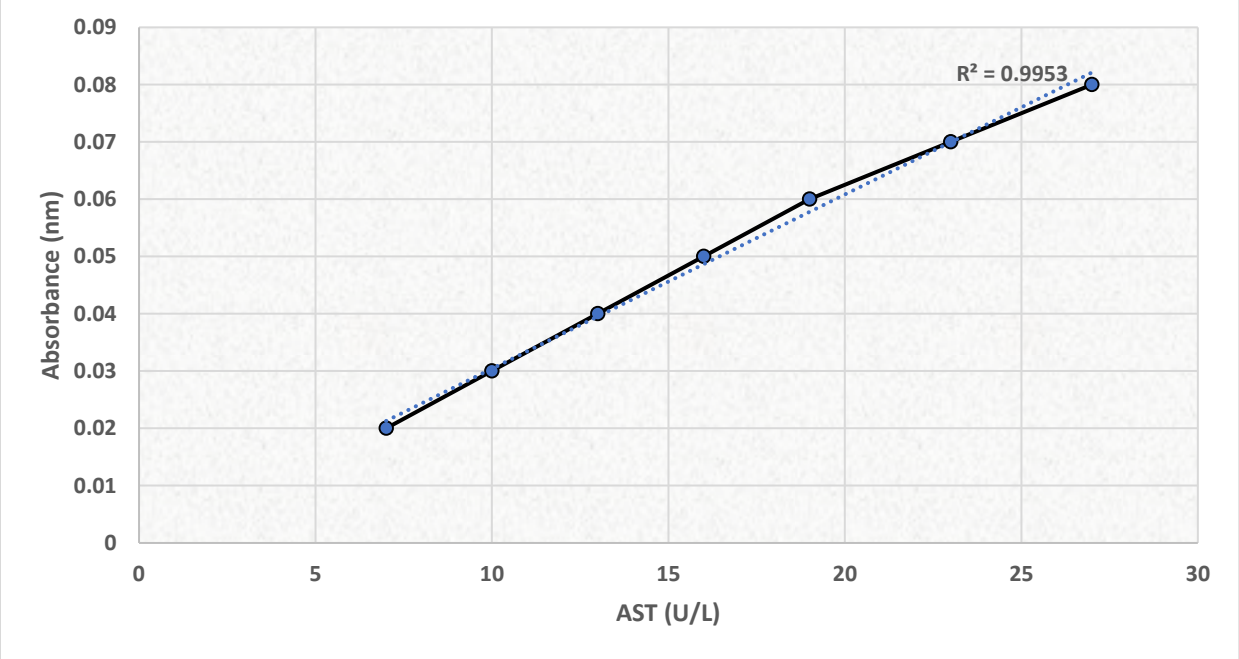


**Figure 2**: Standard curve for the determination of aspartate aminotransferase.
Samples were diluted to fit the range of standard curve, and then multiplied by the dilution factor.

### 3. Estimation of total protein concentration

**Table 3:** Calibration of protein standard (BSA) curve

| Absorbance | Concentration (µg/mL) |
|---|---|
| 0 | 0 |
| 0.014 | 25 |
| 0.0555 | 125 |
| 0.1045 | 250 |
| 0.213 | 500 |
| 0.3075 | 750 |
| 0.4215 | 1000 |
| 0.593 | 1500 |
| 0.7665 | 2000 |

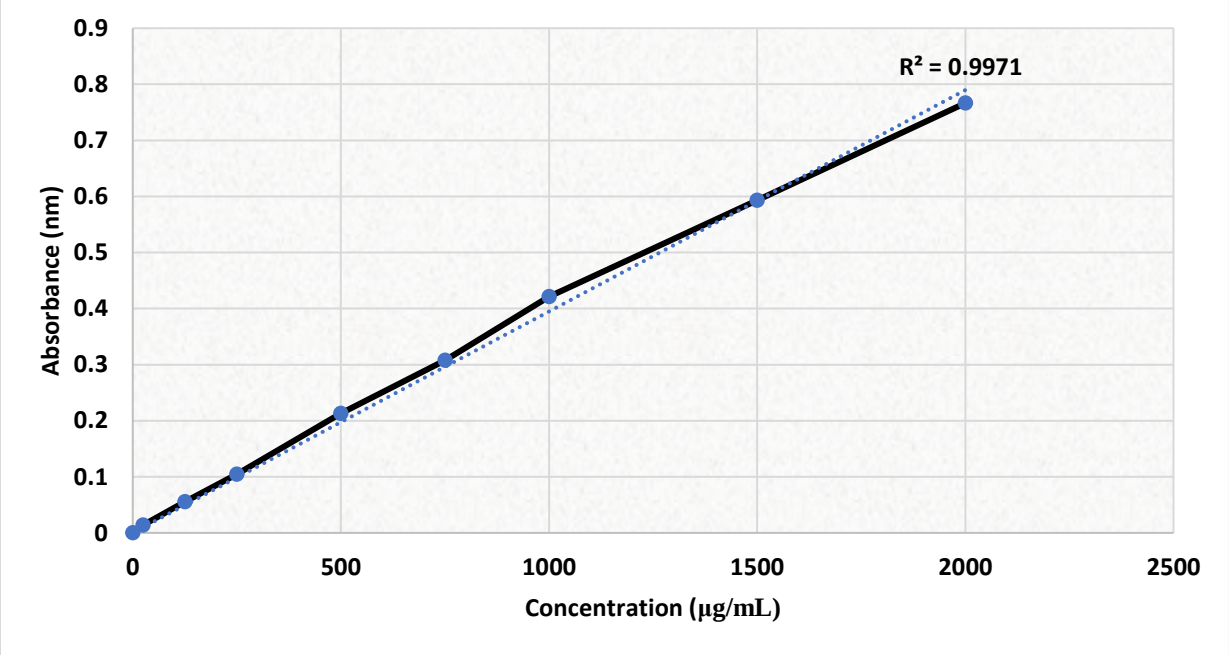


**Figure 3:** Standard curve for the estimation of total protein.